REPUBLIQUE DU CAMEROUN
Paix-Travail-Patrie
················
UNIVERSITE DE YAOUNDE I
················
CENTRE DE RECHERCHE ET DE
FORMATION DOCTORALE EN
SCIENCES, TECHNOLOGIES ET
GEOSCIENCES
················
B. P. 812 Yaoundé
E-mail :crfd_stg@uy1.uninet.com

REPUBLIC OF CAMEROON
Peace-Work-Fatherland
················
THE UNIVERSITY OF YAOUNDE I
················
POSTGRADUATE SCHOOL OF
SCIENCE, TECHNOLOGY AND
GEOSCIENCE
················
P. o. Box 812 Yaounde
E-mail:crfd_stg@uy1.uninet.com
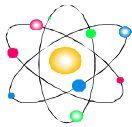
LABORATORY OF NUCLEAR, ATOMIC, MOLECULAR PHYSICS AND BIOPHYSICS
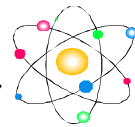
ATMOSPHERIC DISPERSION MODELING OF RADIOACTIVE POLLUTANTS IN FRACTIONAL-DIMENSIONAL SPACE

A dissertation submitted in partial fulfilment of the requirements for the degree of

Doctor of Philosophy in Physics

Option:
Nuclear Physics, Dosimetry and Radioprotection

By:

TANKOU TAGNE Alain Sylvain

Master's degree in physics

Registration number: **02R259**

Under the Supervision:

BEN-BOLIE Germain Hubert, Professor, U Y I

OWONO ATEBA Pierre, Associate Professor, U Y I

2021

UNIVERSITE DE YAOUNDE I
UNIVERSITY OF YAOUNDE I

FACULTE DES SCIENCES
FACULTY OF SCIENCE

DEPARTEMENT DE PHYSIQUE
DEPARTMENT OF PHYSICS

ATTESTATION DE CORRECTION DE LA THESE DE DOCTORAT/PhD

Nous, Professeur **EKOBENA FOUDA Henri Paul** et Professeur **SAIDOU**, respectivement Président du jury et Examinateur de la Thèse de Doctorat/PhD de Monsieur **TANKOU TAGNE Alain Sylvain** Matricule **02R259**, préparée sous la direction du Professeur **BEN-BOLIE Germain Hubert** et sous la supervision du Professeur **OWONO ATEBA Pierre**, intitulée : « **Atmospheric dispersion of radioactive pollutants in fractional-dimensional space**», soutenue le **Mercredi, 20 Octobre 2021**, en vue de l'obtention du grade de Docteur/PhD en Physique, Spécialité Physique Nucléaire , Atomique, Moléculaire, et Biophysique Option Physique Nucléaire, Dosimétrie et Radioprotection, attestons que toutes les corrections demandées par le Jury de soutenance ont été effectuées.

En foi de quoi, la présente attestation lui est délivrée pour servir et valoir ce que de droit.

Fait à Yaoundé le **0 1 NOV 2021**

Examinateur

Pr. SAIDOU

Le Président du Jury

Pr. EKOBENA FOUDA Henri Paul

Le Chef de Département de Physique

Ndjaka Jean-Marie Bienvenu
Professeur

Dedication

To my daughter, **DJUNE TANKOU** Grace Emmanuelle, deep affection.

Acknowledgements

This work is the result of efforts and encouragement from several people without whom it could not have been completed.

We therefore extend our sincere thanks to my Thesis Supervisors; Professor OWONO ATEBA Pierre whose genius inspired the creation of the Nuclear Physics Laboratory.

My great gratitude to Professor BEN-BOLIE Germain Hubert, for the rigorous scientist management and wise advise provided in the context of this work.

Deep gratitude to Professor KOFANE Timoléon Crépin, for having guided my steps on the paths of science.

My gratitude to Professors: SAÏDOU, EMA'A EMA'A Jean Marie, ELE ABIAMA Patrice; *Dra* Daniela BUSKE for their advice and encouragement for the completion of this thesis.

My gratitude to Professors: WOAFO Paul, OWONO OWONO Luc Calvin, EKOBENA FOUDA Henri Paul, NANA NBENDJO Roméo, YIMELE David, NDJAKA Jean-Marie Bienvenu, for their exceptional and permanent support.

My gratitude to the Vice-Chancellor Aurélien Maurice SOSSO, the Dean TCHOUANKEU Jean Claude, the Vice-Dean Alex de Théodore ATCHADE for allowing me to carry out this research work undeniably under their auspices.

All our gratitude goes to everyone the teachers of the University of Yaoundé I, who despite their multiple occupations, have agreed to provide us from precious useful lessons for our education and training. We also thank all those who knew how to cheer us up at the time of the weakening relaxation:

- DJUNE Christine Epse TAGNE ;
- Richard Marie TAGNE ;
- Arch. Bishop ATANGA Joseph ;
- H. E. EYEBE AYISSI Henri ;
- TCHANTCHO NDJAMO Nicaise ;
- My brothers and sisters;

Contents

List of Abbreviations

A B L	Atmospheric Boundary Layer
A D E	Advection Dispersion Equation
α-GM	Alpha-Gaussian Model
AERMOD	American Meteorological Society/Environmental Protection Agency Regulatory Model
A P I	Air Quality Index
A Q I	Air Pollution Index
CO	Carbon Monoxide
CO_2	Carbon Dioxide
C R T W	Random Walk in Continuous Time
F A D E	Fractional Advection-Dispersion Equation
G H G	Greenhouse Effect
G I L T T	Generalized Integral Laplace Transform Technique
K_i	Eddy Diffusivity Coefficient
L	Monin-Obukhov Length
MRAM	Magnetic Random Access Memory
NFPDEs	Nonlinear Fractional Partial Differential Equations
NGOs	Non-Governmental Organizations
NLEEs	Nonlinear Evolution Equations
NO	Nitrogen Oxide
P B L	Planetary Boundary Layer
P S D	Power Spectral Density
RANS	Reynolds-Averaged Navier-Stokes
TRANSCHIM	Transport Chemical Eulerian Model

List of Figures

List of Tables

Résumé

Dans ce travail, une attention particulière est portée sur le calcul fractionnaire omniprésent aujourd'hui dans presque tous les domaines de la science, en physique nucléaire pour simuler le rejet des radionucléides dans l'atmosphère, en dynamique des fluides, en aérodynamique et en mécanique des milieux continus comme modèle pour la formation d'ondes de choc, l'étude des solitons, de la turbulence, du comportement de la couche limite atmosphérique et le transport de masse. La plupart des techniques de la mécanique classique entre dans l'étude de systèmes conservatifs telle que la pollution atmosphérique causée par des effets naturels ou anthropiques et systématiquement modélisée par des équations différentielles d'ordre entier. Mais les processus observés dans le monde physique réel sont non-conservatifs. Dans une démarche méthodologique détaillée, dans le but de générer des solutions α-gaussiennes ou des solutions caractéristiques de la non-linéarité et des effets dispersifs des particules radioactives dans l'atmosphère d'après les profils des équations. Les systèmes d'équations fractionnaires sont utilisés afin de décrire la dynamique des phénomènes physico-chimiques liés à la pollution au niveau de la couche limite atmosphérique (CLA), et l'ordre fractionnaire est équivalent à ses dimensions fractionnaires. Nous nous referons à la topologie différentielle et géométrique de la dynamique des systèmes α-différentiels définissant la diffusion turbulente, justifiée par le comportement non-différentiable du phénomène et par la présence de la diffusion anormale pour construire une équation canonique généralisée dans un espace non-entier, et pour modéliser la dynamique de l'évolution des radionucléides dans un milieu dispersif. L'application physique la plus courante est la génération d'un mouvement brownien fractionnaire avec une structure à corrélation longue portée, caractéristique des mouvements des particules dans un environnement hétérogène et les marches aléatoires de particules en diffusion anormale. Nous retrouvons ainsi, des solutions généralisées sous forme d'expression de dérivée $\mathbb{N}$-tronquée, unifiant un ensemble de solutions à la fois classique et α-gaussiène. En outre, des solutions spatio-temporelles d'ondes solitaires fractales caractéristiques des particules radioactives en mouvement dans l'air. Les conséquences physiques sont discutées, en termes de convergence des solutions pour le nombre N de valeurs propres en utilisant un ensemble de données expérimentales dans des conditions météorologiques stables et instables. Ainsi, pour certaines valeurs, le paramètre α ou indice fractale ne modifie pas la valeur du pic de concentration, qui est l'un des aspects importants dans la pollution atmosphérique, mais il modifie sa position. Alors, l'ordre α peut être appliqué pour modifier la forme de l'onde solitaire sans altération de la non-linéarité et des effets de dispersion du milieu. Ainsi, ce travail démontre que le calcul fractionnaire est devenu un outil décisif dans la description du transport anormal.

Mots clés: Polluants radioactifs, Équations d'advection-dispersion fractionnaires, Équations fractionnaires non-linéaires évolutives.

Abstract

In this work, particular attention is paid to fractional calculus ubiquitous today in almost all fields of science, in nuclear physics to simulate the release of radionuclides into the atmosphere, in fluid dynamics, in aerodynamics and continuum mechanics as a model for the formation of shock waves, the study of solitons, turbulence, atmospheric boundary layer behaviour and mass transport. Most of the techniques of classical mechanics enter into the study of conservative systems such as air pollution caused by natural or anthropogenic effects and systematically modelled by integer order differential equations. But the processes observed in the real physical world are non-conservative. In a detailed methodological approach, with the aim of generating α-Gaussian solutions or solutions characteristic of the non-linearity and dispersive effects of radioactive particles in the atmosphere according to the profiles of the equations. Systems of fractional equations are used in order to describe the dynamics of pollution-related physico-chemical phenomena at the atmospheric boundary layer (CLA), and the fractional order is equivalent to its fractal dimensions. We refer to the differential and geometric topology of the dynamics of α-differentiable systems characterizing turbulent diffusion, justified by the non-differentiable behaviour of the phenomenon and by the presence of anomalous diffusion to construct a generalized canonical equation in a non-integer space, and to model the dynamics of radionuclide evolution in a dispersive medium. The most common physical application is the generation of fractional Brownian motion with a long-range correlation structure, characteristic of particle motions in a heterogeneous environment and random walks particle in anomalous diffusion. We thus find generalized solutions in the form of $\mathbb{N}$-truncated derivative expression, unifying a set of both classical and α-gaussian solutions. In addition, spatio-temporal solutions of fractal solitary waves characteristic of radioactive particles moving into the air. The physical consequences are discussed, in terms of convergence of solutions for the N number of eigenvalues using experimental dataset under stable and unstable meteorological conditions. Therefore, for some values, the parameter α or fractal index does not modify the value of the peak concentration, which is an important aspect in atmospherical pollution, but it modifies its position. Then, the α order can be applied to modify the shape of the solitary wave without altering the non-linearity and dispersive effects of the medium. In this wake, this work demonstrates that fractional calculus have come of age as a decisive tool in the description of anomalous transport.

Keywords: Radioactive pollutants, Fractional advection-dispersion equations, Fractional non-linear evolutive equations.

General Introduction

GENERAL INTRODUCTION

The concern for preserving air quality has increased considerably in recent decades, because excessive emission of pollutants into the atmosphere has heightened with industrial and technological development causing serious environmental damage and causing air to fall short of proper standards. One of the direct consequences of this change is the increasing of air contaminants and the growth in volume in greenhouse gases (GHGs) which contribute directly or indirectly to global warming [1]. Air pollution is caused by natural (e.g. emission of CO_2 by a volcano), anthropogenic (e.g. aerosol emissions) or artificial (e.g. industrial, biotechnology and electromagnetic emissions) effects which damage the ecological balance. To overcome this problem, physico-mathematical models are proposed in order to understand the phenomena that control the transport, dispersion and physico-chemical transformation of pollutants immersed in the atmosphere. We quoted a solid attention in analytical solutions of differential equations, in which some integro-differential operators, particularly fractional differential equations, have been widely explored to characterise many environmental transport phenomena. In the same vein, most of the non-linear evolution equations have been found in a wide range of physics phenomena such as evolution and interaction of non-linear waves, for example the description of the electromagnetic waves in size-quantized films, Alfvén waves in collision ion plasmas, interfacial waves in two-layer liquid systems. Thus, several methods have been attempted to solve fractional differential equations, we cite Laplace Transform Technique [2], Generalized Integral Laplace Transform Technique (GILTT), Fourier Transform Technique [3], Iteration Method [4] and Operational Method [5]. Most of these methods are suitable for special types of fractional differential equations with constant coefficients. However, exact solutions of non-linear evolutive equations are often given using techniques of non-linear analysis such as Fixed-point theorems, Adomian Decomposition Method, Variational Iteration Method [6, 7] and (G'/G, 1/G)-Expansion Method [8, 9].

Therefore, in order to regulate the concentration of pollutants in the atmosphere, two approaches are proposed in this study. The integer order dispersion method based on the

mass conservative properties of objects in the universe and the non-integer model built on the fractional order dispersion method. The main difference between the two models is at variance with traditional diffusion the mean square displacement increases linearly with time. In the contrast, the anomalous diffusion depicts the mean square displacement as not linear [10]. For instantaneous release of solute in the air, the solution given by the Advection Dispersion model (ADE) leads to gaussian spatial concentration distributions or fickian distributions, whereas observed concentrations display a long-tailed distribution or tailing behavior [11].

In the present work, the advection-diffusion equation is not solved as traditionally expressed, but is translated into a more objective mathematical structure in order to give a more realistic representation of the evolution in space and time of the concentration of pollutants dispersed in a turbulent flow environment. Thus, the use of fractional operators into the equation that governs the distribution of contaminants in the atmosphere. Also, are introduced some types of fractional derivatives such as Riemann-Liouville and Caputo derivatives[12, 13]. In Physics, the Reimann-Liouville fractional derivative depicts a long range-dependence or memory effects, and describes the solutes flow at any point affected by the solutes released from all upstream points where solutes may be stored transiently and released gradually. The delayed release of solutes produces an additional flow or concentration at the downstream point.

These realities above, nowadays, justify an excellent deal of attention devoted to application of fractional calculus to almost every field of science [14, 15, 16, 17], in nuclear physics to model fast spreading of radioactive pollutants [18, 19], in fluid dynamics, aerodynamics and continuum mechanics as a model for shock wave formation, solitons, turbulence, boundary layer behavior and mass transport [20]. The real world systems follow non-linear evolution patterns which describe for examplification the propagation of bounded particle of the atmosphere dust-acoustic solitary waves, internal solitary waves in shallow seas and ion acoustic waves in plasmas with negative ion [21, 22]. The classical mechanics techniques have been often used in studies of conservative systems, but most of the processes observed in the physical real world are non-conservative. Therefore, in many cases the real physical processes could be modeled in a realable manner using fractional differential equations rather than integer-order equations.

These considerations emphasize the problem of modeling radioactive (radioactive nuclide, radioisotope or radioactive isotope as an atom that has excess nuclear energy, making it unstable) pollutants including non-conservative and non-linear evolution parameters in non-integer space.

Fractional differential equations can be described best in discontinuous media, and the fractional order is equivalent to its fractional dimensions. Fractal media, which are complex,

appear in different fields of engineering and physics. In addition, this point of view is reinforced by the idea of M-fractional derivative type involving Mittag-Leffler function with α parameter that satisfies the properties of the integer calculation [23, 24]. The truncated M-fractional derivative unifies several types of existing fractional derivatives, also satisfies the product rule and the composition of two-differentiable functions. As diffusion characterizes one of the most fundamental transport process used in physico-chemical systems. Apart from normal diffusion, numerous physical phenomena can be explained through anomalous diffusion [25]. Under these hypothesis, the usual differential equations do not adequately describes the problem of turbulent diffusion. Current derivatives are not well defined in the non-differentiable behavior introduced by turbulence. Therefore, it is expected that traditional advection-diffusion equations do not fully explain the transport of pollutants according to the system parameters that often grow faster than the solutions obtained by conventional models.

The peculiarity of this work consist of obtaining the canonical form of Fractional Advection Dispersion Equations (FADE), keeping in mind that the dispersion model in non-integer space appears as a case of generalization of the solutions formerly obtained from the model of transport and dispersion, including both the gaussian model and the α-gaussian model that derived from the Mittag-Leffler function. Thus, the fractional calculus theory seems useful for modeling problems with fractal geometry in topological space. The most common physical application of fractional calculus is the generation of fractional brownian motion as a representation of acquifer material with a long range correlation structure [26, 27].

The interest of this study lies in its theoretical scope through the exploration of fractional models specific to the analysis of memory effects as a novelty in the dispersion of radionuclides in the atmosphere. The practical value of this study consists in the monitoring and evaluation of the evolution of radioactive pollutants cloud in the atmosphere in order to control its impact on human being and the environment.

This study is structured in three chapters. Chapter 1 reviews litterature on contaminants in the atmosphere. Special emphasis is placed on radioactive pollutants. Also, is examined the theoretical study of the dispersion versus mean square displacement in the Atmospheric Boundary Layer (ABL). Mathematical background of air pollutants modeling gives an overview of conventional models with their limit in order to undertake other models with evolutive solutions. In addition, is investigated the tremendous question of the nature of memory effects in atmospheric diffusion which render perceivable the cumulative effects of pollutants in the environment. Economic and legal aspects of atmospheric pollution are evoked in order to contribute to resilient our planet.

Chapter 2 describes the models and the methods for solving the advection-diffusion equation. we quote the statistical modeling approach that does not allow for detail the characteristics of turbulence and the deterministic approach relies on the formulation of physical mechanisms, chemical and digital resolution of equations, based on physics laws. In a nutshell, diffential topology and geometry of dynamic systems are explored for various dispersion models. Some techniques are used to generate solutions, as the N-truncated fractional derivative type equation versus WKB-approximation method. Special attention is devoted to fractional cases assuming non-linear evolutive solutions, in terms of observing the non-linearity and the dispersive effects of the milieu.

Chapter 3 focuses on the results and discussions. Then is discussed the integer-order versus the non-integer order of dispersion models considering linear and non-linear quadrature schemes. The convergence of the solution including comparison with the exact solution enable to foresight the evolution of the concentration in the Atmospheric Boundary Layer (ABL). The models are validated using datasets for Prairie Grass field experiment and Copenhague campaign. Statistical indices allow to appreciate the degre of correlation between observed and predicted field data. Besides, non-linear fractional partial differential equations direct the findings of exact solution concerning time-fractional evolution problems.

The study ends with a conclusion that opens up perspectives.

Chapter 1

Literature review on radioactive pollutants in the atmosphere

Literature review on radioactive pollutants in the atmosphere

1.1 Introduction

Dealing with information on pollutants or contaminants in air requires good definitional knowledge of the key concepts of air pollution and air quality. Also, sources and external effects processes influencing air quality can be determined by theoretical study of the dispersion versus mean square displacement in the atmospheric boundary layer. Thus, theoretical study of the power-law dynamics in the ABL reveals the impact of cumulative effects of pollutants in the environment. As consequence, the dynamic structure of the atmosphere and its assessment today is subject to an economic and legal framework. These assumptions are the basis for the mathematical modeling theory concerning air pollutants.

1.2 Definitions

1.2.1 Air pollutant

Air pollution characterises all destructive effects of any sources which contribute to the pollution of the atmosphere and/or deterioration of the ecosystem. Air pollution is caused by both human interventions and/or natural phenomena. It is made up of many kinds of pollutants including materials in solid, liquid, and gas phases [28]. In other words, air pollution is a mixture of natural and man-made substances in the air we breathe. It is typically separated into two categories: outdoor air pollution and indoor air pollution. Air pollution can also be defined as the emission of harmful substances to the atmosphere. This broad definition therefore encapsulates a number of pollutants, including : Gases, Fine particles, Noxious gases, greenhouse gases. Air pollution therefore results mainly from heating installations, thermal power stations and industrial plants, means of transport including motor vehicles (except electric) and agriculture.

1.2.2 Air quality

Air quality refers to the condition of the air within our surrounding. Good air quality pertains to the degree which the air is clean, clear and free from pollutants. Air quality is determined by assessing variety of pollution indicators, among them, Air Quality Index (AQI) or Air Pollution Index (API) commonly used to report the level of severity of air pollution to public exposure. Good air quality is a requirement for preserving the exquisite balance of life on earth for humans, plants, animals and natural ressources. As such, human health, plants, animals and natural ressources are threatened when pollution in the air reaches high concentrations. Epidemiological studies have demonstrated adverse health effects due to higher ambient levels of air pollution. These studies indicated that repeated exposures to ambient air pollutants over a prolonged period of time increases the risk of being susceptible to air borne diseases such as cardiovascular disease, respiratory disease, and lung cancer [29].

1.3 Air pollutants, sources and external effects

Air pollutants are divided into several categories. The effects on the environment are multifaceted.

1.3.1 Pollutants from primary sources

A primary pollutant is an air pollutant emitted from a source directly into the atmosphere. The source can be either a natural process or anthropogenic process influenced by humans. Pollutants are emitted from primary sources such as fossil fuel consumption, Volcanic eruption and factories. The major primary pollutants are Oxides of Sulphur, Oxides of Nitrogen, Oxides of Carbon, Particulate Matter, Methane, Ammonia, Chlorofluorocarbons, and Toxic metals.

1.3.2 Pollutants from secondary sources

A secondary pollutant is an air pollutant formed in the atmosphere as a result of the chemical or the physical interactions between the primary pollutants themselves or between the primary pollutants and other atmospheric components. Secondary pollutants are not emitted directly. Secondary pollutants appear after primary pollutants transformation in a chemical reaction. Secondary pollutants are found in photochemical oxidants and secondary particulate matter, such as : Ground Level Ozone, Smog and POPs (Persistent Organic Pollutants).

1.3.3 Fine particles

Fine particles and coarse particles are defined in terms of the modal structure of particle size distributions typically observed in the atmosphere. In a nutshell, suspended particles are all particles carried by water or air, quantifiable by filtration or other physical processes. Particulate matter or PM is the particles suspended in the Earth's atmosphere. The fractions of fine and coarse particles are collected in specific size ranges. Particulate matter (PM) is a term that refers collectively to various particles found in the air, including dust, dirt, soot, smoke, and liquid droplets. Particles can vary greatly in size, ranging from a diameter less than 0.1 microns smaller than a single bacterium to about 10 microns corresponding to 1/7 of the diameter of a human hair, hence PM10 is equivalent to 10 microns, small enough to be inhaled and accumulate. PM2.5 (fine particles) is equivalent to 2,5 microns, this size can go very deep into the lungs.

1.3.4 Ozone

. Ozone, or trioxygen, is a substance with chemical formula O_3 where its molecules are triatomic, formed with three atoms of oxygen. Ozone is thus an allotropic variety of oxygen, but much less stable than the oxygen O_2 , in which it naturally tends to decompose. Ozone can be created by a complex set of chemical and photochemical reactions that involve precursor compounds such as nitrogen oxides (NOx), volatile organic compounds (VOCs) or even methane (CH4). As such, it falls into the category of so-called "secondary" air pollutants; Ozone favor chemical processes, because it involve more or less long times during chemical reaction, can be developed in plumes capable of being transported over long distances. In many cases, for both ozone and other secondary pollutants (some particles), the highest levels of concentrations are far from the sources of precursor pollutants. In the stratosphere, ozone is an essential gas. The ozone layer acts as a ultraviolet (UV) filter, protecting the organisms from this harmful radiation of short wavelength. Ground-level ozone is both a pollutant and a greenhouse gas. It is indeed a very aggressive gas, it easily penetrates to the respiratory tract, causing coughing, pulmonary disorders or eye irritation.

1.3.5 Radioactive and electromagnetic pollutants

Radioactive pollution refers to the observed pollution of living organisms and their environment (atmosphere, hydrosphere, and lithosphere) as a result of release of radioactive substances into the environment during nuclear explosions and testing of nuclear weapons, nuclear

weapon production and decommissioning, mining of radioactive ores, handling and disposal of radioactive waste, and accidents at nuclear power plants [30]. Radiation is the emission of particle or energy in wave form. This is stated as electromagnetic radiation. Examples consist of: visible light, radio waves, microwaves, infrared and ultraviolet lights, X-rays, and gamma-rays. Radiation can be described as two basic types, ionizing and non-ionizing radiation. Radioactive contamination is just radioactive material somewhere it shouldn't be. Radioactive pollution occurs when there is presence or depositions of radioactive materials in the atmosphere or environment, especially where their presence is accidental and when it presents an environmental threat due to radioactive decay. The destruction caused by the radioactive materials is because of the emissions of hazardous ionizing radiation like beta or alpha particles, gamma rays or neurons, protons, heavy charged particles, X-ray and high energy quanta in the environment where they exist. Radioactivity is a phenomenon related to unstable atomic nuclei with excess of energy and/or mass, which spontaneously decompose emitting ionizing radiation in the form of electromagnetic waves (gamma rays) or streams of subatomic (alpha, beta, or neutron) particles [31].

Some radionuclides occur naturally in the environment, and their presence is either cosmogenic or terrestrial. ^{3}H, ^{7,10}Be, ^{14}C, ^{26}Al, and ^{39}Ar are the main radionuclides produced after the interaction of atmospheric gases with cosmic rays. Radioactivity in the air is essentially due to radon (^{222}Rn) in gaseous form, itself derived from uranium (^{238}U). (^{242}Pu) decays to (^{238}U) through alpha decay; will also desintegrate by spontaneous fission. Pollution through uranium depends on the richness of the uranium (^{238}U) in the soil, the porosity of the soil, the building materials and the dwelling air-conditioning which concentrates by confining the diffusion of the radon gas. This gas, as well as the products derived from it, can penetrate in the respiratory tract. The amount of radioactivity in the human body, of the order of 120 Bq / kg, can be induced by the ingestion of food containing radioactive elements. After ingestion, these radionuclides migrate into tissues and bones. Nevertheless, the average admitted values of radionuclides in the human body consist of 4 500 Bq potassium (^{40}K) and 3700 Bq carbon (^{14}C) [32]. Radioactive substance can penetrate into the body by inhalation, ingestion or dermal absorption. In addition, external gamma radiation can penetrate the skin and produce a dose up to the threshold that can affect tissues [33]. In the other side, non-ionizing radiation produces radioactive energy which limited the flux of charged ions when passing through matters inducing enough energy only for excitation. However, it causes biological effects. Thus, hazard depends on the ability to go through the human body and the absorption characteristics

of distinct tissues [34]. In fact, high-energy radiations cause radioactive pollution with serious health risk [35]. The direct consequences on the environment and on humans are the deterministic effects on human organs and air contamination. Common examples of sites pulverized by nuclear fire are Hiroshima and Nagasaki on 6 and 9 August 1945 respectively and Chernobyl in the Ukraine on 26 April 1986.

Human-being is often exposed to ionizing radiations from radioactive isotopes produced by sources such as atomic reactors, and nuclear power plants [36]. The more important health effects described as being caused by radioactive isotopes are blood abnormalities, skin changes, bone changes and so forth. There are three basic tools that can provide protection against radiation source: time, distance and shielding. However, the management of radioactive pollutants can be comforted by the treatment of radioactive waste, the mitigation of nuclear accidents, as well as the control of individual exposure to radiation. Apart from being an inevitable series of negative effects of radiations, it is the duty of humans with regard to Radiation Standards Organizations to help in reducing the harmful effects of this kind of pollution.

Radiation symbolises the term given to a travelling particle or wave and can be splited into three main types:

- Non-ionising radiation: essentially the low-energy parts of the electromagnetic spectrum. This includes all the light you see, radio waves also known as microwaves as in the oven and infrared like heat radiation. Ultra violet falls into the high energy end of this category;

- Ionising radiation: radiation that can remove an electron from its orbital;

- Neutrons: free neutron particles that can collide with other atoms.

Ionising radiation falls into two main particular groups, high-energy electromagnetic radiation including X-ray, gamma rays and alpha and beta particles. These different groups of ionising radiation differ in their capacity to damage and their ability to penetrate materials. Alpha particles, with two neutrons and two protons, are essentially helium ions. These can strip the electrons from another atom in order to become helium atoms. Beta particles are simply free electrons that can be captured by atoms just like any other electron. The difference in terminology is usually that gamma rays come from nuclear decay, while X-rays come from electron orbitals.

Electromagnetic radiation symbolises a form of energy transport without material support. Diverse by the amount of energy that they transport and their possibilities of interactions with the material. Electromagnetic pollution originates from electromagnetic fields and

electromagnetic radiation. One of the oustanding effect concerns the electrical activity of biological cell membranes which can be altered when exposed to electromagnetic radiation, created during the period of ions current exchange as well as during fluctuation in ion concentration. Therefore, it was commonly observed that the electrical activity and oscillating behaviors of biological cells are greatly reduced due to electromagnetic radiation exposure [37].

1.4 Processes influencing air quality

Air pollution study focuses on measuring, monitoring and predicting the concentrations of major chemicals in the atmosphere. The concentrations of chemical species in the atmosphere are controlled by four types of processes (refer, Figure 1.1).
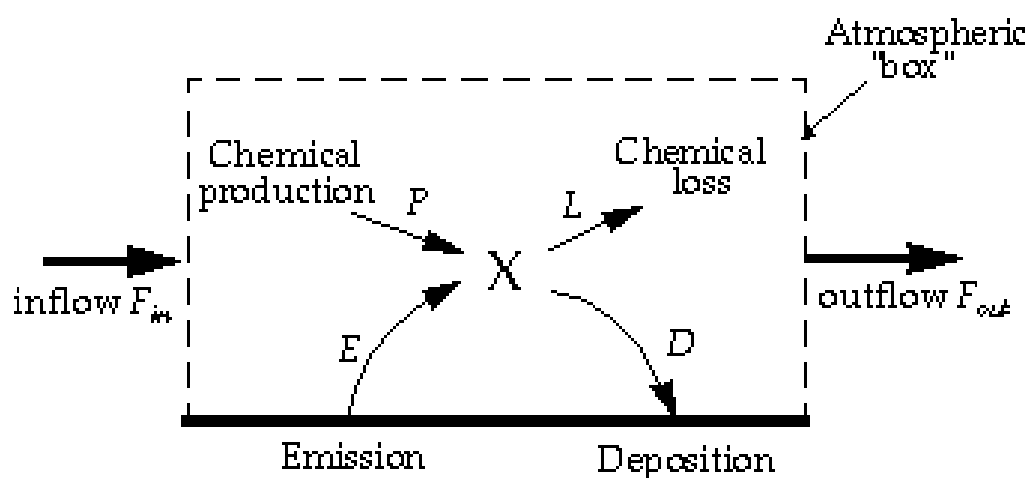
Figure 1.1: One-box model for an atmospheric species X [38].

1.4.1 Emissions

Chemicals are emitted into the atmosphere by a range of sources. Emissions are made up of a variety of solids (particles and aerosols), gases, conversion between gases and solids (and back again) such as fossil fuel combustion. Also, pollution originates from human activity and other mechanisms, such as natural functions of biological organisms. There exist various emission sources, as volcanoes, where gases come from non-biogenic natural processes. Emissions refer to air quality. Thus, the distinction between terms emission (Sources that emit pollutants into the atmosphere) and immission (Amount of polluting substance present in the atmosphere) [39]. Emissions emanate from fixe or mobile source. Emissions inventories are needed to track the evolution of air pollutants and precursors. In addition, air pollution simulation, enables to

assess the impact of pollutants in the environment. For example, emissions of pollutants that lead to ozone formation can be reduced substantially, but this is not reflected in the long-term trend in ozone concentrations.

1.4.2 Transport

The transport of atmospheric species occurs when the wind moves them from their point of origin far from their sources. The transport of inert and passive species can easily be conceived by the mechanisms of advection, diffusion and turbulent diffusion. Advection corresponds to transport of the species or pollutants through the fluid flow. Molecular scattering characterise transport mechanisms that happens at the microscopic scale. The Brownian motion of pollutant molecules leads to a macroscopic flow, oriented in the opposite direction to the concentration gradient (Fick diffusion law). But in practice, both effects coexist and interact. This interaction generally tends to strengthening the total spread of the cloud. Coupling effects can be observed in laminar flows but certainly within the turbulent flows. Most of the air pollutants and their subsequent transport and dispersion occur in the planetary boundary layer (PBL).

1.4.3 Chemical reactions

Chemical changes occur during the movement of pollutants in the atmosphere, they can induce the formation and removal of species. chemical agents can cause, altere or intervene by accelerating reactions. Pollutants observed in the atmosphere are not all emitted directly from their sources. They also result from physico-chemical reactions between chemical components, primary pollutants and other constituents of the atmosphere governed by weather conditions. Secondary pollutants are transported in the atmosphere, and according to their lifespan, interact with the clouds through photochemical or physico-chemical processes, and then end up, for example in a leaching process, by the rains. The knowledge of physico-chemicals reactions, allows us to understand the nature of dry and wet deposition, and concomitantly impacts on climate change and health.

1.4.4 Deposition

Materials thrown away in the atmosphere eventually turn back on the surface of the ground, because of the ground gravitational pull. Deposition behaves in two forms: *dry deposition* involving direct chemical reaction or absorption at the Earth's surface, such as the

uptake of CO_2 by photosynthesis; and *wet deposition* involves scavenging by precipitation and carriers to earth by rain, snow, or fog. During precipitation, two main processes contribute to wet deposition. Firstly, particles facilitate nuclei condensation for cloud drops which can then be converted to raindrops. On the other hand, Gaseous pollutants are captured by dissolution in the aqueous phase. Particulate pollutants are captured when the particle collides with a drop of cloud or rain. These processes take place in the cloud and are generally considered as constituting the *rain-out*. Air pollutants can be deposited on built surfaces, vegetation, soils and surface water by *dry* processes, that is, processes that do not depend on no precipitation. The fundamental processes that lead to dry deposition are the sedimentation, interception and diffusion.
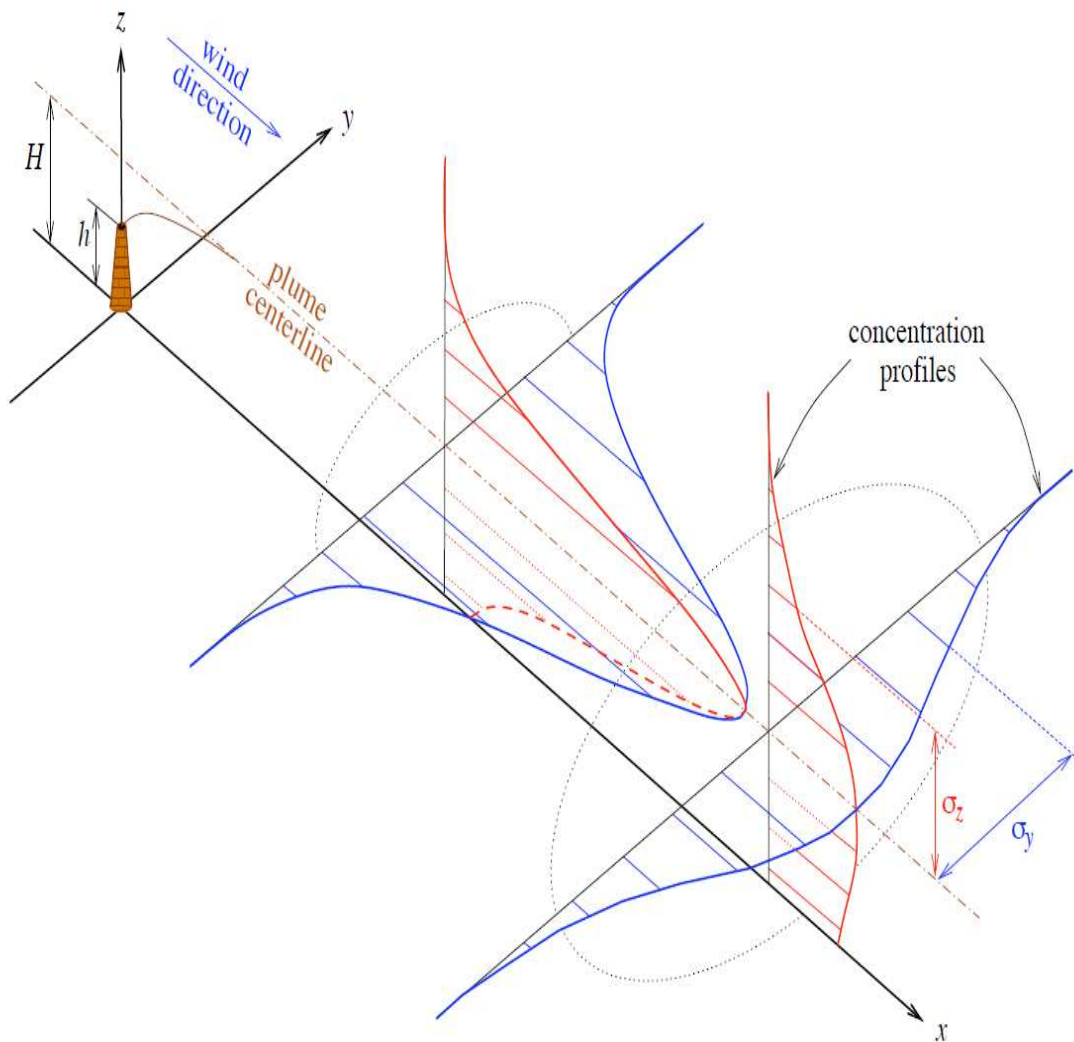
Figure 1.2: A contaminant plume emitted from a continuous point source, with wind direction oriented in the x-axis [40].

Specimen of the standard deviations (σ_i) and Eddy diffusivity coefficients (K_i) necessary for the implementation of the dispersion models reveal that the relevance of a model depends mainly on a correct estimation of the quantities (σ_i) and (K_i). In order to estimate the standard deviations, models allow atmospheric stability in various cases to be expressed as a function of meteorological data fields and the distance to the source [41] or the transfer time [42, 43].

1.5 Theoretical study of the structure and expansion of the Atmospheric Boundary Layer (ABL)

Atmospherical pollution appears at the level of the atmospheric boundary layer (ABL) and implies transformation into the structure and the evolution of the atmosphere.

1.5.1 Atmospheric structure

Atmosphere, corresponds to a mixture of gases and particles that envelops any celestial body: the earth for example, with gravitational field strong enough for preventing escape. Atmosphere is therefore air; the air we breathe considered as mixture of dry air and vapor water. Dry air itself characterizes mixture of several gases. Atmosphere layered structure largely depends on the temperature and energy. In the upper layers, atmosphere is heated by the solar radiation, whereas in the lower layers, it is rather the terrestrial radiation which heated so on and so forth. It is estimated to be about 500 km thick. Temperature variations in the earth's atmosphere are not regular. In some areas, it decreases and in others it increases. The troposphere extends from 0 to on average 12 km altitude. The temperature decreases with altitude. In this layer the main weather phenomena take place. The troposphere concentrates 90 per cent of the air contained in the atmosphere. The stratosphere extends on average from 12 to 50 km of altitude. The temperature increases regularly. The mesosphere extends on average from 50 to 80 km of altitude. Also, the temperature increases regularly. The thermosphere extends on average from 80 to 500 km. An additional layer called exosphere sometimes also included, allows the transition to interplanetary vacuum. This layer is still protected from particles emitted by the Sun than the earth's magnetic field [44].

1.5.2 Spatio-temporal scales in the ABL

ABL represents the part of the atmosphere that is directly influenced by the surface processes (like friction and the diurnal cycle of heating and cooling) and responds to this external forces of about a timescale less than a day [45]. The Atmosphere is characterized by phenomena which space and time scales cover a very wide range. The space scales of these features are determined by their typical size or wavelength, and the time scales by their typical lifetime or period. In time, we distinguish the fast phenomena, which evolve with a periodicity diurnal, which major phases are invariant in principle, but which amplitude will depend on the dynamic and thermal processes related to the studied site. In space, atmospheric phenomena are characterized by their horizontal extension (high and low pressures). The spatial scale can be subdivided according to scales of movements.

As a result, the velocity of the wind at a given point in space has large variations more or less irregular in terms of amplitudes and different frequencies. Large scale movements (synoptic scales) are larger than the hundred kilometers. These movements vary according to some periods: 1 year, due to seasonal variations; 4 days with variations associated with disturbances that cross a region given; and 24 hours, given daily variations, and thermal phenomena day Night. Small scale movements are smaller than a kilometer and have a duration of life of a few minutes maximum (micro-scales). They are related to turbulence and are generated in the atmospheric boundary layer by the presence of obstacles or by the soil roughness. At this scale, the turbulent airflow consists of a multitude of vortices of different sizes, carried away by the overall movement. Intermediate size movements (meso-scales) ensure the transition between precedents. Between small and meso-scales, we sometimes distinguish scales called submeso. The spatio-temporal structure makes use of the concepts of dynamics. It is therefore an estimation of the structure on a time scale, taking into account a given space whose boundaries, if they exist, are to be delimited. The term scale classically refers to the relationship between a dimension in reality and its transcription on the map, so there are different spatio-temporal scales: the global, regional and local scales. The support of a phenomenon, i.e. the portion of the axis of time or space where it occurs, is a geometric object whose fractal dimension can be estimated. By extension, the statistical properties of a multifractal field are defined by laws of scale.

As practical application, the scale of soil moisture uncertainty determines scales of PBL wind predictability when the atmosphere is resistant to upscale error transfer, but when the atmosphere is sensitive the scale and magnitude of soil moisture uncertainty are not important

after a few hours; and non-linear error growth is present whether or not the atmosphere is relatively sensitive to soil moisture uncertainty, leading to doubling times of minutes to hours for finite-sized perturbations.
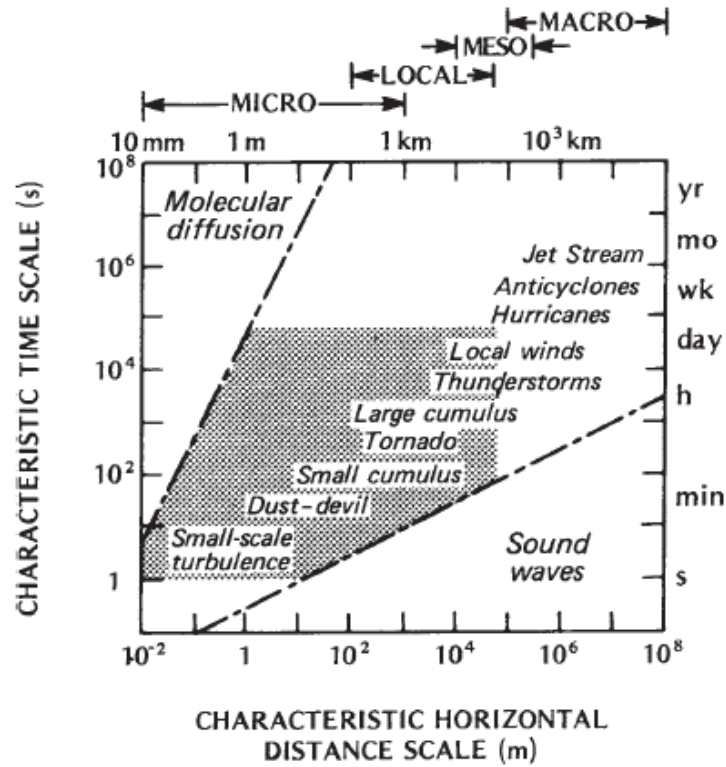
Figure 1.3: Time and space scales of various atmospheric phenomena. The shaded area represents the characteristic domain of ABL features (modified after Smagorinsky, 1974)[46].

At the same time, a spectral analysis makes it possible to find the scale of the fluctuations of the air flow.
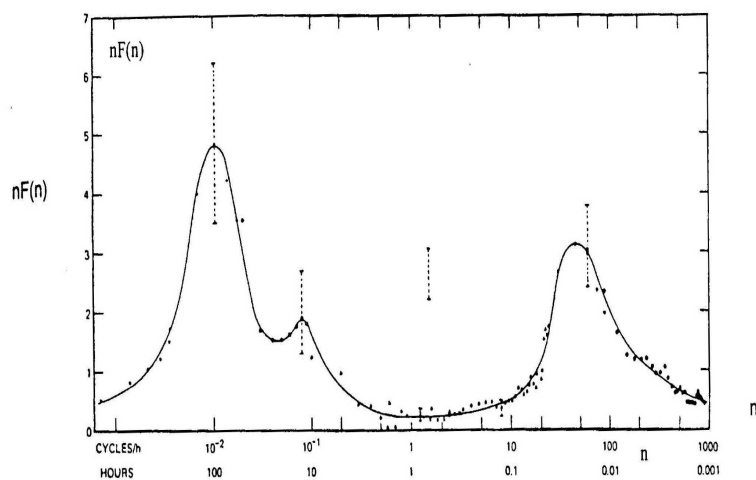
Figure 1.4: Energy spectrum of wind speed[47].

Spectrum peaks depict eddies actually participation in turbulent energy. We find the trends explained above with the peak relative to a period of approximately 100 hours reflecting the speed variations of the wind associated with successive cyclonic and anticyclone crossings; the peak over a period of about 12 hours reflecting the increase in speed wind in the day and its decrease during the night; the peak relative to a period of between 10 s and 10 min reflecting the turbulence of small scale. For the study of product dispersion, in the Atmospheric Boundary Layer (ABL), only the information concerning the structure of movements of small scales (micro-scales) are relevant. At this scale, the shape of the spectrum strongly depends on the thermal stratification of the atmosphere.

1.5.3   Structure and evolution of ABL

The Atmospheric Boundary Layer (ABL) represents the part of the troposphere that is influenced by the presence of soil in a turbulent regime. Its thickness varies from a few hundred meters to a few kilometers, depending on weather conditions, soil type and also meteorological conditions of the day (Figure 1.5). ABL is composed by the surface layer, in contact with the ground, where the turbulent flows of heat, momentum are considered uniform with the altitude, and the layer of mixture or layer of Eckman. The surface layer represents about one-tenth of the ABL. The upper part of the troposphere is non-turbulent because of its thermal stability and is called the free atmosphere.
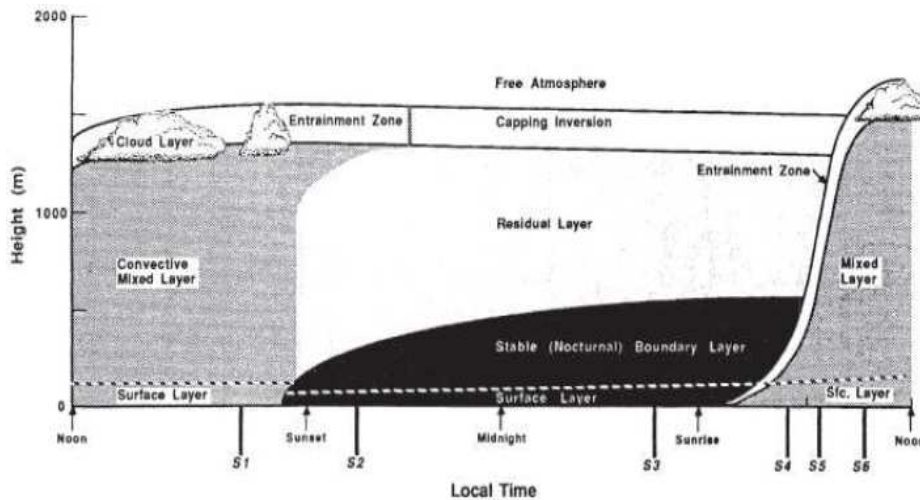
Figure 1.5: Variation in the state and structure of the ABL [48].

Wind transport within the ABL, or advection within the Atmospheric Boundary Layer, they are of the order of 1 to 10 m/s at 10 m altitude for the horizontal components, while the

vertical components rarely exceeds 1 cm/s. Because of the friction of the air on the ground, the wind profile adopts a logarithmic character, more or less disturbed by the thermal processes. Also, transport within the ABL or turbulence, turbulent structures, created mechanically or thermally, allow vertical transport. Their size varies from a few millimeters to 1 km structures.

1.6 Power-law dynamics in the ABL

The study of the power-law dynamics in the ABL displays the dynamics of normal and anomalous diffusion, coupling to the nature of memory effects in atmospheric diffusion. As consequence, a spotlight on physics of the particle movements: Brownian motion and diffusion.

1.6.1 Dynamics of normal and anomalous diffusion

In a homogeneous fluid at rest, concentration of a solute always tends to become uniform. Therefore, a diffusive flux with an uniform field of velocities must add the convective flow, proportional to the macroscopic speed and then concentration must be proportional to the opposite of the concentration gradient, i.e. Fick's law.

$$J_{diff,r} = -A\nabla\rho, \tag{1.1}$$

where A can behave differently, taking the characteristic D value of the molecular diffusion (m/s^2) or the value K which represents the turbulent diffusion (m/s^2). If we set an interval in time, we can also consider J as a measurement in space-time, which converges to a singular measure supported by the trajectory, with

$$\langle J, \varphi \rangle = \int_0^T m\varphi\left(R(t), t\right)dt. \tag{1.2}$$

We can, in certain manner, consider the evolution problem in space and time. The conservation equation including density $\rho(r,t)$ and the field $F = (\rho \times n, J)$ yields divergence null in space time:

$$\nabla_{t,r} \times F = \partial_t\rho + \nabla_r \times J = 0. \tag{1.3}$$

However, considering the time-variable ∇. still represents well the divergence versus the space-variable.

Let's consider substance that propagates according to the vector flow J. The time derivative of the quantity of substance N_ε contained in the immobile sub-domain equals the instantaneous

balance of flows across the frontier. Thus, we end up with the conservation equation in its mathematical formulation:

$$\frac{dN_\varepsilon}{dt} = \frac{d}{dt}\int_\varepsilon \rho\,(r,t)\,dr = -\int_{\partial\varepsilon} J \times n = -\int_\varepsilon \nabla.J. \tag{1.4}$$

This identity being verified for all ε, thus the following equation

$$\frac{d\rho}{dt} + \nabla.J = 0. \tag{1.5}$$

This model can be used to integrate source terms, by considering quantity S of material injected per unit of time and per unit of volume. The instantaneous assessment of material on a volume ε is then written

$$\frac{d}{dt}\int_\varepsilon \rho = -\int_{\partial\varepsilon} J \times n + \int_\varepsilon S. \tag{1.6}$$

At the moment, transport and diffusion phenomena coexist, the flow vector that characterize transport-diffusion, or advection-diffusion can be decomposed into two components

$$J = J_u + J_D, \tag{1.7}$$

then, the derivation of transport master equation:

$$\frac{\partial\rho}{\partial t} + \nabla.(u\rho) = \nabla.A\nabla\rho + S. \tag{1.8}$$

Nevertheless, Fick law admits the same origin as the Brownian movement [49]. The Brownian motion, successively described as cylindrical gaussian measurement, as process with independent increments and stationary, like martingale, as Markov process, finally as model of one-dimensional continuous diffusion. The Brownian movements are often observed on particles in suspension in homogeneous fluid at rest [50]. The similarity enables to consider the normal diffusion in the medium. To go fast, this happens when the consequences of Fick's law are observed, i.e. when the concentration evolves according to the diffusion-advection equation. The simplest way to check the normal diffusion consists in determining the variance (v) of the solute particle positions and to check that evolves while remaining proportional in time. Especially, one observes deviations from the linear time dependence of the mean squared displacement,

$$\left\langle x^2\,(t) \right\rangle \sim A_1 t. \tag{1.9}$$

In various domains or circumstances, different behaviors are observed similar to anomalous diffusion. Anomalous diffusion is found in a wide range of systems, its hallmark being the non-linear growth of the mean squared displacement in the course of time.

$$\left\langle x^2\left(t\right)\right\rangle \sim A_m t^m. \tag{1.10}$$

Anormalous diffusion has been known since 1926 [51]. In particular, this theoretical study was initiated in the description of the dispersive transport in amorphous semiconductors [52]. There are several models of anomalous dispersion: the anomalous diffusion approach highlighting random walk in continuous time (CTRW) gives an over-view of the Brownian movement and provided explanations for a lot of physical magnitudes and phenomena in many experimental fields[53]; Anormalous diffusion with or without velocity field or external force field used to magnified Mandelbrot fractional Brownian movement [54]; Alternative approach of anomalous scattering broadly invoked in fractional differential equations seems well suited to account memory effects observed in numerous complex systems.
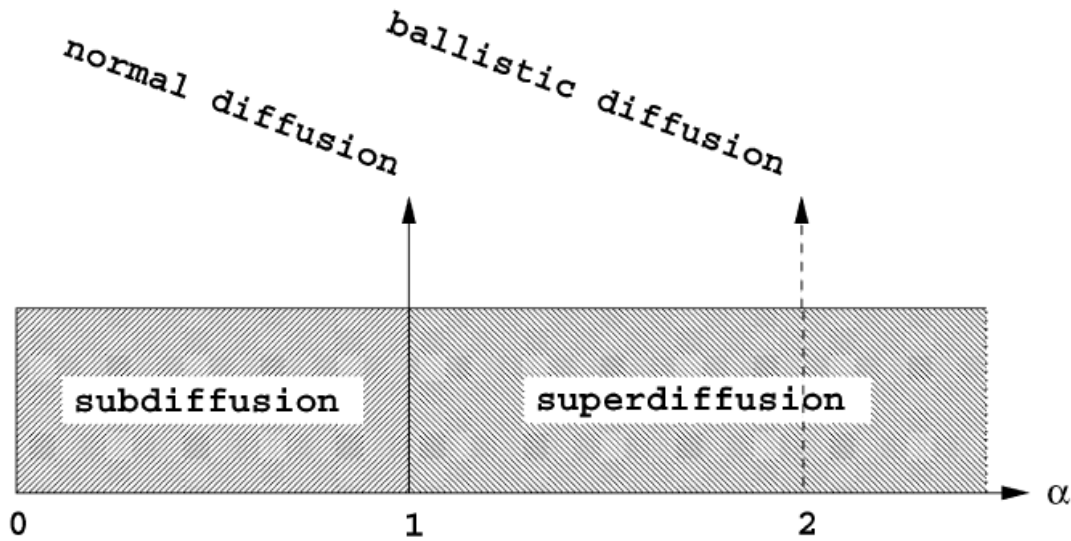
Figure 1.6: Different domains of anomalous diffusion, defined through the mean squared displacement, parametrised by the anomalous diffusion exponent α: (a) subdiffusion for $0 < \alpha < 1$, (b) superdiffusion for $\alpha > 1$. On the threshold between sub and superdiffusion is the normal Brownian diffusion located. Another special case is ballistic motion ($\alpha = 2$) [55].

1.6.2 Nature of memory effects in atmospheric diffusion

In porous media, various observations, made in laboratory columns or in natural environments, show that the transport of mass does not systematically obey Fick's law or Fourier's

law in other words the law of normal dispersion [56]. For example, the medium is able to retain abnormally for long time a fraction of the solute. If this interpretation is correct, the medium keeps a certain memory, and to describe what is going on is needed to go out of the framework of classical models of diffusion based on markovian properties in a small scale. In some porous media, particles appear as trapped by the solid matrix. These particles can be released or not at later times late enough to modify the regime in concentration decay of dispersed mass. This scenario can be referred to the memory effect term [57, 58, 59]. For exemple, the generalized Langevin equation [60], takes into account the system memory in porous media. The disadvantage of the CTRW [61] consists in the way no easy to integrate force fields outside the boundary conditions. But, anomalous diffusion is well symbolised by fractional differential equations that take into account memory effects [62, 63].

The fractional order derivation definition is based on the fractional order integration. Fractional order derivative of a function requires the knowledge of $f(r)$ over the entire interval $]a, r[$, while in the whole case, only the local knowledge of f around r is necessary. This property allows to interpret fractional order systems as long-memory systems, whole systems are then interpretable as short memory systems. Generally, Markovian dynamics occurs when the interaction between system and environment is sufficiently weak and the environment correlations are short-living [64]. Non-Markovian open quantum systems, on the contrary, display memory effects which manifest themselves as information backflow and/or partial return of previously lost quantum properties [65]. The modern approach to non-Markovian dynamics focuses on the physical characterization of memory effects and describes them in terms of a partial, and generally temporary, recovery of previously lost information. A convincing example of the impact of the memory effect on the environment, is the influence of ozone on the ecosystem. Ozone is often considered to play a predominant role in novel forest decline. Ozone has also been supposed to damage conifers through memory effects (*abiotic* pathway) or through predisposition for pathogen attack (*biotic* pathway) [66]. Ozone can induce a variety of normally regulated plant defense reactions. Herbaceous plants such as soybean [67], tobacco [68], parsley [69], and many additional species usually display a close coupling of biochemical responses and visible damage [70]. Absence of this close linkage and the presence of an ozone memory appear to be special properties of conifers [71]. The healthy plant is thereby converted to a distinct metabolic state that may lead to later visible symptoms. Recent literature has emphasized the idea of a cumulative or lifetime dose [72, 73]. In a nutshell, biochemical responses are visible in an early phase of near-ambient ozone exposure. Visible symptoms as well as physiological

effects as such as pigment loss, decreased photosynthesis.

1.6.3 Physics of the particle movements: Brownian motion and diffusion

Brownian motion corresponds to the stochastic motion of particles induced by random collisions with molecules, then becomes relevant only under certain conditions [74, 75]. The molecular disorder that accompanies the transport and diffusion movement of air pollutants intervenes during diffusion of chemical species in the atmosphere. Thus, wet deposit characterized by precipitation, whether in the usual form of rain, or more anecdotal snow and graupels, that is to say the transfer of pollutants from the atmosphere to leached surfaces. This leaching is generally done by two distinct mechanisms: the *in-cloud* and the *below-cloud.* These two anglicisms refer respectively to the mechanisms of condensation and capture that taking place in the cloud or so-called in-cloud around the particles and to the mechanisms of Brownian diffusion due to impact of inertia and interception that taking place under the cloud or so-called below-cloud of drops of rain or snow colliding with the particles. Under the cloud, the particles can be collected by a drop of rain falling due to Brownian diffusion. Some particles have a probability of coming into contact with falling raindrops.

However, the Brownian efficiency decreases sharply with the size of the particles, this mechanism is especially effective for small particle sizes ($< 0.1\,\mu m$) [76]. Dry deposition points-out pollutants transfert from the atmosphere to surfaces by other means than precipitation. Several factors governed by dry deposition include turbulence, the chemical properties of the species, the nature of the surfaces and landscapes encountered. Turbulence, particularly near of surfaces, controls the rate of pollutants deposited. Dry deposition processes, usually is observed through three operating mechanisms: aerodynamic transport into the quasi-laminar thin layer of the atmosphere, Brownian diffusion into the thin layer of the atmosphere and absorption on the surface. Transport into the thin layer is essentially done by turbulent diffusion. Near obstacles as buildings or vegetation, the thin layer of the order of a millimeter is considered as stationary and named *quasi-laminar* layer, within this layer, Brownian diffusion, sedimentation, inertia and impaction processes occur and are more or less effective depending on particle sizes. Finally, while the particles are in contact with the surface, gaseous pollutants can be deposited by adsorption or absorption in the surface.

In general, pollutants can be released into the atmosphere in several ways. For example, radionuclides may be released during normal operation or accidentally. In situations of chronic or accidental release of pollutants into the atmosphere, their dispersion is governed by their

physical properties and those of the atmosphere into which they are released [77]. The effluent enters the atmosphere with a velocity and temperature that are generally different from those of the ambient air, and thus causes a thermokinetic rise in the plume. This rise changes the effective height of the release point and leads to a change in the impact of the pollutants on the ground. The presence of obstacles of different heights also influences the path of the effluent. Following their emission into the atmosphere, radioactive gases or aerosols can be subjected to processes such as: aerosol formation or coagulation; radioactive decay; dry deposition (Brownian diffusion, interception, inertial impaction, gravitational sedimentation...); wet deposition by precipitation (Brownian diffusion, interception, inertial impaction, turbulent diffusion, phoretic effects, electrostatic effects...); resuspension. In the process of direct discharges to the atmosphere, the emission of a pollutant into the atmosphere can be chronic, with emissions into the atmosphere more or less continuous or periodic in time. These releases are related to the normal operation of nuclear power generation facilities or nuclear fuel cycle. The emission of a pollutant into the atmosphere can also be accidental, with one-off and unplanned emissions into the atmosphere. Almost all radionuclides chronically released into the atmosphere are mainly emitted in gaseous form. Nuclear power plants release mainly tritium (^{3}H) and carbon 14 (^{14}C) into the atmosphere. For exemple, the AREVA La Hague spent fuel reprocessing plant releases krypton 85 (^{85}Kr), ^{3}H, ^{14}C and iodine 129 (^{129}I) [78]. Military nuclear centres mainly release ^{3}H. Aerosol emissions are very low and mainly concern the upstream part of the fuel cycle with emissions of uranium 238 (^{238}U) or its descendants [79].

The radionuclides emitted into the atmosphere by a nuclear installation in an accidental release situation can be very varied. In the case of a severe accident in a PWR type nuclear reactor (pressurised water reactor), the main radionuclides released into the atmosphere would be ^{133}Xe and ^{131}I in gaseous form, and ^{90}Sr, ^{137}Cs and ^{131}I in aerosol form. Accidents such as those at Chernobyl and Fukushima injected large numbers of radionuclides into the atmosphere in the form of gases and aerosols. In addition, during the explosion at the Chernobyl power plant, radionuclides such as ^{238}Pu and ^{239}Pu were released into the atmosphere, but in smaller quantities. During a severe accident in a 900 MWe pressurised water reactor, the aerosols emitted in the containment, some of which could be released into the environment, would have a particle size of between a hundred nanometres and ten micrometres [81].

A particular case of releases is to liquids followed by transfer between water and the atmosphere. The oceans, seas, estuaries and rivers constitute a vast sink for many anthropogenic substances. At the water-atmosphere interface, pollutants from the atmosphere are concen-

Table 1.1: Period of the main nuclides emitted or likely to be emitted into the atmosphere and fraction emitted in the event of core meltdown [80].

Radionuclides	period	Fraction emitted in the event of a core meltdown
^{3}H	12 Years	-
^{14}C	5 730 Years	-
^{131}I	8,1 Days	1
^{129}I	$1,6.10^{7}$ Years	1
^{133}Xe	5,2 Days	1
^{85}Kr	10,4 Years	1
^{137}Cs	30 Years	1
^{90}Sr	28 Years	0,1
^{238}U	$4,5\ 10^{9}$ Years	0,001
^{238}Pu	87,7 Years	0,001
^{239}Pu	$2,4\ 10^{4}$ Years	0,001

trated, either directly discharged into the water or desorbed from the sediments; there is an enrichment in stable metals [82] and radionuclides [83]. Similarly, the reappearance towards the continent of artificial radionuclides discharged into the sea, thanks to transport by marine aerosols, is observed by measuring the activity of artificial radionuclides (Caesium ^{137}Cs, Plutonium ^{239}Pu, ^{240}Pu, and Ruthenium ^{106}Ru) in terrestrial bioindicators [84]. Simultaneously with the transfer by marine particles, the outgassing of carbon dioxide (CO_2) can lead to the release of liquid carbon 14 (^{14}C) from the nuclear industry to the atmosphere [85]. The transfer of ^{14}C depends on the physical parameters of the environment but also on biological factors such as photosynthesis, respiration or the degradation of organic matter [86]. The transfer of ^{3}H is mainly influenced by temperature differences between water and air and by wind speed. Analysis of the description of the dry and wet deposition processes of aerosols during dispersion in the atmosphere shows that the plume is depleted of its gaseous and particulate constituents by interaction with surfaces, such as buildings, plants and soil. A gaseous radioactive compound such as carbon-14 ($^{14}CO_2$) emitted into the atmosphere is incorporated into living matrices by the process of photosynthesis, whereas an aerosol is deposited by Brownian diffusion, interception, impaction or sedimentation depending on its size [87].

In reality, in the case of chronic or accidental releases, all the constituents in the form of particles follow the dispersion of the plume, except for particles with diameters greater than

100 ţm for which gravitational sedimentation is important. The particles may also react with the atmospheric aerosol and be transported over long distances. From the above, it follows that atmospheric radioactivity can be of natural origin, such as the release of radon and thoron gas from soil and rocks, or anthropogenic, such as atmospheric military tests or chronic or accidental releases. The fate of atmospheric radioactivity is closely linked to aerosol dynamics. Indeed, natural radionuclides, such as radon and thoron, are emitted in gaseous form and rapidly settle on the atmospheric aerosol. In the case of the Chernobyl accidental release, radionuclides such as caesium (134 or 137), iodine 131 or ruthenium 103, which are volatile when emitted, were preferentially fixed on the atmospheric aerosol and were transported on a continental scale by particles of the accumulation domain [88].

Radioactive particulate pollutants are therefore mainly governed by the same dynamics as atmospheric aerosol. Because of their simplicity of use and speed of calculation, Gaussian models are perfectly suited to the prediction of radioactive atmospheric releases in normal or accidental operating situations. The Gaussian model is a simplified solution of the transport-diffusion equation which describes the spatial evolution of the concentration of a pollutant in the case of a release at a constant flow rate and under homogeneous meteorological conditions. The use of the Gaussian model requires the determination of standard deviations of dispersion. For the so-called first generation Gaussian models, such as the models of Pasquill (1961), Briggs (1985) and Doury (1981), the standard deviations of dispersion have been established from experimental campaigns and are valid under the experimental conditions under which they were determined, mainly from ground releases and on flat or slightly hilly terrain [89].

New-generation Gaussian models, such as ADMS 4.0 developed by CERC (2009), make it possible to determine the dispersion of industrial discharges in the atmosphere according to the characteristics of the atmospheric boundary layer and the characteristics of the site: buildings, relief. Indeed, dispersion characterization campaigns carried out around the world very rarely include measurements of vertical concentration profiles, which are nevertheless very useful for testing models. In addition to integrating the parameters stated by these previous models, the present models developed in this work take into account the memory effects in the dynamics of the propagation of radioactive pollutants.

The main radionuclides emitted or likely to be emitted as gases by the nuclear industry and not chemically inert are tritium (HTO), carbon-14 ($^{14}CO_2$) and iodine (^{129}I, ^{131}I). For all of these radionuclides, there are disagreements between operational model results and environmental measurements. To evaluate the transfers of ^3H and ^{14}C within an ecosystem, the operational

models assume a constant isotopic balance between air and plants. For this type of radionuclide, it should be considered that HTO and ($^{14}CO_2$) mainly follow the water and carbon cycles. Concerning iodine, the 131 isotope of which is harmful to humans because it binds to the thyroid gland, there are still uncertainties about the chemical forms likely to be emitted into the environment during a serious accident in a nuclear reactor.

Nevertheless, if we consider the most reactive chemical form, I_2, and the least reactive, ICH_3, the dry deposition rates and the drawdown coefficients, which are taken as constant in impact calculation models, need to be better quantified according to the environmental parameters. For all of these gases, in situ studies can be carried out using releases from the nuclear industries (^3H, ^{14}C) or stable tracers. From the installations to the environment, the behaviour of aerosols results from the interaction between the properties of the aerosols, the fluid that transports them and the environment in which they evolve. Despite the diversity of these three components, there is a common behaviour of aerosols linked to the physical domains (molecular, continuous, intermediate) characteristic of their dimensions. When radioactive substances are handled, fine solid or liquid particles formed from these substances are frequently suspended in the air: these are called radioactive aerosols. The measurement of alpha radioactive gases, such as radon [90], have clearly shown the formation of large radioactive clusters from radon. An atmospheric aerosol refers to, a suspension, in a gaseous medium, of solid or liquid particles with a negligible falling speed. Atmospheric aerosols are distinguished from hydrometeors, which represent all forms of solid or liquid water present in the atmosphere, excluding clouds, by their speed of fall: hydrometeors have a faster speed of fall than aerosols, which therefore remain suspended in the air for longer.
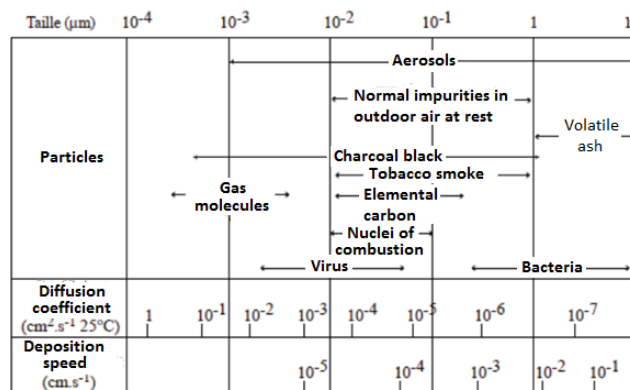
Figure 1.7: physical characterisation of aerosols [91].

Different types of aerosols are characterised by their size, number, volume or mass. The commonly used representation is a particle size distribution representation in the form of log-

normal curves in number (N) or mass. At least three modes are generally distinguished in this type of representation: a coarse mode representing aerosols with a diameter (Dp) greater than or equal to 1 μm, produced mainly by mechanical processes (lifting of desert, volcanic or industrial dust or sea spray by the wind) and eliminated essentially by sedimentation; a so-called accumulation mode representing aerosols with a diameter of between 0.1 and 1 μm, produced by coagulation and condensation from the fine mode and eliminated by leaching or dry deposition; a fine nucleation mode representing aerosols with a diameter of less than 0.1 μm, formed in part by gas-particle conversion (nucleation): Aitken mode. Their number density leads them to coagulate and condense to evolve towards the accumulation mode. The fine and accumulation modes are grouped together in the category of fine particles, whereas the coarse mode corresponds to supermicron coarse particles. The different categories commonly studied in atmospheric chemistry in relation to the study of air quality are particles with an aerodynamic diameter of less than 10 ţm (called PM10), particles with an aerodynamic diameter of less than 2.5 ţm (called PM2.5), particles with an aerodynamic diameter of less than 1 ţm (called PM1).
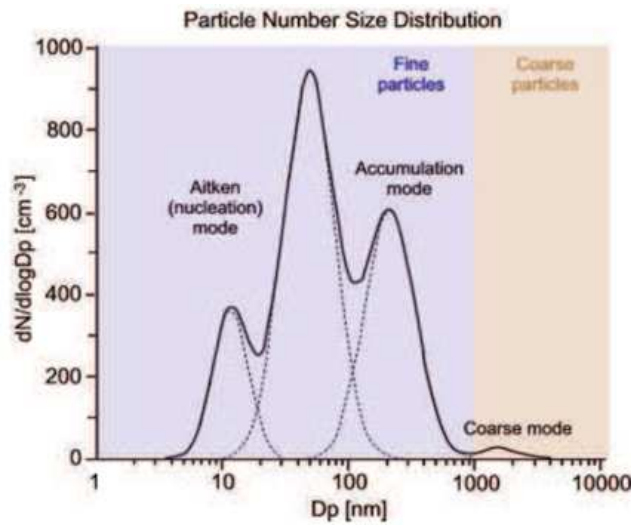
Figure 1.8: particle number distribution as a function of diameter [92].

As an example, the Lagrangian model calculates the trajectories of the particles in the turbulent flow simulated by the dynamic model. The displacement of the particles is a function of the velocity of the flow,

$$U_i = \frac{dx_i}{dt}, \tag{1.11}$$

where U_i are the components of the flow velocity, x_i the particle coordinates, and t the time. This model allows to well define the dispersion of primary pollutants in complex topography.

1.7   Cumulative effects of pollutants in the environment

Exposure to pollutant means the amount of pollutants in contact with the individual or population over time [93]. Many people and communities are located near multiple sources of pollution, including current and former industrial sites, major roads, and farms. They are burdened by higher levels of pollution and more social stressors than others. When facilities and other emission-generating projects or rules are proposed that might affect pollution levels in an area, communities want to know what the cumulative impact might be on their health of the action along with the other stressors in their community. There are existing approaches for characterizing cumulative exposures, cumulative risks, and cumulative health impacts. Among them, we mention the deterministic and stochastic components of environmental change.

1.7.1   Stochastic effects of air pollutants

Carcinogenic chemicals and ionizing radiation whose toxic effects are without threshold are called stochastic. Indeed, we consider the probability that single molecule or particle entering biological tissues is the origin of a cell line cancerous. Radiation protection studies are based on the assumption of no limit value exposure. The threshold of preventive exposure is established according to the criteria of absence of short-term effects and a reduction in the appearance of long-term effects. Exposure to ionizing radiation has effects on health. These effects are called stochastic, let us mention the cancers, whose probability of appearance is considered proportional to the dose received, including for low doses [94]. The stochastic effect is an integral part of the two concepts in the field of radiation protection from exposure. Stochastic effects are those whose frequency, but not severity, is function of exposure. Cancers, for example, are a prototype. Because of the uncertainty associated with the behaviour of these substances on cells at low doses and our ability to define a threshold for the appearance of the effect. It is assumed that there is no threshold for these effects and that at any dose, however small, there is a risk; at least this assumption cannot be rejected for cancers induced by ionizing radiations. Most chemicals causes cancer. Substances known to cause cancer are called carcinogens. Benzene, asbestos, vinyl chloride, radon, and arsenic are examples of toxic substances that can increase the risk of cancer to those who are exposed. Cancer is caused by changes to certain genes that alter the way our cells function. Some of these genetic changes occur naturally when DNA is replicated during the process of cell division. But others are the result of environmental exposures that damage DNA. These exposures may include substances,

such as the chemicals in tobacco smoke, or radiation, such as ultraviolet rays from the sun. Many chemical carcinogens are in food, water, air, household products, and personal care products. Although genetic susceptibility is an important factor in how an individual responds to exposure to a carcinogen, heritable genetic factors alone account for only a minor portion of cancer rates.

1.7.2　Deterministic effects of air pollutants

Intensity, duration, frequency of exposure and the nature of the pollutant are related to biological effects and health effects. Mostly, the toxic effects of chemical components depend on the effective biological or equivalent dose. There is a threshold where exposure to these components leads to irreversible effects when the mechanisms of detoxification, repair and compensation of the organism are out of date. Moreover, exposure to ionizing radiation raises the question of its potential impact on the living organisms.

Pollutants exposure refers to integral part of essential steps in the assessment of environmental risk. The toxicity and pathogenicity of a contaminant also depends on its route of penetration, as well as its rate of transfer into the human body. In the case of chemical pollutants, that is organic and inorganic pollutants, the characteristics of their molecular structure define their physico-chemical properties and especially their pharmacokinetic and toxicokinetic features. During radioactive exposure, the emission of alpha particle is more dangerous after absorption by inhalation or ingestion, only by contact due to its low penetrating power [95]. Other routes of transfer may be considered as the trans-placental route, the pathway percutaneous, and the transcutaneous pathway that can cause the passage of biological contaminants by autoinoculation. Exposed populations do not have the same degree of sensitivity to pollutants and exposure. It depends on the age, the sex, the individual characters physiological, immunological, pathological. To sum up, deterministic effects are those severity depends on the level of exposition. This type of effect also has the characteristic of occurring at a relatively high dose and presenting an action threshold. With the development of industrialization and urbanization, heavy metals contamination has become a major environmental problem. The mechanisms of heavy metals (lead, cadmium, mercury, chromium, and arsenic) contamination can lead to gastric cancer. Heavy metal exposure damages the development of the nervous, hematological, and cardiovascular systems and increases the risk of numerous cancers including kidney, lung, liver, skin, and gastric cancer [96]. We simply cannot escape our exposure to man-made chemicals. But there is a lot we can do to moderate our exposures. For the most

part, it is up to us to become more conscious about the chemicals we are exposed to in the air we breathe, the water we drink, the furniture in our homes, the clothes we wear, and the products we put on our bodies every day. Deterministic effects are dose-related, acute health effects caused by exposure to high levels of radiation that cause large numbers of cells to die or lose their ability to replicate. Organs containing these cells then fail to function correctly. The severity of the effect depends on the level of exposure above its threshold.

In fact,there are some factors that increase the risk of developing cancer exposure to chemicals. Scientists know very little about how contact with most chemicals causes cancer. Coming into contact with a carcinogen does not mean to get cancer. It depends on what, how often, and how much persons were exposed to, among other things. In the 18th century, it was noticed that a large number of chimney sweeps had cancer of the scrotum due to exposure to soot, which contains chemicals known as polycyclic aromatic hydrocarbons. Since then, many more chemicals have been identified as known or suspected causes of cancer. Nowadays, much of what we know about chemicals causing cancer in humans, have been learned from humans exposition. Exposure to chemicals in the outdoors, at home, and at work may add to your chances of getting cancer. Certain chemicals, including benzene, beryllium, asbestos, vinyl chloride, and arsenic are known human carcinogens, meaning they have been found to cause cancer in humans. There are three types of carcinogens which exist : Chemicals that can cause cancer (direct acting carcinogens), Chemicals that do not cause cancer unless they are changed when they are metabolized (procarcinogens), and Chemicals that do not cause cancer by themselves but can act with another chemical to cause cancer (cocarcinogens). In the contrast, The associations between radiation exposure and cancer are mostly based on populations exposed to relatively high levels of ionizing radiation. Cancers associated with high dose exposure include leukemia, breast, bladder, colon, liver, lung, esophagus, ovarian, multiple myeloma, and stomach cancers.

Humans can be adversely affected by exposure to air pollutants in ambient air. In response, the European Union has developed an extensive body of legislation which establishes health based standards and objectives for a number of pollutants present in the air. These standards and objectives (covering a range of environmental values, including human health and wellbeing, protecting the health and biodiversity of ecosystems, protecting the aesthetics of the environment, and protecting agricultural use of the environment) are summarised in the table below. These apply over differing periods of time because the observed health impacts associated with the various contaminants occur over different exposure times.

Table 1.2: Air Quality Standards, Under Directive 2008/50/EU.

Pollutant	Concentration	Averaging period	Legal nature	Permitted exceedences each year
Fine particles (PM2.5)	25 μg/m3***	1 year	Target value to be met as of 1.1.2010	n/a
			Limit value to be met as of 1.1.2015	
Sulphur dioxide (SO2)	350 μg/m3	1 hour	Limit value to be met as of 1.1.2005	24
	125 μg/m3	24 hours	Limit value to be met as of 1.1.2005	3
Nitrogen dioxide (NO2)	200 μg/m3	1 hour	Limit value to be met as of 1.1.2010	18
	40μg/m3	1 year	Limit value to be met as of 1.1.2010 *	n/a
	50μg/m3	24 hours	Limit value to be met as of 1.1.2005 **	35
PM10	40μg/m3	1 year	Limit value to be met as of 1.1.2005 **	n/a
Lead (Pb)	0.5μg/m3	1 year	Limit value to be met as of 1.1.2005	n/a
			(or 1.1.2010 in the immediate vicinity	
			of specific,notified industrial sources;	
			and a 1.0 μg/m3 value applied	
			from 1.1.2005 to 31.12.2009)	
Carbon monoxide (CO)	10μg/m3	Maximum daily 8 hour mean	Limit value to be met as of 1.1.2005	n/a
Benzene	5μg/m3	1 year	Limit value to be met as of 1.1.2010**	n/a
Ozone	120 μg/m3	Maximum daily	Target value to be met as of 1.1.2010	25 days 8 hour mean averaged over 3 years
Arsenic (As)	6 ng/m3	1 year	Target value to be met as of 31.12.2012	n/a
Cadmium (Cd)	5 ng/m3	1 year	Target value to be met as of 31.12.2012	n/a
Nickel (Ni)	20 ng/m3	1 year	Target value to be met as of 31.12.2012	n/a
Polycyclic Aromatic Hydrocarbons	1 ng/m3 (expressed as concentration of Benzo(a)pyrene)	1 year	Target value to be met as of 31.12.2012	n/a

1.7.3   Economic and legal aspects of atmospheric pollution

Economic growth still overtakes the concern of environmental protection. Extraction of raw materials from natural resources is part of a transformation process where industries introduce both final products and pollution in the environment. The negative effects of industrial activity on the environment, which once were perceived exclusively as a local pollution problem, today are widely debated in public policy, aiming not only to preserve the environment, but also to mitigate and adapt to climate change. The impacts of air pollution in the economy include direct economic impacts as well as indirect economic impacts stemming from the human health and environmental effects of air pollution. There exist some emergency measures such as instituting a monitoring system for indoor and outdoor pollution in certain periods. Certain

instrument can also be used like safety standards that can be simply defined as a maximum level for some pollutant in the ambient environment. From a theoretical economic point of view, emission standards are set taking into account what economists define as efficient pollution levels. An efficient pollution level may be defined as the one that maximizes the net benefits of reduction [97]. Air pollution reductions have the potential to directly increase the productivity of the forestry, agriculture, fishing, and tourism industries by decreasing environmental damages suffered by these industries. Reducing air pollution may also lead to innovative new industries and economic spin-offs related to green technology. Industrials ought to specify particular types of technology that polluters must adopt in the production process and it appears necessary the implementation of monetary penalties to noncomplying sources. Also, is valuable the idea that in the presence of an externality such as air pollution, imposing a per unit tax on the emissions firms would internalize the externality. The tax rate would be equal to the marginal social damage caused by the last unit of pollution at the efficient allocation [98].

Environmental protection has a constitutional value. The French Constitution, through the Charter for the environment declares the constitutional value, Article 1 states that Everyone has a right to live in a balanced and healthy environment. Also, we can state the Berne Convention on the Conservation of European Wildlife and Natural Habitats 1979. And Law No 96 / 12 of 5 August 1996. Relating to environmental management in Cameroon. In this vein, Cameroon's initiative is prominent through the the Decree No 2009/410 establishing the creation, organization and functions of the National Observatory on Climate Change (ONACC) as a national legal implementing body of climate change policies, to serve as operational instrument for nature protection and sustainable development. Also, Decree No. 2005/0577/PM laying down rules for carrying out Environmental Impact Studies (EIS) and Order No. 0070/MINEP of 22/04/2005 fixing activities subject to the achievement of a EIS. NGO^s, associations or legal persons can also take action if they have a sufficient interest. But, there are restrictions on the application of environmental legislation. Including the burden of proof and compensation for the damage caused. The local regulations are not often observed.

1.8 Dynamic structure of the atmosphere

The dynamic structure of the atmosphere depends on the environmental features and the dispersion overall roughness.

1.8.1   Atmospheric stability: Monin Obukhov's length approach (LMO)

To model velocity, temperature and turbulence profiles in the Atmospheric Boundary Layer, Monin-Obukhov theory is often used. It extends the log-linear profile considering the conservation of the momentum under the neutral condition to stable and unstable. Monin-Obukhov lenght (L) [99], represents the criterion of stability recognized by meteorologists as appropriate for the characterisation of the Atmospheric Boundary Layer. It essentially depends on the heat flow and the speed of friction. Its interpretation will make it possible to determine the stratification of the terrestrial boundary layer. Indeed, the thickness of the atmospheric layer that is of interest in the pollution problem extends of the order of 500 to 1000 m.

Meteorologists divide the Atmospheric Boundary Layer into two zones: a surface layer where it is assumed that both frictional tension and heat flux are approximately constant as a function of height. The thickness of this layer is of the order of a few tenths of the thickness of the Atmospheric Boundary Layer; a so-called transition layer up to the upper limit of the Atmospheric Boundary Layer, the structure of the wind flow and the temperature field is still under the influence of frictional stresses and heat flux at the surface of the ground, but moreover the Coriolis force intervenes. However, our concern lies in the study and understanding of how the surface layer works. In the boundary layer surface, the vertical production of the kinematic turbulence decreases, and this faster than the vertical production of the turbulence by buoyancy. The altitude at which the buoyancy output term equals the kinematic output is a characteristic length scale for the surface boundary layer and corresponds to the Monin-Obukhov length and is noted L_{MO}. Therefore properties of the surface layer are well known, for example, in the case of neutral atmosphere, the vertical distribution of velocities obeys to the classical logarithmic laws.

$$\frac{U}{U_*} = \frac{1}{k}\log_e\frac{U_*z}{\nu} + Cte\,(\text{smooth ground}), \quad \frac{U}{U_*} = \frac{1}{k}\log_e\frac{z}{z_0} + Cte\ (\text{rough soil}). \quad (1.12)$$

with k : Karman constant ($k = 0.4$), U_* : speed of friction and z_0 : length characterizing the surface roughness.

In the case where the temperature gradient differs from the adiabatic temperature gradient, the formulas based on the theory of similarity of Monin and Obukhov are used frequently [100, 101], assuming that in the surface boundary layer the only scale of velocities is U_* and the only scale of lengths is:

$$L = -\frac{U_*^3 \rho C_\rho T}{gkq}, \tag{1.13}$$

with :

T : absolute average temperature in the surface boundary layer;

q : average heat flow in the vertical direction;

C_ρ : specific heat of air at constant pressure;

g : acceleration due to gravity;

ρ : density of the air.

L is infinite in the case of an adiabatic temperature gradient ($q = 0$), positive for a negative heat flux (stable athmosphere), negative for a positive heat flux (unstable atmosphere). The absolute value of the Obukhov length characterizes the height below which shear is the dominant degeneration process of turbulence. For a convective situation, the buoyancy and shear turbulence production terms are approximately equal for $z \sim$ - 0.5 |L|.

1.8.2 Influence of the environment on dispersion : overall roughness

Pollutants emitted are dispersed either by horizontal transport in the wind direction or mixing vertically by atmospheric turbulence due to the effects of the Atmospheric Boundary Layer [102]. Roughness acts directly where the structures are born and can potentially change their behavior significantly. The analysis of the effect of roughness in the boundary layer is also complicated by the fact that the geometry and scales of the rough elements vary a lot. The roughness of a surface not only increases the friction of the wall but it has a significant influence on the transport of momentum, mass and heat in the flow, such as dynamic effects, associated with wind shear, and thermal convective effects [103]. Physical characteristics of roughness, include the radioactive properties of the soil and the environmental aspects of the earth, the sea, the city, the countryside, but also the action of meteorological parameters such as temperature and wind surface, involve dynamic and thermal effects causing significant turbulence that favors the vertical exchange of energy and matter, thus allowing the dilution of pollutants [104]. Winds are not disturbed only by the immediately surrounding obstacles, the overall roughness of the grounds also exerts an influence. Any non-smooth surface corresponds actually to friction force for the wind. In other words, the roughness corresponds to the disturbance of the flows as a function of the micro-reliefs which represent more or less strong adhesion. The roughness length is the height above the ground z_o of the plane where the adhesion condition applies and where the average wind vector is equal to the null vector. It depends, for each direction, on the

homogeneity of the terrain, the type of obstacles and the distance which these two conditions apply.

Strong roughness significantly reduces the speed of the wind, so a forest or an urban landscape will slow much more the wind than a plain landscape. On the other hand, the surface of the sea with even lower roughness has very little influence on the flow of air. While long grass, bushes and shrubs slow down the wind considerably. In a nutshell, two terms are used when assessing the wind potential of a given location: The roughness class and the roughness length. The environment also influences the dispersion of pollutants in the atmosphere. A distinction is made between mechanical disturbances linked to the nature of the soil, the presence of obstacles or the topography and disturbances linked to strong soil discontinuities leading to thermal effects. The length of roughness, expressed in metres, characterises the overall influence of the rough sublayer (surface layer) on the wind profile. It is also referred to as the characteristic size of vortices at ground level. This roughness is correlated with the height of obstacles on the ground. The flow around a building or group of buildings is a very complex phenomenon. The presence of an obstacle significantly modifies the velocity field downstream and upstream of the obstacle. Urban form controls the overall aerodynamic roughness of a city, and hence plays a significant role in how air flow interacts with the urban landscape, reducing surface roughness in a city centre can increase ground-level pollutant concentrations, both locally in the area of reduced roughness and downwind of that area. The ventilation of a city is intricately linked with urban form because urban form controls the overall aerodynamic roughness of the area.
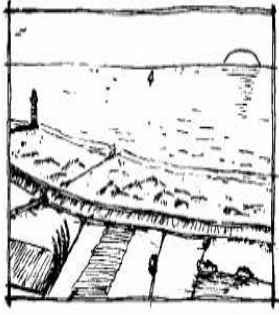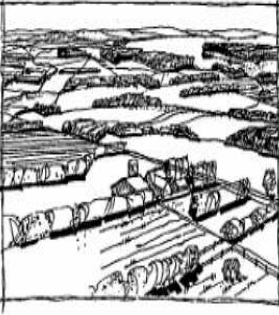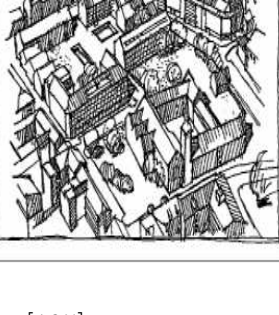
Classe	Roughness Length (M)	Landscape type	Illustration
0	0,003	Wide expanses of water, coastal areas	
I	0,01	Rase campaign, with or without some isolated obstacles (trees, buildings, airports).	
II	0,05	Countryside with hedges, orchards, small woods, hedgerow, scattered habitat	
III	0,3	Industrialized, urban or forest zone	
IV	1	Large cities with big buildings	

Figure 1.9: Roughness length according to the landscape [105].

1.9   Mathematical background of air pollutants modeling

Modeling air pollutants involves complex techniques and procedures. Among these, we quote physical models under controlled conditions which use statistical and deterministic approaches. Well-known traditional models like analytical models: semi-empirical Gaussian plume model and Gaussian puff model. In this circumstance the Sharan ITT model is dedicated to weak winds. Numerical models also play a large role in the study of contaminants in the air. We lay emphasis on Numerical models like Lagrangian stochastic model: AERMOD and Eulerian diffusive model: TRANSCHIM. Semi-analytical models form the backbone of research today, as the Generalized Integral Laplace Transform Technique (GILTT) that includes the expansion of the concentration in series of eigenfunctions derived to an auxiliary problem. Nevertheless, the complexity of existing phenomena, as a result of the non-conservative laws that govern real world process, arouses the curiosity of scientists even more.

1.9.1   Physical models under controlled conditions

Statistical approach

Since the atmospheric boundary layer is the seat of turbulent flows, there exist random characteristic variables. Major changes in these turbulent variables are nevertheless made accessible by the use of statistical tools. However, statistical tools are good for the study of medium fields, especially when one is interested in flows around complex geometries. For example, Reynolds Averaged Navier Stokes (RANS) approach consists in applying the reynolds mean operator to Navier Stokes equations characteristic of the fluid flow, assumes to be Newtonian and incompressible. The decomposition proposed by Reynolds describes any random variable x as the sum of its overall mean $\overline{x}$ and a random fluctuation x′ centered on the average value [106]. The system governing the fundamental equations is described in the following paragraph.

Firstly, let's rewrite the Navier-Stokes equations considering average Reynolds assumptions. The Boussinesq approximation is considered, the actual thermodynamic state of the atmosphere deviates little from a reference or rest state, considered hydrostatic and adiabatic. In particular, it is considered that the density fluctuation ρ remains low in the Atmospheric Boundary Layer, except for the buoyancy effects that happen in atmospheric stratification. The density is substituted by its mean value and the conservation equation of the mass is then written, for $\alpha = 1, 2, 3$:

$$\frac{\partial \overline{\rho}\,\overline{u}_\alpha}{\partial X_\alpha} = 0. \tag{1.14}$$

Secondly, the conservation of momentum introducing the Reynolds-averaged Navier Stokes equations, under the Boussinesq approximation and neglecting the Coriolis forces, is written for $\alpha = 1, 2, 3$ and $j = 1, 2, 3$:

$$\overline{\rho}\left(\frac{\partial \overline{u}_\alpha}{\partial t} + \overline{u}_j\frac{\partial \overline{u}_\alpha}{\partial x_j}\right) = -\overline{\rho}g\delta_{\alpha 3} + \overline{\rho}g\delta_{\alpha 3}\beta\left(\overline{\theta} - \theta_{ref}\right) - \frac{\partial \overline{p}}{\partial x_\alpha} + \frac{\partial}{\partial x_j}\left[\mu\left(\frac{\partial \overline{u}_\alpha}{\partial x_j} + \frac{\partial \overline{u}_j}{\partial x_\alpha}\right) - \left(\overline{\rho u'_j u'_\alpha}\right)\right], \tag{1.15}$$

with β the buoyancy coefficient and μ the dynamic viscosity.

Let consider the turbulence in the conservation expression of the momentum, this reveals double correlation terms between velocity fluctuations corresponding to the terms $\overline{u'_j u'_\alpha}$. These additional unknowns, called Reynolds tensors, require a particular treatment, given by a model of closure of turbulence.

For energy conservation, in a similar way, the Reynolds mean operator is applied to the equation of heat to give the following relation, for $j = 1, 2, 3$:

$$\frac{\partial \overline{\theta}}{\partial t} + \overline{u}_j\frac{\partial \overline{\theta}}{\partial x_j} = -\frac{1}{\overline{\rho}C_p}\frac{\partial}{\partial x_j}\left(\lambda\frac{\partial \overline{\theta}}{\partial x_j} - \left(\overline{\theta' u'_j}\right)\right) + \overline{S}_\theta, \tag{1.16}$$

with θ the temperature potential, C_p the mass heat capacity at constant pressure, λ the molecular thermal conductivity and S_θ the potential temperature source term. This last relation again reveals double correlations terms $\overline{\theta' u'_j}$ between temperature fluctuations and speed fluctuations. These terms, as previously stated are treated by the chosen closure model. Application of the Reynolds mean operator to the conservation principle of the mass of species i. The advection-diffusion equation then becomes for C_i the mass concentration of the chemical species i, for $j = 1, 2, 3$:

$$\frac{\partial \overline{C}_i}{\partial t} + \overline{u}_j\frac{\partial \overline{C}_i}{\partial x_j} = \frac{\partial}{\partial x_j}\left(D_i\frac{\partial \overline{C}_i}{\partial x_j} - \overline{C'_i u'_j}\right) + \overline{S}_i + \overline{R}_i, \tag{1.17}$$

with D_i the molecular diffusivity resulting from Fick's law, S_i the positive source term for a rejection, negative for a sample and R_i the term of production or destruction of the chemical species i by chemical reaction. In the case where, we will consider the rejection of a passive tracer, without taking into account the chemical reactions likely to occur ($R_i = 0$) and neglect the molecular diffusivity ($D_i = 0$). The turbulence closure model will once again attempt to resolve the double correlations terms $\overline{C'_i u'_j}$. The previously described turbulent flows of

momentum, energy and pollutant concentration are treated by a closure model [107]. The goal is to obtain a system with many equations as unknown to solve the flow.

Then it is possible to generate solutions using *Saturn _Code* software that can use a first-order closure model, consisting of connecting the turbulent flows $\overline{u'_j u'_\alpha}$, $\overline{\theta' u'_j}$ and $\overline{C'_i u'_j}$ to the average fields $\overline{u}_j$, $\overline{\theta}$ and $\overline{p}$, using a constitutive law, called turbulent viscosity model. The first-order closure of turbulent fluxes is based on the Boussinesq hypothesis, establishing an analogy between turbulent flows and diffusive-type mass fluxes, governed by a Fick law [108]. Any turbulent flow can thus be modeled using the average gradients and a coefficient of diffusivity or turbulent viscosity v_t. Unlike molecular diffusivity, which is an intrinsic property of the fluid, this turbulent viscosity depends on the flow studied. The double correlations terms, constituting the unknowns of the previously described system, are then written:

Reynolds Tensors:

$$-\overline{u'_j u'_\alpha} = v_t \left(\frac{\partial \overline{u}_\alpha}{\partial x_j} + \frac{\partial \overline{u}_j}{\partial x_\alpha} \right) - \frac{2}{3} k \delta_{ij}, \tag{1.18}$$

Turbulent heat flow:

$$-\overline{\theta' u'_j} = \frac{v_t}{pr_t} \frac{\partial \overline{\theta}}{\partial x_j}, \tag{1.19}$$

Turbulent flow of matter:

$$-\overline{C'_i u'_j} = \frac{v_t}{S_{ct}} \frac{\partial \overline{C}_i}{\partial x_j}. \tag{1.20}$$

with k the kinetic energy of turbulence, defined as: $k = \frac{1}{2} \overline{u'_j u'_j}$

The use of a closure model makes it possible to obtain the turbulent viscosity parameter v_t, to go back to the turbulent flows and then enables the resolution of the conservation equations in order to determine the flow.

Deterministic approach

Modeling atmospheric phenomena can be possible using two types of approaches: statistical modeling (empirical) and deterministic (physical) modeling. The first approach uses a panel of data as key variables in the system (concentration measurements, emission estimates, meteorological observations ...) in linear regression equations (or delinearized) type, without involving chemical equations and physical evolution of the environment. The second

approach, discussed below, relies on the formulation of physical mechanisms, chemical and digital resolution equations, based on physical laws (laws of thermodynamics, mechanics of fluids, etc.). Deterministic models rank themselves into three categories according to the Eulerian, Lagrangian, or Gaussians schematic representation of pollutants dispersal. These models require different input datasets (sources of pollution, geography, meteorology, etc.), restore the mapping of pollutant fields and make forecasts. Also, they produce sequential data of pollutant concentrations.

Deterministic models based on mathematical and numerical descriptions of phenomena can be used to track or reconstruct meteorological or atmospheric event in order to diagnose the origin of pollutants and precursors [109]. But, according to the initial hypotheses, the model does not always generate its own analytical solution, nevertheless gives an approximate numerical solution. The random nature of environmental processes leads to an irreducible and inherent uncertainty [110]. The advantage of using deterministic numerical models, the physicochemical processes are explicitly treated by the set of equations and depend only on the input data at the initial moment, subsequently evolving independently with their own numerical schemes.

1.9.2 Analytical models: Semi-empirical

Gaussian plume model

Resolution of the Advection-Diffusion Equation (ADE) requires complex modeling techniques. However, in some cases there are analytical solutions that provide quick and easy way to study turbulent dispersion. Let's focus on the gaussian solution of the advection-diffusion equation. For a punctual instantaneous emission at the origin $(t = 0)$, the concentration is given by the initial condition $C(x, y, z, 0) = S\delta(x)\delta(y)\delta(z)$, with δ the Dirac delta function. In practice, there are many situations, depending on the assumptions about the source of emission and boundary conditions on the ground. Assumptions often used for gaussian models are quite differents:

- The mass transfer due to the transport of the elementary volume in the x-direction is much greater than that due to the diffusion of the gas;

- The state is considered stationary i.e. $\frac{\partial C}{\partial t} = 0$. This hypothesis requires that the concentrations of all points in space be constant over time;

- The wind speed is considered constant, and it blows in the x-direction;

- The mass diffusion coefficients K_x, K_y and K_z are independent of the considered point (homogeneous turbulence) and do not depend on time;

- The concentration of the pollutant comes from a continuous source;

- The atmosphere is considered homogeneous (this implies that the experimental site is flat and the surface of the ground uniform);

- The vertical component of the wind is negligible compared to the horizontal component.

In infinite dimension situation i.e. thin plume, the gaussian solution is written:

$$C(x, y, t) = \frac{S}{(2\pi t)^{3/2}\sqrt{K_x K_y K_z}} \exp\left[-\frac{(x - Ut)^2}{4K_z t} - \frac{y^2}{4K_y t} - \frac{z^2}{4K_z t}\right], \qquad (1.21)$$

Assuming that the distribution of concentrations in the perpendicular planes is approximately gaussian. The pollutant plume therefore has a spread, in the x, y, z-directions, given by $2K_x t$; $2K_y t$; $2K_z t$ variances usually defined by σ_x^2; σ_y^2; and σ_z^2 [111]. This implies that the distribution of the pollutants follows gaussian law whose standard deviations depend on the leeward distance (x) or the time elapsed during the emission, also called the transport time [112]. Relations between the standard deviations of dispersion and the diffusion coefficients are then defined as follows [113]:

$$\sigma_x^2 \simeq \frac{2K_x x}{\overline{u}}, \ \sigma_y^2 \simeq \frac{2K_y x}{\overline{u}}, \ \sigma_z^2 \simeq \frac{2K_z x}{\overline{u}}. \qquad (1.22)$$

The distribution occurs along the vertical and transverse axes and constitutes the gaussian conical plume distribution (Figure 1.10)[114].
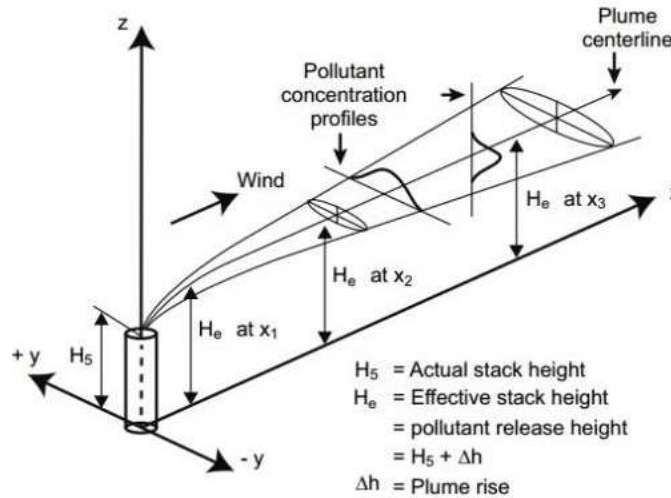
Figure 1.10: Schematic representation of Gaussian plume [115].

The limits of the gaussian models depend in part on the simplifying hypotheses emitted during their development [116]. These limits include:

- The plume diffusion formula assumes long emission and sampling times in front of the pollutants travel time so that it can be distributed in the form of a plume;

- No material is removed from the plume by chemical reaction or deposition on the surface;

- For moderate to strong wind conditions, pollutants own diffusion is neglected compared to advection when it occurs in the mean wind axis. This hypothesis is also known as the thin plume approximation. The validity of this hypothesis is weakened as we move away from the source due to weak correlations of wind for the chosen distances;

- Assumption on stationary flow and constant weather conditions is not valid in the case where there is a rapid change of weather conditions (low winds, for example);

- Beyond distances greater than 100 m and beyond 10 km, the results are no longer valid because other turbulence and diffusion phenomena must be considered;

- Assumption on the gaussian distribution in the vertical direction is doubtful but does not seem to adversely affect the model estimating ground-level concentrations;

- On complex terrain, the condition of flat and homogeneous terrains necessary for the functioning of the Gaussian models is no longer valid.

Gaussian puff model

The logical extension of gaussian rectilinear model in stationary case for continuous source in time emitted ($x = y = 0$), at the height h, with total reflection hypothesis on the ground) behaves as puff model, which represents the variation in emissions over time as well as weather conditions. It is assumed that a single puff is emitted in N successive intervals of duration Δt, each puff evolves independently of the other puffs in a gaussian mode. The concentration is then calculated by summing over all the puffs.

$\forall t \geq N\Delta t$,

$$
\begin{aligned}
C(x, y, z, t) = \frac{1}{(2\pi)^{3/2}} \sum_{i=1}^{i=N} \frac{S_i \Delta t}{\sigma_x \sigma_y \sigma_z} \exp\left[-\frac{(x-x_i(t))^2}{2\sigma_x^2} - \frac{(y-y_i(t))^2}{2\sigma_y^2}\right] \\
\times \left[\exp\left(\frac{(z-z_i(t)-h)^2}{2\sigma_z^2}\right) + \exp\left(\frac{(z-z_i(t)+h)^2}{2\sigma_z^2}\right)\right],
\end{aligned}
\tag{1.23}
$$

with $S_i \Delta t$ the emission at the origin of the time t. The position of the center of mass of the puff i is given for example for the x-axis, by:

$$x_i(t) = x_i(t - \Delta t) + u(x_i(t - \Delta t), t - \Delta t)\Delta t, \qquad (1.24)$$

with $u(x, t)$ the wind component along the x-axis. Modeling the evolution of the size of the puffs is one of the thorny points of such models; many parameterizations describe the evolution of σ_*^2 in time and space for puffs.
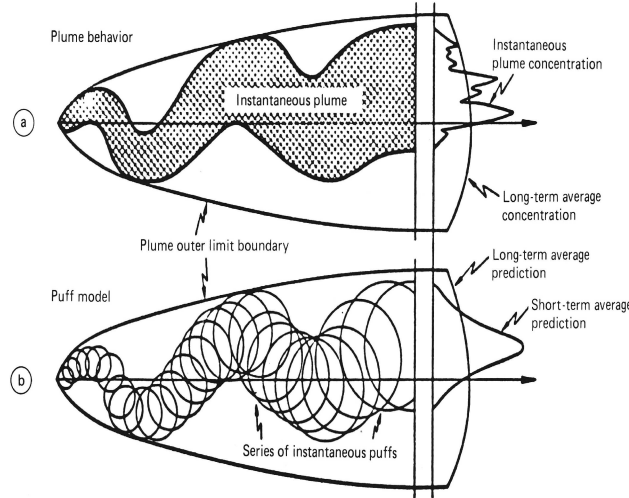
Figure 1.11: Instantaneous behavior of a typical plume and a series of puffs from a puff-diffusion model [117].

In this model, most dispersion processes and physico-chemical processes are taken into account using specific parameterizations, without solving equations. These models are well suited to real-time operational studies, impact studies because they require limited computation time and thus allow the study of a large number of cases.

ITT Sharan model

The Sharan ITT model is dedicated to weak winds [118], this model is obtained from an analytical resolution of the stationary transport-diffusion equation. The transport of contaminant emitted from a source primarily depends on the wind speed U. Here, is used the following power-law profile for wind speed [119].

$$U(z) = az^{\alpha}, \; a = U(z_r)z_r^{-\alpha}. \qquad (1.25)$$

The form of eddy diffusivity is given in terms of both downwind distance x and the height z above the ground, to deal with the near source dispersion [120].

$$K_z = K'_z(z)f(x), \tag{1.26}$$

where $K'_z(z)$ gives the form of eddy diffusivity depending on z and $f(x)$ represents the correction term near source dispersion and the dimensionless integrable function of x. $K'_z(z)$ characterises the parameterization parameter as power-law profile in z:

$$K'_z(z) = bz^\beta, \; b = K'_z(z_r)z_r^{-\beta}. \tag{1.27}$$

where $K'_z(z_r)$ equals the value of K'_z at the height $z = z_r$ and β corresponds to the power-law exponent appearing in the diffusion coefficient. For these profiles of wind speed Eq. (1.25) and eddy diffusivity Eq. (1.27), the newmann type conditions, yields the analytical solution:

$$
\begin{aligned}
C(x,z) = Q \times \Bigg[&\frac{\alpha+1}{ah^{\alpha+1}} + \frac{\alpha-\beta+2}{ah^{\alpha-\beta+2}}(zH_s)^{(1-\beta)/2} \\
&\times \sum_{n=1}^{\infty} \frac{J_{-\mu}\big[\gamma_n(z/h)^{(\alpha-\beta+2)/2}\big]J_{-\mu}\big[\gamma_n(H_s/h)^{(\alpha-\beta+2)/2}\big]}{J^2_{-\mu}(\gamma_n)} \times \exp\left(-\frac{b(\alpha-\beta+2)^2\gamma_n^2}{4ah^{\alpha-\beta+2}}\right) \int_0^x f(x')dx' \Bigg],
\end{aligned}
\tag{1.28}
$$

where $\mu = (1-\beta)/(\alpha-\beta+2)$ depict the Bessel function of order $-\mu$ $J_{-\mu}$ and $\gamma_n'^s$ are the zeros of the equation:

$$J_{-\mu+1}(\gamma_n) = 0. \tag{1.29}$$

Eq. (1.28) gives the crosswind integrated concentration released from an elevated source point in the atmosphere when the wind speed is parameterized as a power-law profile of z and eddy diffusivity varies according to terms of both x and z.

Special cases

Case I: ground level source

The crosswind integrated concentration for a ground level source point is obtained by taking the limit $H_s \to 0$ in Eq. (1.28) then introducing Bessel properties for small function arguments [121]:

$$
\begin{aligned}
C(x,z) = Q \times \Bigg[&\frac{\alpha+1}{ah^{\alpha+1}} + \frac{\alpha-\beta+2}{ah^{\alpha-\beta+2}} \frac{(zh)^{(1-\beta)/2}\Gamma(\mu)\sin(\pi\mu)2^\mu}{\pi} \times \sum_{n=1}^{\infty} \frac{J_{-\mu}\big[\gamma_n(z/h)^{(\alpha-\beta+2)/2}\big]}{\gamma_n^\mu J^2_{-\mu}(\gamma_n)} \\
&\times \exp\left(-\frac{b(\alpha-\beta+2)^2\gamma_n^2}{4ah^{\alpha-\beta+2}}\right) \int_0^x f(x')dx' \Bigg],
\end{aligned}
\tag{1.30}
$$

where $\Gamma(.)$ represents the gamma function.

Case II: ground level source

Supposing wind speed as constant and eddy diffusivity emerging as function of x only, i.e. $K_z(x,z) = f(x) = K(x)$ (for $\beta = 0$ and $b = 1.0$ Eq. (1.27)), the expression of the concentration distribution is obtained from Eq. (1.28) by taking the limit $\alpha \to 0$ (equivalently $U(z) = U(Z_r) = U$) as:

$$C(x, z) = \frac{Q}{hU}\left[1 + 2\sum_{n=1}^{\infty} \cos(\lambda_n H_s)\cos(\lambda_n z)\exp\left(-\frac{\lambda_n^2}{U}\int_0^x K(x')dx'\right)\right],\qquad(1.31)$$

where $\lambda_n = \frac{n\pi}{h}$. Eq. (1.31) equals the solution previously obtained for uniform wind speed and eddy diffusivity as a generalized function of downwind distance x [122]. If the eddy diffusivity in Eq. (1.31) is taken as a constant and expressed in terms of the dispersion parameters using the relation $K = \frac{U\sigma_z^2}{2x}$ [123], after integration, the resulting expression becomes

$$C(x, z) = \frac{Q}{hU}\left[1 + 2\sum_{n=1}^{\infty} \cos(\lambda_n H_s)\cos(\lambda_n z)\exp\left(-\frac{\lambda_n^2}{2}\sigma_z^2\right)\right],\qquad(1.32)$$

Also equivalent to the classical gaussian plume model for an elevated source with reflections from two parallel boundaries at $z = 0$ and $z = h$ [124].

A similar solution was obtained in the analysis of theory-K using first order WKB-approximation method for air pollutants dispersion [125].

1.9.3 Numerical models

Lagrangian stochastic model: AERMOD

American Meteorological Society/Environmental Protection Agency Regulatory Model (AERMOD) is a computer model defined by the normal distribution curve, also called the gauss curve (see Eq. (1.33)). The equations defining the concentration of pollutants in the model are based on the probability density equation according to normal law or Laplace-Gauss law Eq. (1.33):

With:

$$f(x) = y = -\frac{1}{\sqrt{2\pi}\sigma}\exp\left(-\frac{1}{2}\left(\frac{x - \overline{x}}{\sigma}\right)^2\right),\qquad(1.33)$$

With:

σ = standard deviation of the gaussian distribution (m)

x = distance in the abscisse (m)

$\overline{x} = \mu$ = average value (m)

In particular, AERMOD simulates the dispersion of atmospheric pollutants in the field near the source (less than 50 km, local level). The AERMOD model was developed by the American Meteorological Society and the Environmental Protection Agency (EPA) in 1991 to introduce the Atmospheric Layer (ABL) concepts into regulatory compliance models [126, 127]. This model also makes it possible to simulate both surface sources and high point sources volumes for a simple or complex site topography [128]. Depending on the stability of the atmosphere and the location below the ABL, AERMOD can simulate five different types of plumes: direct, indirect, penetrating, injected, and stable. If the atmosphere is stable, the plume is modeled by two gaussians in the lateral and vertical direction. Under convective conditions, the horizontal distribution remains gaussian, while the concentration of the vertical distribution is the result of the combination of three different plumes [129]:

- A direct plume: part of the plume will fall, but all the above part will escape and will be lost in the modeling;

- A penetrating plume: the code will simulate the part of the plume that will remain at altitude and compensate for the part of the direct plume lost by penetration into the high stable layer;

- An indirect plume: it is not exactly the symmetric of the direct plume, but allows the code to simulate the concentration increase related to the nonplanar geometries of the ground or buildings. This source compensates for the loss of both previous sources and represents the majority of the fallout of the plume.

Eulerian diffusive model: TRANSCHIM

Transchim relies on the three-dimensional resolution of the Eulerian species transport equation. This equation is for a given species i in the form:

$$\frac{\partial C_i}{\partial t} + div\left(V(\overrightarrow{x}, t)C_i\right) = div\left(D(\overrightarrow{x}, t)\Delta C_i\right) + R_i + S_i, \tag{1.34}$$

where $\overrightarrow{x}$ and t respectively represent the space and time variable. C_i is the concentration scalar for species i. V represents the vector of wind speed following the horizontal, the vertical component of the wind not being taken into account in the version used by TRANSCHIM, $V(\overrightarrow{x}, t) = V_x \overrightarrow{e}_x + V_y \overrightarrow{e}_y$. The turbulent diffusivity of the atmosphere $D(\overrightarrow{x}, t)$ is calculated either by the parameterization model [130] or by the representation [131, 132]. R_i represents

the term of production and chemical disappearance of species i, which can be written in the form:

$$R_i = P_i - L_i.C \tag{1.35}$$

where P_i represents the production vector and $L_i C$ the dissipation term L_i is a diagonalisable matrix. The last term of the equation represents the emissions of polluting sources E_i and the deposition of species

$$S_i = E_i(x, t) - vdep_i C_i \tag{1.36}$$

$vdep$ represents the rate of deposition of species.

To solve satisfactorily the transport problem of chemical pollutants in the atmosphere, numerous variables are taken into account: the displacement due to the wind, the emissions, the deposits of species, the diffusion, the chemistry intervening between the various species emitted and those present in the atmosphere, the relief, the weather, the development of the Atmospheric Boundary Layer [133]. TRANSCHIM solves the problem of transport chemistry numerically and parametrically by taking into account the development of the Atmospheric Boundary Layer and the diffusivity of the atmosphere. Meteorological parameters and flow emitted are input data to be interpolated at each point in the domain. The relief is not taken into account, but only flat areas. To solve Eq. (1.34), the choice of discretization technique is essential. There are three types [133]: the finite difference method, the finite volume method and the finite element method. This choice is not insignificant, because the discretization techniques are coupled to the types of meshes used. A structured mesh (Figure 1.12 a), where all the points are marked by the indices (i, j, k) and have the same number of neighbors, is generally used with finite difference or finite volume methods. Whereas an unstructured mesh (Figure 1.12 b), where the points are numbered and may not have the same number of neighbors, is used instead for the finite element method. TRANSCHIM uses the finite difference method.

In order to assess the impact of long-term exposure to air pollution, simulations over long periods several months or even years are necessary. In some cases, such as photochemical pollution, the calculation time is prohibitive. This leads either to an intensification of the calculations thanks to parallelisation, or to the simulation of representative scenarios: this is the whole reason to proceed with the parallelisation of the TRANSCHIM code. The efficiency obtained for simulations with photo-oxidising chemistry is satisfactory, but the time saving remains limited for inert simulations.
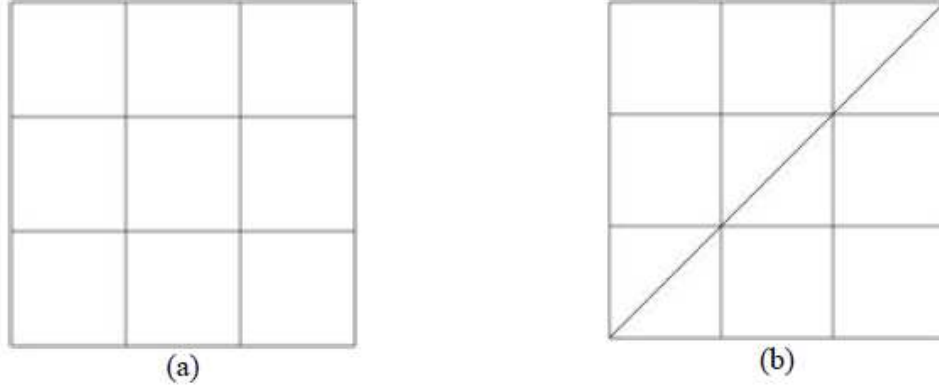
Figure 1.12: Mesh structure (a) structured and (b) unstructured.

The aim of the finite difference method is to obtain approximate values of the continuous solution in a number of points. The discretization technique consists in establishing relations allowing to evaluate approximately the derivatives of the solution to the nodes of the mesh. Then the differential equation, where the derivatives have been replaced by their approximate expression, must be satisfied at each node of the domain. For example, on a two-dimensional grid where each node is marked by the indices (i, j) in (x, y), the displacement of the solution $u(x, y)$ in Taylor series of point (x_o, y_o) is given by:

$$u(x_0 + \Delta x, y_0) = u_{i+1,j} = u_{i,j} + \Delta x \left(\frac{\partial u}{\partial x}\right)_{i,j} + \frac{\Delta x^2}{2!} \left(\frac{\partial u}{\partial x^2}\right)_{i,j} + \dots \qquad (1.37)$$

In this case the development has been limited to the second order, but it can be continued to any higher order. The expression of the first derivative is thus obtained:

$$\left(\frac{\partial u}{\partial x}\right)_{i,j} = \frac{U_{i+1,j} - u_{i,j}}{\Delta x} + O(\Delta x). \qquad (1.38)$$

The notation $O(\Delta x)$ denotes the truncation error ε such that for $\Delta x \to 0$, we have $\varepsilon \leq K |\Delta x|$, where K is a positive constant. In the study of finite differences, the truncation error is always of the form $O(\Delta x^q)$; q is therefore called the order of precision of the formula. The expression established in Eq. (1.38), for the first derivative is not unique. Indeed by doing the development of Taylor for the point $(x_0 - \Delta x, y_0)$ (the node $(i-1, j)$), we obtain a formula for the first derivative of the rear difference in the following form:

$$\left(\frac{\partial u}{\partial x}\right)_{i,j} = \frac{u_{i,j} - u_{i-1,j}}{\Delta x} + \frac{\Delta x}{2} \left(\frac{\partial^2 u}{\partial x^2}\right)_{i,j} + \dots = \frac{u_{i,j} - u_{i-1,j}}{\Delta x} + O(\Delta x). \qquad (1.39)$$

By combining the rear and front difference formulas $(in(i+1, j))$, we obtain a centered difference formula:

$$\left(\frac{\partial u}{\partial x}\right)_{i,j} = \frac{u_{i,j} - u_{i-1,j}}{2\Delta x} + O(\Delta x^2). \tag{1.40}$$

The order of precision is not limited. It suffices to recombine the values of u for a larger number of points, for example at order 4:

$$\left(\frac{\partial u}{\partial x}\right)_{i,j} = \frac{-u_{i+2,j} + 8u_{i+1,j} - 8u_{i-1,j} + u_{i-2,j}}{12\Delta x} + O(\Delta x^4). \tag{1.41}$$

However, the increase in the precision of the diagram leads to an increase in the number of points to be considered, and consequently the increase in the number of operations to be solved, and therefore the increase in the calculation time. It turns out that the higher the order of precision, the slower the return of results will be. Note that even-order schemes tend to favor oscillations, and odd order schemes tend to introduce dissipation. In the area of air pollution, emissions create discontinuities that tend to oscillate solutions and lead to non-convergence.

1.9.4 Semi-analytical models

GILTT method

The scheme of the GILTT (Generalized Integral Laplace Transform Technique) approach includes the following steps: expansion of the serial concentration of eigenfunctions obtained from an auxiliary problem, substitution of this equation in the Advection-Diffusion Equation (ADE), resulting in a matrix Ordinary Differential Equation (ODE) which is then solved analytically by the Laplace Transform technique [134, 135, 136, 137]. Considering the following pollutant transport equation:

$$\frac{\partial c(z,t)}{\partial t} = K_z' \frac{\partial c(z,t)}{\partial z} + K_z \frac{\partial^2 c(z,t)}{\partial z^2} + Q\delta(z - H_s)\delta(t - t_0). \tag{1.42}$$

This equation obeys to the following limiting conditions:

- The Neumann boundary condition on the vertical

$$-K_z'(x,z)\frac{\partial c}{\partial z} = 0, \; at \; z \to 0 \; z \to z_i. \tag{1.43}$$

- The concentration $c(z,t) = 0$ at $t = 0$.

The solution of the problem (1.42) takes the form [138]:

$$c(z,t) = \sum_{n=0}^{N} c_n(t)\zeta_n(z). \tag{1.44}$$

where $\zeta_n(t) = \cos(\lambda_n z)$ and $\lambda_n = \frac{n\pi}{z_i}$ are respectively the eigenfunctions and eigenvalues, and $c_n(t)$ is the solution of the transformed problem. Replacing the Eq. (1.44) in Eq. (1.42) and taking moments:

$$
\begin{aligned}
&\sum_{n=0}^{N} c_n'(t) \int_0^{z_i} \zeta_n(z)\zeta_m(z)dz \\
&+ \sum_{n=0}^{N} c_n(t) \left[\lambda_n^2 \int_0^{z_i} K_z \zeta_n(z)\zeta_n(z)dz - \int_0^{z_i} K_z \zeta_n'(z)\zeta_m(z)dz \right] \\
&= Q\delta(t-t_0) \int_0^{z_i} \delta(z-H_s)\zeta_m(z)dz.
\end{aligned}
\tag{1.45}
$$

The above equation can be rewritten as a first order linear matrix equation:

$$
Y'(t) + FY(t) = \eta\delta(t-t_0).
\tag{1.46}
$$

For $t > 0$, where the matrix F is defined as $F = A^{-1}B$ with entries of matrices A and B defined as:

$$
A = (a)_{n,m} = \int_0^{z_i} \zeta_n(z)\zeta_m(z)dz
\tag{1.47}
$$

$$
B = (b)_{n,m} = \lambda_n^2 \int_0^{z_i} K_z \zeta_n(z)\zeta_m(z)dz - \int_0^{z_i} K_z' \zeta_n'(z)\zeta_m(z)dz
\tag{1.48}
$$

and η is the vector $\eta = A^{-1}Q\zeta_m(H_s)$. For the initial condition, the procedure is analogous and after the substitutions due and integrations, the result is: $Y(0) = c(z,0) = 0$.

In this work the transformed problem represented by Eq. (1.46) is solved by the Laplace Transform Technique and diagonalization [139]. Thus, the final solution is given by

$$
Y(t) = X.G(t).X^{-1}.\eta
\tag{1.49}
$$

where $G(t)$ is the diagonal matrix which elements are $e^{-d_i(t-t_0)}$, X is the eigenfunction matrix and d_i are the eigenvalues of the matrix F.

Fractional Brownian approach

Complex functional-structure processes could be efficiently analysed by adopting principles and methodologies derived from the fractal geometry. For example, let consider the following fractal time random walk system[140], where the characteristic waiting time

T diverges, but the jump length variance Σ^2 is still kept finite. To this end, a long-tailed waiting time pdf with the asymptotic behaviour [141, 142].

$$C(t) \sim A_\alpha(\tau/t)^{1+\alpha}, \tag{1.50}$$

for $0 < \alpha < 1$ corresponds Laplace asymptotics space [143, 144]. Assuming that $\psi(u = 0)$, i.e. $\lim_{u\to 0} \int_0^\alpha dt e^{-ut}\psi(t)$ is the normalisation of the waiting time pdf, i.e. $\psi(u = 0) = 1$.

$$C(u) \sim 1 - (u\tau)^\alpha. \tag{1.51}$$

Again, the specific form of $C(t)$ is of minor importance. Consequently, together with the gaussian jump length pdf characterised through this asumption: the long-time limit corresponds to Brownian motion. For instance, a Poissonian waiting time pdf $C(t) \sim \tau^{-1}\exp(-t/\tau)$ with $T = \tau$, together with a gaussian jump length pdf

$$\lambda(x) = \left(4\pi\sigma^2\right)^{-1/2}\exp\left[-x^2/(4\sigma^2)\right], \tag{1.52}$$

leading to $\Sigma^2 = 2\sigma^2$. Then, the corresponding Laplace and Fourier transforms are of the forms

$$\lambda(k) \sim 1 - \sigma^2 k^2 + 0(k^4), \tag{1.53}$$

the pdf in Fourier Laplace space becomes

$$C(k, u) = \frac{[C_0(k)/u]}{1 + K_\alpha u^{-\alpha}k^2} \tag{1.54}$$

in the $(k, u) \to (0, 0)$ diffusion limit. Employing the integration rule for fractional integrals [145]

$$\mathscr{L}\left\{{}_0D_t^{-p}C(x,t)\right\} = u^{-p}C(x,u),\ p \geq 0, \tag{1.55}$$

one infers the fractional integral equation

$$C(x,t) - C_0(x) = {}_0D_t^{-\alpha}K_\alpha\frac{\partial^2}{\partial x^2}C(x,t). \tag{1.56}$$

The Riemann-Liouville operator $_0D_t^{1-\alpha} = (\partial/\partial t)\,_0D_t^{-\alpha}$, for $0 < \alpha < 1$, is defined through the relation [146, 147].

$$_0D_t^{1-\alpha}C(x,t) = \frac{1}{\Gamma(\alpha)}\frac{\partial}{\partial t}\int_0^t dt' \frac{C(x,t')}{(t-t')^{1-\alpha}}, \tag{1.57}$$

the Riemann-Liouville derivative can be replaced by a Caputo derivative since they are directly related

$$_0^C D_t^{\alpha}C(x,t) = \,_0D_t^{\alpha}C(x,t) - \frac{C_0(x)}{\Gamma(1-\alpha)}t^{-\alpha}. \tag{1.58}$$

The fundamental property Eq. (1.57) is the fractional order differentiation of α power,

$$_0D_t^{1-\alpha}t^p = \frac{\Gamma(1+p)}{\Gamma(p+\alpha)}t^{p+\alpha-1}. \tag{1.59}$$

In reality, it can be shown the more general relation

$$_0D_t^q t^p = \frac{\Gamma(1+p)}{\Gamma(1+p-q)}t^{p-q}. \tag{1.60}$$

Therefore, the integro-differential nature of the Riemann-Liouville fractional operator $_0D_t^{1-\alpha}$ according to Eq. (1.57), with the integral kernel $M(t) \propto t^{\alpha-1}$, ensures the non-Markovian nature of the subdiffusive process defined by the FADE. Indeed, calculating the mean squared displacement from relation Eq. (1.54) by using the relation $\langle x^2 \rangle = \lim_{k\to 0}\{-(d^2/dk^2)\,C(k,u)\}$ and subsequent Laplace inversion, then results

$$\left\langle x^2(t)\right\rangle = \frac{2K}{\Gamma(1+\alpha)}t^{\alpha}. \tag{1.61}$$

is obtained. Alternatively, it can be inferred from the FADE through integration over $\int_{-\infty}^{+\infty}dx\,x^2$, leading to $(d/dt)\langle x^2(t)\rangle = \,_0D_t^{1-\alpha}2K = 2Kt^{\alpha-1}/\Gamma(\alpha)$.

we obtain after some manipulations

$$_0D_t^{\alpha}C - \frac{t^{-\alpha}}{\Gamma(1-\alpha)}C_0(x) = K\frac{\partial^2}{\partial x^2}.C(x,t), \tag{1.62}$$

The initial value $C_0(x)$ is seen to decay with the inverse power-law form $\frac{t^{-\alpha}}{\Gamma(1-\alpha)}C_0(x)$, and not exponentially fast as for standard diffusion [148].

By application of the differential operator $\partial/\partial t$, one finally arrives at the FADE

$$\frac{\partial C}{\partial t} = {}_0 D_t^{1-\alpha} K \frac{\partial^2}{\partial x^2} C(x,t). \tag{1.63}$$

Given that for continuum functions $f(x)$ we have ${}_0 I_x^\alpha {}_0 D_x^\alpha f(x) = {}_0 D_x^\alpha {}_0 I_x^\alpha f(x) = f(x)$ and ${}_0 I_x^{\alpha+\beta} = {}_0 I_x^\alpha {}_0 I_x^\beta$ we obtain after some stricky manipulations:

$$\frac{\partial^\alpha C(x,t)}{\partial x^\alpha} - \frac{t^{-\alpha}}{\Gamma(1-\alpha)} C(0,t) = K_z \frac{\partial^2 C(x,t)}{\partial z^2}. \tag{1.64}$$

Finally, the Riemann-Liouville derivative in Eq. (1.64) can be replaced by a Caputo derivative since they are directly related

$$ {}_0^C D_x^\alpha f(x,t) = {}_0 D_x^\alpha f(x,t) - \frac{f(0)}{\Gamma(1-\alpha)} t^{-\alpha}. \tag{1.65}$$

Consequently, the general steady-state fractional advection-diffusion equation displaying the anomalous power-law mean squared displacement Eq. (1.61) is given by

$$u \frac{{}^C \partial^\alpha C(x,t)}{\partial t^\alpha} = K_z \frac{\partial^\alpha C(x,t)}{\partial z^2}. \tag{1.66}$$
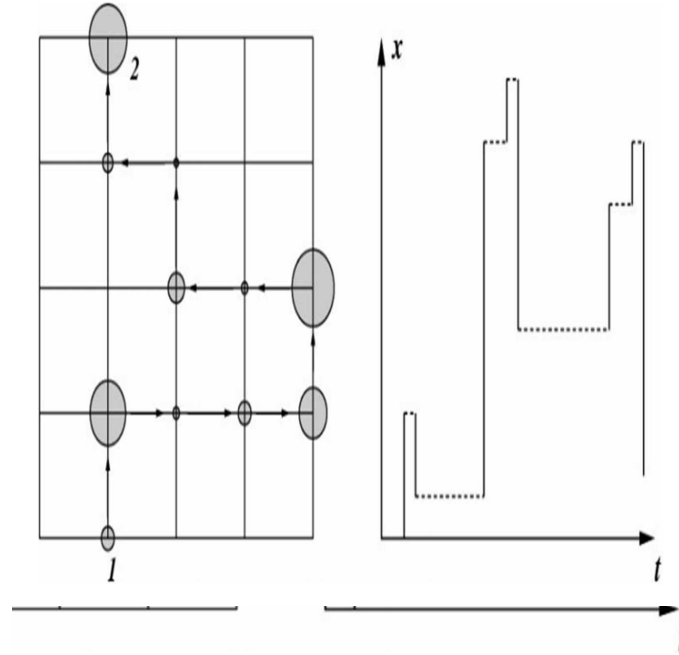
Figure 1.13: Continuous time random walk (CTRW) model. Left: CTRW process on a two-dimensional latticegeneralising the Brownian situation. Right: (x, t) diagram of a one-dimensional CTRW process where both jump lengths and waiting times are drawn from pdfs which allow for a broad variation of the corresponding random variables.
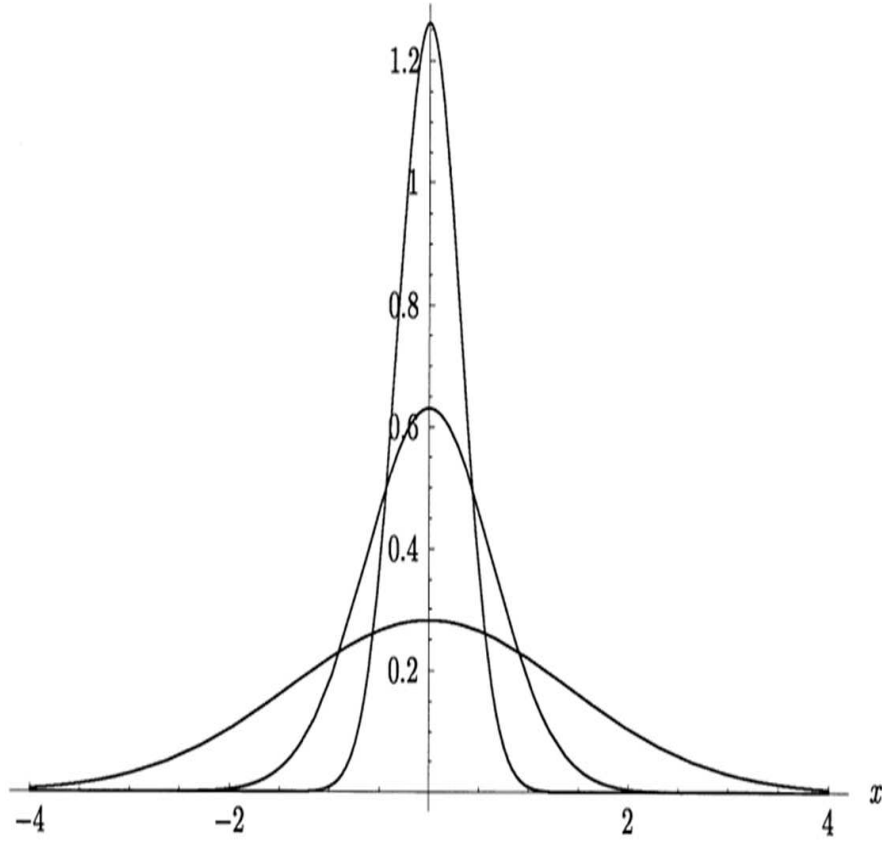
Figure 1.14: Propagator W(x, t) for Brownian diffusion (α=1) for the times t=0.05, 0.2 and 1. Galilei invariant Brownian model: The propagator is symmetric with respect to its maximum which is translated with velocity v=1.
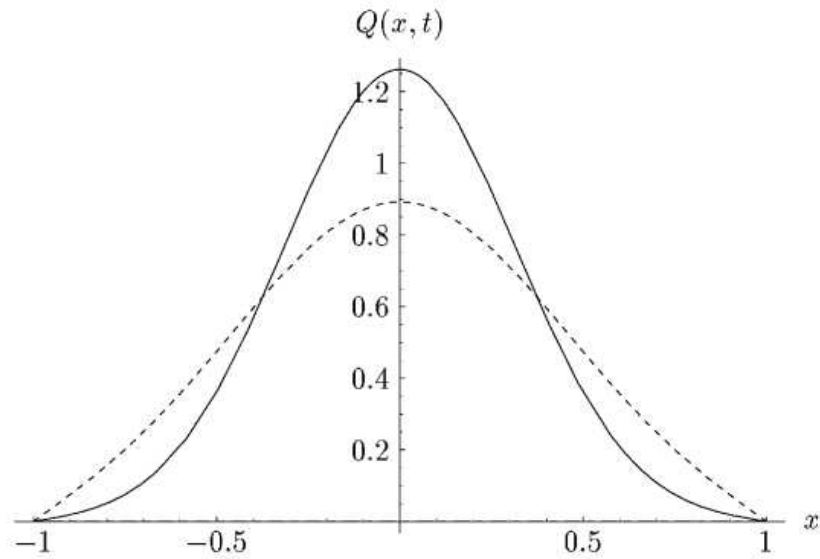
Figure 1.15: Image solution Q(x, t) for absorbing boundaries at x=$\pm$1. Top: The subdiffusive case, α=1/2. Bottom: The Brownian case, γ=1.
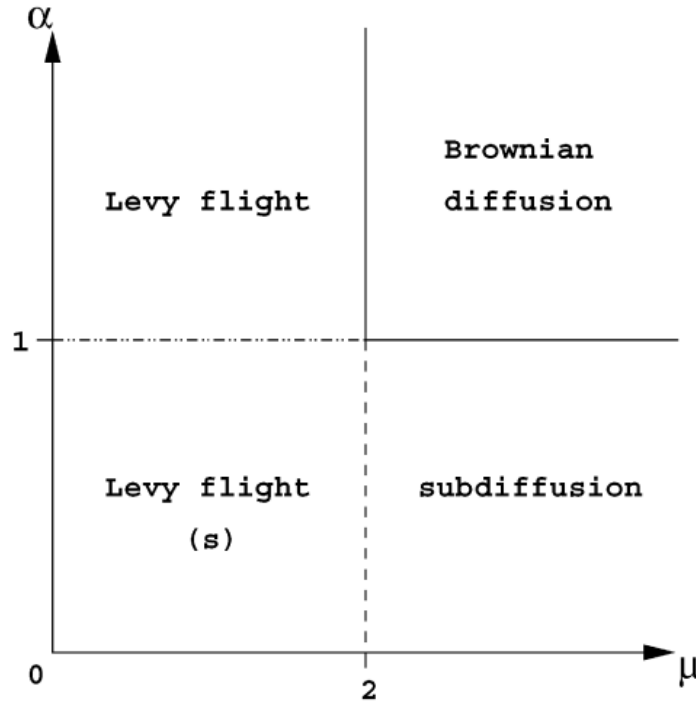
Figure 1.16: Phase diagram for the FDE. The different phases characterise the four domains which can be distinguished according to diverging or finite characteristic waiting time T and jump length variance Σ^2.

Remark 1.

The free (linear) equation will be said to be dispersive if the solutions, even if they are initially well localised in space, tend to disperse throughout the space in large time. One of the mathematical consequences of dispersion for linear equations is the presence of local regularizing effects. These regularizing effects are linked to dispersion. The more dispersive the equation is, the more important these effects will be. For non-linear equations, this phenomenon can result in two very different behaviours: non-linearity reinforces the dispersion and the solutions have a linear behaviour. If, on the other hand, non-linearity and dispersion compensate each other, then we generally observe localised solutions which propagate without any change in shape, such as progressive waves or stationary states sometimes called solitons. The interest of physicists and modellers in non-linear dispersive equations is undoubtedly due to the existence of soliton waves, i.e. solutions propagating at constant speed without shape change.

In addition, most of the classical mechanics techniques have been used in studies of conservative systems, such as almost all the models studied above, but most of the processes observed in the physical real world are non-conservative. A system is said to be conservative when there is mass, energy, momentum conservation.

1.10   Conclusion

Litterature review on pollutants in the atmosphere starts with an assimilation of definitions on air pollution and air quality, including methods for assessing like variety of pollution indicators. There are many air pollutants sources inducing external effects, such as radioactive and electromagnetic pollutants. These processes influencing air quality are caused by a series of chemical reactions. As it is also important to mention, the atmospherical pollution phenomenon appears at the level of the Atmospheric Boundary Layer (ABL) and implies the structure and the evolution of the atmosphere. A general overview of the techniques that implement the dispersion of pollutants in the atmosphere, allows to explore the strong points and to elucidate the shortcomings in the optimal exploitation of these models. It is on this basis that the study of the power-law dynamics in the ABL displays the dynamics of normal and anomalous diffusion, coupling to the nature of memory effects in atmospheric diffusion. As consequence, a spotlight on physics of the particle movements: Brownian motion and diffusion. This shows that, cumulative effects of pollutants in the environment through the dynamic structure of the atmosphere depends on the environment and dispersion overall roughness. Which has implications on economic and legal aspects of air pollution.

Chapter 2

Models and Methodology

Models and Methodology

2.1 Introduction

Conduct a study on the models and methodology, comes back to explore the dynamic structure of the atmosphere. By means of an analysis of differential topology and geometry which caracterized dispersion models under controlled conditions. This approach highlights, a variety of models, thus fractional equations solving methods are explored in comparison with the existing models. A special case is underlined, reflecting the dynamics of non-linear fractional equations evolving in the atmosphere.

2.2 Differential topology and geometry of dynamics systems

This work research is concerned with an investigation of the smoothness properties of fractional spaces in differential topology and geometry.

2.2.1 Differential calculus in linear topological spaces

Linear topological space means an abstract linear space with a Hausdorff topology in which the functions such that addition and scalar multiplication are respectively continuous functions of both variables. Let T_1 and T_2 be any two linear topological spaces. A function $g(x)$ on T_1 to T_2 is termed linear if it is additive and continuous-hence homogeneous of degree one [149]. We recall that a real respectively complex linear space or a vector space is a non-void set for example E and two operations called addition and scalar multiplication which satisfies the some axioms. A base for the neighborhood system of 0 is called a local base or a local base for the topology or a system of nuclei. The straightforward sort of linear topological space is that in which the topology is defined by means of a norm. Recall that a norm p for a linear space E is a subadditive ($p(x + y) \leqq p(x) + p(y)$), absolutely homogeneous ($p(tx) = |t| \, p(x)$), non-negative functional on E, such that $p(x) = 0$ if and only if $x = 0$. If p is a norm for E, then

the metric associated with p is defined by $d(x, y) = p(x - y)$. Each linear topological space E can be mapped by a topological isomorphism onto a dense subspace of a complete linear topological space $E^{\wedge}$.

Let f be a map of linear space X to a linear space Y. The first difference of f at a point $x \in X$ for the increment $h \in X$ is, as usual, the name for the expression

$$\Delta f(x; h) = f(x + h) - f(x). \tag{2.1}$$

Now let Y be a linear topological space A map f: X $\rightarrow$ Y is called differentiable at the point $x \in X$ in the direction $h \in X$ if the expression $\frac{\Delta f(x; \tau h)}{\tau}$ has a limit as $\tau \rightarrow 0$, $\tau \in \mathcal{R}$. This limit is called the first variation (or simply the variation) of f at x for the increment h and is written $\delta f(x; h)$.

Therefore [150]

$$\delta f(x; h) \underline{\det} = \lim_{\tau \to 0} \frac{\Delta f(x; \tau h)}{\tau} = \lim_{\tau \to 0} \frac{\Delta f(x + h) - f(x)}{\tau} = \left. \frac{\partial}{\partial \tau} \right|_{\tau=0} f(x + \tau h). \tag{2.2}$$

Evidently, if the variation for the increment h at x exists, then for any real number α the variation for the increment α h at x exists and

$$\delta f(x; h) = \alpha \delta f(x; h). \tag{2.3}$$

Let X be a linear space, Y and H_i linear topology spaces, $H_i \Subset X$, σ_i a system of subsets of H_i, β_i a system of bounded subsets of H_i (i = 1, 2, ..., n). We always suppose that each of the systems σ_i, β_i contains all the one-point subsets of H_i. Thus, the definition of the higher order derivatives by induction. The $(\sigma_1, \beta_1; ...; \sigma_n, \beta_n)$ - derivative f^n along the subspaces $H_1, ..., H_n$

(briefly, the $(H_1, \sigma_1, \beta_1; ...; H_n, \sigma_n, \beta_n)$-derivative) of the map $f : X \rightarrow Y$ is defined as

the (H_n, σ_n, β_n) - derivative of the $(H_1, \sigma_1, \beta_1; ...; H_{n-1}, \sigma_{n-1}, \beta_{n-1})$ - derivative f^{n-1}.

The map f is called $(H_1, \sigma_1, \beta_1; ...; H_n, \sigma_n)$ - differentiable at $x \in X$ if (for some β_n) the derivative $f^{(n)}$ is defined at x the value $f^{(n)}(x)$ of this derivative at x is called:

the $(H_1, \sigma_1, \beta_1; ...; H_{n-1}, \sigma_{n-1}, \beta_{n-1}, H_n, \sigma_n)$ - derivative at x.

2.2.2 Fractional calculus in geometric spaces

The change of dimensionality at different scales and its acquiring non-integer values is typical of multi-fractals, so it is customary to describe dimensional flow as a fractal property of space-time. Fractional measures have the desired characteristics of having anomalous scaling

and inducing power-counting renormalizability. Although realistic models of Nature should include gravity, the introduction of the present formalism of fractional dynamics in a flat non-dynamical space will help in clarifying how to construct a covariant notion of space-time with non-integer dimension [151].

Fractional space ε_α^D is a novel object and all related statements are pointed out here, where D is the number of topological dimensions and $0 < \alpha \leqslant 1$ is a real parameter interpreted as running with the scale. Contrary to ordinary calculus, there is no unique definition of derivative, we quote Riemann-Liouville or Caputo derivative. The output of fractional operators is almost always quite different from that of ordinary calculus and, in this respect, counterintuitive. The definitions of fractional derivatives are related to one another in a precise way, eventually, differences amount both to the convergence properties of the functional space on which these operators act and to boundary terms in the formula. Fractional operators are regularly employed in a number of fields in physics and mathematics, such as statistics, diffusing or dissipative processes with residual memory like weather and stochastic financial models [152].

Following these assumptions, thus it have been established the basic definition of integral derivatives following integro-differential operators. Let $x \in [x_0, x_1]$ be a real coordinate variable defined on an interval with constant extrema x_0 and x_1, which may be taken to infinity if desired. We define a space of functions $f(x)$ on this interval, such that all the following integro-differential operators will be well defined. A space of particular interest is $AC^n[x_0, x_1]$, that of functions which are absolutely continuous on $[x_0, x_1]$ up to their n-1 derivative.

Let $f \in L_p(x_0, x_1)$ and let θ be the Heaviside distribution:

$$\theta(x) = \begin{cases} 1, & x > 0 \\ 0, & x < 0 \end{cases} \tag{2.4}$$

We introduce the left fractional integral of order α as

$$\left(\mathrm{I}^\alpha f\right)(x) := \frac{1}{\Gamma(\alpha)} \int_{x_0}^{x_1} \frac{dx'}{(x - x')^{1-\alpha}} \theta(x - x') f(x'). \tag{2.5}$$

Here $\alpha \in \mathbb{C}$ is a complex constant parameter, which we shall restrict to be real for our purposes. This formula is naturally suggested as a generalization to non-integer n of the Cauchy formula for the n-time repeated integration:

$$\left(I^n f\right)(x) = \int_{x_0}^{x} dy_1 \int_{x_0}^{y_1} dy_2 \cdots \int_{x_0}^{y_{n-1}} dy_n f(y_n). \tag{2.6}$$

One can also define the right fractional integral of order α

$$\left(\bar{I}^{\alpha} f\right)(x) := \frac{1}{\Gamma(\alpha)} \int_{x_0}^{x_1} \frac{dx'}{(x'-x)^{1-\alpha}} \theta(x'-x) f(x'). \qquad (2.7)$$

where integration now is from x to the end of the interval. Because of the x dependence in the step function, the output of fractional integrals is a function of x. These operators are bounded if $f \in L_p(x_0, x_1)$, for every $1 \leqslant p \leqslant +\infty$ [153].

Fractional gradients admit a geometric interpretation [154], in one dimension, the fractional derivative of a differentiable function f on $\mathbb{R}$ can be expressed as

$$\left(\partial^{\alpha} f\right)(x) = \lim_{y \to x^+} \frac{(T_{\alpha} f)(y, x) - (T_{\alpha} f)(x, x)}{(y-x)^{\alpha}}. \qquad (2.8)$$

where T is a mapping [155]. Thus, the definition of a fractional Euclidean space ε_{α}^{D} of order α as Euclidean space $\mathbb{R}^D$ endowed with a set of rules $\text{Calc}^{\alpha} = \{\partial^{\alpha}, I^{\alpha}, ...\}$ of integro-differential calculus, a measure ϱ_{α} with a given support, a natural norm $\|\cdot\|$, and a Laplacian $\mathcal{K}$:

$$\varepsilon_{\alpha}^{D} = (\mathbb{R}^D, Calc^{\alpha}, \varrho_{\alpha}, \|\cdot\|, \mathcal{K}). \qquad (2.9)$$

Different sets of fractional operators in Calc^{α} can correspond to inequivalent fractional spaces.

The sighsight of calculus can be justify:

Fractional opposite to non-fractional calculus is among the most studied and best manageable frameworks generalizing ordinary calculus and, to the best of our knowledge, there are almost no other examples of calculi mimicking fractal behaviours in physics and statistics such as anomalous scaling of dimensionality and discrete scale invariance [156]. While left operators involve integration from an initial point x_0 up to the arbitrary point x, right operators integrate over the complementary sub-interval $[x_0, x_1]$. $0 < \alpha \leqslant 1$: This choice is empirical. One wishes to obtain a model of space whose dimension is smaller than the topological dimension D of the embedding space. For a natural isotropic distribution of fractional charge over the D coordinates, this is achieved precisely for this range of the order parameter. The Caputo derivative carries several advantages over the Riemann-Liouville operator. the Caputo derivative of a constant is zero for any x_0, while for the Riemann-Liouville derivative it is so only when $x_0 = +\infty$. Also, we quote the existence, in the former case, of a standard Cauchy problem, where one needs to specify only the first n ordinary derivatives [157]. On the other hand, the Riemann-Liouville operator requires the specification of n initial conditions of the form $\lim_{x \to x_0} \left(I^{k-\alpha} f\right)(x), k = 1, ..., n$ which have no clear physical interpretation. The relation

between the integer classical derivative, on the left-hand side, and the derivative in the sense of distributions on the right-hand side establishes the relationship between Caputo and Riemann derivatives:

$$(\partial^n f)(x) = ({}_{RL}\partial^n f)(x) - \sum_{i=0}^{n-1} \partial^{n-1-i}\delta(x-x_0)\left(\partial^i f\right)(x_0). \tag{2.10}$$

Therefore, one can consider the Caputo derivative as the fractional generalization of classical differentiation, and the Riemann-Liouville derivative as the fractional generalization of functional differentiation. In this respect, the Caputo operator is a much more natural choice for the fractional derivative in actions defined on ε_α^D.

The determination of the spectral dimension of fractional spaces highlights once again the main difference between fractal geometry and ordinary space constructions in field theory. In the first case, geometry and topology are defined by the symmetry and harmonic structures of the fractal, which are given at the outset. On the other hand, in field theory the harmonic structure stems from physical considerations. More specifically, we can say that the symmetry structure is first dictated by the action measure ϱ and then imposed on the Lagrangian density $\mathscr{L}$, but the harmonic structure is determined both by the symmetries and by the form of the kinetic operator.

2.3 A note on fractional order derivatives

2.3.1 A truncated $\mathscr{M}$-series fractional derivative function

Definition 1.

Let $f :]-\infty, +\infty[\to \mathbb{R}$. For $0 < \alpha < 1$ a N-truncated derivative type of f of order α, denoted by ${}_iD_N^{\alpha,\beta}$, is

$$_iD_N^{\alpha,\beta} f(x) := \lim_{h \to 0} \frac{f(x_i\mathbb{E}_\beta(|h|x^{-\alpha})) - f(x)}{h}, \tag{2.11}$$

$\forall x > 0$ and ${}_i\mathbb{E}_\beta(.), \beta > 0$ is a truncated Mittag-Leffler function of one parameter as defined as: ${}_i\mathbb{E}_\beta(z) = \sum_{k=0}^{i} \frac{z^k}{\Gamma(\beta k+1)}$, with $\beta > 0$ and $z \in \mathbb{C}$. We note that, if f is α-differentiable in some open intervals $(0, a)$, $a > 0$, and $\lim_{x \to 0^+} ({}_iD_N^{\alpha,\beta} f(x))$ exist, then we have ${}_iD_N^{\alpha,\beta} f(0) = \lim_{x \to 0^+} ({}_iD_N^{\alpha,\beta} f(x))$.

Property

Let us consider the mathematical problem of defining fractional integration and differentiation [158]. In a nutshell, for every complex function $f(x + iy)$, of a sufficiently wide class, and every number α, irrational, fractional or complex, a function $^C D_z^\alpha f(z) = g(z)$, or $^C D_x^\alpha f(x) = g(x)$, z simply as real, should satisfy the following criteria:

- The derivative $^C D_x^\alpha f$ of an analytic function f is analytic. In this case, this purpose is verified by (Chain rule);

- Backward compatibility, the operation $^C D_x^\alpha f$ must give the same result as ordinary differentiation when the order α is a positive integer. In this context, this point is justified by the obtained solution (2.151);

- The zero order derivative leaves the function unchanged : $^C D_x^0 f(x) = f(x)$. We recall that $_i D_N^{\alpha,\beta} f(x) = \lim_{h \to 0} \frac{f(x_i \mathbb{E}_\beta(|h|x^{-\alpha})) - f(x)}{h}$, by choosing $\beta = 1$ as we have $_1 \mathbb{E}_{\Bbbk}(hx^{-\alpha}) = \sum_{k=0}^i \frac{(hx^{-\alpha})^k}{\Gamma(\beta k + 1)} = 1 + hx^{-\alpha}$, for $\alpha = 0$, we conclude that the operation of order zero returns the function itself;

- The fractional operators must be linear, ie : $^C D_x^\alpha(af(x) + bg(x))$

  $= a \cdot^C D_x^\alpha f(x) + b \cdot^C D_x^\alpha g(x)$, following it, with the main equation behaves in its form is linear;

- The index law of exponents for integration of arbitrary order holds,

  $^C D_x^\alpha \cdot^C D_x^\beta f(x) =^C D_x^{\alpha+\beta} f(x)$, we suppose f be a continuous function such that $_N I_b^{\alpha,\beta} f$ then $_i D_N^{\alpha,\beta}(_N I_b^{\alpha,\beta} f(x)) = \frac{x^{1-\alpha}}{\Gamma(1+\beta)} \frac{d}{dx}(_N I_b^{\alpha,\beta} f(x))$ in the same line

  $\frac{x^{1-\alpha}}{\Gamma(1+\beta)} \frac{d}{dx}(\Gamma(1+\beta)) \int_b^x \frac{f(x)}{x^{1-\alpha}} dx = f(x)$, hence this calculation can therefore be extended to prove the assumption.

  A definition that meets these criteria finds a logical application in the Riemann-Liouville integral.

Definition 2.

- $g(x)$ represents a function defined throughout certain interval containing x_0 and all point near x_0, thus $g(x)$ appears to be local fractional calculus at $x = x_0$, depict by $\lim_{x \to x_0} g(x) = g(x_0)$, if to each ε and constant r positives corresponds δ as [159]

$$|g(x) - g(x_0)| < k\varepsilon^{\alpha}, \ 0 < \alpha \leq 1. \tag{2.12}$$

$|x - x_0| < \delta, \ \varepsilon, \ \delta > 0$ and $\varepsilon, \ \delta > 0$ and $\varepsilon, \ \delta \in \mathbb{R}$. Consequently, the function $g(x)$ is designated local fractional continuous on the interval (a,b), denoted by

$$g(x) \in C_{\alpha}(a, b), \tag{2.13}$$

where α represents the fractal dimension with $0 < \alpha \leq 1$.

- g(x): $\mathbb{R} \to -\mathbb{R}$, $X \mapsto g(X)$ is designated a non-differentiable function of exponent α, $0 < \alpha \leq 1$ which satisfies Hölder function of exponent α, then for $x, \ y \in X$ we obtain [160, 161]

$$|g(x) - g(y)| \leq C |x - y|^{\alpha}. \tag{2.14}$$

- g(x): $\mathbb{R} \to -\mathbb{R}$, $X \mapsto g(X)$ is designated to be local fractional continuous of order α, $0 < \alpha \leq 1$, or shortly α-local fractional continuous, [159, 160]

$$g(x) - g(x_0) = 0((x - x_0)^{\alpha}). \tag{2.15}$$

As remark $g(x)$ is designated to be in the space $C_{\alpha}[a, b]$ if and only if it is in the form

$$g(x) - g(x_0) = 0((x - x_0)^{\alpha}) \tag{2.16}$$

where any $x_0 \in [a, b]$ and $0 < \alpha \leq 1$.

.

Local fractional derivative

Let consider $g(x) \in C_{\alpha}(a, b)$. Local fractional derivative of $g(x)$ of order α at $x = x_0$ is writen as [159]

$$f^{(\alpha)}(x_0) = \frac{d^{\alpha} f(x)}{dx^{\alpha}}\bigg|_{x=x_0} = \lim_{x \to x_0} \frac{\Delta^{\alpha} (f(x) - f(x_0))}{(x - x_0)^{\alpha}} \tag{2.17}$$

with $\Delta^{\alpha} (f(x) - f(x_0)) \simeq \Gamma(1 + \alpha) (f(x) - f(x_0))$ and $0 < \alpha \leq 1$.

Therefore [161, 162]

$$\frac{d^\alpha x^{k\alpha}}{dx^\alpha} = \frac{\Gamma\left(1+k\alpha\right)}{\Gamma\left(1+(k-1)\alpha\right)} x^{(k-1)\alpha}$$
$$\frac{d^\alpha E_\alpha\left(kx^\alpha\right)}{dx^\alpha} = kE_\alpha\left(kx^\alpha\right), k \; constant. \tag{2.18}$$

As stated earlier [162]

If $h(x) = (fou)(x)$ with $u(x) = g(x)$ one gets

$$\frac{d^\alpha h(x)}{dx^\alpha} = f^{(\alpha)}(g(x))\left(g^{(1)}(x)\right)^\alpha, \tag{2.19}$$

when $f^{(\alpha)}(g(x))$ and $g^{(1)}(x)$ exist.

If $h(x) = (fou)(x)$ with $u(x) = g(x)$ one gets

$$\frac{d^\alpha h(x)}{dx^\alpha} = f^{(1)}(g(x))g^{(\alpha)}(x), \tag{2.20}$$

when $f^{(1)}(g(x))$ and $g^{(\alpha)}(x)$ exist.

2.4 Dispersion models in differential topology and geometry

Pollutants released into the atmosphere are carried by wind speed and dispersed by turbulence. In general, for moderate and strong winds, diffusion is negligible in front of the advection. However, for low speeds, diffusion is not negligible. These aspects related to wind speed are atypical for regions in hemispheres. Thus, this part is structured in such a way as to study two typical dispersion models: the classical integer-order dispersion model under medium, strong and weak wind conditions. The fractional dimensional order dispersion model.

2.4.1 Dispersion model in integer-dimensional space

Numerous dispersion models have been established taking into account a number of natural and physical parameters. In general, when the wind is strong, the mechanical turbulence is predominant and the atmosphere is neutral. When the wind is light, if the thermal energy close to the ground is important, convection sets in, the atmosphere is unstable. Otherwise, it remains stable. Without losing sight of these generalities, we consider a problem of pollutant dispersion in ABL by assuming that the velocities v and w take the value zero, the diffusion component is also neglected.

The traditional approach to the characterization of distribution in framed within the context of Euclidian geometry was mostly perfected by the mid-20th century. Partial differential

equations, ordinary differential or integral equations, are functional equations. That means that the unknown, or unknowns, for possible determination are functions. A general partial differential equation in $\mathbb{R}^d$ of order k is of the form:

$$G(x, \Lambda^k u(x) = 0). \tag{2.21}$$

where G is a specified function. We also consider N X N systems in which case G and u are column N-vectors. A function u of class C^k is said to be a classical solution (2.21) if it verifies the equation as all points x in a specified domain of $\mathbb{R}^d$. Consider first the one dimensional situation d = 1 in which case (2.21) becomes an ordinary differential equation (ODE), or system of ODE. For k = 1 and N = 1, that is the case of an ordinary differential equation of order k = 1. Then (2.21) is simply, $G(x, u(x), \partial_x u(x)) = 0$ where G is a given function of the three variables x, u and $p = \partial_x$. The case of a second order ODE, i.e. d = N = 1 and k = 2. Then (2.21) becomes, $G(x, u(x), \partial_x u(x), \partial_x^2 u(x)) = 0$, where G now depends on the four variables x, u, $p = \partial_x$, $q = \partial_x^2$. In a nutshell, an integer giving the differential order of the PDE with respect to the space variable.

Global scale dispersion models can be classified into two categories. The first category uses a description of turbulent motions allowing for transport by organized circulations. Since it is believed that uniformity is achieved much more quickly in the zonal direction than in the meridional or vertical directions, this kind of model is usually simplified to two dimensions viz vertical and north-south [163]. The second category of models uses three-dimensional winds at a series of grid points over the globe to transport effluent on a synoptic and global scale. These motions include turbulent and mean movements. The turbulent transport on subgrid scale must still be parameterized such as by Particle-in-cell (PIC) methods, among the fully parameterized models [164, 165].

The topological dimension of the system, consider fractal dimension estimates based. Essentially, a fractal dimension refers to the spatial dimension of an object whose dimension falls between the standard Euclidean integer dimensions of one, two or three [166]. Euclidean objects only occupy integer dimensions, 1 for a line, 2 for a square, and so on. Fractals, however, may occupy non-integer dimensions, dimensions that fall in between 1 and 2 or between 2 and 3. Space-fractional advection-dispersion equation (SFADE) can describe particle transport in a variety of fields more accurately than the classical models of integer-order derivative. Because of non-local property of integro-differential operator of space-fractional derivative.

2.4.2   Classical ADE model in integer dimensional space

The steady-state advection-dispersion equation of a non-reactive contaminant relaease in the ABL base on K-theory is given by

$$u(z)\frac{\partial C}{\partial x} = \frac{\partial}{\partial x}\left(K_x(x,z)\frac{\partial C}{\partial x}\right) + \frac{\partial}{\partial z}\left(K_z'(x,z)\frac{\partial c}{\partial z}\right) \tag{2.22}$$

Where $u(z)$ is the wind profile in x-direction and K_x and K_z are the longitudinal and verticales eddy diffusivities in the x-and z-directions respectively.

Eq. (2.22) is subjected to the following boundary and initial conditions:

a) The pollutants are released from a continuous point source with the emission rate Q for the occasion located at the point $(0, 0, hs)$, with a fixed enclosure and the x-axis coinciding with the plume [167]

$$C(0, z) = \frac{Q}{u(z)}\delta(z - h_s)\delta(y), \qquad at \qquad x = 0, \tag{2.23}$$

hs is the effective stack height and δ is the Dirac-delta function.

b) The ground and Atmospheric Boundary Layer (ABL) top are assumed to be impermeable, with the diffusive flux vanishes close to the surface [168]

$$K_z'(x, z)\frac{\partial C}{\partial z} = 0, \ z = z_0, \ z = h, \tag{2.24}$$

h is the height of Planetary Boundary Layer (PBL).

c) C moves to zero as x tends to infinity.

$$C \to 0 \qquad as \qquad x \to \infty$$

.

where z_0 is the surface roughness length.

Eq. (2.22) is associated with the Sturm-Liouville auxiliary problem

$$\frac{d}{dz}\left(K_z(z)\frac{d\phi_n(z)}{dz}\right) + \gamma_n^2 u(z)\phi_n(z) = 0. \tag{2.25}$$

With $0 \leq z \leq h$ and the function ϕ_n verify the following boundary conditions

$$K_z(z)\frac{d\phi_n(z)}{dz} = 0 \text{ when } z = 0..h. \tag{2.26}$$

Eqs. (2.25) and (2.26) verify the Sturm-Liouville problem which concedes solutions when $\gamma_1 < \gamma_2 < \gamma_3 < \gamma_4... < \gamma_n < ....$ however, in order to obtain an exact solution, for $\gamma_n \gg 0$ Eq. (2.25) can be approximated. Using the first-order WKB approximation [169, 170]

$$\phi_n(z) \sim \frac{1}{(u(z)K_z(z))^{1/4}} \cos\left(\gamma_n \int_0^z \sqrt{\frac{u(q)}{K_z(q)}} dq\right). \tag{2.27}$$

In addition, the concentration can be expressed as follows:

$$C = B_0(x,y) + \sum_{n=1}^{\infty} B_n(x,y)\phi_n(z). \tag{2.28}$$

Use of the proposed method and scheme [167, 170, 171], the general solution C takes the form

$$\simeq \frac{Q}{\sqrt{2\pi}\sigma_y} \exp\left(-\frac{y^2}{2\sigma_y^2}\right) \times \left[\frac{1}{\int_0^h u(z)dz} + \sum_{n=1}^{\infty} \frac{2\exp\left(-\gamma_n^2 \int_0^x f(x')dx'\right)}{\int_0^h \sqrt{\frac{u(z)}{K_z(z)}}dz} \times \right.$$
$$\left. \frac{1}{(u(h_s)K_z(h_s)u(z)K_z(z))^{1/4}} \times \cos\left(n\pi \frac{\int_0^{h_s}\sqrt{\frac{u(q)}{K_z(q)}}dq}{\int_0^h \sqrt{\frac{u(q)}{K_z(q)}}dq}\right) \times \cos\left(n\pi \frac{\int_0^z \sqrt{\frac{u(q)}{K_z(q)}}dq}{\int_0^h \sqrt{\frac{u(q)}{K_z(q)}}dq}\right)\right]. \tag{2.29}$$

2.4.3 Comparison with existing models

- 1 $K_z'(x,z)$ depends on z only. Eq. (2.29) is the generalisation of the derived solution [169], which is deduced by taking f(x)=1

$$\simeq \frac{Q}{\sqrt{2\pi}\sigma_y} \exp\left(-\frac{y^2}{2\sigma_y^2}\right) \times \left[\frac{1}{\int_0^h u(z)dz} + \sum_{n=1}^{\infty} \frac{2\exp\left(-\gamma_n^2 x\right)}{\int_0^h \sqrt{\frac{u(z)}{K_z(z)}}dz} \times \right.$$
$$\left. \frac{1}{(u(h_s)K_z(h_s)u(z)K_z(z))^{1/4}} \times \cos\left(n\pi \frac{\int_0^{h_s}\sqrt{\frac{u(q)}{K_z(q)}}dq}{\int_0^h \sqrt{\frac{u(q)}{K_z(q)}}dq}\right) \times \cos\left(n\pi \frac{\int_0^z \sqrt{\frac{u(q)}{K_z(q)}}dq}{\int_0^h \sqrt{\frac{u(q)}{K_z(q)}}dq}\right)\right]. \tag{2.30}$$

$K_y(x,z)$, $K_z(x,z)$ and $u(z)$ constants, $\left(\frac{\int_0^{h_s}\sqrt{\frac{u(q)}{K_z(q)}}dq}{\int_0^h \sqrt{\frac{u(q)}{K_z(q)}}dq}\right) \equiv \frac{h_s}{h}$ and $\left(\frac{\int_0^{h_s}\sqrt{\frac{u(q)}{K_z(q)}}dq}{\int_0^h \sqrt{\frac{u(q)}{K_z(q)}}dq}\right) \equiv \frac{z}{h}$

$$C = \frac{Q}{\sqrt{(2\pi)}u\sigma_y h} \exp\left(-\frac{y^2}{2\sigma_y^2}\right)\left[1 + 2\sum_{n=1}^{\infty} \cos(\lambda_n z)\cos(\lambda_n h_s)\exp\left(-\frac{(n\pi)^2 K_z x}{uh^2}\right)\right], \tag{2.31}$$

which is a gaussian solution.

- In the case, $K_z(x, z) = f(x)$ and $u(z)$ depends on z

$$
\simeq \frac{Q}{\sqrt{2\pi}\sigma_y} \exp\left(-\frac{y^2}{2\sigma_y^2}\right) \times \left[\frac{1}{\int_0^h u(z)dz} + \sum_{n=1}^{\infty} \frac{2\exp\left(-\gamma_n^2 \int_0^x f(x')dx'\right)}{\int_0^h \sqrt{u(z)}dz} \times \right.
$$
$$
\left. \frac{1}{[u(h_s)u(z)]^{1/4}} \times \cos\left(n\pi \frac{\int_0^{h_s} \sqrt{\frac{u(q)}{K_z(q)}}dq}{\int_0^h \sqrt{\frac{u(q)}{K_z(q)}}dq}\right) \times \cos\left(n\pi \frac{\int_0^z \sqrt{\frac{u(q)}{K_z(q)}}dq}{\int_0^h \sqrt{\frac{u(q)}{K_z(q)}}dq}\right) \right].
$$

(2.32)

Assuming that $\int_0^z u(q)dq \equiv l_1$ and $\int_0^z \sqrt{u(q)}dq \equiv l_2$, if l_1 and $l_2 \to \infty$ when $h \to \infty$, the limit value of the series of Eq. (2.32) is obtained by converting the series into an integral using Riemman's summation property [172], u(z) constant, this solution takes gaussian form.

$$
c = \frac{Q}{2\pi u \sigma_z \sigma_y} \exp\left(-\frac{y^2}{2\sigma_y^2}\right) \times \left[\exp^{\left(-\frac{(z+h_s)^2}{2\sigma_z^2}\right)} + \exp^{\left(-\frac{(z-h_s)^2}{2\sigma_z^2}\right)} \right].
$$

(2.33)

2.4.4 Models behaviour under wind conditions

Pollutants released into the atmosphere are carried by wind speed and are dispersed by its fluctuations. This process is characterised by weak and strong winds.

Low wind conditions

These diffusion models are established taking into account the longitudinal diffusion coefficient. These models are linked to the following assumptions:

- Diffusion is not limited in the vertical direction ($0 \leqslant z < \infty$).

- The height of the ABL is limited ($0 \leqslant z < h$).

For most of the case studies, diffusion coefficients are assumed to be constant or x functions. These considerations do not focus on experiences that show that diffusion coefficients are functions of x and z [173]. In addition, some of the models consider generalized forms of expressions for wind speed and eddy diffusivity. But they are obtained by approximating these variables [174], this approximation does not realistically simulate air pollution processes. Generally, the fundamental equation is solved by associating it with boundary conditions. Assuming that the solution can be expressed as an Ansatz. The initial problem is associated with an auxiliary Sturm-Liouville problem.

Strong wind conditions

In another approach, there are models that solve the dispersion equation by considering the generalized forms of expressions for wind speed and diffusion coefficients. We quote, the models: Alternating Direction Multipliers Method (ADDM) [175], Matrix Form [176], Polynomial Form [177]; Classic Integral Transform Technique (CITT) [178] and Generalized Integral Laplace Transform Technique (GILTT) [179]. The dispersion of pollutants is linked to the strong turbulence. For moderate to strong wind conditions, the diffusion of the pollutant is neglected compared to advection when we are in the middle wind axis. This assumption is also known as the thin plume approximation. The validity of this hypothesis is weakened as we move away from the source due to weak wind correlations for these distances. Wind speed also influences the flow of the plume. It is also involved in the calculation of the plume elevation linked to the thermal and dynamic effects of smoke. So, more the wind is strong, more the plume will be folded towards the ground. Turbulence has two origins, one thermal and the other mechanical. Mechanical turbulence is predominant in strong wind and tends to return the atmosphere thermally neutral. Thermal turbulence leads to high instabilities when the ground is overheated and the wind allows natural convection to settle.

2.4.5   Dispersion model in fractional-dimensional space

The fractional advection-dispersion equation (FADE) known as its non-local dispersion was used in the modeling of the turbulent and chaotic dynamics of classical conservative systems. To model a type of diffusion: continuous time random walks, fractional differential equations seem well suited to take into account the effects of memory. The anomalous diffusion law on fractals is characterized by the walk dimension [180]:

$$d_W := 2\frac{d_H}{d_s}. \tag{2.34}$$

Since $d_S \leqslant d_H$ for a fractal, $d_H \geqslant 2$. The mean-square displacement of a random walker is a power law in diffusion time, $\langle r^2(\sigma) \rangle \sim \sigma^{2/d_W}$. Processes with $d_W > 2$ are of sub-diffusion, since the diffusion speed is lower than for normal diffusion (Gaussian process, $d_W = 2$). Systems with $d_W < 2$ are caller of super-diffusion or jump processes and do not correspond to fractals [181]. The determination of the spectral dimension of fractional spaces highlights once again the main difference between fractal geometry and ordinary space. Fractal geometry, and topology are defined by the symmetry and harmonic structures of the fractal, which are given at the outset.

Harmonic structure is characterized both by the symmetries and by the form of the kinetic operator. Depending on the choice of laplacian and of the operator D_σ^β, the diffusion equation will depicted different diffusion processes, determined by different values of the walk dimension. When anomalous dimensions are involved, there is no unique way to determine the diffusion equation, except on heuristic or phenomenological grounds [182].

$$\left(D_\sigma^\beta - \mathcal{K}\right) P\left(x, x', \sigma\right) = 0, P\left(x, x', \sigma\right) = \delta_\alpha\left(x, x'\right), 0 < \beta \leqslant 1, \quad (2.35)$$

where

$$D_\sigma^\beta \in \left\{\partial_\sigma, \partial_{0,\sigma}^\beta, {}_\infty \bar{\partial}_\sigma^\beta\right\}, \quad (2.36)$$

and we chose the fractional delta as the natural initial condition. Generalized to $\left(D_\sigma^\beta - \bar{\mathcal{K}}_\gamma\right) P\left(x, x', \sigma\right) = 0$ is often called fractional wave equation.

When $\beta = 1 = \gamma$, this is ordinary diffusion (Brownian motion).

When $\beta \neq 1$ and $\gamma = 1$, it corresponds to fractional sub-diffusion.

Finally, when $\beta = 1$ and $\gamma \neq 1$ the process is a Lévy flight [183].

2.4.6 Canonical form of the generalized FADE model in non-integer space

Let consider an equation for the spatial distribution of concentration of a pollutant in the Atmospheric Boundary Layer (ABL), in a Cartesian coordinate system, the spatial distribution of concentration $\bar{c} = \bar{c}(x, y, z)$ of the substance, where the flows are represented by the K-theory can be described by the following advection-diffusion equation [184].

$$u(z)\frac{\partial \bar{c}}{\partial x} = \frac{\partial}{\partial x}\left(K_x \frac{\partial \bar{c}}{\partial x}\right) + \frac{\partial}{\partial y}\left(K_y \frac{\partial \bar{c}}{\partial y}\right) + \frac{\partial}{\partial z}\left(K_z \frac{\partial \bar{c}}{\partial z}\right), \quad (2.37)$$

where $\bar{c}$ is the average concentration, $u(z)$ and K_x, K_y, K_z are the Cartesian components of wind velocity and eddy diffusivity along the x, y and z-directions, respectively. The following assumptions are taking into consideration: under moderate to strong wind conditions, the diffusion term in the x-direction is smaller than the advection term. In addition, eddy diffusivities are represented by the considered expressions:

$$K_y(x, z) = f_1(x)u(z), \quad K_z(x, z) = f(x)K_z(z), \quad (2.38)$$

where $f(x)$ is a dimensionless function of x call attention to a correction $K_z(z)$ in the vicinity of the source, and $K_z(z)$ is the far-field eddy diffusivity coefficient that is a function of z. The

three dimensional concentration [185], using the variable separations method can be deduced from Eq. (2.37) by taking $f(x) = \frac{1}{2}\frac{d}{dx}\sigma_z^2(x)$ and $f_1(x) = \frac{1}{2}\frac{d}{dx}\sigma_y^2(x)$, where σ_y and σ_z are the dispersion coefficient in the y-direction and z-direction respectively. The functional form of K_y is characterized to allow a gaussian distribution for the transverse concentration. In agreement with these considerations, Eq. (2.37) becomes,

$$u(z)\frac{\partial \overline{c}_y}{\partial x} = \frac{\partial}{\partial y}\left(K_y\frac{\partial \overline{c}_y}{\partial y}\right) + \frac{\partial}{\partial z}\left(K_z(z)\frac{\partial \overline{c}_y}{\partial z}\right). \tag{2.39}$$

When the process is governed by the steady state regime of the advection-diffusion equation with K_z constant with a sharp boundary condition $\overline{c}_y(0, z) = \lim_{x \to 0^+} \overline{c}_y(x, z) = \delta(z)$ in the domain $0 \leq x < \infty$ and $-\infty < z < \infty$ the above solution is given in terms of the Brownian solution by the Galilei shifted Gaussian. It is well-known that the advantage to random walk models, within the fractional approach it is feasible to insert external fields in a direct way. Thus the taking into account of transport in the phase space extended by both position and velocity coordinate is possible within the same methodology. The equation of the cross-wind integrated concentration ($\overline{c}_y = \overline{c}_y(x, z)$) is obtained by integrating the above equation with respect to y from $-\infty$ to $+\infty$ (neglecting the longitudinal diffusion). Besides, the assessment of boundary value problems is similar to the method for the analogous classical equations [186]. Diffusion law in the fractals is characterized by the walk dimension [187]:

$$\overline{c}_y(x, z) = \frac{1}{\sqrt{4\pi K_z x}} \exp\left(-\frac{z^2}{4K_z x}\right). \tag{2.40}$$

By introducing the well-known scaling rules for the Fourier and Laplace transforms one gets:

$$f(ax) \underset{\mathcal{F}}{\longleftrightarrow} |a|^{-1} \widehat{f}\left(k/a\right), a \in \mathbb{R}, f(bt) \underset{\mathcal{L}}{\longleftrightarrow} b^{-1}\widetilde{f}\left(s/b\right), b > 0. \tag{2.41}$$

As reported [188] and [189] the tridimensional solution, for ground level sources is proposed. Thus, the modified CTRW scheme is introduced, and applied to an extended Taylor formula, supposing the initial condition $\overline{c}_y(x, 0) = \delta(x)$. The corresponding equation in Fourier-Laplace space takes the form

$$u(s)\frac{\partial \overline{c}_y(x, s)}{\partial x} = -s^2 K_y \overline{c}_y(x, s) - s^2 K_s(s)\overline{c}_y(x, s), \tag{2.42}$$

$$= -s^2 \sum_{n=0}^{\infty} \frac{(i)^n}{n!} K_n^{(1)} \overline{c}_y^{(n)}(x, s) - s^2 \sum_{n=0}^{\infty} \frac{(i)^n}{n!} K_n^{(2)} \overline{c}_y^{(n)}(x, s). \tag{2.43}$$

Supposing a waiting time distribution, especially for the choice of a long-tailed distribution for ψ, $\psi(u) \sim 1 - (u\tau)^\gamma$ for $u \to 0$ and $k \to 0$, in the asymptotic forms $\lambda_e(k) \sim 1 - \sigma^\mu |k|^\mu$ for

the cosine transform, after a tricky development. We encounter a situation where the Laplace transform of the sticking probability is:

$$\phi(k, u) = \frac{1 - \psi(u)}{u} \frac{1}{1 - \psi(k, u)}, \tag{2.44}$$

the term $\frac{[1 - \psi(u)]}{u}$ is the Laplace transformed sticking probability

$$\Phi(t) = 1 - \int_0^t dt' \psi(t'). \tag{2.45}$$

Accordingly to Weiss treatise [189], in the Fourier-Laplace space

$$u\bar{c}_y(k, u) - \bar{c}_y(k, 0) = u\psi(u)\phi(k)\bar{c}_y(k, u) - \psi(u)\bar{c}_y(k, 0), \tag{2.46}$$

the Fourier transform of $\phi(k)$ correspond to an operator in k, thus

$$\phi(k)\bar{c}_y(k, x) \equiv \lambda_c(k)\bar{c}_y(k, x). \tag{2.47}$$

Assuming that sub-diffusion is symbolized by a finite transfer variance Σ^2, for small k, yields

$$\bar{c}_y(k, u) - \frac{\bar{c}_y(k, 0)}{u} = u^{-\alpha} L(y, z)\bar{c}_y(k, u). \tag{2.48}$$

Using the definition of the Riemann-Liouville fractional differentiation of order $1 - \alpha$, $0 < \alpha < 1$

$$_0D_x^{1-\alpha}\bar{c}_y(k, u) = \frac{1}{\Gamma(\alpha)} \frac{\partial}{\partial x} \int_0^x dx' \frac{\bar{c}_y(k, x')}{(x - x')^{1-\alpha}}. \tag{2.49}$$

By integrating the corresponding formula

$$\mathscr{L}\left\{_0D_x^{-\alpha}\bar{c}_y(k, x)\right\} = u^{-\alpha}\bar{c}_y(k, u), \tag{2.50}$$

we obtain the fractional partial equation

$$\frac{\partial \bar{c}_y(k, u)}{\partial x} =_0 D_x^{1-\alpha} L(y, z)\bar{c}_y(k, u), \tag{2.51}$$

considering the operator

$$L(y, z) = \frac{\partial}{\partial z}\left[K_z\frac{\partial}{\partial z}\right] + K_y\frac{\partial^2}{\partial y^2}. \tag{2.52}$$

Let introduce the ansatz

$$\bar{c}(x, y, z) = X_n(x)Y_n(y)Z_n(z), \tag{2.53}$$

The resulting equation

$$\frac{dX(x)}{dx}({}_0D_x^{1-\alpha}X)^{-1} = \frac{L(y, z)YZ}{YZ} \tag{2.54}$$

is then separated into the pair of eigen-equations [190]

$$_0D_x^\alpha X(x) - \frac{x^{-\alpha}\delta(0)}{\Gamma(1-\alpha)} = L(y, z). \tag{2.55}$$

for an eigenvalue $\lambda_{n,\alpha}$ of $L(y, z)$ and $u(z) = 1$ for simplification. We find, the fractional generalized diffusion equation:

$$\frac{\partial^\alpha \bar{c}(x, y, z)}{\partial x^\alpha} - \frac{x^{-\alpha}\delta(x)}{\Gamma(1-\alpha)} = \frac{K_y}{u(z)}\frac{\partial^2 \bar{c}(x, y, z)}{\partial y^2} + \frac{K_z}{u(z)}\frac{\partial^2 \bar{c}(x, y, z)}{\partial z^2}. \tag{2.56}$$

The practical advantage of the FADE solution is that, although the differential equations containing Caputo derivatives require regular physical boundary conditions, the differential equations containing the Riemann-Liouville derivatives require non-regular boundary conditions, which are not as easy to implement and give the physical meaning of the solution [191]. Commonly, in current atmospheric dispersion models, the study parameters u and K_z are generally chosen in terms of x and z in order to counterbalance the anomalous diffusion introduced by turbulence. For the above Equation describing a feasible real problem of dispersion in the Planetary Boundary Layer (PBL). Therefore, FADE is subjected to the boundary conditions [167, 192] and [168, 193].

The solution can be obtained in the form of an ansatz

$$\bar{c}_n(x, y, z) = X_n(x)B_n(y, z). \tag{2.57}$$

This leads to two differential system equations

$$\frac{\partial^\alpha X}{\partial x^\alpha} - \frac{x^{-\alpha}}{\Gamma(1-\alpha)} + \lambda_n^2 X = 0, \tag{2.58}$$

$$\frac{K_y}{u(z)}\frac{\partial^2 B(y, z)}{\partial y^2} + \frac{1}{u(z)}\left[\frac{\partial}{\partial z}K_z\frac{\partial B(y, z)}{\partial z}\right] + \lambda_n^2 B(y, z) = 0. \tag{2.59}$$

As $\bar{c}_y(x, 0) = X(x)B(y, 0)$ for $B(y, 0) = 1$ the solution Eq. (2.58) is well-known, and given by the Mittag-Leffler function

$$X_n(x) = E_\alpha \left[-\kappa \lambda_n^2 x^\alpha \right], \tag{2.60}$$

as previously stated [194],

$$E_\alpha(x) = \sum_{n=0}^\infty \frac{x^n}{\Gamma(\alpha n + 1)}, \tag{2.61}$$

represents the Mittag-Leffler function, which can be reduced into the exponential form for $\alpha \to 1$, $E_1 \left[-\kappa \lambda_n^2 x \right] \sim \exp \left[-\kappa \lambda_n^2 x \right]$,

$$X_n(x) = A \exp \left[-\kappa \lambda_n^2 x \right], \tag{2.62}$$

, with $\lambda_n = \frac{n\pi}{h}$. The corresponding asymptotic properties [195]

$$E_\alpha \left[-\kappa \lambda_n^2 x^\alpha \right] \sim \begin{cases} 1, \ x \leqslant \lambda_n^{1/\alpha} \\ \kappa \lambda_n^{-2} x^{-\alpha}, \ x \geqslant \lambda_n^{1/\alpha}. \end{cases} \tag{2.63}$$

by choosing,

$$B_n(y, z) = Y_n(y) \psi_n(z). \tag{2.64}$$

Eq. (2.59) can be rewritten in two system equations:

$$\frac{d^2 Y_n(y)}{dy^2} + \beta_n^2 Y_n(y) = 0, \tag{2.65}$$

and

$$\frac{d}{dz} \left[K_z(z) \frac{d\psi_n(z)}{dz} \right] + \left(\lambda_n^2 u(z) - \beta_n^2 K_y \right) \psi_n(z) = 0. \tag{2.66}$$

The new eigen-equations problem Eqs. (2.65) and (2.66) can be solve considering the following method.

In the case $\alpha = 1$

Eq. (2.59) follows the traditional gaussian solution form [196]. Thus, can be expand in the form:

$$A_n(y, z) = \sum_{n=1}^\infty Y_n(y) \psi_n(z). \tag{2.67}$$

Eq. (2.59) can also be rewritten as a system of two differential equations refer (Eqs. (2.65) and (2.66)), where eigenvalues are presented in a more convenient form. The solution for Eq.

(2.65) is in the form

$$Y_\beta(y) = A(\beta)\cos(\beta y). \tag{2.68}$$

We recall that γ, β, λ are separation constants

$$\lambda_n^2(x) = \beta_n^2 f_1(x) + \gamma_n^2 f(x). \tag{2.69}$$

and

$$\sum_{j=0}^{\infty} \rightarrow \sum_{j=0}^{\infty}\sum_{i=0}^{\infty}, \int_{\Omega} dydz = \int_{-y_s}^{y_s}\int_{z_0}^{h} \tag{2.70}$$

According to the above relation, the solution of the initial problem is given in a product form like

$$c_{\gamma,\beta}(x,y,z) = [\psi_\gamma(x)Z_\gamma(z)]\,[\psi_\beta(x)Y_\beta(y)]. \tag{2.71}$$

Eq. (2.71) can be rewritten

$$\psi_\beta(x,y) = \psi_\beta(x)Y_\beta(y) = Y_\beta(y)\exp\left(-\int_0^x \beta^2 f_1(x')dx'\right). \tag{2.72}$$

i.e.,

$$\psi_\gamma(x,z) = \psi_\gamma(x)Z_\beta(z) = Z_\gamma(z)\exp\left(-\int_0^x \gamma^2 f_2(x')dx'\right). \tag{2.73}$$

Eq. (2.71) can be recasts in the form

$$c_{\gamma,\beta}(x,y,z) = \int_0^\infty B(\gamma)\psi_\gamma(x,z)d\gamma \int_0^\infty A(\beta)\psi_\beta(x,y)d\beta. \tag{2.74}$$

To determine expressions of the functions $\psi_\gamma(z)$ and $\psi_\beta(x,y)$ the source term and the initial conditions are used and enable to establish that $A(0,y) = \delta(y)$ and $B(0,z) = \delta(z - h_s)/u$. Then to find the integral related to the eigenvalues β. By using the term related to the integral one gets the following equation:

$$\psi(x,y) = \int_0^\infty A(\beta)\psi_\beta(x,y)d\beta = \int_0^\infty A(\beta)\exp^{-\beta_n^2 \frac{k_y x}{u(z)}}\cos(\beta y)d\beta. \tag{2.75}$$

Application of the initial condition yields

$$F(y) = \int_0^\infty A(\beta)\chi(\beta,y)d\beta \tag{2.76}$$

$F(y)$ represents an arbitrary function defined in a semi-interval, in terms of the solution of the auxiliary problem Eq. (2.65). Analogous procedure was found when solving transport diffusion problem [196], by the transform technique and that result can be indicated in the form

$$F(y) = \int\limits_0^\infty \chi(\beta, y) \left[\frac{2}{\pi} \int\limits_0^\infty \chi(\beta, y')F(y')dy' \right] d\beta \qquad (2.77)$$

The above equation is well-founded when $F(y)$ and $\frac{dF}{dx}$ are sectionally continuous on each finite interval of the domain. By equating Eq. (2.76) and Eq. (2.77) we obtain the representation of the coefficient $A(\beta)$

$$A(\beta) = \frac{2}{\pi} \int\limits_0^\infty \chi(\beta, y')F(y')dy'. \qquad (2.78)$$

Substituting Eq. (2.78) into Eq. (2.75) yields the solution of the initial problem

$$\psi(x, y) = \int\limits_0^\infty \exp^{-\beta_n^2 \frac{k_y x}{u(z)}} \frac{2}{\pi} \chi(\beta, y) \int\limits_0^\infty \chi(\beta, y')F(y')dy' \qquad (2.79)$$

By substituting the boundary condition in the Eq. (2.79)

$$\psi(x, y) = \frac{2}{\pi} \int\limits_0^\infty \int\limits_0^\infty \exp^{-\beta_n^2 \frac{k_y x}{u(z)}} \delta(y - y') \cos(\beta y) \cos(\beta y')d\beta dy'. \qquad (2.80)$$

$$\psi(x, y) = \frac{2}{\pi} \int\limits_0^\infty \delta(y - y') \left[\frac{1}{4} \sqrt{\frac{\pi}{\frac{k_y x}{u(z)}}} \left(\exp\left[-\frac{(y - y')^2}{4\frac{k_y x}{u(z)}} \right] + \exp\left[-\frac{(y + y')^2}{4\frac{k_y x}{u(z)}} \right] \right) \right] dy'. \qquad (2.81)$$

$$\psi(x, y) = \frac{1}{2} \sqrt{\frac{1}{\pi \frac{k_y x}{u(z)}}} \exp\left[-\frac{(y - y')^2}{4\frac{k_y x}{u(z)}} \right]. \qquad (2.82)$$

Similarly, one gets

$$Z_\gamma(z) = B(\gamma)\cos(\gamma z). \qquad (2.83)$$

$$\psi(x, z) = \int\limits_0^\infty B(\gamma)\psi_\gamma(x, z)d\gamma = \int\limits_0^\infty B(\gamma)\exp^{-\gamma_n^2 \frac{k_z x}{u(z)}} \cos(\gamma z)d\gamma. \qquad (2.84)$$

The application of the initial condition yields

$$G(z) = \int\limits_0^\infty B(\gamma)\chi(\gamma, z)d\gamma \qquad (2.85)$$

$G(z)$ represents an arbitrary function defined in a semi-interval, in terms of the solution of the auxiliary problem. Using the transform technique one gets

$$G(z) = \int_0^\infty \chi(\gamma, z) \left[\frac{2}{\pi} \int_0^\infty \chi(\gamma, z')G(z')dz' \right] d\gamma \qquad (2.86)$$

The above equation is well-founded when $G(z)$ and $\frac{dG}{dx}$ are sectionally continuous on each finite interval of the domain. By equating Eqs. (2.85) and (2.86) we obtain the representation of the coefficient $B(\gamma)$

$$B(\gamma) = \frac{Q}{\pi} \int_0^\infty \chi(\gamma, z')G(z')dz'. \qquad (2.87)$$

The substitution of the Eq. (2.87) into Eq. (2.84) yields the solution of the initial problem

$$\psi(x, z) = \int_0^\infty \exp^{-\gamma_n^2 \frac{k_z x}{u(z)}} \frac{Q}{\pi} \chi(\gamma, z) \int_0^\infty \chi(\gamma, z')G(z')dz' \qquad (2.88)$$

By substituting the boundary condition in the Eq. (2.88)

$$\psi(x, z) = \frac{Q}{\pi} \int_0^\infty \int_0^\infty \exp^{-\gamma_n^2 \frac{k_z x}{u(z)}} \delta(z - z') \cos(\gamma z) \cos(\gamma z') d\gamma dz'. \qquad (2.89)$$

$$\psi(x, z) = \frac{Q}{\pi} \int_0^\infty \delta(z - z') \left[\frac{1}{4} \sqrt{\frac{\pi}{\frac{k_z x}{u(z)}}} \left(\exp\left[-\frac{(z - z')^2}{4\frac{k_z x}{u(z)}} \right] + \exp\left[-\frac{(z + z')^2}{4\frac{k_z x}{u(z)}} \right] \right) \right] dy'. \qquad (2.90)$$

$$\psi(x, z) = \frac{Q}{\sqrt{4\pi \frac{k_z x}{u(z)} U}} \left(\exp\left[-\frac{(z - z')^2}{4\frac{k_z x}{u(z)}} \right] + \exp\left[-\frac{(z + z')^2}{4\frac{k_z x}{u(z)}} \right] \right). \qquad (2.91)$$

Considering the following relation

$$\int_{-\infty}^{+\infty} exp^{-\frac{y^2}{\sigma_y^2}} dy = \sqrt{2}\sqrt{\pi}\sigma_y \qquad (2.92)$$

The crosswind-integrated solution is obtained

$$\bar{c}_y(x, z) = \frac{Q}{\sqrt{2\pi}U\sigma_z} \left(\exp\left[-\frac{(z + h_s)^2}{\sigma_z} \right] + \exp\left[-\frac{(z - h_s)^2}{\sigma_z} \right] \right). \qquad (2.93)$$

In the case $0 < \alpha \leq 1$

By introducing these properties

1. [197] if $\text{Re}(\alpha) \geq 0$ and $\beta \in \mathbb{C}\,(\text{Re}(\beta) > 0)$, then the equations

$$(J_{a+}^\alpha J_{a+}^\beta f)(x) = \left(J_{a+}^{\alpha+\beta} f\right)(x),\ (J_{b-}^\alpha J_{b-}^\beta f)(x) = \left(J_{b-}^{\alpha+\beta} f\right)(x) \tag{2.94}$$

are satisfied on almost all points $x \in [a, b]$ for $f \in L_p(a, b)$, $(1 \leqslant p \leqslant \infty)$; if $\alpha + \beta > 1$, then the above relations hold at any point of $[a, b]$.

2. The relation between Caputo fractional derivative and Riemanna-Liouville fractional derivative is given by the following formulas [198]

$$D_{a+}^\alpha f(x) = {}^C D_{a+}^\alpha f(x) + \sum_{i=0}^{n-1} \frac{f^{(i)}(a)}{\Gamma(i-\alpha+1)}(x-a)^{i-\alpha}. \tag{2.95}$$

As noted [199, 200], Eq. (2.58) can be solved using fractional approach solution. Thus, this equation can then be transformed using Eq. (2.95) to arrive at a known classical integral form

$$u(z)\frac{{}^C\partial^\alpha \overline{c}_y(x,z)}{\partial x^\alpha} = \frac{\partial}{\partial z}\left(K_z(z)\frac{\partial \overline{c}_y(x,z)}{\partial z}\right). \tag{2.96}$$

The analytical solution of the above equation with the boundary conditions Eqs. (2.23) and (2.24) has been obtained by taking the solution of the form

$$\overline{c}_y(x,z) = \sum_{n=0}^{N} X_n(x)c_{\lambda,\beta}(y,z). \tag{2.97}$$

Where $X_n(x)$, n =0, 1, 2, . . . are the unknown coefficients of the series. To find these coefficients $X_n(x)$ we choose the solution (2.97) to satisfy the partial differential equation (2.96) and by using properties from (2.94) and (2.95) as a result, one gets

$$\sum_{n=0}^{\infty} \frac{d^\alpha X_n(x)}{dx^\alpha} u(z)\psi_{n,m} = \sum_{n=0}^{\infty} X_n(x)\left[-K_z\alpha_{\lambda,\beta}^2\psi_{n,m} + \frac{\partial K_z}{\partial z}\left(\frac{d\psi_{n,m}}{dz}\right)\right]. \tag{2.98}$$

Multiplying both the sides of the above equation by eigenfunctions $\psi_{n,m}$ $(n, m = 0, 1, 2, ...)$ and integrating it with respect to z, we obtain a following set of first-order ordinary differential equations (ODEs)

$$\sum_{n=0}^{\infty}\left(\int_z u(z)\psi_{n,m}(z)\psi_{n,m}(z)dz\right)\frac{d^\alpha X_n(x)}{dx^\alpha}$$
$$= \sum_{n=0}^{\infty}\left[\int_z \psi_{n,m}(z)\left\{-K_z\alpha_{\lambda,\beta}^2\psi_{n,m} + \frac{\partial K_z}{\partial z}\left(\frac{d\psi_{n,m}}{dz}\right)\right\}dz\right]X_n(x). \tag{2.99}$$

This can be recasted in the matrix notation

$$\frac{d^\alpha X}{dx^\alpha} = \mathbf{F}X,\tag{2.100}$$

for $x > 0$ and $0 < \alpha \leqslant 1$.

Where $X(x)$ is a vector, the matrix $\mathbf{F}$ is defined as $\mathbf{F} = \mathbf{B}^{-1}\mathbf{E}$, α is an arbritrary non-integer value. The elements of matrices $\mathbf{B}$ and $\mathbf{E}$ are, respectively,

$$b_{n,m} = \int_z u(z)\psi_{n,m}(z)\psi_{n,m}(z)dz\tag{2.101}$$

and

$$e_{n,m} = \int_z \psi_{n,m}(z)\left\{-K_z\alpha_{\lambda,\beta}^2\psi_{n,m} + \frac{\partial K_z}{\partial z}\left(\frac{d\psi_{n,m}}{dz}\right)\right\}dz.\tag{2.102}$$

In Eqs. (2.100)-(2.102) matrices $\mathbf{B}$ and $\mathbf{E}$ are constant matrices of dimension N X N and in Eq. (2.100) $\mathbf{F}$ is a N X N matrix of the real-valued continuous functions of real variable x. The system of the non-integer dimensions differential (2.100) will have a unique solution [201]

$$X(x^\alpha) = E_\alpha\left(-d_i x^\alpha\right)X_0.\tag{2.103}$$

where d_i are the eigenvalues of matrix $\mathbf{F}$, and E_α is the Mittag-Leffler function:

$$E_\alpha\left(-d_i x^\alpha\right) = \sum_{j=0}^{\infty}\frac{(-d_i x^\alpha)^j}{\Gamma\left(j\alpha + 1\right)}\tag{2.104}$$

X_0 is a known vector with N components. To determine X_0, solution (2.97) is replaced into the source condition (Eq. (2.23))

$$u(z)\sum_{n=0}^{\infty}X_n(0)\psi_{n,m}(z) = Q\delta(z - H_s),\tag{2.105}$$

Multiplying both sides of Eq. (2.105) by eigenfunction $\psi_{n,m}$ and integrating it with respect to z, we get :

$$\sum_{n=0}^{\infty}\left(\int_z u(z)\psi_{n,m}(z)\psi_{n,m}(z)dz\right)X_n(0) = Q\psi_{n,m}(H_s)\tag{2.106}$$

or in matrix notation

$$X(0) = B^{-1}G,\tag{2.107}$$

$G = Q\psi_{n,1}(H_s)$ is a N X 1 column matrix and B is given by Eq. (2.101). Given a function f of scalar arguments and a matrix $\mathbf{F}$, thus the problem of finding a suitable definition for f(M) goes back [202]. For the choosen functional form of $K_z(x,z)$ derived in the Eq. (2.38), the matrix $\mathbf{F}$ in Eq. (2.100) can be expressed as

$$F(x) = f(x)M, \tag{2.108}$$

where M is a square matrix with elements independent of the variable x, thus refers to a constant matrix. Let M be a N X N matrix with s distinct eigenvalues $\lambda_1, ..., \lambda_s$ and let N_i be the index of λ_i, i.e the smallest integer q in order that $(M - \lambda_i I)^q = 0$ with I denoting the N X N identity matrix. Therefore, the function f is said to be defined on the spectrum of A if the values $f^{(j)}(\lambda_i)$, $j = 0, ..., n_i - 1, i = 1, ..., s$ exist. Thus for functions defined on the spectrum of M the Jordan canonical form can be of use to define matrix functions. The matrix M can be transformed into the following Jordan canonical form [203].

$$M = PJP^{-1} \tag{2.109}$$

J represents the Jordan matrix of all eigenvalues of M then P is the corresponding matrix of all linearly independent eigenvectors. As all the eigenvalues of M are distinct, J appears as a diagonal matrix. Diagonalizable matrices are favorable arguments for simple calculations; indeed a matrix is diagonalizable if there exist a non-singular matrix P and a diagonal matrix $D = diag(\lambda_1, ..., \lambda_n)$ so that $M = P^{-1}DP$. In this case $f(M) = P^{-1}f(D)P$. and $f(D)$ is still a diagonal matrix with principal entries $f(\lambda_i)$. First we find the general solution to the homogeneous system Eq. (2.100), for this we need to introduce a generalisation of the α-exponential function [204] and [205]

$$e_\alpha^{\lambda(x-l)} = (x-l)^{\alpha-1} \sum_{k=0}^{\infty} \frac{\lambda^k(x-l)^{k\alpha}}{\Gamma[(k+1)\alpha]}, \tag{2.110}$$

where $\lambda, \nu \in \mathbb{C}$, $\alpha \in \mathbb{R}^+$ and $a \in \mathbb{R}$.

Moreover, has also been established the explicit solution to the same problem expressed in terms of a certain Mittag-Leffler function; more in the form of the following general power series:

$$X(x^\alpha) = x^q \sum_{j=0}^{\infty} d_i \frac{x^{j\alpha}}{\Gamma(j\alpha + \beta)}, \tag{2.111}$$

where $0 < \alpha < 1$, and q, β are constants.

where d_i are the eigenvalues of the matrix $\mathbf{F}$ given in Eq. (2.100).

Matrix from Eq. (2.111) is a fundamental solution matrix to system (2.100); and this matrix can be written as

$$P^{-1}DP = P^{-1}\begin{bmatrix} E_\alpha(-d_1 x^\alpha) & 0 & \cdots & 0 \\ 0 & E_\alpha(-d_2 x^\alpha) & \cdots & 0 \\ \vdots & \vdots & \ddots & \ddots \\ 0 & 0 & \cdots & E_\alpha(-d_N x^\alpha) \end{bmatrix} P. \qquad (2.112)$$

The similar matrix form was obtained in a different approach by using GILTT method [206].

2.5 Analysis with existing models

In order to check the accuracy of the employed analytical solution technique given in the previous section, the solution of Eq. (2.58) given by Eq. (2.97) is reduced into some particular cases. Uniform wind speed. For the rest, we consider the crosswind-integrated concentration. The matrix B becomes a scalar matrix with the scalar u and E is a diagonal matrix with the elements

$$e_{n,n} = -\lambda_n^2 K. \qquad (2.113)$$

Therefore, the matrix F in Eq. (2.100) will be a diagonal matrix with diagonal elements

$$d_i = -\left(K/u\right)\lambda_n^2 \qquad (2.114)$$

In Eq. (2.104), the diagonalization of matrix F at once calculates the integration of F by just integrating the diagonal elements and then taking their value leading to

$$X_n\left(x^\alpha\right) = E_\alpha\left(-\left(K/u\right)\lambda_n^2 x^\alpha\right) X_n(0). \qquad (2.115)$$

In the case where from the above relation $\alpha = 1$, we end up with the classical exponential solution

$$X_n\left(x\right) = \exp\left(-\left(K/u\right)\lambda_n^2 x\right) X_n(0). \qquad (2.116)$$

The solutions $\psi_n(z)$ (n = 0, 1, 2, 3, ...) of (2.96) that satisfy the boundary conditions (2.23) with $\psi_0 = 0$ are $\psi_n(\text{z}) = b_n \cos(\lambda_n z)$ where $\lambda_n = \frac{n\pi}{h}$, and b_n is a constant. As a reult, starting

from the superposition principle, and from (2.26), by using the boundary condition (2.23), and using the identity below

$$\delta\left(x - H_s\right) = \frac{1}{h}\left[1 + 2\sum_{n=1}^{\infty}\cos\left(\lambda_n H_s\right)\cos\left(\lambda_n x\right)\right].$$ (2.117)

we obtain the crosswind integrated concentration formula (i.e. $\alpha = 1$)

$$\bar{c}_y(x, z) = \frac{Q}{Uh}\left[1 + 2\sum_{n=1}^{\infty}\cos\left(\lambda_n H_s\right)\cos\left(\lambda_n z\right)\exp\left(-k\lambda_n^2 x\right)\right].$$ (2.118)

$$\bar{c}_y(x, z) = b_0 + \sum_{n=1}^{\infty} b_n \cos(\lambda_n z) E_\alpha(-\kappa\lambda_n^2 x^\alpha).$$ (2.119)

The coefficients $X_n(0)$ in Eq. (2.107) are given by

$$X_n(0) = \frac{Q}{u}\psi_n(H_s).$$ (2.120)

In the same vein, Eq. (2.116) leads to the classical gaussian plume solution [207], for an elevated source with reflections from two parallel boundaries at z $=0$ and $z = h$.

2.6 N-truncated fractional derivative order model

The advantage of using this sort of equation is constructed on the assumptions that the solution of the cross-wind integrated concentration $\bar{c}_y = \bar{c}_y(x, z)$ is obtained by integrating the Eq. (2.56) with respect to y parameter from the initial function $\bar{c}(x, y, z)$ in the interval $-\infty$ to ∞ (refer, [208]), when $\alpha = 1$ and by neglecting the longitudinal diffusion. We operate in our calculations a translation into the space of the different equations that we have so carefully formulated. On the other hand, by taking a Fourier transform of the reshaped equation

$$u\frac{\partial\bar{c}}{\partial x} = \frac{\partial}{\partial z}\left[K_z\frac{\partial\bar{c}}{\partial z}\right],$$ (2.121)

we obtain a relaxation equation for a fixed wave number k,

$$u\frac{\partial\bar{c}(x, k)}{\partial x} = -K_z k^2 \bar{c}(x, k),$$ (2.122)

$\bar{c}(x, k)$ from (2.122) is called the propagator this means that individual modes of the above equation on rectangular domains decay exponentially in space

$$\bar{c}(x, k) = \bar{c}(0, k)\exp\left(-K_z k^2 x\right),$$ (2.123)

where we set for some practical requirements $u = 1$. Therefore, for a gaussian process, individual modes of the concentration pursues an exponential distribution in the longitudinal spatial x-direction. Indeed, the Gaussian distribution for the concentration (2.122) and its individual modes exponential distribution (2.123) are indicative of the normal diffusive process, displaying a linear mean squared displacement

$$\left\langle z^2(x) \right\rangle = -\lim_{k \to 0} \frac{d^2}{dk^2} \overline{c}(x, k) = 2K_z x. \tag{2.124}$$

under other conditions, in most cases, the anomalous process highlights a power-law mean squared displacement $\langle z^2 \rangle \propto x^\alpha$ with $0 < \alpha < 1$ [209]. This power law follows directly from the Fourier-Laplace concentration function [209]

$$\overline{c}(s, k) = \frac{\overline{c}(o, k)}{s + K_z s^{1-\alpha} k^2}, \tag{2.125}$$

since

$$\left\langle z^2(x) \right\rangle = -\mathscr{L}^{-1} \left\{ \lim_{k \to 0} \frac{d^2}{dk^2} \overline{c}(s, k) \right\} = \frac{2K_z}{\Gamma(\alpha + 1)} x^\alpha, \tag{2.126}$$

where $\Gamma(\cdot)$ represents the Gamma function and $\mathscr{L}^{-1}$ stands for the inverse Laplace transform. Besides, from the Laplace transform for fractional Riemann-Liouville integrals [210, 211]

$$\mathscr{L}\left\{ {}_0I_x^\alpha f(x) \right\} = s^{-\alpha} f(s), \tag{2.127}$$

we can deduce from (2.125) the steady-state fractional advection-diffusion integral equation

$$\overline{c}(x, z) - \overline{c}(0, z) = {}_0I_x^\alpha K_z \frac{\partial^2 \overline{c}(x, z)}{\partial z^2}. \tag{2.128}$$

by taking $u = 1$. Here and for a logical continuation of our work we set without loss of generality $a = 0$. Furthermore, by taking the derivative of (2.128) in the spatial domain we obtain a Riemann-Liouville fractional differential equation

$$\frac{\partial \overline{c}(x, z)}{\partial x} = \frac{\partial^{1-\alpha}}{\partial x^{1-\alpha}} K_z \frac{\partial^2 \overline{c}(x, z)}{\partial z^2}. \tag{2.129}$$

Albeit it is well known that fractional differential equations depict more practically the time evolution of anomalous diffusive systems [212, 213, 214], let us recast (2.129) in a more adequate expression. Given that for continuum functions $f(x)$ we obtain ${}_0I_x^\alpha {}_0D_x^\alpha f(x) = {}_0D_x^\alpha {}_0I_x^\alpha f(x) = f(x)$, and ${}_0I_x^\alpha {}_0I_x^\beta = {}_0I_x^{\alpha+\beta}$ [215, 216, 217, 218], after some tricky manipulations we arrive at

$$\frac{\partial^\alpha \overline{c}(x, z)}{\partial x^\alpha} - \frac{x^{-\alpha}}{\Gamma(1-\alpha)} \overline{c}(0, z) = K_z \frac{\partial^2 \overline{c}(x, z)}{\partial z^2}. \tag{2.130}$$

At last

$$^{C}_{0}D^{\alpha}_{x}f(x) = {}_{0}D^{\alpha}_{x}f(x) - \frac{f(0)}{\Gamma(1-\alpha)}x^{-\alpha} \tag{2.131}$$

for $0 < \alpha < 1$ [219, 220]

$$u\frac{^{C}\partial^{\alpha}\overline{c}(x,z)}{\partial x^{\alpha}} = K_{z}\frac{\partial^{2}\overline{c}(x,z)}{\partial z^{2}}. \tag{2.132}$$

Now, Eq. (2.132) can be analytically solved by using separation of variables method to obtain the solution of the M-fractional advection dispersion equation. We arrive at the main Eq. (2.132) that describes the mathematical model of our study case. We assumed that (2.132) has a solution of the form

$$\overline{c}_{y}(x,z) = P(x)Q(z). \tag{2.133}$$

Then, considering the above relation, from this equation, we obtain a system of differential equations, given by

$$^{C}_{0}D^{\alpha,\beta}_{x}P(x) + \kappa\lambda^{2}P(x) = 0, \tag{2.134}$$

and

$$\frac{d^{2}Q(z)}{dz^{2}} + \lambda^{2}Q(z) = 0. \tag{2.135}$$

We start, considering the so-called M-fractional linear differential equation with constant coefficients Eq. (2.134), where λ^{2} is a positive constant. The above equation can be written as follows:

$$\frac{x^{1-\alpha}}{\Gamma(\beta+1)}\frac{dP(x)}{dx} \pm \kappa\lambda^{2}P(x) = 0, \tag{2.136}$$

using chain rule Eq. (2.11) (Property), the Eq. (2.136) can be expressed in the form :

$$_{i}D^{\alpha,\beta}_{N}P(x) - \kappa\lambda^{2}P(x) = 0, \tag{2.137}$$

with $\kappa \sim \gamma \cdot x^{\alpha}$

whose solution is:

$$P(x) = C \cdot \mathbb{E}_{\beta}(-\lambda^{2}_{n}\kappa x^{\alpha}). \tag{2.138}$$

in a parallel approach:

We are now studying a particular case involving fractional derivative. Choosing $\beta = 1$ and applying the limit $i \to 0$ on either side of Eq. (2.11), we have:

$$_iD_N^{\alpha,\beta}f(x) = \lim_{h \to 0} \frac{f(x_i\mathbb{E}_\beta(hx^{-\alpha})) - f(x)}{h}, \tag{2.139}$$

it is also known that

$$_1\mathbb{E}_{\beta_1}(hx^{-\alpha})) = \sum_{k=0}^{1} \frac{(hx^{-\alpha})^k}{\Gamma(k+1)} = 1 + hx^{-\alpha}, \tag{2.140}$$

so, we conclude that

$$_iD_N^{\alpha,\beta}f(x) = \lim_{h \to 0} \frac{f(x_i\mathbb{E}_\beta(hx^{-\alpha})) - f(x)}{h} = f^\alpha(x). \tag{2.141}$$

so that a trivial solution of Eq. (2.137) can be in the form:

$$P(x^\alpha) = P_0\mathbb{E}_\alpha\left(-\lambda_n^2\kappa x^\alpha\right), \tag{2.142}$$

where $\mathbb{E}_\alpha$ represents the Mittag-Leffler function.

In the same line, the solutions $Q_n(z)(n = 0, 1, 2, 3, ...)$ of (2.135) that satisfy the boundary conditions

$$K_z\frac{\partial\bar{c}_y}{\partial z} = 0, \; z = z_0 \cdots h \text{ with } z_0 = 0 \tag{2.143}$$

are obtained at the same time, using the equation: $Q_n(z) = Q_n cos(\lambda_n z)$ where $\lambda_n = \frac{n\pi}{h}$, and assuming that Q_n is a constant, from the superposition principle, we arrive at the following formula:

$$\bar{c}_y(x,z) = Q_0 + \sum_{n=1}^{+\infty} Q_n cos(\lambda_n z)\mathbb{E}_\beta(-\lambda_n^2\kappa x^\alpha). \tag{2.144}$$

Finally, by introducing the boundary condition (2.23) and using the identity

$$\delta(z - h_s) \times h = 1 + 2\sum_{n=1}^{+\infty} Q_n cos(\lambda_n z)cos(\lambda_n h_s), \tag{2.145}$$

we end up at the final Eq. (2.118).

2.7 Comparison with existing models

2.7.1 FADE equation solutions

Eq. (2.37) is frequently simplified by integrating over all cross-wind directions to obtain an equation in two dimensions (x, z) the so-called cross-wind integrated concentration.

2.7.2 $K_z^{'}(x,z)$ as a function of z only

f(x)=1

$$\bar{c} \simeq \frac{Q}{Uh} \left[1 + 2 \sum_{n=1}^{\infty} \cos(\lambda_n z) \cos(\lambda_n h_s) \exp(-\lambda_n^2 \sigma_z^2) \right], \tag{2.146}$$

2.7.3 U(z) and $K_z^{'}(x,z)$ are constant

- **Classical gaussian plume model**

$$\bar{c}_1 \simeq \frac{Q}{Uh} \left[1 + 2 \sum_{n=1}^{\infty} \cos(\lambda_n z) \cos(\lambda_n h_s) \exp\left(-\frac{(n\pi)^2 K_z x}{Uh^2} \right) \right], \tag{2.147}$$

- **α-gaussian model**

$$\bar{c}_2 \simeq \frac{Q}{Uh} \left[1 + 2 \sum_{n=1}^{\infty} \cos(\lambda_n z)) \cos(\lambda_n h_s) E_\alpha \left(-\frac{(n\pi)^2 K_z x^\alpha}{Uh^2} \right) \right], \tag{2.148}$$

2.7.4 U(z) and $K_z(x,z) = f(x)$ as a function of z only

$$\bar{c} \simeq \frac{Q}{\sqrt{2\pi}U\sigma_z} \left[\exp^{\left(-\frac{(z+h_s)^2}{\sigma_z^2} \right)} + \exp^{\left(-\frac{(z-h_s)^2}{\sigma_z^2} \right)} \right]. \tag{2.149}$$

2.7.5 M-fractional type equation solutions

So, using the theorem mentioned in the beginning and Eq. (2.132), the solution for the M-fractional type subject to the boundary conditions Eq. (2.23) and Eq. (2.143) can be obtained with $z_0 \sim 0$

$$\bar{c}_y(x,z) = \frac{Q}{uh} \left[1 + 2 \sum_{n=1}^{\infty} cos(\lambda_n h_s) cos(\lambda_n z) \mathbb{E}_\beta \left(-\lambda_n^2 \kappa x^\alpha \right) \right]. \tag{2.150}$$

The crosswind-integrated concentration, is intrinsically a smoother variable because it integrated over a collection of samplers and is thus less susceptible to minor variations in sample performance. Moreover, it avoids difficulties which occur when its distribution is found to be non-gaussian.

2.7.6 Classical gaussian model

On the other hand, taking the limit $\beta \to 1$ and $\alpha \to 1$, using Eq. (2.11), we recover the solution of traditional advection dispersion equation of integer order

$$\bar{c}_y(x,z) = \frac{Q}{uh} \left[1 + 2 \sum_{n=1}^{\infty} cos(\lambda_n h_s) cos(\lambda_n z) exp \left(-\lambda_n^2 \kappa x \right) \right]. \tag{2.151}$$

2.7.7 α-gaussian model

Otherwise, taking the limit $\beta \to 1$ and $i \to 0$, using Eq. (2.11) we recover, as previously noted [221] the solution of the solution for the $\alpha-$Gaussian model

$$\overline{c}_y(x,z) = \frac{Q}{uh}\left[1 + 2\sum_{n=1}^{\infty} cos(\lambda_n h_s)cos(\lambda_n z)\mathbb{E}_\alpha\left(-\lambda_n^2 \kappa x^\alpha\right)\right]. \qquad (2.152)$$

2.8 Dynamics of the non-linear fractional evolutive equations in the atmosphere

In this decades, an excellent deal of attention is devoted to application of fractional calculus to almost every field of science. We notice that more pronounced effects and deeper insight into the formation and properties of the resulting traveling waves by additionally considering the fractional order derivative beside the non-linearity and dispersion terms.

2.8.1 Mathematical analysis of the solutions

In this section, we describe the main steps of the (G'/G, 1/G)-expansion method for finding of the time-fractional KdV-mKdV equation [222, 223, 224]. As introductions, consider the second order linear ordinary differential equation (ODE)

$$G''(\xi) + \lambda G(\xi) = \mu, \qquad (2.153)$$

and we bring out

$$\phi = \frac{G'}{G}, \text{and } \psi = \frac{1}{G} \qquad (2.154)$$

for practicability henceforward

$$\phi' = -\phi^2 + \mu\psi - \lambda, \ \psi' = -\phi\psi. \qquad (2.155)$$

From the three scenarii of the general solutions of the Linear ordinary differential equation (2.153), one gets:

Observation 1 If $\lambda < 0$, the general solutions of (2.153)

$$G(\xi) = A_1 \sinh(\sqrt{-\lambda}\xi) + A_2 \cosh(\sqrt{-\lambda}\xi) + \frac{\mu}{\lambda}, \qquad (2.156)$$

in this case,

$$\psi^2 = \frac{-\lambda}{\lambda^2\sigma + \mu^2}(\phi^2 - 2\mu\psi + \lambda) \tag{2.157}$$

where A_1 and A_2 are two arbitrary constants and $\sigma = A_1^2 - A_2^2$.

Observation 2 If $\lambda > 0$, the general solutions of (2.153)

$$G(\xi) = A_1\sin(\xi\sqrt{\lambda}) + A_2\cos(\xi\sqrt{\lambda}) + \frac{\mu}{\lambda} \tag{2.158}$$

and thus,

$$\psi^2 = \frac{\lambda}{\lambda^2\sigma - \mu^2}(\phi^2 - 2\mu\psi + \lambda), \tag{2.159}$$

where $\sigma = A_1^2 - A_2^2$.

Observation 3 If $\lambda = 0$, the general solutions of (2.153)

$$G(\xi) = \frac{\mu}{2}\xi^2 + A_1\xi + A_2, \tag{2.160}$$

therefore,

$$\psi^2 = \frac{1}{A_1^2 - 2\mu A_2}(\phi^2 - 2\mu\psi). \tag{2.161}$$

At once, is given an illustration how this method operates. Thus, consider a non-linear evolution equation, say in two independent variables x and t,

$$Q = (u, u_t, u_x, u_{xx}, u_{tt}, ...), \tag{2.162}$$

with $u = u(x,t)$ as an unknown function. By wave transformation $u(x,t) = u(\xi)$, $\xi = x - Vt$ Eq. (2.162) can be reduced to an ODE for $u(\xi)$

$$Q' = (u, u', u''...) = 0. \tag{2.163}$$

Introducing the assumption that the solution of ODE (2.163) can be expressed by a polynomial ϕ and ψ as

$$u(\xi) = \sum_{i=0}^{N} a_i\phi^i + \sum_{i=1}^{N} b_i\phi^{i-1}\psi, \tag{2.164}$$

where $a_i(i = 0, 1, ..., N)$ and $b_i(i = 1, ..., N)$ are constants to be determined later. N represents a positive integer that can be determined by employing homogeneous balance between

the highest order derivative and the highest nonlinear term emerging in ODE (2.163). Substituting (2.164) into (2.163) along with (2.155) and (2.157), Eq. (2.163) can be converted into a polynomial in ϕ and in ψ. Matching the coefficients of each power of $\phi^i \psi^j$ to zero gives a system of algebraic equation for $a_i b_i V \mu A_1 A_2$ and λ. The algebraic system is solved with the aid of maple. Therefore, is obtained the general solutions in terms of the hyperbolic functions for $\lambda < 0$. Also, is get the general solutions in terms of the trigonometric function for $\lambda > 0$. And is retrieved the general solutions in terms of the rational function for $\lambda = 0$.

2.8.2 Motion of the bounded particle of the atmosphere solitary waves

The KdV-mKdV equation primarily characterizes the propagation of bounded particle of the atmosphere dust-acoustic solitary waves, internal solitary waves in shallow seas and ions acoustic waves in plasmas with negative ions [225]. The regular KdV-mKdV equation is given by [226]

$$u_t(x,t) + au(x,t)u_x(x,t) + bu^2(x,t)u_x(x,t) + \gamma u_{xxx}(x,t) = 0 \qquad (2.165)$$

u depends on $u(x,t)$ and $u(x,t)$ is a field variable, $x \in \Omega$ is a space coordinate in the propagation direction of the field and $t \in T$ is the time. Applying a potential function $v(x,t)$, specifying $u(x,t) = v_x(x,t)$, yields the potential equation of the KdV-mKdV Eq. (2.165) in the form

$$v_{xt}(x,t) + av_x(x,t)v_{xx}(x,t) + bv_x^2(x,t)v_{xx}(x,t) + \gamma v_{xxxx}(x,t) = 0 \qquad (2.166)$$

The indices indicate the partial differentiation of the function according to the parameter. The Lagrangian of the KdV-mKdV equation (2.165) can be defined implementing the semi-inverse method [227] in such a way

$$\begin{aligned} J(v) = \int\limits_{\Omega} dx \int\limits_{T} dt (v(x,t)(c_1 v_{xt}(x,t) + c_2 av_x(x,t)v_{xx}(x,t) + bc_3 v_x^2(x,t)v_{xx}(x,t) \\ + \gamma c_4 v_{xxxx}(x,t)), \end{aligned} \qquad (2.167)$$

where $c_i(i \cdot \cdot 4)$ are unidentified constants to be adjusted next [228].

Note that the unidentified constants turn to

$c_1 = -\frac{1}{2}$, $c_2 = -\frac{1}{3}$, $c_3 = -\frac{1}{4}$, $c_4 = -\frac{1}{2}$.

Hence, the functional expression given leads immediately the Lagrangian form of the KdV-mKdV equation,

$$L(v_t, v_x, v_{xx}) = \frac{1}{2} v_x(x,t) v_t(x,t) + \frac{1}{6} a v_x^3(x,t) + \frac{1}{12} b v_x^4(x,t) + \frac{1}{2} \gamma v_{xx}^2(x,t). \tag{2.168}$$

Since $\alpha < 1$, the fractional operator $_0^R D_t^\alpha$ can be reduced to the fractional integral one. This involves that, one can depict the fractional operator as the Riesz fractional integral [229]

$$_0^R D_t^\alpha g(t) = \frac{1}{2} \left[_0 D_t^\alpha g(t) +_t D_{T0}^\alpha g(t) \right] = \frac{1}{2} \frac{1}{\Gamma(\alpha)} \int_a^b d\tau \, |t - \tau|^{\alpha-1} f(\tau), \alpha > 0. \tag{2.169}$$

Assuming that $_0 D_t^\alpha g(t)$ and $_t D_{T0}^\alpha g(t)$ are left and right Riemann-Liouville fractional integrals, respectively.

Physical meaning, if t indicates the time-variable, the right Riemann-Liouville fractional derivative is perceived as a future state of the process. For this justification, the right-derivative is often neglected in applications, when the present state of the process does not depend on the results of the upcoming process [230]. Thus, the right-derivative is regarded as equal to zero in the framework below. The time-fractional KdV-mKdV equation can be written as

$$_0 D_t^\alpha u(x,t) + au(x,t)u_x(x,t) + bu^2(x,t)u_x(x,t) + \gamma u_{xxx}(x,t) = 0, \text{where } 0 < \alpha \le 1. \tag{2.170}$$

Thus, the governing equation, the time-fractional combined KdV-mKdV equation [231], is given by

$$D_t^\alpha u + auu_x + bu^2 u_x + \gamma u_{xxx} = 0 \tag{2.171}$$

where a, b, γ are the constants and α represents the fractional order whose range is $0 < \alpha \le 1$.

The non-linear fractional partial differential equation with two independent variables is considered as follows

$$F(u, u_x, u_{xx}, u_{xxx}, ... D_t^\alpha u, ...) = 0, \; 0 < \alpha \le 1 \tag{2.172}$$

where F is a polynomial in $u(x,t)$ and other highest order partial derivatives with non-linear terms also involved. The solution of equation (2.172) is given here using fractional complex transform [232] characterized in the following form

$$u(x,t) = \Phi(\xi), \; \xi = cx + \frac{kt^\alpha}{\Gamma(\alpha + 1)} \tag{2.173}$$

where c and k are constants. Using (2.173)[233, 234], the FPDE (2.172) can be reduced to the following (ODE)

$$F(\Phi, c\Phi', c^2\Phi'', c^3\Phi''', ..., k\Phi', ...) = 0. \qquad (2.174)$$

The method has been applied for obtaining the exact solution for (2.171). Now using the fractional complex transform (2.173) in (2.171) we have the non-linear (ODE) as follows

$$k\Phi'(\xi) + ac\Phi(\xi)\Phi'(\xi) + bc^3\Phi^2(\xi)\Phi'(\xi) + \gamma c^3\Phi'''(\xi) = 0. \qquad (2.175)$$

Eq. (2.175) is integrable, thus integrating with respect to ξ once yield

$$k\Phi(\xi) + \frac{1}{2}ac\Phi^2(\xi) + \frac{1}{3}bc^3\Phi^3(\xi) + \gamma c^3\Phi''(\xi) = 0. \qquad (2.176)$$

where integration constants are considered as zero. By balancing $\Phi^3(\xi)$ and $\Phi''(\xi)$ one gets

$$N + 2 = 3N$$
$$N = 1. \qquad (2.177)$$

Therefore from (2.177) the solution of (2.176) is of the form

$$\Phi(\xi) = a_0 + a_1\phi(\xi) + b_1\psi(\xi). \qquad (2.178)$$

Where a_0, a_1 and b_1 are constants to be determined later.

The general solutions of NPDEs give information about the character of the physical phenomena. For better understanding of non-linear phenomena as well as further applications in practical life, it is more significant to establish exact traveling wave solutions. Non-linear partial differential equations (PDEs) play a vital role in the field of science and engineering, such as fluid mechanics, plasma physics, solid state physics, chemical physics, quantum mechanics, optical fibres, electricity, geochemistry, meteorology and many others. Due to important applications of non-linear PDEs in real world problems, it is required to generate their analytical solutions. With the help of analytical solutions, if exist, the phenomena modelled can be better understood by these non-linear PDEs. On the other hand, the Korteweg-de Vries (KdV) equation has been used to describe a wide range of physics phenomena as a model for the evolution and interaction of non-linear waves. It was first derived as an evolution equation that governing a one dimensional, small amplitude, long surface gravity waves propagating in a shallow channel of water.

Case 1 For $\lambda < 0$, resulting to hyperbolic function solutions, substituting (2.178) into (2.176), using (2.155) and (2.157). We have a polynomial in ϕ and ψ which yields a set of algebraic equations.

$$
\left[2\gamma c^3 a_1 - \frac{bc^3 a_1 b_1^2 \lambda}{\lambda^2 \sigma + \mu^2} + \frac{1}{3} bc^3 a_1^3 \right] \phi^3(\xi)
$$

$$
+ \left[\left(-\frac{2}{3} \frac{bc^3 b_1^3 \lambda}{2\lambda^2 \sigma + 2\mu^2} + bc^3 a_1^2 b_1 + 2\gamma c^3 b_1 \right) \psi(\xi) - \frac{bc^3 a_0 b_1^2 \lambda}{\lambda^2 \sigma + \mu^2} - \frac{1}{2} \frac{acb_1^2 \lambda}{\lambda^2 \sigma + \mu^2} + \frac{1}{2} aca_1^2 \right.
$$

$$
\left. + bc^3 a_0 a_1^2 - \frac{4}{3} \frac{bc^3 b_1^3 \lambda^2 \mu}{(\lambda^2 \sigma + \mu^2)(2\lambda^2 \sigma + 2\mu^2)} + \frac{\gamma c^3 b_1 \mu \lambda}{\lambda^2 \sigma + \mu^2} \right] \phi^2(\xi)
$$

$$
+ \left[\left(\frac{2bc^3 a_1 b_1^2 \lambda \mu}{\lambda^2 \sigma + \mu^2} - 3\gamma c^3 a_1 \mu + 2bc^3 a_0 a_1 b_1 + aca_1 b_1 \right) \psi(\xi) + \right.
$$

$$
ka_1 - \frac{bc^3 a_1 b_1^2 \lambda^2}{\lambda^2 \sigma + \mu^2} + aca_0 a_1 + 2\gamma c^3 a_1 \lambda + bc^3 a_0^2 a_1 \right] \phi(\xi) + \left[aca_0 b_1 + kb_1 - \frac{1}{3} \frac{bc^3 b_1^3 \lambda \left(-\frac{8\lambda \mu^2}{\lambda^2 \sigma + \mu^2} + 2\lambda \right)}{2\lambda^2 \sigma + 2\mu^2} \right.
$$

$$
\left. + \frac{acb_1^2 \lambda \mu}{\lambda^2 \sigma + \mu^2} + \frac{2bc^3 a_0 b_1^2 \lambda \mu}{\lambda^2 \sigma + \mu^2} + bc^3 a_0^2 b_1 + \gamma c^3 b_1 \left(-\frac{2\lambda \mu^2}{\lambda^2 \sigma + \mu^2} + \lambda \right) \right] \psi(\xi) +
$$

$$
ka_0 - \frac{bc^3 a_0 b_1^2 \lambda^2}{\lambda^2 \sigma + \mu^2} - \frac{4}{3} \frac{bc^3 b_1^3 \lambda^3 \mu}{(\lambda^2 \sigma + \mu^2)(2\lambda^2 \sigma + 2\mu^2)} + \frac{1}{2} aca_0^2 - \frac{1}{2} \frac{acb_1^2 \lambda^2}{\lambda^2 \sigma + \mu^2} + \frac{1}{3} bc^3 a_0^3 + \frac{\gamma c^3 b_1 \mu \lambda^2}{\lambda^2 \sigma + \mu^2}.
\tag{2.179}
$$

Solving the algebraic equations by Maple, we obtain the roots of Eq. (2.179).

$$
a_0 = -\frac{1}{2} \frac{a}{bc^2}, \ a_1 = \pm \frac{3\gamma}{\sqrt{-6b\gamma}}, \ b_1 = \pm \sqrt{\lambda(\lambda^2 \sigma + \mu^2)} \left(\pm \frac{3\gamma}{\lambda\sqrt{-6b\gamma}} \right),
$$

$$
k = \frac{\alpha a^2 + 2\beta b \gamma c^4}{4bc}, \ i = \sqrt{-1}, \ \lambda^2 \sigma + \mu^2 \neq 0.
\tag{2.180}
$$

Where $\alpha = \frac{2\mu^2}{3\lambda^2 \sigma}$ and $\beta = \frac{2\lambda(\sigma \lambda^2 + \mu^2)}{\sigma}$. By choosen parameters α and $\beta \sim 1$ namely terms embedded specifics to the dispersive milieu which has be found to describe physical phenomenon as turbulence [235] or theory of flow through wave traveling in viscous fluid [236]. We retrieve the same value $k = \frac{a^2 + 2b\gamma c^4}{4bc}$ in the method approach used by [237] to solve the time-fractional KdV-mKdV equation. Substituting (2.180) into (2.178) we obtain the following solutions of Eq. (2.171)

Family 1.1

$$
\Phi(\xi) = -\frac{1}{2} \frac{a}{bc^2} \pm \frac{3\gamma}{\sqrt{-6b\gamma}} \left(\frac{A_1\sqrt{-\lambda}\cosh(\sqrt{-\lambda}\xi) + A_2\sqrt{-\lambda}\sinh(\sqrt{-\lambda}\xi)}{A_1\sinh(\sqrt{-\lambda}\xi) + A_2\cosh(\sqrt{-\lambda}\xi) + \frac{\mu}{\lambda}} \right)
$$

$$
\pm \sqrt{\lambda(\lambda^2 \sigma + \mu^2)} \left(\pm \frac{3\gamma}{\lambda\sqrt{-6b\gamma}} \right) \left(\frac{1}{A_1\sinh(\sqrt{-\lambda}\xi) + A_2\cosh(\sqrt{-\lambda}\xi) + \frac{\mu}{\lambda}} \right)
\tag{2.181}
$$

where $\sigma = A_1^2 - A_2^2$.

Family 1.2 In particular if we set $A_1 = 0$, $A_2 > 0$ and $\mu = 0$ in (2.181) then we obtain solitary solution

$$
\Phi(\xi) = -\frac{1}{2}\frac{a}{bc^2} \pm \frac{3\gamma}{\sqrt{-6b\gamma}}\left(\sqrt{-\lambda}\tanh(\sqrt{-\lambda}\xi)\right)
$$
$$
\pm\sqrt{\lambda\sigma}\left(\pm\frac{3\gamma}{\sqrt{-6b\gamma}}\right)\left(\frac{1}{A_2}\sec h(\sqrt{-\lambda}\xi)\right)
\tag{2.182}
$$

Family 1.3 For $A_2 = 0$, $A_1 > 0$ and $\mu = 0$ in (2.181) then we have the solitary solution

$$
\Phi(\xi) = -\frac{1}{2}\frac{a}{bc^2} \pm \frac{3\gamma}{\sqrt{-6b\gamma}}\sqrt{-\lambda}\coth(\sqrt{-\lambda}\xi)
$$
$$
\pm\sqrt{\lambda\sigma}\left(\pm\frac{3\gamma}{\sqrt{-6b\gamma}}\right)\frac{1}{A_1}\csc h(\sqrt{-\lambda}\xi).
\tag{2.183}
$$

Case 2 For $\lambda > 0$ arising from Trigonometric function solutions, substituting (2.178) into (2.176) and using (2.155) and (2.159). We have a polynomial in ϕ and ψ. Vanishing each coefficient yields a set of algebraic equations

$$
\left(\frac{bc^3a_1b_1^2\lambda}{\lambda^2\sigma - \mu^2} + 2\gamma c^3 a_1 + \frac{1}{3}bc^3 a_1^3\right)\phi^3(\xi)
$$
$$
+\left[\left(\frac{2}{3}\frac{bc^3b_1^3\lambda}{2(\lambda^2\sigma - \mu^2)} + bc^3 a_1^2 b_1 + 2\gamma c^3 b_1\right)\psi(\xi) + \frac{bc^3 a_0 b_1^2\lambda}{\lambda^2\sigma - \mu^2} + \frac{1}{2}\frac{acb_1^2\lambda}{\lambda^2\sigma - \mu^2} + \frac{1}{2}aca_1^2\right.
$$
$$
\left. +bc^3 a_0 a_1^2 - \frac{4}{3}\frac{bc^3 b_1^3\lambda^2\mu}{2(\lambda^2\sigma - \mu^2)(\lambda^2\sigma - \mu^2)} - \frac{\gamma c^3 b_1 \mu\lambda}{\lambda^2\sigma - \mu^2}\right]\phi^2(\xi)+
$$
$$
\left[\left(-\frac{2bc^3 a_1 b_1^2\lambda\mu}{\lambda^2\sigma - \mu^2} + 2bc^3 a_0 a_1 b_1 + aca_1 b_1 - 3\gamma c^3 a_1\mu\right)\psi(\xi)+\right.
$$
$$
\frac{bc^3 a_1 b_1^2\lambda^2}{\lambda^2\sigma - \mu^2} + bc^3 a_0^2 a_1 + aca_0 a_1 + ka_1 + 2\gamma c^3 a_1\lambda\Bigg]\phi(\xi) + \Bigg[aca_0 b_1 + kb_1 + \frac{1}{3}\frac{bc^3 b_1^3\lambda\left(\frac{8\mu^2\lambda}{\lambda^2\sigma - \mu^2} + 2\lambda\right)}{2(\lambda^2\sigma - \mu^2)}
$$
$$
-\frac{acb_1^2\lambda\mu}{\lambda^2\sigma - \mu^2} - \frac{2bc^3 a_0 b_1^2\lambda\mu}{\lambda^2\sigma - \mu^2} + bc^3 a_0^2 b_1 + \gamma c^3 b_1\left(\frac{2\mu^2\lambda}{\lambda^2\sigma - \mu^2} + \lambda\right)\Bigg]\psi(\xi)+
$$
$$
ka_0 + \frac{bc^3 a_0 b_1^2\lambda^2}{\lambda^2\sigma - \mu^2} - \frac{4}{3}\frac{bc^3 b_1^3\lambda^3\mu}{2(\lambda^2\sigma - \mu^2)(\lambda^2\sigma - \mu^2)} + \frac{1}{2}aca_0^2 + \frac{1}{2}\frac{acb_1^2\lambda^2}{\lambda^2\sigma - \mu^2} + \frac{1}{3}bc^3 a_0^3 - \frac{\gamma c^3 b_1\mu\lambda^2}{\lambda^2\sigma - \mu^2}
\tag{2.184}
$$

Solving the algebraic equations by Maple, we obtain the roots of Eq. (2.184)

$$
a_0 = -\frac{1}{2}\frac{a}{bc^2},\ a_1 = \pm\frac{3\gamma}{\sqrt{-6b\gamma}},\ b_1 = \pm\sqrt{\lambda(\lambda^2\sigma - \mu^2)}\left(\pm\frac{3\gamma}{\lambda\sqrt{-6b\gamma}}\right),
$$
$$
k = \frac{\alpha a^2 + 2\beta b\gamma c^4}{4bc},\ i = \sqrt{-1},\ \lambda^2\sigma - \mu^2 \neq 0.
\tag{2.185}
$$

Substituting (2.185) into (2.178) we obtain the following solutions of Eq. (2.171)

Family 2.1

$$\Phi(\xi) = -\frac{1}{2}\frac{a}{bc^2} \pm \frac{3\gamma}{\sqrt{-6b\gamma}}\left(\frac{A_1\sqrt{\lambda}\cos(\sqrt{\lambda}\xi) - A_2\sqrt{\lambda}\sin(\sqrt{\lambda}\xi)}{A_1\sin(\sqrt{\lambda}\xi) + A_2\cos(\sqrt{\lambda}\xi) + \frac{\mu}{\lambda}}\right)$$
$$\pm\sqrt{\lambda(\lambda^2\sigma - \mu^2)}\left(\pm\frac{3\gamma}{\lambda\sqrt{-6b\gamma}}\right)\left(\frac{1}{A_1\sin(\sqrt{\lambda}\xi) + A_2\cos(\sqrt{\lambda}\xi) + \frac{\mu}{\lambda}}\right) \tag{2.186}$$

where $\sigma = A_1^2 + A_2^2$.

Family 2.2 In particular if we set $A_1 = 0$, $A_2 > 0$ and $\mu = 0$ in (2.186) then we obtain solitary solution

$$\Phi(\xi) = -\frac{1}{2}\frac{a}{bc^2} \pm \left(\frac{3\gamma}{\sqrt{-6b\gamma}}\right)\sqrt{\lambda}\tan\left(\sqrt{\lambda}\xi\right) \pm \sqrt{\lambda\sigma}\left(\pm\frac{3\gamma}{\sqrt{-6b\gamma}}\right)\frac{1}{A_2}\sec(\sqrt{\lambda}\xi). \tag{2.187}$$

Family 2.3 For $A_2 = 0$, $A_1 > 0$ and $\mu = 0$ in (2.186) then we have the solitary solution

$$\Phi(\xi) = -\frac{1}{2}\frac{a}{bc^2} \pm \left(\frac{3\gamma}{\sqrt{-6b\gamma}}\right)\sqrt{\lambda}\cot\left(\sqrt{\lambda}\xi\right) \pm \sqrt{\lambda\sigma}\left(\pm\frac{3\gamma}{\sqrt{-6b\gamma}}\right)\frac{1}{A_1}\csc(\sqrt{\lambda}\xi). \tag{2.188}$$

Case 3 For $\lambda = 0$ resulting to Rational function solution, substituting (2.178) into (2.176) and using (2.155) and (2.161). We have a polynomial in ψ and ϕ, vanishing each coefficient yield a set of system of algebraic equations

$$\left[\frac{bc^3a_1b_1^2}{A_1^2 - 2\mu A_2} + 2\gamma c^3 a_1 + \frac{1}{3}bc^3a_1^3\right]\phi^3(\xi)$$
$$+ \left[\left(\frac{2}{3}\frac{bc^3b_1^3}{2A_1^2 - 4\mu A_2} + bc^3a_1^2b_1 + 2\gamma c^3 b_1\right)\psi(\xi) + \frac{bc^3a_0b_1^2}{A_1^2 - 2\mu A_2} + \frac{1}{2}\frac{acb_1^2}{A_1^2 - 2\mu A_2} + \frac{1}{2}aca_1^2 + bc^3a_0a_1^2\right.$$
$$\left. - \frac{4}{3}\frac{bc^3b_1^3\mu}{(2A_1^2 - 4\mu A_2)(A_1^2 - 2\mu A_2)} - \frac{\gamma c^3b_1\mu}{A_1^2 - 2\mu A_2}\right]\phi^2(\xi)$$
$$+ \left[\left(-\frac{2bc^3a_1b_1^2\mu}{A_1^2 - 2\mu A_2} + 2bc^3a_0a_1b_1 + aca_1b_1 - 3\gamma c^3a_1\mu\right)\psi(\xi)\right.$$
$$+ bc^3a_0^2a_1 + aca_0a_1 + ka_1\Big]\phi(\xi) + \left[aca_0b_1 - \frac{acb_1^2\mu}{A_1^2 - 2\mu A_2} + \frac{8}{3}\frac{bc^3b_1^3\mu^2}{(2A_1^2 - 4\mu A_2)(A_1^2 - 2\mu A_2)}\right.$$
$$+ kb_1 - \frac{2bc^3a_0b_1^2\mu}{A_1^2 - 2\mu A_2} + bc^3a_0^2b_1 + \frac{2\gamma c^3b_1\mu^2}{A_1^2 - 2\mu A_2}\Big]\psi(\xi) + ka_0 + \frac{1}{3}bc^3a_0^3 + \frac{1}{2}aca_0^2. \tag{2.189}$$

Solving the algebraic equations by Maple, we obtain the roots of Eq. (2.189).

$$a_1 = \pm\frac{3\gamma}{\sqrt{-6b\gamma}}, \quad b_1 = \pm\sqrt{A_1^2 - 2\mu A_2}\left(\frac{3\gamma}{\sqrt{-6b\gamma}}\right), \quad k = 0, \ A_1^2 - 2\mu A_2 \neq 0. \tag{2.190}$$

Substituting (2.190) in (2.178), we obtain the solution of (2.171) as follows

Family 3.1

$$
\begin{aligned}
\Phi(\xi) = &\pm \frac{3\gamma}{\sqrt{-6b\gamma}} \left(\frac{\mu\xi + A_1}{\frac{\mu}{2}\xi^2 + A_1\xi + A_2} \right) \\
&\pm \sqrt{A_1^2 - 2\mu A_2} \left(\frac{3\gamma}{\sqrt{-6b\gamma}} \right) \left(\frac{1}{\frac{\mu}{2}\xi^2 + A_1\xi + A_2} \right).
\end{aligned}
\tag{2.191}
$$

2.8.3 Atmospherical dynamic in two-layer fluid systems

Let consider a function $g : \mathbb{R} \to \mathbb{R}, x \to g(x)$ represents a continuous but not necessarily differentiable function. Thus the Jumarie modified Riemann-Liouville derivative of order α is described as follows [238]

$$
D_x^\alpha g(x) =
\begin{cases}
\frac{1}{\Gamma(1-\alpha)} \int\limits_0^x (x-\xi)^{-\alpha-1} [g(\xi) - g(0)] \, d\xi, \ \alpha < 0, \\
\frac{1}{\Gamma(1-\alpha)} \int\limits_0^x (x-\xi)^{-\alpha} [g(\xi) - g(0)] \, d\xi, \ 0 < \alpha < 1, \\
[g^{\alpha-n}(x)]^n, \ n \le \alpha \le n+1, \ n \ge 1.
\end{cases}
\tag{2.192}
$$

We list some important properties of the fractional modified Riemann-Liouville derivative as

$$
D_x^\alpha x^\beta = \frac{\Gamma(\beta+1)}{\Gamma(\beta+1-\alpha)} x^{\beta-\alpha},
\tag{2.193}
$$

$$
D_x^\alpha (h(x)g(x)) = g(x)(D_x^\alpha h(x)) + h(x)(D_x^\alpha g(x)),
\tag{2.194}
$$

$$
D_x^\alpha h[g(x)] = h_g'[g(x)] D_x^\alpha g(x) = \left(D_g^\alpha h[g(x)] \right) (g'(x))^\alpha.
\tag{2.195}
$$

2.8.4 Traveling wave solutions for space-time fractal order

The objective of this work consist of obtaining analytical solutions, by using the (G'/G, 1/G)-expansion method [239], for the space-time fractional coupled mKdV equation

$$
\begin{aligned}
D_t^\alpha u &= \frac{1}{2} D_x^{3\alpha} u - 3u^2 D_x^\alpha u + \frac{3}{2} D_x^{2\alpha} v + D_x^\alpha(uv) - 3\lambda D_x^\alpha u, \\
D_t^\alpha v &= -D_x^{3\alpha} v - 3v D_x^\alpha v - 3(D_x^\alpha u)(D_x^\alpha v) + 3u^2 D_x^\alpha(v) + 3\lambda D_x^\alpha v,
\end{aligned}
\tag{2.196}
$$

$$
t > 0, \ 0 < \alpha \le 1,
\tag{2.197}
$$

where D_t^α and D_x^α are the Jumarie's modified Riemann-Liouville derivatives. λ is a constant and α represents the parameter characterizing the order of the fractional derivatives of $u(x,t)$ and $v(x,t)$. By investigating the traveling wave transformation

$$u(x,t) = u(\xi), \ v(x,t) = v(\xi)$$
$$\text{with } \xi = \frac{kx^\alpha + ct^\alpha}{\Gamma(1+\alpha)}, \tag{2.198}$$

where k and c are assumed constants, substituting (2.198) into (2.196). Therefore (2.196) can be reduced into an ordinary differential equation (ODE)

$$cu'(\xi) = \frac{k^3}{2}u'''(\xi) + \frac{3}{2}k^2v''(\xi) + 3k(u(\xi)v(\xi))' - 3ku^2(\xi)u'(\xi) - 3\alpha ku'(\xi),$$
$$cv'(\xi) = -k^3v'''(\xi) - 3kv(\xi)v'(\xi) - 3k^2u'(\xi)v'(\xi) + 3\alpha kv'(\xi). \tag{2.199}$$

For our analysis, let consider the ansätz

$$v(\xi) = a + bu(\xi), \tag{2.200}$$

where a and b as coefficients are supposed to be determined later. The main non-linear evolutive equation is in the form

$$u''(\xi) = \frac{1}{k^2b}\left[(c + \lambda k - ka) - 3kbu(\xi) + ku^2(\xi)\right]u'(\xi) + \frac{1}{b}(u'(\xi))^2. \tag{2.201}$$

Associating this first integral, with the two-dimensional autonomous system. In order to use the Feng's first integral method [240]. We consider the space-time fractional differential equation with independant variables x_1, x_2, x_3,...x_m,t and dependant variable u

$$G\left(u, D_t^\alpha u, D_{x_1}^\alpha u, D_{x_2}^\alpha u D_{x_3}^\alpha u, ..., D_t^{2\alpha} u, D_{x_1}^{2\alpha} u, D_{x_2}^{2\alpha} u, D_{x_3}^{2\alpha} u, ...\right) = 0. \tag{2.202}$$

Introducing the variable transformation

$$u\left(x_1, x_2, ..., x_m, t\right) = U\left(\xi\right),$$
$$\xi = \frac{k_1x_1^\alpha + k_2x_2^\alpha + \cdots + k_mx_m^\alpha + ct^\alpha}{\Gamma\left(1+\alpha\right)}, \tag{2.203}$$

where k_i and c are constants to be investigated. The fractional differential equation (2.203) is transformed to a linear ordinary differential equation

$$L = L\left(U(\xi), U'(\xi), U''(\xi), ...\right), \tag{2.204}$$

with $U'(\xi) = \frac{dU(\xi)}{d\xi}$. We suppose that (2.203) has a solution in the form

$$U(\xi) = R(\xi), \tag{2.205}$$

- and using a new independant variable $S(\xi) = R'(\xi)$, which yields to the following system of non-linear ordinary differential equations

$$\begin{aligned} R'(\xi) &= S(\xi), \\ S'(\xi) &= F(R(\xi), S(\xi)). \end{aligned} \tag{2.206}$$

Using the main idea of the Feng's first integral method. By introducing the division theorem for two variables in the complex domain which is constructed on the Hilbert-Nullstellensatz theorem [241], we arrive at one first integral to (2.206) that transform (2.205) to a first-order integrable ordinary differential equation. An exact solution to (2.203) is thus derived by solving this relevant equation. We assume the division theorem : $H(x,y)$ and $P(x,y)$ are polynomials in $\mathbb{C}[(x,y)]$ and $H(x,y)$ is reductible in $\mathbb{C}[(x,y)]$. If $P(x,y)$ vanish at all zero points of $H(x,y)$, then there exists a polynomial $L(x,y)$ in $\mathbb{C}[(x,y)]$ such that

$$P(x,y) = H(x,y)L(x,y), \tag{2.207}$$

therefore the exact traveling wave solutions to the mKdV system (2.196) can be recasted in terms of the solution of the first order differential equation below

$$\frac{dR(\xi)}{d\xi} = -\left[\frac{\beta}{\kappa}\left(\delta - \frac{1}{\kappa^2}\right) - \frac{\beta}{\kappa^2}R + \frac{\beta}{\kappa}R^2\right]. \tag{2.208}$$

The general solution for the space-time fractional mKdV (2.196) is achieved by solving the first order differential equation (ODE), which can be reshaped as

$$\frac{dR(\xi)}{d\xi} = r + pR + qR^2. \tag{2.209}$$

with

$$r = q\left(\delta - \frac{1}{\kappa^2}\right) = -\frac{1}{k}\left(\frac{b^2}{2} - \frac{c}{k}\right), \ p = -\frac{q}{\kappa} = \frac{b}{k}, \ q = -\frac{1}{k} = -\frac{\beta}{\kappa}. \tag{2.210}$$

When balancing R' and R^2, we have $m = 1$ therefore we choose solution of (2.210) as

$$R(\xi) = d_0 + d_1\phi(\xi) + d_2\psi(\xi). \tag{2.211}$$

Case 1. For $\lambda < 0$ substituting (2.211) into (2.209) and using (2.155) and (2.157) yield a system of algebraic equations in d_0, d_1, d_2, λ and σ, we obtain

$$
\left(-a_1 - qa_1^2 + \frac{qb_1^2\lambda}{\lambda^2\sigma + \mu^2}\right)\phi^2(\xi) + \left[(-b_1 - 2qa_1b_1)\,\psi(\xi) - pa_1 - 2qa_0a_1\right]\phi(\xi)
$$
$$
+ \left(a_1\mu - 2qa_0b_1 - pb_1 - \frac{2qb_1^2\lambda\mu}{\lambda^2\sigma + \mu^2}\right)\psi(\xi) - a_1\lambda - pa_0 - qa_0^2 + \frac{qb_1^2\lambda^2}{\lambda^2\sigma + \mu^2} - r.
$$

(2.212)

Solving the algebraic equation by Maple, we obtain the roots of (2.212)

$$
a_0 = -\frac{p}{2q}, \ a_1 = -\frac{1}{2q}, \ b_1 = \pm\frac{1}{2}\frac{\sqrt{(p^2 - 4rq)(\sigma p^4 - 8\sigma p^2 rq + 16\sigma r^2 q^2 + \mu^2)}}{(p^2 - 4rq)\,q},
$$
$$
r = \frac{1}{4}\frac{\lambda + p^2}{q}, \ \lambda^2\sigma + \mu^2 \neq 0, \ i = \sqrt{-1}.
$$

(2.213)

substituting (2.213) into (2.211) yields the following solution of (2.196) Since $M = p^2$ and $N = 4rq$ we have the following relation

$$
M^2 - N^2 = (M - N)(M + N) + 2MN.
$$

(2.214)

Family 1.1.

$$
R(\xi) = \frac{1}{2q}\left(-p - \frac{A_1\sqrt{-\lambda}\cosh(\sqrt{-\lambda}\xi) + A_2\sqrt{-\lambda}\sinh(\sqrt{-\lambda}\xi)}{A_1\sinh\sqrt{-\lambda}\xi + A_2\cosh(\sqrt{-\lambda}\xi) + \frac{\mu}{\lambda}}\right)
$$
$$
\pm\frac{1}{2}\frac{\sqrt{(p^2 - 4rq)(\sigma p^4 - 8\sigma p^2 rq + 16\sigma r^2 q^2 + \mu^2)}}{(p^2 - 4rq)\,q}
$$
$$
\times\left(\frac{1}{A_1\sinh\sqrt{-\lambda}\xi + A_2\cosh(\sqrt{-\lambda}\xi) + \frac{\mu}{\lambda}}\right),
$$

(2.215)

where $\sigma = A_1^2 - A_2^2$.

Family 1.2. For $A_1 = 0, \quad A_2 > 0, \quad \mu = 0$ in (2.215) we obtain the solitary wave

$$
R(\xi) = \frac{1}{2q}\left(-p - \sqrt{-\lambda}\tanh\left(\sqrt{-\lambda}\xi\right)\right)
$$
$$
\pm\frac{1}{2}\frac{\sqrt{(p^2 - 4rq)(p^4 - 8p^2 rq + 16r^2 q^2)}}{(p^2 - 4rq)\,q}\sec h\left(\sqrt{-\lambda}\xi\right).
$$

(2.216)

Family 1.3. For $A_2 = 0, \quad A_1 > 0, \quad \mu = 0$ in (2.215) we obtain the solitary wave

$$
R(\xi) = \frac{1}{2q}\left(-p - \sqrt{-\lambda}\coth\left(\sqrt{-\lambda}\xi\right)\right)
$$
$$
\pm\frac{1}{2}\frac{\sqrt{-(p^2 - 4rq)(p^4 - 8p^2 rq + 16r^2 q^2)}}{(p^2 - 4rq)\,q}\csc h\left(\sqrt{-\lambda}\xi\right).
$$

(2.217)

Case 2. For $\lambda > 0$ substituting (2.211) into (2.209) and using (2.155) and (2.159) yield a system of algebraic equations in d_0, d_1, d_2, λ and σ, we have

$$
\begin{aligned}
&\left(-a_1 - qa_1^2 - \frac{qb_1^2\lambda}{\lambda^2\sigma - \mu^2}\right)\phi^2(\xi) + \left[(-b_1 - 2qa_1b_1)\psi(\xi) - pa_1 - 2qa_0a_1\right]\phi(\xi) + \\
&\left(a_1\mu - 2qa_0b_1 - pb_1 + \frac{2qb_1^2\lambda\mu}{\lambda^2\sigma - \mu^2}\right)\psi(\xi) - a_1\lambda - pa_0 - qa_0^2 - \frac{qb_1^2\lambda^2}{\lambda^2\sigma - \mu^2} - r.
\end{aligned}
\tag{2.218}
$$

We obtain the roots of equations (2.218), with the aid of Maple,

$$
a_0 = -\frac{p}{2q}, \; a_1 = -\frac{1}{2q}, \; b_1 = \pm\frac{1}{2}\frac{\sqrt{(p^2 - 4rq)(-\sigma p^4 + 8\sigma p^2 rq - 16\sigma r^2 q^2 + \mu^2)}}{(p^2 - 4rq)q},
$$
$$
r = \frac{1}{4}\frac{\lambda + p^2}{q}, \; \lambda^2\sigma + \mu^2 \neq 0, \; i = \sqrt{-1}.
\tag{2.219}
$$

Substituting (2.219) into (2.211) we obtain the following solution of (2.196)

Family 2.1.

$$
\begin{aligned}
R(\xi) = &\frac{1}{2q}\left(-p - \frac{A_1\sqrt{\lambda}\cos(\sqrt{\lambda}\xi) - A_2\sqrt{\lambda}\sin(\sqrt{\lambda}\xi)}{A_1\sin(\sqrt{\lambda}\xi) + A_2\cos(\sqrt{\lambda}\xi) + \frac{\mu}{\lambda}}\right) \\
&\pm\frac{1}{2}\frac{\sqrt{(p^2 - 4rq)(-\sigma p^4 + 8\sigma p^2 rq - 16\sigma r^2 q^2 + \mu^2)}}{(p^2 - 4rq)q} \\
&\times\left(\frac{1}{A_1\sin(\sqrt{\lambda}\xi) + A_2\cos(\sqrt{\lambda}\xi) + \frac{\mu}{\lambda}}\right).
\end{aligned}
\tag{2.220}
$$

$\sigma = A_1^2 + A_2^2$

Family 2.2. For $A_1 = 0, \quad A_2 > 0, \quad \mu = 0$ in (2.220) we obtain the solitary wave

$$
\begin{aligned}
R(\xi) = &\frac{1}{2q}\left(-p + \sqrt{\lambda}\tan(\sqrt{\lambda}\xi)\right) \\
&\pm\sqrt{\frac{(p^2 - 4rq)(-p^4 + 8p^2 rq - 16r^2 q^2)}{(p^2 - 4rq)q}}\sec(\sqrt{\lambda}\xi).
\end{aligned}
\tag{2.221}
$$

Family 2.3. For $A_2 = 0, \quad A_1 > 0, \quad \mu = 0$ in (2.220) we obtain the solitary wave

$$
\begin{aligned}
R(\xi) = &\frac{1}{2q}\left(-p + \sqrt{\lambda}\cot(\sqrt{\lambda}\xi)\right) \\
&\pm\sqrt{\frac{(p^2 - 4rq)(-p^4 + 8p^2 rq - 16r^2 q^2)}{(p^2 - 4rq)q}}\csc(\sqrt{\lambda}\xi).
\end{aligned}
\tag{2.222}
$$

Case 3. For $\lambda = 0$ substituting (2.211) into (2.209) and using (2.155) and (2.161) yield a system of algebraic equations in d_0, d_1, d_2, λ and σ, we have

$$\left(-a_1 - qa_1^2 - \frac{qb_1^2}{A_1^2 - 2\mu A_2}\right)\phi^2(\xi) + \left[(-b_1 - 2qa_1b_1)\,\psi(\xi) - pa_1 - 2qa_0a_1\right]\phi(\xi)+ \tag{2.223}$$
$$\left(-pb_1 + a_1\mu - 2qa_0b_1 + \frac{2qb_1^2\mu}{A_1^2 - 2\mu A_2}\right)\psi(\xi) - pa_0 - qa_0^2 - r.$$

We obtain the roots of (2.223) with the aid of Maple

$$
\begin{aligned}
a_0 &= -\frac{p}{2q}, \ a_1 = -\frac{1}{2q}, \\
b_1 &= \pm\frac{1}{2}\frac{\sqrt{A_1^2 - 2\mu A_2}}{q}, \\
r &= \frac{1}{4}\frac{p^2}{q}, \\
A_1^2 &- 2\mu A_2 \neq 0.
\end{aligned}
\tag{2.224}
$$

Family 3.1.

$$R(\xi) = \frac{1}{2q}\left(-p - \frac{\mu\xi + A_1}{\frac{\mu}{2}\xi^2 + A_1\xi + A_2}\right) \pm \frac{1}{2}\frac{\sqrt{A_1^2 - 2\mu A_2}}{q}\left(\frac{1}{\frac{\mu}{2}\xi^2 + A_1\xi + A_2}\right) \tag{2.225}$$

In order to simplify the expression $\sqrt{p^2 - 4qr}$ we have in a more suitable form

$$\sqrt{p^2 - 4qr} = \lambda = \frac{1}{k}\sqrt{3b^2 - 4\left(\frac{c}{k}\right)}, \tag{2.226}$$

$$c = \frac{3kb^2}{4} - \frac{\lambda^2 k^3}{4}, \tag{2.227}$$

$$\xi = \frac{kx^\alpha + ct^\alpha}{\Gamma\left(1 + \alpha\right)}. \tag{2.228}$$

We recall that $R(\xi) = u(\xi)$ and $v(\xi) = a + bu(\xi)$.

Remark 2. Since $R(\xi)$ satisfies the generalized Riccati equation (2.196). Similar solutions of type extended tanh-function method for (2.196) are obtained by using the sub-equation method in the integer order limit case [242]. Also, we find more different solutions and rational solution.

2.9 Tools for models validation

The performance of the fractional derivative models expressed in Eq. (2.11) and Eq. (2.56) was evaluated against experimental ground-level concentration using the Copenhagen campaign and Prairie Grass experiments [243]. Usually, to evaluate the performance of the dispersion models, the Environmental Protection Agency (EPA) recommends a well known set of statistical indices defined as follows [244]:

Normalized mean square error (NMSE):

$NMSE = \overline{(c_p - c_o)^2}/\bar{c}_o\bar{c}_p$

Fractional bias (FB):

$FB = (\bar{c}_o - \bar{c}_p)/0.5(\bar{c}_o + \bar{c}_p)$

Correlation coefficient (R):

$R = \overline{(c_o - \bar{c}_o)(c_p - \bar{c}_p)}/(\sigma_o\sigma_p)$

Fractional variance:

$FS = (\sigma_o - \sigma_p)/0.5(\sigma_o + \sigma_p)$

Factor of Two (FA2):

$FA2 = 0.5 \leq c_p/c_o \leq 2$

therefore, σ_p and σ_o represent the standard deviations of c_p and c_o respectively. Where the over bars indicate the average over all measurement terms (N). These parameters focus on the agreement between model predictions and observations [245]. A model appears to be perfect for ideal values:

$NMSE \leq 0.4, -0.3 \leq FB \leq 0.3$ and COR=FA2=1.

These parameters focus on the agreement between model predictions and observations [246]. The data in red in the Table 3.1 indicate the extreme values of the Monin-Obhukov length.

The present model shows that the modified form of eddy diffusivity is given in the form $K_z(x, z) = f(x)u(z)$, in which $u(z)$ is any form of eddy diffusivity depending on z and $f(x)$ is the correction of $u(z)$ near of the source dispersion and represents a dimensionless integrable function of x, i.e. a power-law parameterisation of $u(z)$. The micrometeorological conditions used in the initial simulations of this study are those from the experiment conducted at Copenhagen, where u_{10} is the mean wind speed at 10m, u_* is the friction velocity and L the Monin-Obukhov length.

2.10   Conclusion

Since the atmospheric boundary layer is the seat of turbulent flows, several theories of mathematical physics attempt to solve the Navier Stokes equations characteristic of the fluid flow at this level. Via deterministic approach, to model a phenomenon, it is possible to differentiate two types of approaches: statistical modeling (empirical) and deterministic (physical) modeling. Statistical approach does not allow for detail turbulence characteristics. Deterministic approach, relies on the physical mechanisms, chemical and digital systems, based on physical laws. Then Advection-Diffusion Equation (ADE) or Non-linear Evolutive Equations (NLEEs) require complex modeling techniques. In some cases there are analytical solutions that provide a quick and easy way to study turbulent dispersion. But, in the context of anomalous diffusion that takes into account complex processes of functional structure processes, FADE could be efficiently analyzed by adopting principles and methodologies derived from the Fractal Geometry. In addition, there are methods adapted to particular types of fractional differential equations, namely linear equations with constant coefficients. There are some that deal with the existence and multiplicity of solutions of non-linear fractional differential equations using non-linear analysis techniques such as the $(G'/G, 1/G)$-Expansion method. These solutions help us in estimating the role of the fractional derivative in terms of non-linearity and dispersion.

Chapter 3

Results and discussion

3.1 Introduction

Physico-mathematical models are powerful tools in the study of air pollution phenom-
ena. They are realistic models designed for the most part on fundamental characteristics of
chemistry-transport models including the large dimension and the strong uncertainties that
falsify the data. The dimension of the model is the size of the state, that is to say the number
of point values of concentration used to describe the continuous fields of concentrations. As in
most environmental systems, the data used are biased by uncertainties. Among which there
are two types of data; Raw data which are compiled from micro-meteorological data and the
parameterized fields as the vertical diffusion coefficients in the tensor $\overrightarrow{K}$. In a nutshell, these
models use physical parameters from experiments. These experiments make it possible to test
the validity and performance of the models under similar conditions. Because validation is a
necessary and sufficient condition for the efficient and effective implementation of a model. For
model performance evaluation, practical tool intended to serve as a common frame of reference,
we quote WinDimula model evaluation including the model Validation kit [247]. Following
these assumptions, we proceed to the evaluation of the models Eqs. (2.146)-(2.150) with the
experiments of Prairie Grass and Copenhagen respectively. Then, examination of the behavior
of the (FADE) and the (NLEEs).

3.2 Physical behavior of the solution

3.2.1 Convergence of the solutions

Fractional derivatives definitions are related to one another in a detailed scheme. At last,
differences result in the convergence properties of the functional space on which these operators
act. The convergence shows that the modified equations are more reliable in predicting the
movement of pollution. Eqs. (2.146)-(2.150) are applicable unambiguously if they converge.

In Figure 3.1 we have represented the evolution of the concentration as a function of distance from the source for different values of α in comparison with data from Copenhagen experiment n^o4.
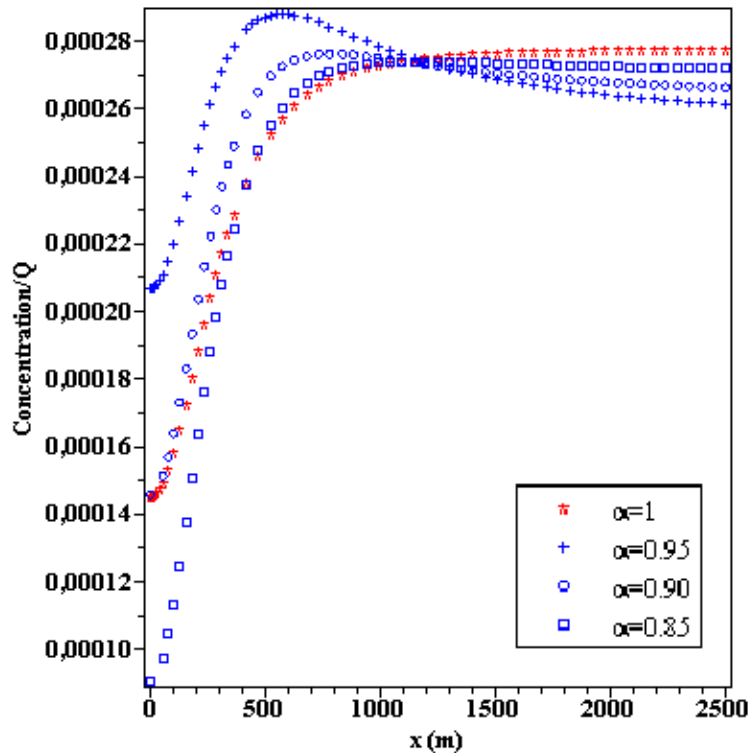
Figure 3.1: Laterally integrated concentration as a function of distance from the source for different values of α in comparison with data from Copenhagen experiment n^o4.

Thus, numerical convergence of the proposed solutions for the concentration with increasing numbers of eigenvalues is reached taking into account the conventional integer atmospheric diffusion equation and the fractional diffusion equation for different α parameters. From a practical point of view, we considered $N = 150$. At all simulated distances that we observe, there is an obvious distinction between the results of the α-GM extended to the fractional type models, which considers continuous profiles of the wind velocity and diffusion coefficient parameters. Although they exist many different approaches to fractional calculus, several known formulations are one way or another connected with the analytical continuity of Cauchy formula for n-fold integration, that give us a definition for an integration $_aI_x^\alpha$ of non-integer. For $f \in L_1[a,b]$ even when $0 < \alpha < 1$, applied to the suggested fractional operator, it is possible to proof the convergence of f [248]. Thus, to cross-check the model physical flexibility, this study laid emphasis on the conventional experimental data. In order to investigated the sensitivity of an analytical solution of steady-state fractional advection-diffusion equation, for estimating

the concentrations of pollutants in the Planetary Boundary Layer.

3.2.2 Comparison with the exact solution

In order to check the accuracy of the chosen analytical solution technique. practically, the solution of Eqs. (2.146)-(2.150) given by the master equations (2.56) which is reduced into some particular cases. The proposed models are compared with the exact analytical solution obtained by taking the particular forms of U(z) and K_z(x, z). The exact solution is given by Eq. (1.28)[249]. It is represented in blue dashed line and the approximate Eq. (2.147) is in green solid line. Figure 3.2 is plotted with data from Copenhagen experiment n^o8. This figure shows that for a jet point close to the source ($h_s = 9$ m) the exact solution is confused with the approximate solution, while for a high source ($h_s = 115$ m) the approximate solution has a significant offset from the exact solution.
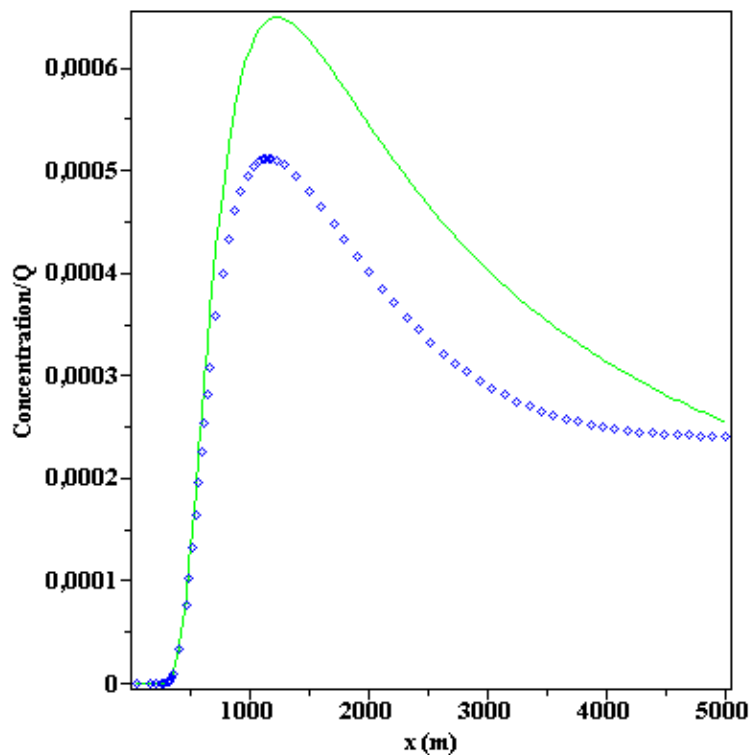
Figure 3.2: Convergence of the present model (Eq. (1.28)) and comparison with the exact solution [249].

As the analytical models in the literature are derived by considering the lower boundary at the ground, for the comparison purposes we have considered z_0=0. These models can be broadly classified first into two groups based on the wind field as uniform wind speed and variable wind speed as function of z. The models differ with the choice of the eddy diffusivity.

3.2.3 Evolution of the concentration in the ABL

To verify the models' physical consistency. It's taken as its basis the conventionals experimental data from Copenhagen [250] and the experimental datasets from Prairie Grass campaign [251]. The results obtained by the fractional models take into consideration the mean values of different diffusion coefficients that dependent on the longitudinal distance in the height direction of the Planetary Boundary Layer (PBL). Figures 3.3-3.5 and Figures 3.6-3.7 highlight the graph of the vertical profiles of laterally integrated concentration for different distances from the source, using data from Copenhagen experiment n[o]4 and from Prairie Grass experiment n[o]1.
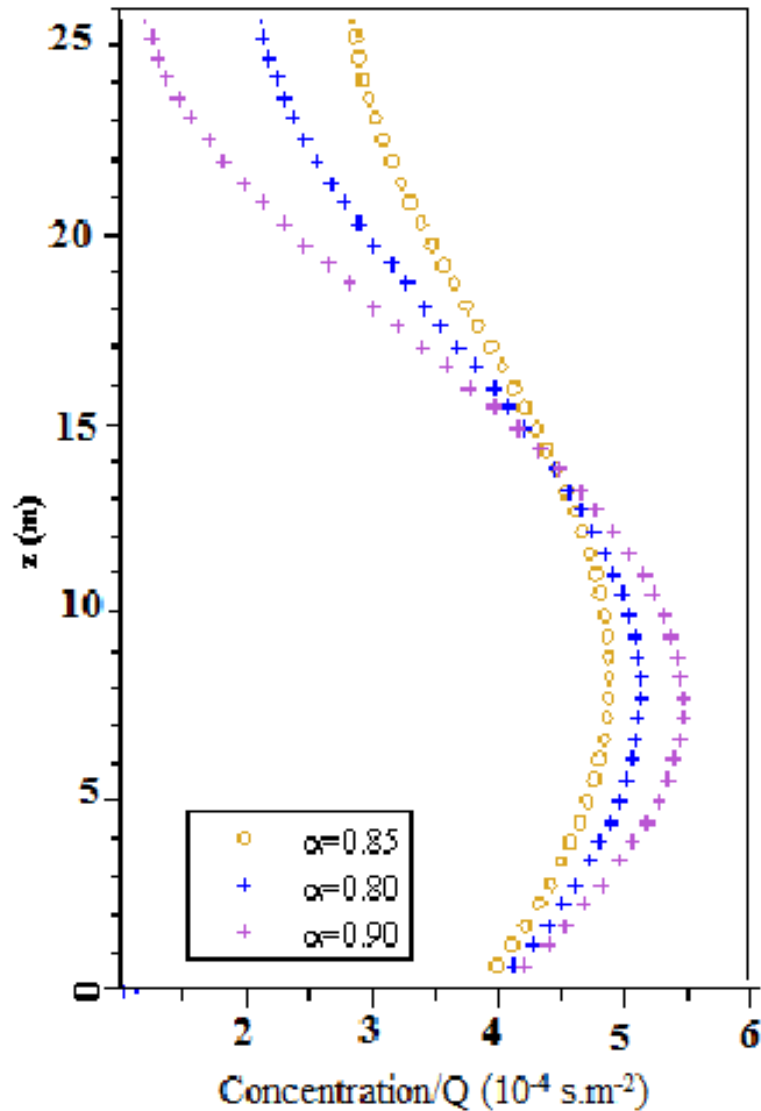
Figure 3.3: Vertical profile of laterally integrated concentration for a distance x=3 km from the source (the data are from Prairie Grass experiment n[o]1).
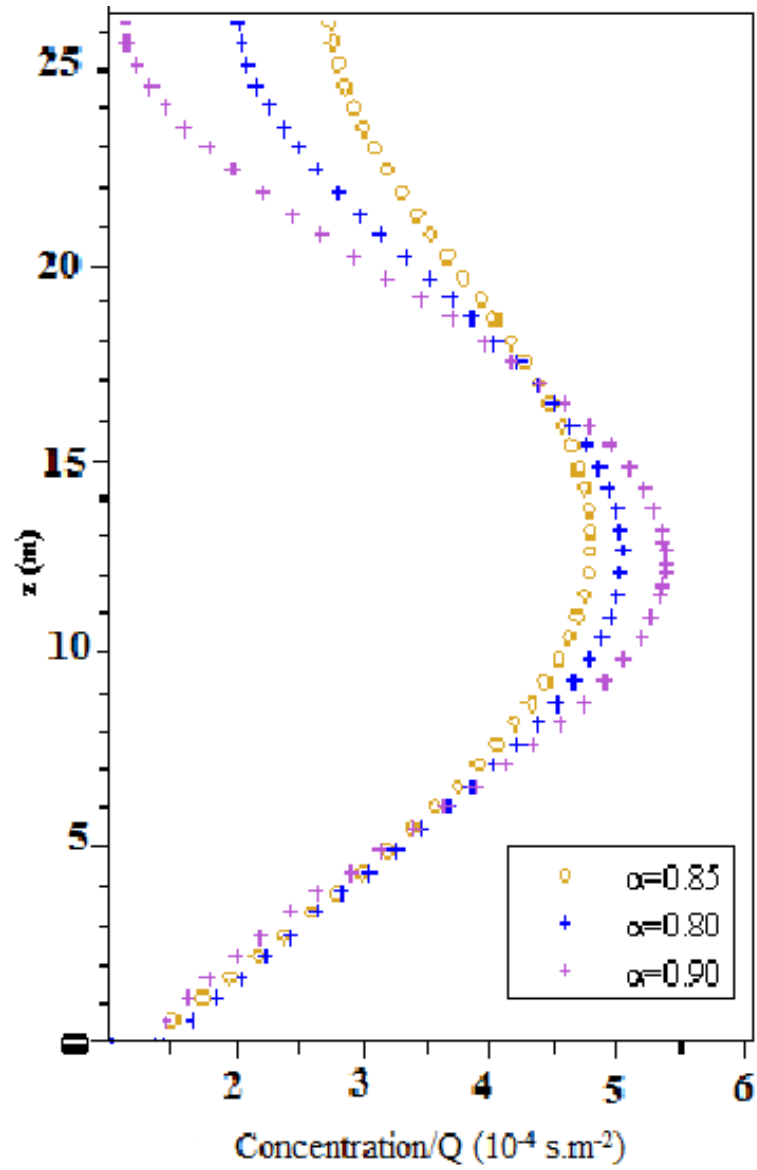
Figure 3.4: Vertical profile of laterally integrated concentration for a distance x=4 km from the source (the data are from Prairie Grass experiment n°1).

Figure 3.5: Vertical profile of laterally integrated concentration for a distance x=5 km from the source (the data are from Prairie Grass experiment n°1).

Figures 3.3, 3.4 and 3.5 displayed in their series the vertical concentration profiles for different distances from the source point 3 km, 4 km and 5 km. It's noticed the influence of the α term in the models, especially in Figure 3.3. For the pollutant progression distance nearest to the source (1 km), In the figures, we mention that the concentrations closely depend on the vertical component. According to the values of the exponent α, often it's distinguished several domains of anomalous transport which correspond to $0 < \alpha < 1$ that prevails on fractal structures.

Figures 3.6 and 3.7 show the vertical concentration profiles for a distance from the point source. This qualitative analysis is used to illustrate the asymmetry of the turbulent flow with the solution of Eq. (2.148). Without difficulty observe the influence of the α term on the model in Figures 3.6 and 3.7. For the distance closest to the source a few kilometer (1 km), a concentration peak is observed in the region of the source's height that is stronger in the present α-model and sharpens when parameter α decreases. As the distance from the source intensifies, we observe a depletion of the peak and of the concentration's numerical value with a propensity for vertical homogenization. This behavior is most precisely observed for distances greater than 60 km. At this level, complete homogenization of the concentration in the vertical direction is observed, both for $\alpha = 0.95$, α=0.90 and $\alpha = 0.85$, complete homogenization in the vertical direction has not been observed up to date. At all simulated distances, which takes into account continuous profiles of the wind velocity and diffusion coefficient parameters.

Figures 3.9 and 3.10 displayed in their series the vertical concentration profiles for different distances from the source 10 and 20 km. Also, noticed the influence of the α term in the models. In closing, the substitution of the local coordinate derivative in the diffusion equation by a fractional operator accounts for the memory effects which are connected with many complex systems. In all proposed models, the mean wind speed in longitudinal direction (u) is obtained from Table 3.4. In accordance to the evolution of concentration as a function of distance Figure 3.8 reveals that the present model Eq. (2.119) performs far better than the α-GILTT model and the α-GM model to describe the data of Copenhagen experiment Table 3.8, as can be seen from the statistical indices. The present predicted model behaves well as regarding observed data than the other models. The correlation of α-GILTT, and α-GM predicated models equals (0.70, and 0.75 respectively) and present model equals (0.80) in the other hand, the NMSE values as shown in Table 3.7, for the present, α-GILTT and α-GM models are 0.03 and 0.22, 0.12 respectively. The good performance of the present model highlights the impact of a downwind correction function in the vicinity of the source related to eddy diffusivity coefficients.

Figure 3.6: Vertical profile of laterally integrated concentration for a distance x=10 km from the source (the data are from Copenhagen experiment n°4).

Figure 3.7: Vertical profile of laterally integrated concentration for a distance x=1 km from the source (the data are from Copenhagen experiment n°4).

Figure 3.8: Laterally integrated concentration as a function of distance from the source for values of α 0.85, and 0.90 in comparison with data from Copenhagen experiment n°4).
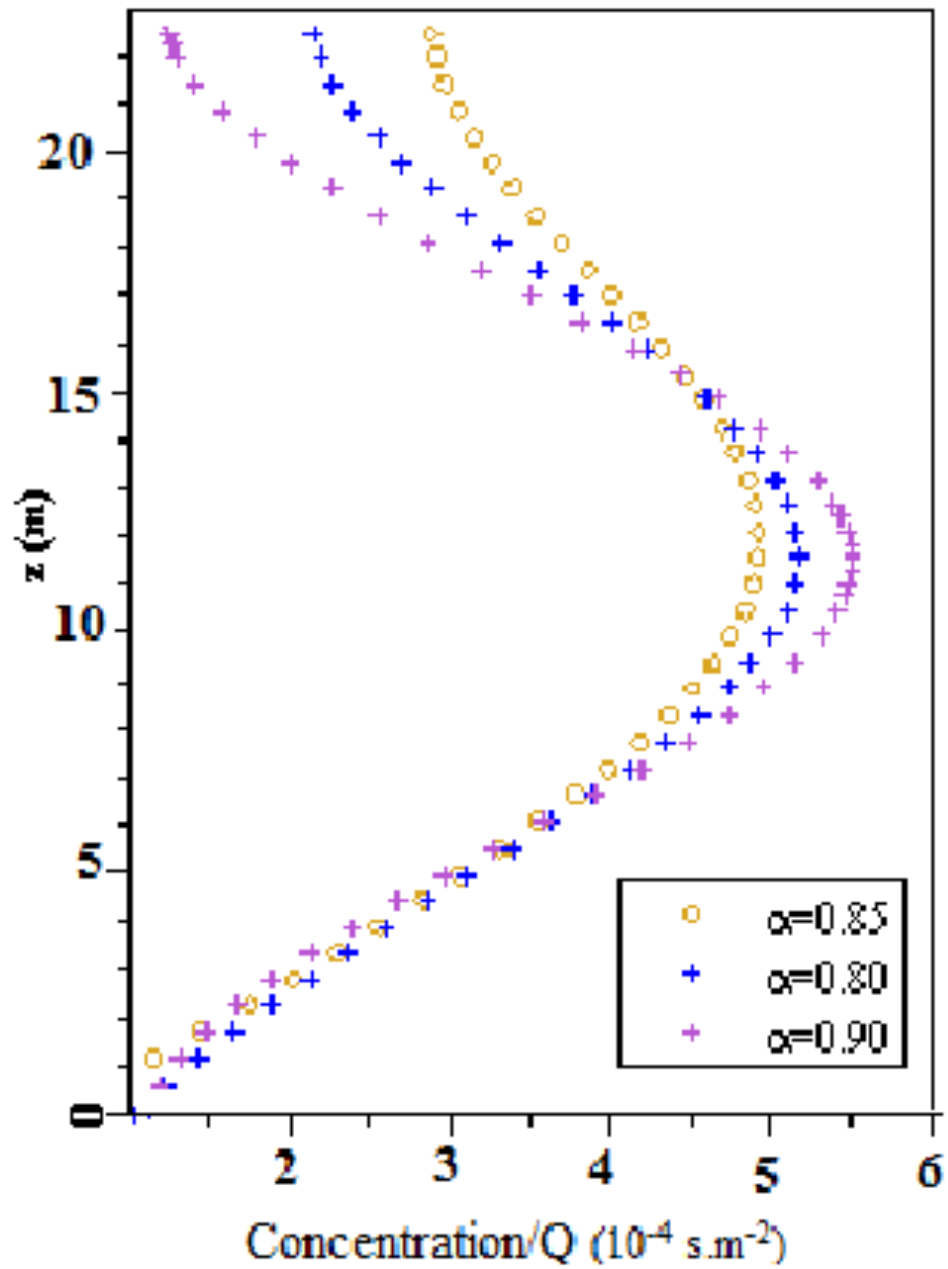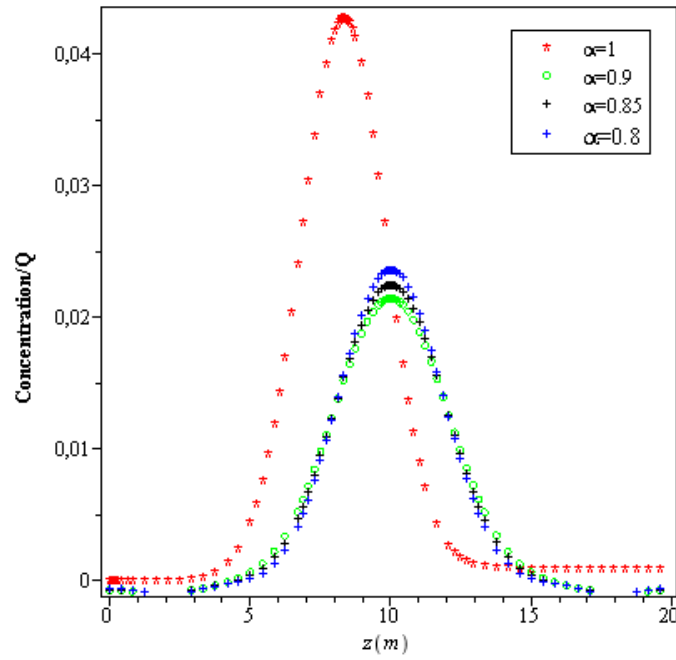
Figure 3.9: Vertical profile of laterally integrated concentration for a distance x=10 km from the source (the data are from Prairie Grass experiment n°1).
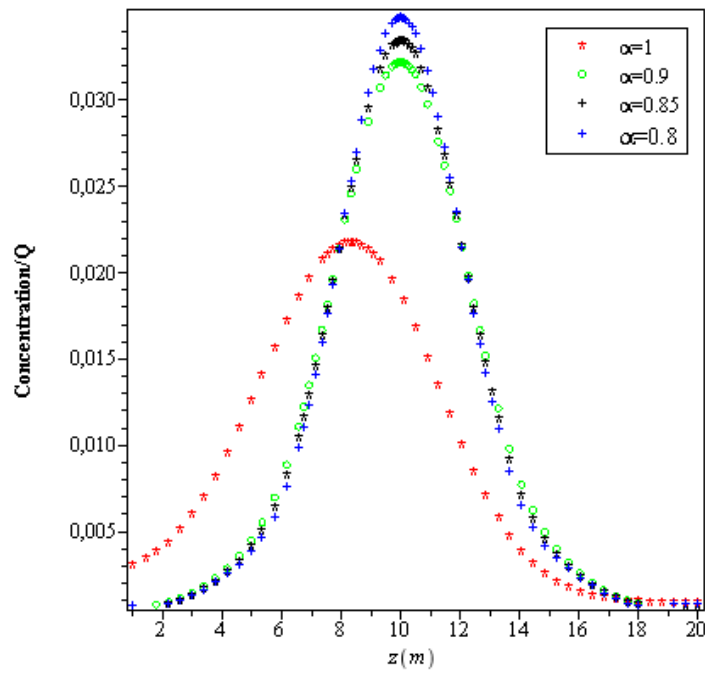
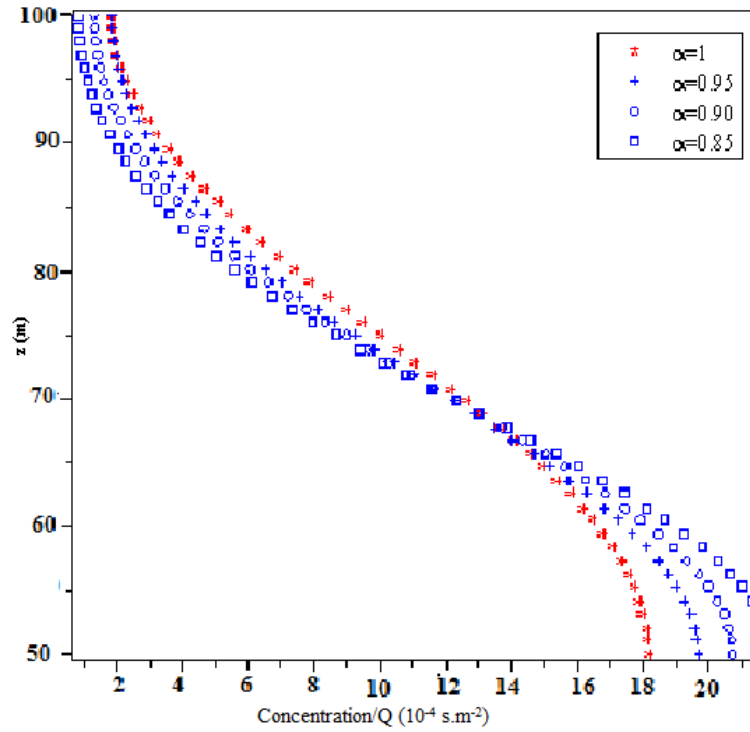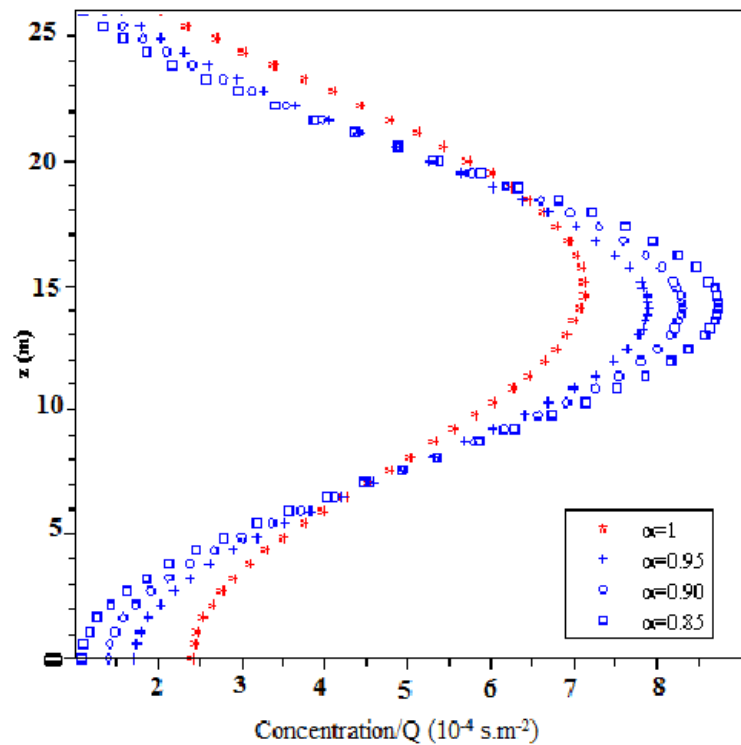Figure 3.10: Vertical profile of laterally integrated concentration for a distance x=20 km from the source (the data are from Prairie Grass experiment n° 1).
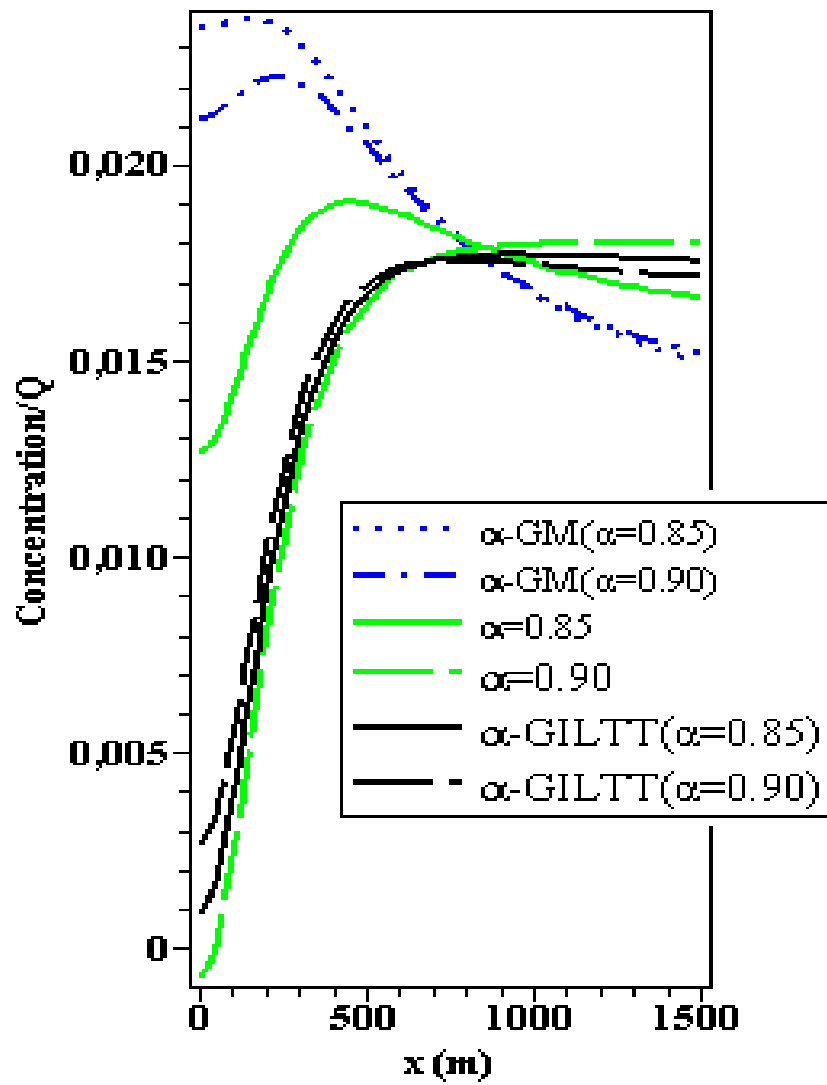
In order to estimate the better α value, by using the datasets in unstable conditions of the classical Prairie Grass experiment we examine the solutions from different values, $\alpha = 0.60$ to $\alpha = 0.99$ by steps of 0.1. The results obtained from the α-gaussian equation (2.148) are shown in Table 3.1 and for $\alpha = 0.80$. For this value of α, the model has its best statistical indice. Also, It was worth noticed, that the Mittag-Leffler function is the accurate relaxation function for an underlying fractal random walk process. Thus, the advantage of the α-gaussian model emerges as a consequence of the anomalous diffusion present in turbulent diffusion that results in a distribution with a power-law mean squared displacement. The anomalous diffusion behavior manifest in Eq. (2.148) is connected closely with the breakdown of the central limit theorem, caused by either broad distributions or long-range correlations [252].

Similarly, assuming the Copenhagen experiment, the α-models result from the anomalous diffusion present through turbulent diffusion in a distribution with a power-law mean squared displacement. That is once more the consequence of the replacement of the local coordinate derivative in the diffusion equation by a fractional operator accounts for the memory effects which are connected with many complex systems. At least, in order to estimate the better α value for the proposed model, we analyzed the solutions from $\alpha = 0.6$ to $\alpha = 0.99 \sim 1$ by steps of 0.05. The best performance occurs when $\alpha = 0.85$. As mentioned in Figures 3.6 and 3.7. This α parameter does not change the value of the maximum concentration, which is one of most important aspects in the context of air pollution, but it changes its position. This difference in the best α value is related to different diffusion coefficients employed in any cases. This supposes a correlation between the order of the equation and the quality of diffusion coefficient to the model best describe the observed concentration data. The conventional models ($\alpha = 1$) arise from the equation of molecular diffusion i.e. Fickian's law, which assumes a gaussian distribution that displays a linear mean square displacement. Asymmetries related to turbulent flow in the atmosphere are depicted by the diffusion coefficient. So far the fractional model takes on an anomalous probability distribution with a power-law mean squared displacement (2.148). This anomalous distribution has been demonstrated to be more efficient to describe the motion of particles in a turbulent flow [253]. In fact, turbulence provides the real explanation for the pollutants dispersion, given that the turbulence in the pollution models is directed after the field lines of mean wind speeds. showing minimal diffusion in other directions. Anomalous diffusion processes are found complex systems, with characteristic being the non-linear growth of the mean squared displacement in the course of time. But, traditional diffusion often follows Gaussian statistics, thus Fick's second law fails to outline the related transport behaviour.

3.3 Campaigns' for model validation

3.3.1 Prairie Grass measurements campaign

The performance of the analytical solutions is evaluated against datasets in unstable conditions of the classical Prairie Grass experiment conducted by O'Neill, NE, USA, in July and August 1956 [254]. For comparison purposes, we use the same digital version of the datasets [255], available at http://www2.dmu.dk/ atmospheric environment/Docs /PrairieGrass.xls which gives crosswind integrated concentrations under meteorological variable conditions with a surface roughness length $z_0 = 0.006$ m. Prairie Grass experiment is a classic experiment conducted in July-August 1956. A release took place from a point source close to ground level (46 cm height, except for 4 runs). SO_2 was used as a tracer, and concentrations were measured on arcs at distances of 50 m, 100 m, 200 m, 400 m and 800 m. The duration of each of the 68 sampling periods was 10 minutes. The micro-meteorological data including wind speed, temperature, etc., were also measured. Our evaluation does not include some runs, especially runs (3, 4, 5, 14, 19, 24, 25, 30, 38, 40, 41, 53) of very stable conditions ($h/L > 10$) in which turbulence becomes very weak, sporadic, intermittent and no longer continuous in time and space [256]. We are aware that inclusion or not of those abnormal runs modifies statistical performance measures. However, many users of the Prairie Grass datasets discarded these runs [257]. We also excluded these data, so it is worth noting that they exist.
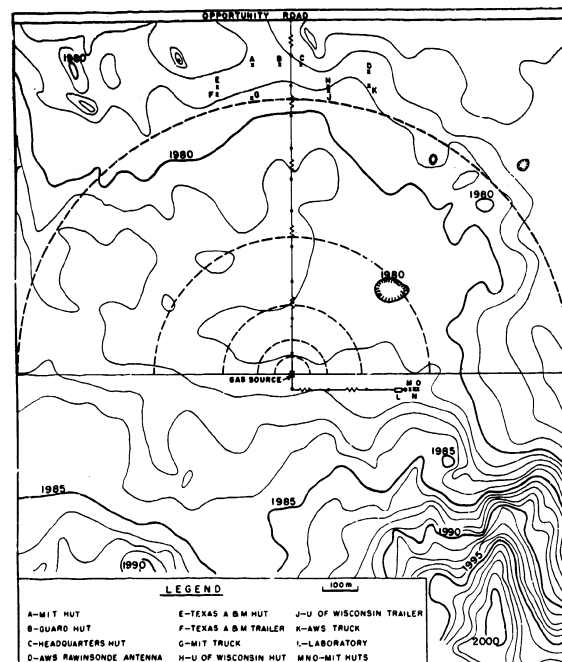
Figure 3.11: Topography of field site and layout of equipment [258].

3.3.2 Copenhague measurements campaign

The data report from a series of tracer experiment was carried out in the Copenhagen area in 1978/79 under neutral and unstable atmospheric conditions. The report contains sulphurhexafluoride of tracer concentration and meteorological measurements. The tracer was released without buoyancy from a tower at a height of 115 m, and collection of tracer sampling units at the ground-level positions at the maximum of three crosswind arcs (Figure 3.12). The sampling units were positioned at 2 to 6 km from the point of release. The site was mainly residential with a roughness length of the 0.6 m. These stations are considered to be on the ground. Each arc consisted of 20 measuring stations almost regularly spaced. These Copenhagen experiments have been widely used for the evaluation of air pollution models. They are also part of the Harmonization Initiative Model Evaluation Package [259]. This experiment was set up to obtain data that was necessary for the parameterization of the terms of the Monin-Obukhov similarity theory, as well as the development of Pasquill's classification of stability classes. The dataset includes among others the Monin-Obukhov length (L), the boundary layer height (h), the friction velocity (u_*) and the lateral dispersion parameter (σ_ω); these data are recorded in (Table 3.4).
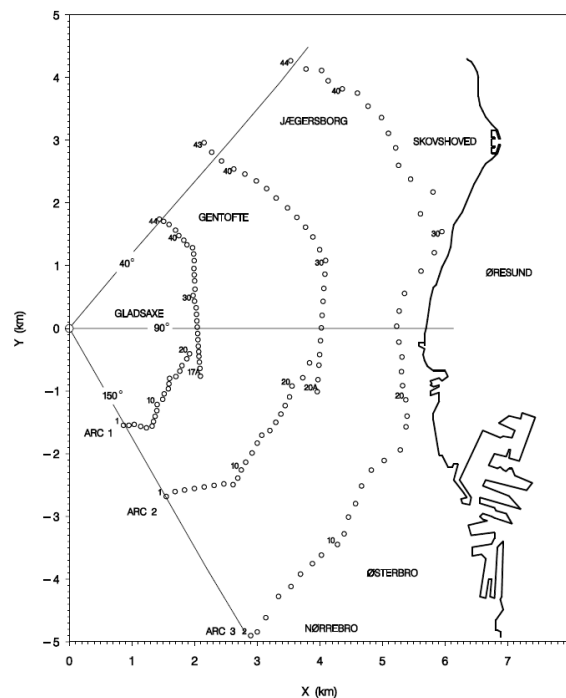
Figure 3.12: Area for the tracer experiment. The x-axis is pointing towards East, the y-axis towards North and the sampling unit positions are indicating by circles. The positions are distributed in 3 arcs [260].

3.4   Results analysis

3.4.1   Prairie Grass experiment

For a practical application of solution Eqs. (2.147) and (2.148), a comparison is made with the exact solution, the three plots are confined in the same Figure 3.13. The exact solution is that given by the ITT model [143](red color) where $u(z)$ depicted the wind speed at a reference height z and α emphasize the power-law exponent that depends on the atmospheric stability (α-uPL). The approximate solution is that obtained by Eq. (2.148) (α-GM) (green color).
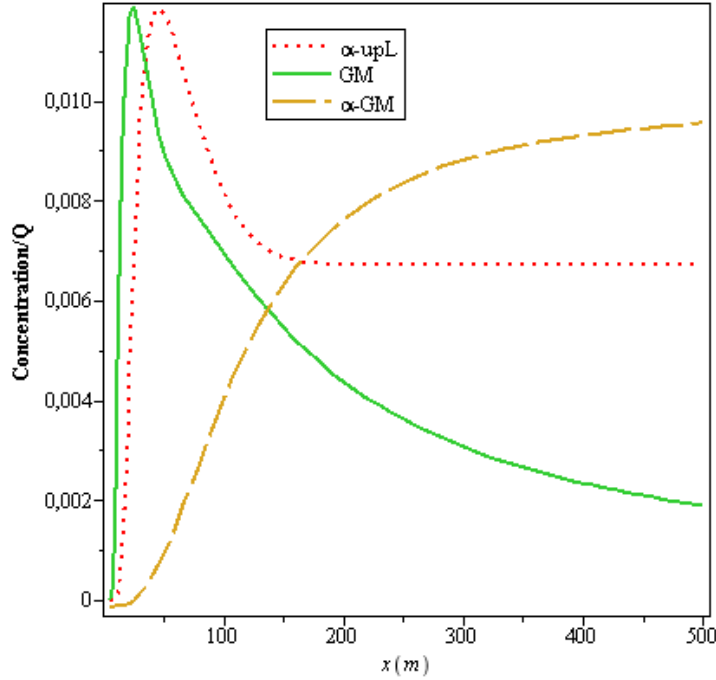
Figure 3.13: Cross-wind integrated concentration as a function of distance from the source point in comparison with data from Prairie Grass experiment n°1.

Parameter α does not change the value of the peak concentration, which is one of the most significant aspects in the understanding of air pollution. This result is valuable comparatively to the traditional gaussian model (GM). The Figure 3.13 shows that for a low source (h_s) appreciably very small, the exact solution is confused with the approximate solution. The proposed model with $\alpha = 1$ (refer, Eq. 2.116) underlining common diffusion.

Figures 3.14 and 3.15 depicted a scatter diagram between observed and predicted crosswind integrated concentrations. At this point, both predicted and observed concentrations are normalized with the source strength Q. These figures reveal that the predicted concentrations from the present model are in good agreement with the observed ones.
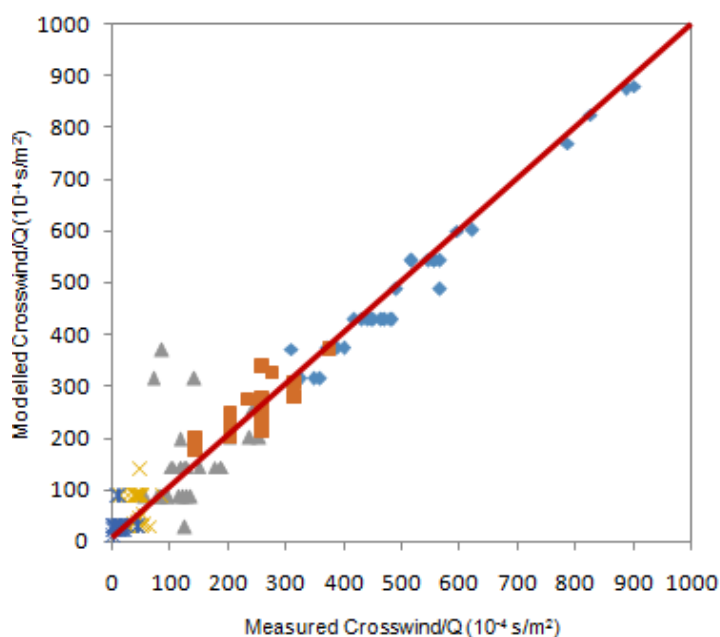
Figure 3.14: Represents a scatter plot of observed and predicted concentration normalized by source strength Q for the present model ($\alpha = 1$).
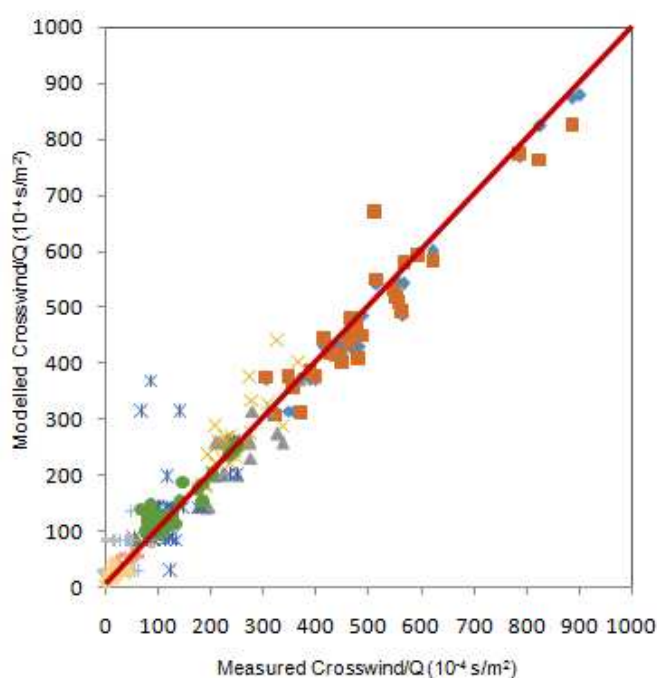
Figure 3.15: Represents a scatter plot of observed and predicted concentration normalized by source strength Q for the present model ($\alpha = 1$) and OML model. In both figures, the solid lines is a one-to-one line; data between dotted lines correspond to factor of two.

The performance of the fractional derivative model expressed in Eq. (2.148) was evaluated against experimental ground-level concentration, as mention earlier using the Prairie-Grass dispersion experiment. The datasets in Table 3.2 give an assessment of the evolution of the solution for the three models highlighted. Predictably, from these data there emerges a convergence between the observed and computed values. Therefore, at different positions x=50, 100, 200, 400 and 800 m, some results overestimate and others underestimate the experimental values. Similar results was obtained in previous works [261]. In a nutshell, the effects of overestimation and underestimation of the experimental values can be appreciated in the scatter diagrams of Figures 3.14 and 3.15, where the higher proportion of overestimated values occurs for the smaller normalized concentrations. Though, almost the majority of observed crosswind-integrated concentrations are predicted within a factor of 2.

In Table 3.2, the results of the estimated crosswind-integrated concentrations for the Prairie Grass experiment obtained for the fractional models are compared with experimental data, against the gaussian model Eq. (2.148), and with results obtained from the OML model [259].

Considering gaussian model Eq. (2.146) and α-gaussian model Eq. (2.148) the micro-meteorological values are given in Table 3.1. The good performance of the proposed fractional model is shown in Tables 3.2 and 3.3. The statistical indices used to evaluate our models performance are shown in Table 3.3. In fact, as indicated by the statistical indices. The α-gaussian model Eq. (2.148) performs far better than the gaussian model Eq. (2.147) and the OML model in accordance with the data of Prairie Grass experiment. Then, anomalous diffusion is an involved field with fascinating elusiveness. Accordingly, parameters and exponents can change in the course of time or when an external force is switched on. Diffusion processes in numerous complex systems usually no longer follow gaussian statistics, and then Fick's second law fails to describe the related transport behavior. For the most part, it's observed deviations from the linear coordinate dependence of the mean squared displacement. It was revealed, that the Mittag-Leffler function is the exact relaxation function for an underlying fractal time random walk process. Thus, in the Laplace domain, the sub-diffusive system passes through the same states as its normal counterpart, for a reshaped Laplace variable. A basic feature arising in that context is the substitution of the exponential decay of modes by the Mittag-Leffler pattern. Hence, the advantage of the α-gaussian model is a consequence of the anomalous diffusion presents in turbulent diffusion that results in a distribution with a power-law mean squared displacement. This feature involves the slow decay of the initial condition, slower dispersion, memory effects, and consequently a relatively slow approaching of the stationary state.

Table 3.1: Micrometeorological and emission data for unstable run of the Prairie Grass experiment (the top of the ABL Z_1=260 m).

run n^o	$w*(m/s)$	$u_0*(m/s^{-1})$	L(m)	Z_1/L	$Q(gs^{-1})$	$Z_s(m)$
1	0.84	0.20	-8.89	-29.24	81.50	0.0057
2	0.91	0.147	-7.71	-33.72	83.90	0.0052
6	1.64	0.413	-31.25	-8.32	77.80	0.0060
7	1.25	0.472	-117.99	-2.20	89.50	0.0059
8	2.15	0.332	-12.41	-20.95	89.90	0.0058
9	1.70	0.327	-24.81	-10.47	91.09	0.0058
10	1.44	0.485	-53.00	-4.900	92.00	0.0060
11	1.75	0.338	-17.17	-15.14	92.09	0.0057
12	0.94	0.535	-87.52	-2.97	95.90	0.0061
13	1.49	0.572	-59.15	-4.39	99.09	0.0061
16	0.70	0.242	-9.82	-26.47	95.50	0.0056
17	1.33	0.252	-6.75	-38.51	93.00	0.0058
20	1.50	0.426	-37.08	-7.01	101.80	0.0058
21	2.07	0.655	-63.65	-4.08	101.19	0.0058
26	1.22	0.208	-8.57	-30.34	101.40	0.0051
27	1.76	0.453	-41.78	-6.22	97.59	0.0057
28	2.05	0.433	-30.52	-8.51	98.80	0.0058
31	2.19	0.500	-46.13	-5.63	98.40	0.0060
32	2.09	0.545	-93.67	-2.77	96.00	0.0059
34	1.48	0.545	-80.71	-3.22	94.69	0.0061
35	1.70	0.667	-104.84	-2.48	97.40	0.0061
45	1.54	0.379	-21.38	-12.16	98.90	0.0059
46	2.13	0.433	-27.84	-9.34	100.69	0.0060
47	1.13	0.419	-105.09	-2.47	100.80	0.0059
49	1.23	0.257	-7.00	-37.14	103.09	0.0061
50	1.68	0.233	-8.16	-31.86	104.00	0.0058
51	1.32	0.547	-74.11	-3.51	104.09	0.0059
52	1.61	0.482	-37.23	-6.98	102.00	0.0060
53	1.91	0.486	-31.13	-8.35	02.80	0.0060
54	2.33	0.492	-44.32	-5.87	102.40	0.0061
55	1.98	0.335	-11.51	-22.59	104.00	0.0060

Table 3.2: Observed and predicted normalized crosswind-integrated concentration $c_y(x,z)/Q(sm^{-2})$ for unstable conditions of the Prairie Grass experiment (x=50 m).

run n^o	α-Gaussian	Gaussian	OML	Measured
1	756.15	874.00	824.12	886.18
2	756.32	879.00	1040.08	900.10
6	420.79	429.00	478.29	468.09
7	420.71	431.17	436.81	464.36
8	528.95	543.34	530.67	545.00
9	539.61	600.20	591.90	595.19
10	539.50	429.00	417.97	431.11
11	515.31	543.41	551.09	515.86
12	293.67	372.65	389.29	387.14
13	299.41	315.54	357.26	357.27
16	753.96	768.61	772.93	786.62
17	480.79	544.02	578.08	565.48
20	403.85	429.69	468.92	479.42
21	358.94	372.60	310.87	370.41
26	751.42	824.45	764.80	825.95
27	424.23	429.67	442.59	417.69
28	424.27	429.97	454.40	462.68
31	424.22	429.65	401.67	450.09
32	329.63	372.58	375.60	399.25
34	293.67	372.65	389.29	387.14
35	309.03	315.53	308.80	323.50
45	545.58	543.28	506.87	555.87
46	461.58	486.68	451.33	489.77
47	461.48	486.47	491.48	565.11
49	546.25	600.58	582.46	620.50
50	546.11	543.86	668.52	513.55
51	369.44	372.26	376.14	307.42
52	421.69	429.69	415.18	439.53
53	421.71	429.71	406.41	445.97
54	396.93	429.67	407.11	481.04
55	514.38	543.26	517.81	554.82

Table 3.3: Comparison between the three methods according to standard statistical performance measure.

Model	$K_z(x,z)$	NMSE	FA2	FB	COR	FS
Ideal		0	1	0	1	0
Gaussian	$K_z(z)$	0.30	73%	-0.052	0.82	-0.27
OML	f(x)	0.03	97%	0.010	0.96	-0.02
α-Gaussian	$K_z(z)f(x)$	0.03	97%	0.020	0.96	0.06

3.4.2 Copenhagen experiment

The crosswind-integrated concentration, at ground level, as a function of the distance from the source using data from Copenhagen experiment. Enables to observe that the concentration generated by the models with different α provides the best results with the parameterizations used. In comparison with the traditional case highlighted, we observe that, for the range of tracer collection points in this experiment ($2 \sim 6$ km), the results are similar but the results from the fractional present model are still better. The statistical indices from the mathematical models and the results obtained in the Copenhagen dispersion experiment [250], used to evaluate our models performance are shown in Tables 3.6 and 3.7. In all proposed models the mean wind speed in longitudinal direction (u) is obtained from Table 3.4. The present model (2.150) performs far better than the α-GILTT model and the α-GM model to describe the data of Copenhagen experiment, as can be seen from the statistical indices.

The present predicted model performs well with observed data than the other models. The correlation of α-GILTT, and α-GM predicated models equals (0.70, 0.75 respectively) and present model equals (0.80). In the otherhand, The NMSE values as shown in Table 3.6, indicates that the present and α-GILTT, α-GM models are 0.03 and 0.22, 0.12 respectively. The good performance of the present model highlights the impact of a downwind correction function in the vicinity of the source related to eddy diffusivity coefficients. The conventional models (α = 1) arise from the equation of molecular diffusion i.e. Fickian's law, which assumes a gaussian distribution that displays a linear mean square displacement. Asymmetries related to turbulent flow in the atmosphere are depicted by the diffusion coefficient. So far the fractional model takes on an anomalous probability distribution with a power-law mean squared displacement (2.144). This anomalous distribution has been demonstrated to be more efficient to describe the motion of particles in a turbulent flow [262].

Table 3.4: Meteorological conditions during the Copenhagen experiment [250].

Exp.	Stability	$u_{10}(ms^{-1})$	$u_*(ms^{-1})$	L(m)	$\sigma_\omega(ms^{-1})$	h(m)
1	Very unstable (A)	2.1	0.37	-46	0.83	1980
2	Slightly unstable (C)	4.9	0.74	-384	1.07	1920
3	Moderately unstable (B)	2.4	0.39	-108	0.68	1120
4	Slightly unstable (C)	2.5	0.39	-173	0.47	390
5	Slightly unstable (C)	3.1	0.46	-577	0.71	820
6	Slightly unstable (C)	7.2	1.07	-569	1.33	1300
7	Moderately unstable (B)	4.1	0.65	-136	0.87	1850
8	Neutral (D)	4.2	0.70	-72	0.72	810
9	Slightly unstable (C)	5.1	0.77	-382	0.98	2090

Table 3.5: Observed and estimated crosswind-integrated concentrations $\bar{c}_y/Q(10^{-4}sm^{-2})$ for Copenhagen experiment.

Exp.	Distance(m)	Observed	Gaussian	α-Gaussian	M-Gaussian
1	1900	6.48	3.58	6.09	6.31
1	3700	2.31	2.47	4.04	4.10
2	2100	5.38	2.47	4.14	4.18
2	4200	2.95	1.75	3.05	3.30
3	1900	8.20	4.45	6.71	6.91
3	3700	6.22	3.73	5.38	5.44
3	5400	4.30	3.72	4.27	4.29
4	4000	11.7	10.25	10.74	10.75
5	2100	6.72	4.17	5.79	5.88
5	4200	5.84	3.93	4.79	4.81
5	6100	4.97	3.93	4.98	5.00
6	2000	3.96	2.00	2.26	2.28
6	4200	2.22	1.53	2.27	2.35
6	5900	1.83	1.17	2.06	2.13
7	2000	6.70	2.86	4.68	5.52
7	4100	3.25	1.94	3.65	3.89
7	5300	2.23	1.73	3.35	3.58
8	1900	4.16	4.02	5.52	5.73
8	3600	2.02	3.01	4.97	5.01
8	5300	1.52	2.94	4.29	4.42
9	2100	4.82	2.95	3.77	4.52
9	4200	3.11	1.64	3.01	3.27
9	6000	2.59	1.95	2.91	3.15

Table 3.6: Comparison between the three methods according to standard statistical performance measure

Model	NMSE	FA2	FB	COR	FS
Ideal	0	1	0	1	0
Gaussian	0.23	0.73	-0.39	0.82	0.27
α-Gaussian	0.07	0.87	0.001	0.83	0.30
M-Gaussian	0.06	0.88	-0.03	0.86	0.28

Table 3.7: Observed and estimated crosswind-integrated concentrations $\bar{c}_y/Q(10^{-4}sm^{-2})$ for Copenhagen experiment.

Exp.	Distance(m)	Observed	α-GILTT	α-Gaussian	*Present*
1	1900	6.48	6.38	6.34	6.30
1	3700	2.31	2.47	4.95	4.10
2	2100	5.38	4.87	4.18	4.14
2	4200	2.95	3.27	3.27	3.30
3	1900	8.20	8.70	6.51	6.40
3	3700	6.22	5.07	5.22	5.00
3	5400	4.30	3.72	4.67	3.95
4	4000	11.70	10.75	10.70	10.60
5	2100	6.72	4.17	5.79	5.88
5	4200	5.84	3.93	5.69	5.61
5	6100	4.97	5.00	4.48	4.10
6	2000	3.96	2.00	2.26	2.28
6	4200	2.22	1.53	2.27	2.35
6	5900	1.83	1.17	2.06	2.13
7	2000	6.70	2.86	4.68	5.52
7	4100	3.25	2.23	2.28	2.22
7	5300	2.23	1.95	1.73	1.70
8	1900	4.16	4.02	3.51	4.73
8	3600	2.02	3.00	3.01	2.96
8	5300	1.52	2.94	2.29	2.18
9	2100	4.82	2.95	2.26	2.22
9	4200	3.11	2.44	1.64	3.27
9	6000	2.59	1.95	2.00	3.15

Table 3.8: Statistical performance indicators of the models for different values of α

Dispersion Model	NMSE	FA2	FB	COR	FS
α-GM	0.12	0.91	-0.04	0.75	0.28
α-GILTT	0.22	0.87	-0.30	0.70	0.01
Present	0.03	0.96	-0.17	0.88	-0.04

3.5   Non-linear fractional evolutive equations profiles

3.5.1   Profile of the atmosphere dust-particles

The present section discloses the numerical simulations for the time-fractional mKdV equation. we have displayed the solution graphs for time-fractional mKdV equation for both classical and fractional order. Figures (3.16)-(3.19) and (3.20)-(3.23) show the evolution of the traveling wave solutions for Eqs. (2.181) and (2.186). From earlier study, the proposed solutions have distinctive scenarios from other methods and have various kinds of parameters. However, our solutions include similarities with the solutions derived by other methods as fractional complex transform which has been analyzed applying the space-time fractional mKdV equation in the non-integer order, called sigmoid-function method [263].

However, our estimations are performed on the solutions of the time-fractional generalized mKdV equation including the values of the coefficients and some sensible values, respectively $\alpha = 1, 0.5, 0.75$. It can be observed that the amplitudes and velocities of the solitons depend on both k and α, where α is a parameter related to non-linearity. Figures (3.24) and (3.25) show the one soliton (peakon) and the one soliton (shock wave) using solution (2.191). The traveling wave soliton solutions of the time-fractional mKdV equation are obtained. Futhermore, 3-dimensional pattern of the solution $u(x, t)$ for the time-fractional mKdV equation with space x and the time t for different values of the order α is indicated, respectively.

In figures (3.16)-(3.19) highlighting Hyperbolic equation (2.181) the solution $u(x, t)$ is at all time a single soliton wave for all values of order α. It prove that the balancing scenario between non-linearity and dispersion is still valid. Figures (3.20)-(3.23) emphasize the Trigonometric equation (2.186) the solution depict the change of the amplitude and width of the soliton arising from the variation of the order α. The behaviour shows that the increasing of the value α is regular in both height and the width of the traveling wave solution. i.e., the order α can be applied to modify the shape of the solitary wave free of alteration of the non-linearity and the dispersion effects of the milieu.

The outcome of this method is reliable and offer more solutions that other analytical methods. These equations with time-dependant coefficient and the stochastic perturbation terms will be introduced in the next work by using this method.we obtain some exact solutions of the time-fractional mKdV equation. By using the two variables (G$'$/G, 1/G)-expansion method. The method used in this study, can be applied for searching some exact solutions of the NPDEs.

Hyperbolic functions

Figure 3.16: Profile of one-soliton solution (2.181) of the time-fractional KdV-mKdV equation for $k = 3/4$, $c = a_0 = \alpha = 1$.

Figure 3.17: contour plot of graph (3.16).
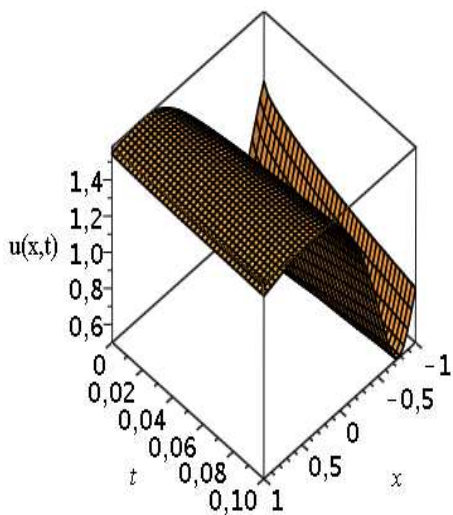
Figure 3.18: Profile of the single-soliton solution (2.181) of the clannish random walker Hyperbolic equation for $k = 0.62$, $c = a_0 = 1$, $\alpha = 0.5$.
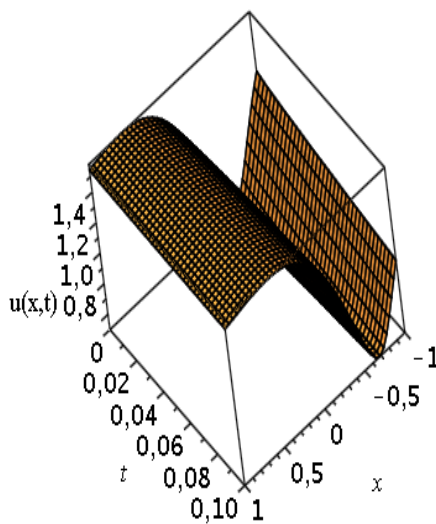
Figure 3.19: Profile of the single-soliton solution (2.181) of the clannish random walker Hyperbolic equation for $k = 0.68$, $c = a_0 = 1$, $\alpha = 0.75$.
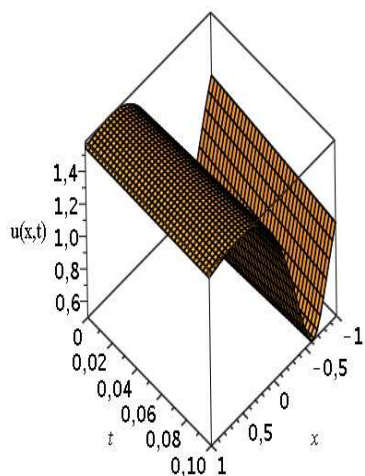
Trigonometric functions
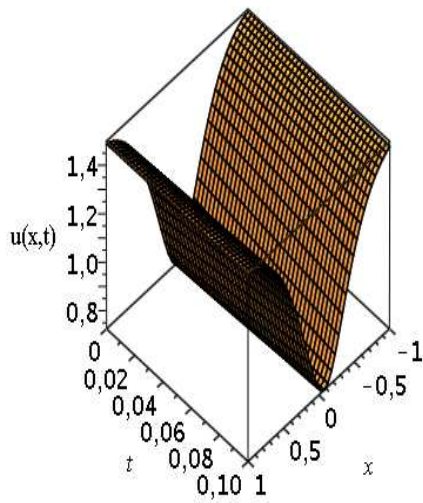
Figure 3.20: Profile of one-soliton solution (2.186) of the time-fractional KdV-mKdV equation for $k = 3/4$, $c = a_0 = \alpha = 1$.
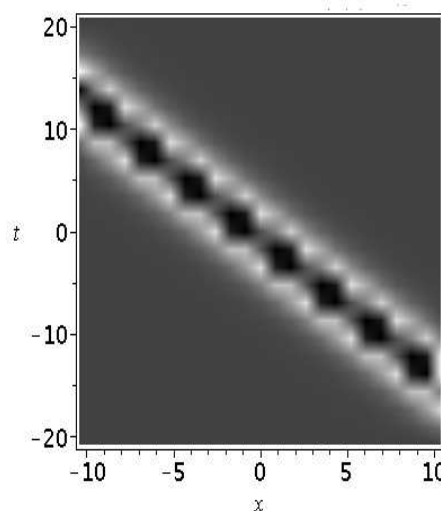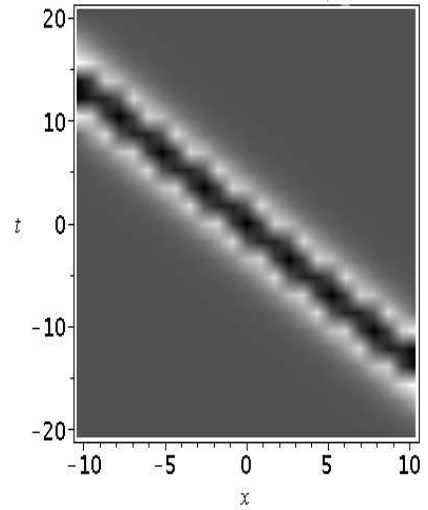

Figure 3.21: contour plot of graph (3.20).
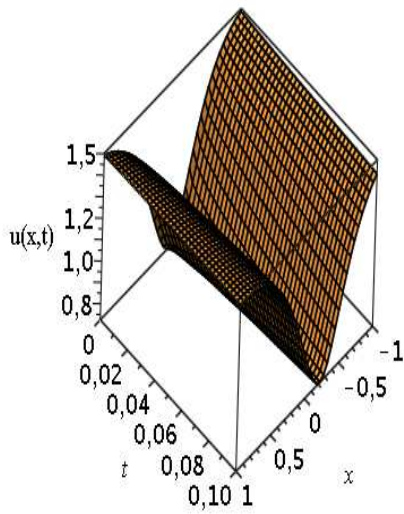
Figure 3.22: Profile of the single-soliton solution (2.186) of the clannish random walker Trigonometric equation for $k = 0.62$, $c = a_0 = 1$, $\alpha = 0.5$.
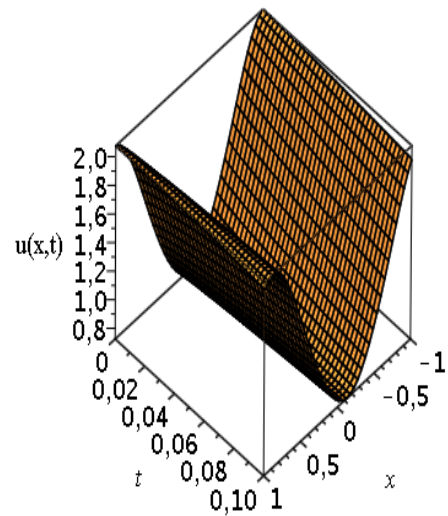
Figure 3.23: Profile of the single-soliton solution (2.186) of the clannish random walker Trigonometric equation for $k = 0.68$, $c = a_0 = 1$, $\alpha = 0.75$.

Rational function
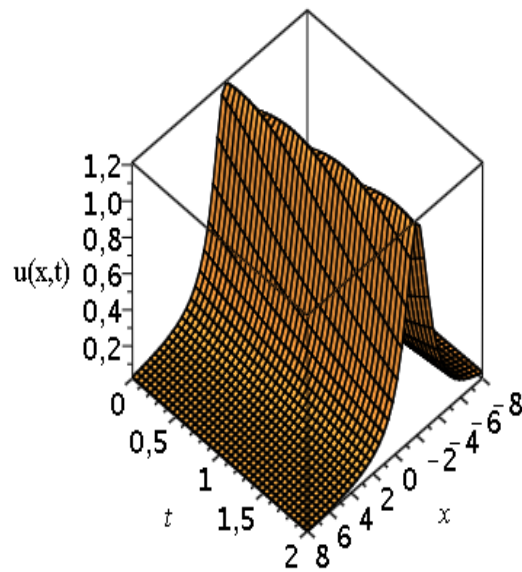
Figure 3.24: Profile of one-soliton (a peakon) solution (2.191) of the time-fractional KdV-mKdV equation for $k = 3/4$, $c = \alpha = 1$ (Real part).
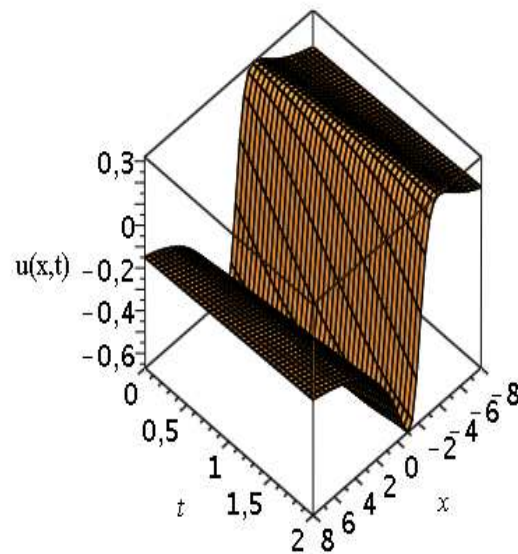
Figure 3.25: Profile of one-soliton (a shock wave) solution (2.191) of the time-fractional KdV-mKdV equation for $k = 3/4$, $c = \alpha = 1$ (Imaginary part).

3.5.2 Scattering of interfacial traveling waves in a two-layer fluid systems

It is established that the non-linear partial differential equations described as evolution equations provide a special type of elementary solution. These solutions so-called as solitons display the form of localized waves that maintain their properties even after mutual interaction, and then behave a bit like particles. On another note, the balancing scheme between non-linearity and dispersion is one of the most recuring patterns for solitary waves to occur, they can also arise as a consequence of other balancing mechanisms. Therefore our objective is to study carefully, the effects of fractional order derivatives on the structure and propagation of the resulting solitary waves obtained from FmKdV equations. The basic advantage of the suggested method comparatively to the generalized and improved $(G'/G, 1/G)$-Expansion method consist of that this method offers new and more general type exact traveling wave solutions with numerous real parameters. In a nutshell, the traveling wave solutions of some non-linear evolution equations (NLEEs) have its relevance to disclose the internal effect of the physical phenomena. The traveling solitary wave solutions of the non-linear space-time fractional mKdV equation obtained by the given method are different from those obtained by other researchers due to the following reasons.

- The proposed solution (2.211) has a distinctive architecture from other methods and has various kinds of parameters;

- By introducing several values of d_n's $(n = 0, 1, 2)$, (2.211) outline multiple types of special solutions in the form of trigonometric, hyperbolic, exponential and rational functions;

However, our solutions include similarities with the solutions derived by other methods as setted out thereafter.

- For the particular solution $u(\xi)$, using certains approximations in terms given by the global expression, we have retrieved the previously well-known solution (2.187) that have been found in litterature [264, 265];

- Authors obtained new traveling wave solutions in Ref. [266] for the non-linear mKdV space-time fractional partial differential equation by extended tanh-function method are similar with our solutions in family 1.2 and 2.1 for the space-time fractional coupled mKdV equation;

- To our knowledge the general solutions (2.181), (2.186) and (2.191) that report on travelling wave type solutions, have not been yet obtained in the litterature.

The remaining of our solutions are new and has not developed previously. No any other study proposed exact traveling wave solutions for coupled mKdV equation. Since the coupled mKdV equation depictes approximatively the motion phenomena occuring in a two-layer fluid systems [267]. The new analytical solutions (2.215), (2.220) and (2.225) will be hepful in the study of the physical behavior of these fluid systems. The purpose of the present study is the effect of the fractional-order derivative on the structure and propagation of the resulting traveling waves obtained from coupled mKdV equation. The fractional derivative in the sens of the modified Riemann-Liouville derivative and the Feng's first integral method are employed to obtain the first order differential equation (2.211) from the non-linear coupled space-time fractional mKdV partial differential equation (2.196). Using An improved (G'/G, 1/G)-Expansion method yields a set of algebraic equations that leads to the general solution of space-time fractional mKdV equation (2.196). However, our approximative calculations are carried out on the solution of the time-fractional mKdV equation regarding some values of the coefficients and some relevant values respectively, $\alpha = 1$, 0.5 and 0.75. The traveling waves soliton solutions of the coupled time-fractional mKdV equations are obtained. Moreover, 3-dimensional and 2-dimensional representations of the solutions $u(x,t)$ and $v(x,t)$ for the time-fractional generalized mKdV equations with space x and time t for different values of the order are presented, namely. In Figures (3.26) and (3.29) the solutions u and v are still single soliton waves solutions for all values of the order α. This demonstrates that the balancing schemes between non-linearity and dispersion remain in effect. Figures (3.26) and (3.28) illustrated the change of amplitude and width of the soliton arising from the variation of the order α. 2-and 3-dimensional graphs characterized the behaviour of the solutions $u(x,t)$ and $v(x,t)$ at time t respective to diffrents values of the order α. The shape demonstrates that the increasing of the values α is uniform in both height and width of the traveling waves solutions. That is the order α can be applied to modify the behavior of the traveling waves without change of the non-linearity and the dispersion effects in the milieu. Figure (3.28) is devoted to the analysis of the term of the relation between the amplitude of the traveling wave soliton and the fractional order at different time values. The figures depict that at the same time, the increasing of the fractional α increases the amplitude of the traveling wave to some values of α.

It can be noticed that in Figures (3.30) and (3.31) the amplitudes and velocities of the traveling waves solitons depend on both k and α, where α is a parameter connected to non-linearity. Figure (3.32) and (3.33) point out the two-soliton solutions and their evolution in time and space. Overtaking collisions between the two solitons for two different amplitude

modes are displayed in figure (3.34). In figure (3.35), the plot of the fusion phenomenon of the two solitons with the parameters for $k_1 = 0.5$, $k_2 = 1$, it is seen that two single soliton fusions become one resonant soliton after their interaction, that is, after a specific time t = 0. That means, when the two bodies behave nearer to each other after interaction between them with different characteristics as different sizes, different behaviour for examplification and tend to be a single clannish, which is completely different from the previous nature i.e., different sizes, different behaviour and so forth. From a careful analysis of (3.34) and (3.35), it is concluded that, for all the ranges of the two arbitrary parameters k_1, k_2, only fusion occurs. Neither elastic scattering nor fission does exist. That is, the two waves with different amplitudes and velocities collide at t = 0. The waves keeps their shapes and sizes the same before and after collision except for shifting the phase for any parametric values in the solution. Therefore, we conclude that during the interaction of waves in the presence of weakly non-linear surface and internal waves in a medium, the two solitons keep their initial shapes and velocities except for shifting the phase.

The non-linear partial differential equations described as evolution equations provide a special type of elementary solution. These solutions so-called as solitons display the form of localized waves that maintain their properties even after mutual interaction, and then behave a bit like particles. On another note, the balancing scheme between non-linearity and dispersion is one of the most recuring patterns for solitary waves to occur, they can also arise as a consequence of other balancing mechanisms. Therefore our objective is to study carefuly, the effects of fractional order derivatives on the structure and propagation of the resulting solitary waves obtained from FmKdV equations. The basic advantage of the suggested method comparatively to the generalized and improved (G′/G, 1/G)-Expansion method consist of that this method offers new and more general type exact traveling wave solutions with numerous real parameters. In a nutshell, the traveling wave solutions of some non-linear evolution equations (NLEEs) have its relevance to disclose the internal effect of the physical phenomena. The (G′/G, 1/G)-Expansion method to derived new exact solution of traveling wave solutions of the coupled time-fractional mKdV equation. This method has more advantages, it is direct, precise and concise. Therefore, the proposed method can be found potentially useful to solve many systems of non-linear fractional partial differential equations in mathematics and physics. The advantages of this method is that it avoids tedious calculations and provides exact and explicit traveling wave solutions with acuracy. Therefore it can be used to construct the exact solutions for some time-fractional differential equations.
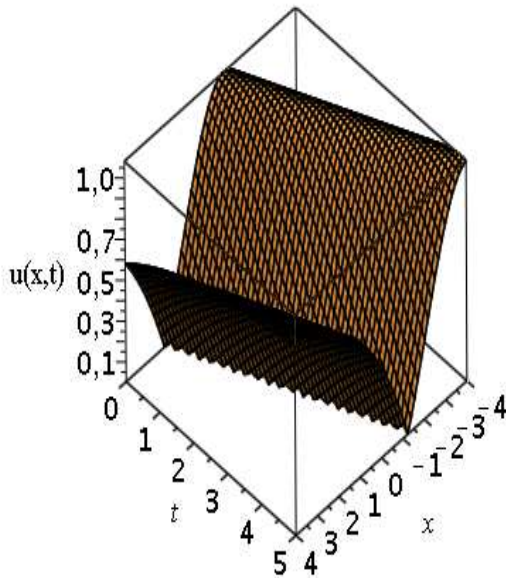
Figure 3.26: The distribution function u(x,t) as a 3-dimensions graph for value of fractional order $\alpha = 1$.
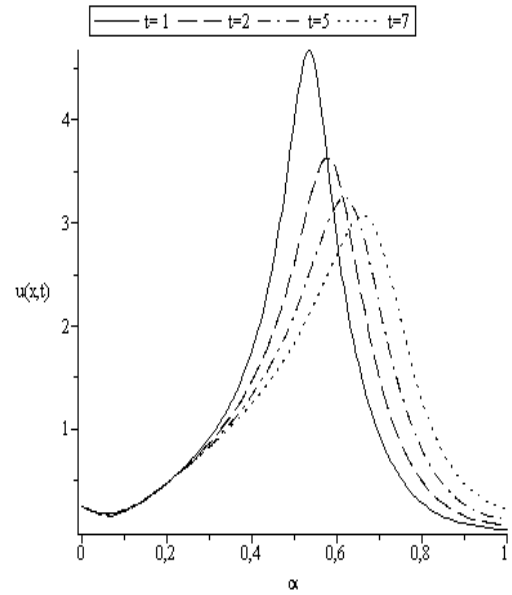
Figure 3.27: The amplitude of the distribution function u(x,t) as a function of the fractional order (α) at different time values : 2-dimensions graph.
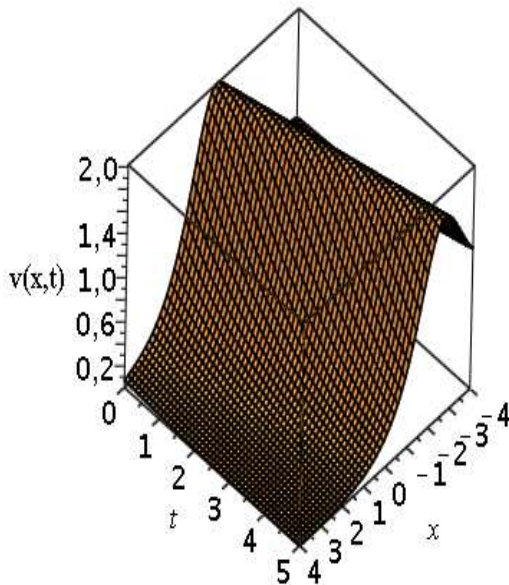
Figure 3.28: The distribution function v(x,t) as a 3-dimensions graph for value of fractional order $\alpha = 1$.
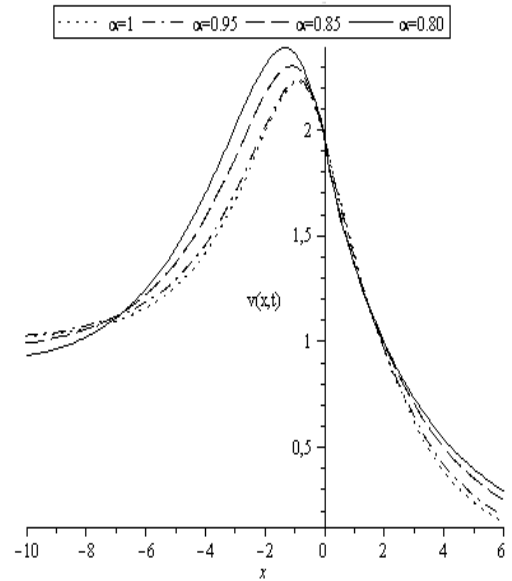
Figure 3.29: The distribution function v(x,t) as a function of space x at time t=1 for different values of the fractional order (α) : 2-dimensions graph.
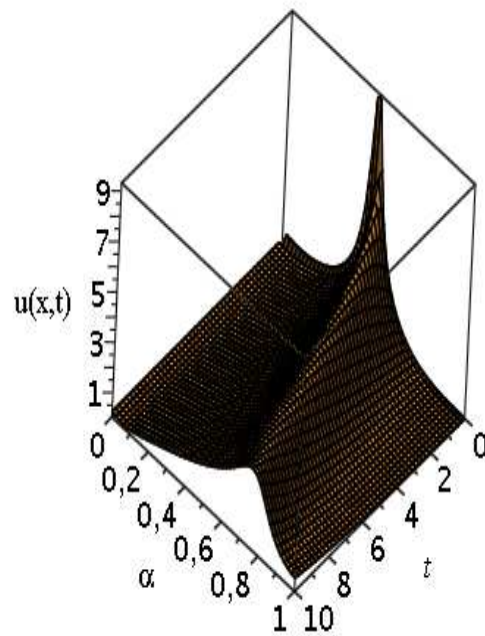
Figure 3.30: Profile of the single-soliton (a traveling wave type) solution for $k_1 = 0.5$ including different values of the fractional order α.
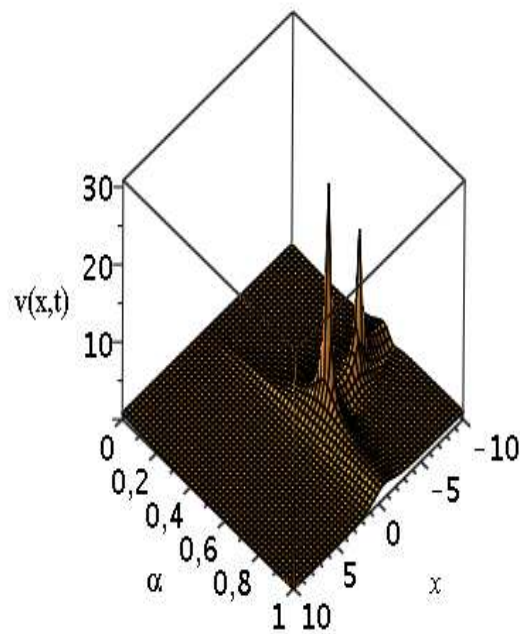
Figure 3.31: Profile of the single-soliton (a traveling wave type) solution for $k_2 = 1$ of space x at time t=1 for different values of the fractional order α.
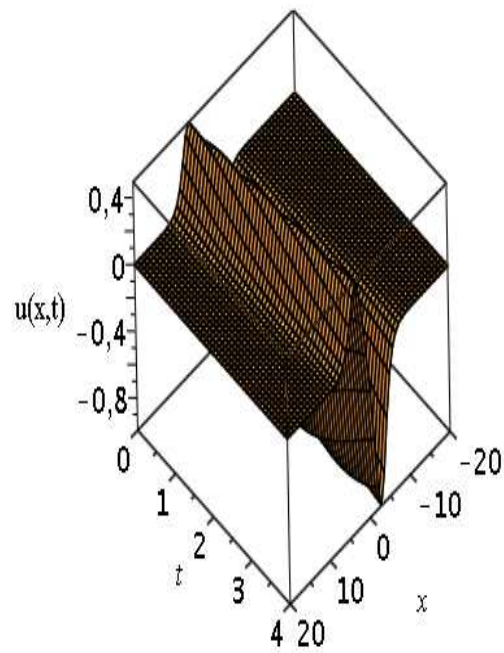
Figure 3.32: Profile of the two traveling waves with different amplitudes and velocities for $k_1 = 0.5$ and $k_2 = 0.002$ of the coupled mKdV equation.
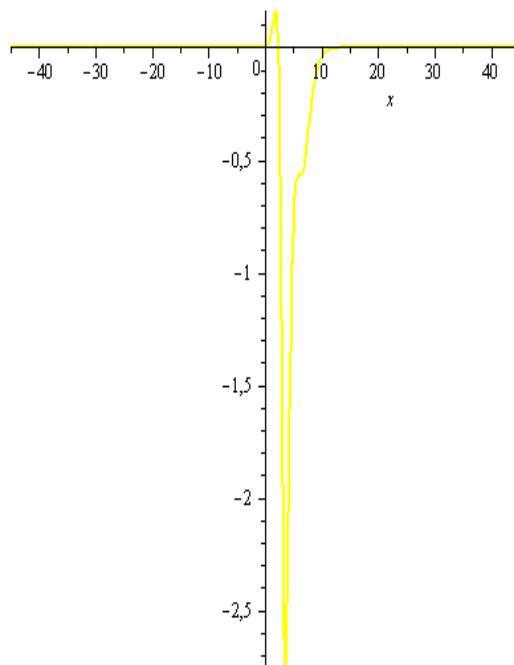
Figure 3.33: Evolution of the two traveling waves type soliton solutions in space and time.
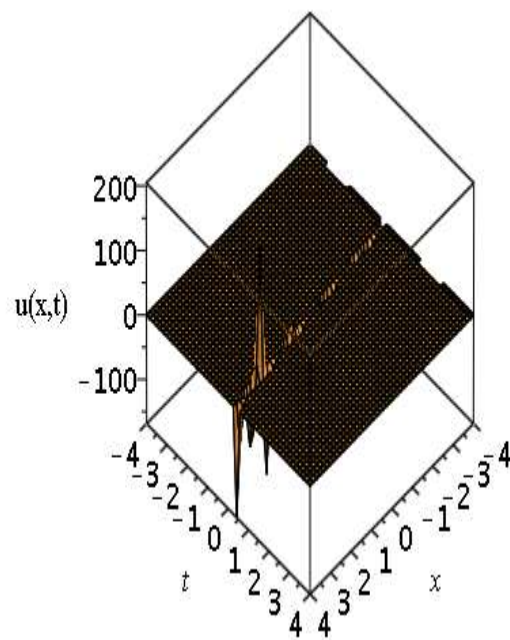
Figure 3.34: Profile of interaction of two-soliton solutions of the coupled mKdV equation for $k_1 = 6.5$, $k_2 = 5$, and $\alpha = 1$.
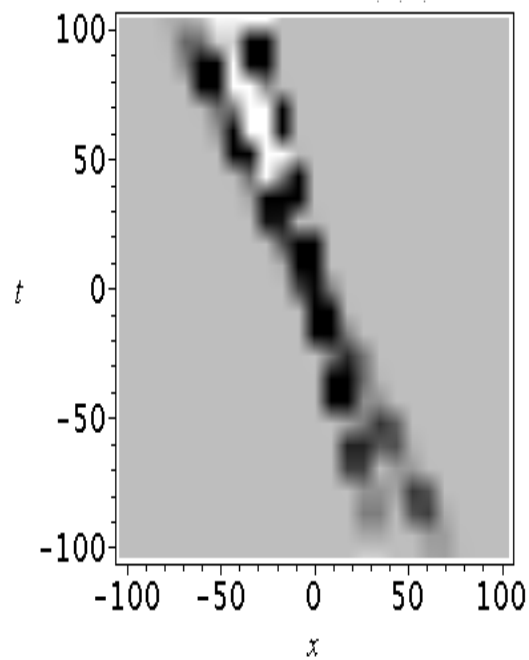
Figure 3.35: Evolution and collision of the two traveling waves type soliton solutions at $(0,0)$ point for $k_1 = 0.5$ and $k_2 = 1$.

3.6 Physical consequences in non-integer domains

3.6.1 Power-law pattern

The statistical indices used to assess the performance of the mathematical models are summarized in (Tables 3.3, 3.6 and 3.8). The results of the crosswind-integrated concentrations estimated in Table 3.6 for the Copenhagen experiment [268], obtained for the fractional models are compared with the experimental data and the gaussian model Eq. (2.151). The gaussian model and α-gaussian model Eq. (2.152), show that the average wind speed in the longitudinal direction (u) is obtained from Table 3.4 and the coefficient K is chosen, in order of comparison, as being the average of the diffusion coefficient given by Eq. (2.151) (with $\alpha = 1$) over the longest x distance of each experiment. Tables 3.6 and 3.8 show good performance for the proposed fractional models. In particular, Table 3.6 from the statistical indices obtained from the mathematical models and the results obtained in the evolution of the Copenhagen dispersion experiment [269], shows that the α-gaussian model works much better than the gaussian model equation (2.151), as shown by the statistical indices.

The advantage of the M-gaussian model consist of generalization of both gaussian and α-fractional models, it comes forth from the expression of the rates of increase which are the basis of the formulation of expressions and derivative terms. From the point of view of statistical physics, normal diffusion is the basis of the well-known Brownian motion of particles. The advantage of fractional models over standard integer derivative models is that the former can very well describe the inherent processes of unusually exponential or heavy tail decay. As an illustration, compared to the gaussian models, the fractional models are consequence of the anomalous diffusion presents on the turbulent diffusion which leads a distribution with a power-law of average quadratic displacement. It is important to note that the M-gaussian model also has better performance. For convenience to our analysis, it was considered that the diffusion coefficient is a function $K(x) = \frac{\kappa}{u} = \rho . \left(\frac{\sigma_\omega}{u}\right)^2 .x$ to give full meaning to the anomalous diffusion formulated in the problem [270].

Finally, in order to estimate the best approximated value for each model, the analysis is conducted on the basis of the values of $\alpha = 0.8$, $\beta = 0.99$, and $\beta = 0.7$, $\beta = 0.8$ in steps of 10^{-2}. For the α-gaussian model equation (2.150), the best performance occurs when it is close to 0.90. The variations noted in the choice of values proceed from the importance of the characterization of the different diffusion coefficients used throughout the process. In the Gaussian model equation (2.151), the diffusion coefficient (K) is constant, this subsumes a correlation between

the order of the equation and the quality of the diffusion coefficient compared to the model that best describes the observed concentration data. The traditional models ($\alpha = 1$) come from the molecular diffusion equation, inspired by the Fickian law, which assumes a gaussian distribution displaying a linear mean square displacement whose asymmetries is related to the turbulent flow in the atmosphere. That is described by a particular coefficient of diffusion. The fractional model assumes an anomalous probability distribution with a mean quadratic displacement power-law Eq. (2.152). This anomalous distribution proved more effective in describing particle motion in turbulent flow [270, 271]. The fractional derivative models have an obvious physical meaning and are easy to obtain from an adjustment of experimental or field measurement data.

3.6.2 Memory effect design

There is at least a century that we notes the existence of series of observations with persistent memory. Since then, phenomena of the same type have been observed, notably in chemistry, hydrology, climatology, thermodynamic and economics. Such series obviously pose interesting statistical problems and their modeling as well as their statistical behavior have already been the subject of several research works. There are some historical examples processed by fractional Brownian modeling. Also, approach based on fractional derivatives enables to describe viscous phenomena [272]. We distinguish long memory processes. They are so called because of the strong correlation between the observations widely separated over time. They are characterized by a decrease in their auto-correlogram according to a power function $\left(\gamma(h) = \gamma h^\delta\right)$. A random process is said to have a long memory if its autocorrelation function $\rho(k)$ is such that $\rho(k) \sim Ck^{-\alpha}$ [273], when $k \to \infty$ where $C > 0$ and $\alpha =]0,1[$ and $\sim$ represents asymptotic equivalence. $\rho(k)$ geometrical decrease (therefore slowly) when the delay increases. In the contrary, the advantage of short memory is that it induces, most often, many limiting theories such as the laws of large numbers, central functional theories and major deviation theories.

There are many short memory stochastic models, let's name a few one such as independent variables, m-independent variables, certain processes from Markov [274]. So, a process is said to have short memory if it has self-correlation $\rho(k)$; such as $\rho(k) \leq Ck^{-\alpha}$ when $k \to \infty$, where $C > 0, 0 < r < 1$ and $k = 1, 2, ...$, $\rho(k)$ decreases exponentially (so quickly) when the delay increases. Fractional differential equations are more stable than equations of integer ($\alpha = 1$) this is because memory systems are generally more stable than their equivalents which are of weak

memory [275]. A fundamental difference between fractional order models and integer order models is that the fractional models have memory, that is to say the fractional model depends on the history of the system. Furthermore, the non-local character of fractional operators also makes them useful in taking into account memory effects [276]. It has been proven that the fractional order of the function derivative has a significant influence on the pollutant concentration. For small values of the fractional parameter, the concentration has maximum values in the central area of the geometrical domain. If the fractional parameter increases, the concentration has a minimum in the same area. This behavior is due to the memory kernel of the time-fractional function derivative [277]. In contrast to gaussian diffusion, fractional diffusion is non-universal in that it involves a parameter α which is the order of the fractional derivative, hence fractional diffusion equations account for the typical anomalous features which are observed in many systems [278]. Also, the fractional approach is in some sense equivalent to the generalized master equation approach. The advantage of the fractional model again lies in the straightforward way of including external force terms and of calculating boundary value problems; Similar findings were revealed in a recent study [279].

Indeed, from the statistical indices obtained from the mathematical models and the results obtained in the evolution of the Copenhagen dispersion experiment, it is shown that the α-gaussian model works much better than the gaussian model, as shown by the statistical indices. The advantage of the M-gaussian model developed assuming a generalization of both gaussian and α-fractional models, it comes forth from the expression of the rates of increase which are the basis of the formulation of expressions and derivative terms. From the point of view of statistical physics, normal diffusion is the basis of the well-known Brownian motion of particles. The advantage of fractional models over standard integer derivative models is that the former can very well describe the inherent processes of unusually exponential or heavy tail decay. The traditional models ($\alpha = 1$) originate from the equation of molecular diffusion (Fick's law), which assumes a gaussian distribution that displays a linear mean square displacement. Henceforth, it was realized that the replacement of the local time derivative in the diffusion equation by a fractional operator accounts for the memory effects which are connected with many complex systems.

3.6.3   Complexity on nature-inspired fractal design-based flexible

A wide variety of natural phenomena is characterized by power-law behavior of their parameters. This type of behavior is also called scaling. The first observation of scaling

probably goes back to Kepler [280], who empirically discovered that squares of the periods of planet revolution around the sun scale as cubes of their orbits radii. This empirical law allowed Newton to discover his famous inverse-square law of gravity. In the Nineteenth century, it was realized that many physical phenomena, for example diffusion, can be described by partial differential equations. In turn, the solutions of these equations give rise to universal scaling laws. For example, the root mean square displacement of a diffusing particle scales as the square root of time. A class of large chemical reaction networks that exist not only outside the living, but on spatial scales many orders of magnitude larger than organisms. These are the chemical reaction networks of planetary atmospheres, networks whose structure is largely determined by the photo-chemistry of their component substrates.

The chemical reaction *networks* in these atmospheres, despite being tremendously different in chemistry, have a degree distribution consistent with a power-law [281]. Fractional derivatives inherit certain non-local behaviors, which leads to many interesting applications, including memory effects and future dependency. In particular, fractional equations offer a real advantage over integer differential equations, for the description of anomalous diffusion that can be easily followed from M-fractional type models. As a result, the concentration of pollutants in Eq. (2.152) decreases slowly for a given distance from the traditional gaussian model Eq. (2.151), since the Mittag-Leffler function, as defined initially for $0 < \alpha < 1$ decreases more than the exponential function. This can be further justified by the fact that the fractional models obey to a power law of the mean quadratic displacement [282]. In addition, the function $\mathbb{E}_\alpha\left(-\kappa\lambda_n^2 x^\alpha\right)$ is characteristic of the anomalous diffusion process, such as continuous time random walk, Levy statistics, fractional Brownian motion.

We recall that magnetic fields are able to couple the spin and the electron to facilitate electron transfer and enhance the rate of CO oxidation potentials, likely to induce magnetobiological or magnetophysiological effects. Carbon monoxide causes mental illnesses and worsens cardiovascular disease. Air pollution would also tend to decrease life expectancy [283]. The impact of pollution on health therefore depends on the nature of the pollutants, the type of people involved but also the dose received by the body. Factors affecting this dose are pollutant concentration, duration of exposure and physical activity. Fine particles (PM 2.5) can bind in the bronchi, or even impede the circulation in the pulmonary alveoli and cause cardiovascular disorders [284]. Thus it was generally observed that the electrical activity and oscillating behaviors of biological cells are greatly reduced due to electromagnetic radiation exposure and which is consistent with biological experiments. The analysis of the mechanisms underlying

spatial structures of activity in the neuronal network is relevant in discerning a wide range of both naturally occurring and pathological phenomena. Looking biological processes in nature, the metabolism of living creatures depends upon the oxygen dissolution process into water. It is important to mention that magnetic materials are used in a multitude of data storage systems, such as hard disks and MRAM devices. For instance, the principle of operation of a magnetic memory relies on the capacity to locally control the magnetization. Typically, upon writing, the magnetic moments. A magnetic moment is a quantity that represents the magnetic strength and orientation of a magnet or other object that produces a magnetic field.

Fractal structures are generally very difficult, but their formulation and the geometric understanding of the objects concerned have been considerably simplified. This certainly explains the concept in all phenomena where an appearance of disorder is encountered. Complex geometric structures. The existence of such structures in nature is either the result of the disorder present or is the result of functional optimization. This is the case of trees or lungs, which maximize their surface/volume ratio. The notion of fractality is basically geometric. Fractal structures are present in many natural or man-made "objects" and processes. This is the case of the prodigious branching of the bronchi in the lungs, clouds, rocky coasts, mountains or the roots of a plant. For instance, the increase of carbon dioxide in the atmosphere can cause climatic and geographical changes. Recently, our planet has begun to experience an increase in the volume of atmospheric CO_2 gases, which is thought to be life-threatening if it continues. Many reasons for the increased generation of CO_2 gases have been investigated and discussed with the aim of preventing or even reversing their release and the combination of magnetic field gradients and the susceptibility gradient enhance gas flow convection. The mass of a structure (gas cloud, galaxy, galaxy cluster) is proportional to a D power of its size, this power being a fractal dimension; a fractal is an object whose geometry can be described by a non-integer dimension.

3.7   On the fractal design in the pollutants exposure

The power-law (also called the scaling law) states that a relative change in one quantity results in a proportional relative change in another. Also, long range correlations and random walks Multiple biological networks show a connectivity or degree distribution that is broad-tailed and often consistent with a power-law.

3.7.1 Power-law scaling

The power law (also called the scaling law) states that a relative change in one quantity results in a proportional relative change in another. Recent studies have identified broadband phenomena in the electric potentials produced by the brain [285, 286]. As well as power-law scaling in these signals using subdural electrocorticographic recordings from the surface of human cortex. The power spectral density (PSD) of the electric potential has the power-law form $p(f) \sim A f^{-\alpha}$ from 80 to 500 Hz corresponding to this scaling index, $\alpha = 4.0 \pm 0.1$ [287]. For most multicellular creatures, the extent of cell number variability is unknown. Several scaling relationships are important in cell structure, biological systems obey a host of remarkably simple and systematic empirical scaling laws which relate how organismal features change with size over many orders of magnitude [288, 289]. For example, Kleiber's law implies that the power required to sustain unit mass of an organism, decreases with size; and the origin of these so-called allometric scaling relationships was stated earlier when studiying the phenomenon of relative growth [290], where x is body size, y is organ size, $\log b$ is the intercept of the line on the y-axis and a is the slope of the line, also known as the allometric coefficient. Following the ongoing revolution in biology. Certainly, sequencing of the human genome [291], the key words for these concerns are complexity, network, and power-law. In nature, a fractal object is defined by its structural properties, namely by surface roughness, intricacy, irregularity and absence of smoothness, form invariance, geometrical or statistical self-similarity, power-law scaling, morpho-functional complexity, iteration of simple generators, expressed by a numerical descriptor i.e. a fractional/non-integer dimension [292].

A mere but potentially powerful acumen into the nature of biological complexity i.e., typically, any complex system can be abstracted in the form of a network graph where the vertices are the elements of the systems and the edges are interactions between them. Specially in the cell the variety of interactions between genes, proteins and metabolites are well captured by networks. The latter can be, in the most forthright situation, physical interactions between proteins, but also similarities between expression profiles of genes, relationships between regulators and the regulated genes, links between neurons or other cells, and a variety of other types of links between biological entities. These biological networks share with each other and with other types of networks. The distribution of the number of connections per node in these networks more or less precisely follows a power-law. In a nutshell, for a sample including the metabolic network of 43 organisms [293], the protein interaction network of S. cerevisiae [294] and various food webs [295]. If the degree distribution instead was single-peaked as like Poisson

or gaussian, the majority of the nodes would be well described by the average degree, and therefore the notion of a typical node. Versus for networks with a power-law degree distribution, the majority of the nodes have only one or two neighbors while coexisting with many nodes with hundreds and some even with thousands of neighbors. For these networks there exists no typical node, and they are therefore often referred to as scale-free.

3.7.2 Long range correlations and random walks

The degree or connectivity of a node is the number of edges or the number of its neighbors in the graph. Multiple biological networks show a degree distribution that is broad-tailed and often consistent with a power-law. A network's degree distribution could be a simple consequence of chemistry, the chemistry of DNA, RNA, and proteins, and the patterns of molecular interactions this chemistry allows. Also, the degree distribution of genetic networks might somehow reflect their history. Molecular networks have their degree distribution, because this structure is somehow best suited to the network's biological function. Nowadays, recent hypothesis postulates that the observed broad-tailed degree distribution of biological networks is indeed a product of natural selection [296]. [296] made available information on a class of large chemical reaction networks that exist not only outside the living, but on spatial scales many orders of magnitude larger than organisms. These are the chemical reaction networks of planetary atmospheres, networks whose structure is largely determined by the photochemistry of their component substrates. The chemical reaction networks in these atmospheres, despite being vastly different in chemistry, have a degree distribution consistent with a power-law [297]. A remarkable feature of biological networks, also represented in social networks and air travel networks, is the existence of hubs, a colloquial term for vertices with a high number of connections compared to typical vertices. The vertex degree distribution shows a decay much slower than the gaussian-like distribution for random networks. In the twentieth century, power- laws were found to describe various systems in the vicinity of critical points. These include not only systems of interacting particles such as liquids and magnets [298] but also purely geometric systems, such as random networks [299]. Scaling is also found to hold for polymeric systems, including both linear and branched polymers [300]. Since then, the list of systems characterized by power-laws has grown rapidly including models of rough surfaces [301], turbulence and earthquakes. Empirical power-laws are found to characterize also many physiological, ecological, and socio-economic systems. These facts give rise to the increasingly appreciated fractal geometry of nature [302, 303, 304].

The term long range correlations, implying some long-range interactions or information propagation in space. In diffusion process it is characterise by the mean-square displacement of random walks. As a function of space it is assumed to have a power-like behavior. In such systems, super-diffusion may be attributed to long-range positive correlations. In fractal systems, random walks are usually sub-diffusive, assuming a smaller, non-trivial value, and one defines the so-called walk fractal dimension. So if fractals are in fact so widespread it makes sense to anticipate that long-range power-law correlations may be similarly widespread. Indeed recognizing the ubiquity of long-range power-law correlations can help us to understand nature since as soon as we find power-law correlations we can quantify them with a critical exponent quantification of this kind of scaling behavior for apparently unrelated systems enables us to notice similarities between different systems leading to underlying unifications that might under other conditions have gone pushed aside. In order to study the scale-invariant long-range correlations of a system sequence which we term a fractal landscape. It is notice that for the conventional random walk model, for the case of an uncorrelated walk the direction of each step is independent of the previous steps. For the case of a correlated random walk the direction of each step depends on the history memory of the walker [305, 306]. For describing space-time variations in the particle activity, we use the ADE as one of the most widespread equations in physics. Phenomenological laws are often sufficient to derive this equation and clarify its terms. Stochastic models can also be used to derive it, with the significant advantage that they provide information on the statistical properties of particle activity. Among these stochastic models, the most common approach consists of random walk models.

Remark 3. For practical aspects [307, 308], a KdV-like advection-dispersion equation $u_t + (3(1 - \delta)u + (\delta + 1)\frac{u_{xx}}{u_x})u_x =\in u_{xxx}$ or a scale-invariant analogue of the KdV equation $u_t + 2u_{xx}u_x/u =\in u_{xxx}$, which we named the SIdV equation. SIdV is one of the two simplest translation, scale and space-time parity-invariant non-linear advection-dispersion equation. The dimensionless parameter $\in$ measures the strenght of dispersion relative to advection. For $\in= 1$, SIdV shares the sech^2 solitary wave with KdV, as originally discovered by genetic programming. When $\in= \pm2/3, 0$. The equation reduces to the integrable mKdV equation, to a linear dispersive wave equation and to a non-linear diffusion equation. Like KdV, SIdV admits similarity solutions, solitary and cnoidal tavelling waves and remarkably even plane waves. The equation may be written in conservation law form in two ways [309, 310], leading to two integrals of motions. In general, we found a Lagrangian in a different variable at $\in= -2/3$ and a Hamiltonian when $\in= 2/3$.

3.8   Conclusion

Physico-mathematical models are powerful tools in the study of air pollution phenomena. They are realistic models designed for the most part on fundamental characteristics of chemistry-transport models. To verify the models' physical consistency. It's taken as its basis the conventionals experimental data from Copenhagen and the experimental datasets from Prairie Grass campaign. So far the fractional model takes on an anomalous probability distribution with a power-law mean squared displacement. Then, anomalous diffusion is an involved field with fascinating elusiveness. Fractional derivatives definitions are related to one another in a detailed scheme. At last, differences amount both to the convergence properties of the functional space on which these operators act and to boundary terms in the formula. The α-models as a consequence of the anomalous diffusion present in turbulent diffusion, results in a distribution with a power-law mean squared displacement. It is established that the non-linear partial differential equations described as evolution equations provide a special type of elementary solution. These solutions so-called as solitons display the form of localized waves that maintain their properties even after mutual interaction, and then behave a bit like particles. On another note, the balancing scheme between non-linearity and dispersion is one of the most recuring patterns for solitary waves to occur, they can also arise as a consequence of other balancing mechanisms. Therefore, our purpose is also to study carefuly, the effects of fractional order derivatives on the structure and propagation of the resulting solitary waves obtained from non-linear evolutive fractional equations.

General Conclusion

GENERAL CONCLUSION

Our final analysis begin by remembering that Cauchy-Kowalewsky's theorem guarantees the existence and uniqueness of an analytical solution for the advection-diffusion equation. We recall that analytical solutions can be written in two ways equivalent forms: solution expressed either in integral form or with a series formulation.

We look back on the scientific problem which gave rise to this study, in other words modeling of radioactive pollutants including non-conservative and non-linear evolution parameters in non-integer space.

In order to solve the initial problem, in a methodological approach, is considered step by step. The literature review which focuses on the transport and dispersion of radioactive pollutants in the atmosphere ; is recalled, at this stage the theoretical study of the dispersion versus mean square displacement in the Atmospheric Boundary Layer (ABL). Alike, mathematical background of air pollutants modeling gives an overview of conventional models with their limit in order to undertake other models with evolutive solutions. The interest of our research question appears as soon as arises the tremendous question of the nature of memory effects in atmospheric diffusion. The transport within the ABL, can be effective by advection-dispersion. Thus, the study of the power-law dynamics in the ABL displays the dynamics of normal and anomalous diffusion, coupling to the nature of memory effects in atmospheric dispersion. Besides, cumulative effets of pollutants in the environment, which requires a suitable understanding of the dynamic structure of the atmosphere. Economic and legal aspects of atmospheric pollution are evoked in order to contribute to resilient our planet.

Significantly more, a range of models and methods for solving the advection-diffusion equation is explored. We quote the statistical modeling approach that does not allow for detail the characteristics of turbulence and the deterministic approach relies on the formulation of physical mechanisms, chemical and digital resolution of equations, based on physics laws. All encompassing, diffential topology and geometry of dynamic systems for various dispersion models. Some techniques are used to generate solutions, as the N-truncated fractional derivative

type equation versus WKB-approximation method. Special attention is devoted to fractional cases assuming non-linear evolutive solutions, in terms of observing the non-linearity and the dispersive effects of the milieu. These analyzes lead to groundworks on tools for models validation. Finally, results and discussions highlight merging points by examining the integer-order versus the non-integer order of dispersion models considering linear and non-linear quadrature schemes. The convergence of the solution including comparison with the exact solution enable to foresight the evolution of the concentration in the Atmospheric Boundary Layer (ABL). The models are validated using datasets for Prairie Grass field experiment and Copenhagen campaign. Statistical indices allow to appreciate the degree of correlation between observed and predicted field data. Besides, non-linear fractional partial differential equations direct the findings of exact solution concerning time-fractional evolution problems. The study ends with a conclusion that opens up perspectives.

There are different types of risks classified according to the time of exposure at source with the harmful effects caused by atmospheric radioactive pollution: As evidence, planetary pollution today is as stake. Alerting the general public to air pollution is one of the most efficient solution against the environmental damage. The negative effects of industrial activity on the environment, which once were perceived exclusively as a local pollution problem, today are widely debated in public policy, aiming not only to preserve the environment, but also to mitigate and adapt to climate change produced by greenhouse gases. Then, the modeling of air pollutants involves complex techniques and procedures. However, in some cases there are analytical solutions that provide a quick and easy way to study turbulent dispersion. These models are well suited to real-time operational studies and impact studies because they require limited computation time and thus allow the study of a large number of cases.

Classical mechanics approaches are gaining importance in the study of the dynamics of systems that govern the world, for example the transport and dispersion of contaminants by dint of air. In most cases, these studies involve conservative systems, such as almost all the models studied above, but most of the processes observed in the physical real world are non-conservative. A system is said to be conservative when there is conservation of mass, energy, momentum. Thus, in many cases the real physical processes could be modeled in a real-able manner using fractional differential equations rather integer-order equations. Conduct a study on the models and methodology, comes back to explore the dynamic structure of the atmosphere; By means of an analysis of differential topology and geometry which caracterized dispersion models under controlled conditions. The change of dimensionality at different scales

and its acquiring non-integer values is typical of multi-fractals, so it is customary to describe dimensional flow as a fractal property of spacetime. Fractional measures have the desired characteristics of having anomalous scaling and inducing power-counting renormalizability. The fractional advection-dispersion equation (FADE) known as its non-local dispersion was used in the modeling of the turbulent and chaotic dynamics of classical conservative systems. The practical advantage of the FADE solution is that, although the differential equations containing Caputo derivatives require regular physical boundary conditions, the differential equations containing the Riemann-Liouville derivatives require non-regular boundary conditions, which are not as easy to implement and give the physical meaning of the solution. It was revealed, that the Mittag-Leffler function is the exact relaxation function for an underlying fractal time random walk process. In our context, fractional master equation is presented in a canonical forms and then solved with multiple methods. In order to check the accuracy of the employed analytical solution technique, cross-check analysis with previously existing solutions as fractional advection-dispersion equation and N-truncated type fractional model equation. Moreover, is envisaged the study of the the non-linear fractional partial differential equation.

For model performance evaluation, practical tools intended to serve as a common frame of reference. Fractional derivatives definitions are related to one another in a detailed scheme. At last, differences amount both to the convergence properties of the functional space on which these operators act and to boundary terms in the formula. Thus, numerical convergence of the proposed solution for the concentration with increasing numbers of eigenvalues is reached taking into account the conventional integer atmospheric diffusion equation and the fractional diffusion equation for different α parameters. Moreover, From earlier study, the proposed non-linear evolutive fractional solutions have distinctive scenarios from other methods and have various kinds of parameters. However, our solutions include similarities with the solutions derived by other methods as fractional complex transform which has been analyzed applying the space-time fractional mKdV equation in the non-integer order, called sigmoid-function method. In a nutshell, the traveling wave solutions of some non-linear evolution equations (NLEEs) have its relevance to disclose the internal effect of the physical phenomena. From the point of view of statistical physics, normal diffusion is the basis of the well-known Brownian motion of particles. The advantage of fractional models over standard integer derivative models consist of the former can very well describe the inherent processes of unusually exponential or heavy tail decay. There are some historical examples processed by fractional Brownian modeling. Also, approach based on fractional derivatives enables to describe viscous phenomena. Also, there are many short

memory stochastic models, let's name a few one such as independent variables, m-independent variables, certain processes from Markov. A fundamental difference between fractional order models and integer order models is based on the fact that the fractional models have memory, that is to say the fractional model depends on the history of the system. Hence the physical sens of memory effect; the shortening of life time of a material or substance. In fact, fractal structures are not easy in term of appreciation of their behavior, but their formulation and the geometric about the understanding of the objects concerned have been considerably simplified. The notion of fractality is basically geometric. Fractal structures are present in many natural or man-made "objects" and processes. A fractal is an object whose geometry can be described by a non-integer dimension.

To improve this innovative pattern in the study of the dispersion of radioactive pollutants in fractional domains, must be integrated and taken into account in the future:

- Models including the momentum transfer coefficient (surface drag coefficient) in a tropical environment under convective conditions;

- Parameterization schemes for velocity and diffusivity coefficient that reflect the realities of tropical zones;

- Investigate Fractional complex transforms for Fractional advection-dispersion equations;

- Introduce new tuning design schemes of Fractional complex-order PI, seeking control design with Fractional-order dispersive equations;

- Expand use of derivative of complex order in the Fractal dispersive models;

- Discuss disaster prevention by comparing experimental atmospheric dynamic parameters and its normalized atmospheric equivalent.

References

References

[1] M. Thaghavi, S. Cautenet, G. Foret, *Atmospheric Chemistry and Physics*. **4**, 825 (2004).

[2] J. Boussinesq, *Mémoires présentés par divers savants de l'Académie des Sciences de l'Institut Nationale de France*. **XXIII**, 1 (1877).

[3] D. J. Korteweg, F. de Vries, *Philosophical Magazine Series 5*. **39(240)** 422 (1895).

[4] A. A. Kilbas, H. M. Srivastava, J. J. Trujillo, *Theory and applications of fractional differential equations*. Elsevier, Amsterdam, (2006).

[5] I. Podlubny, *Fractional Differential Equations*. Academic Press, San Diego, (1999).

[6] S. G. Samko, A. A. Kilbas, O. I. Marichev, *Fractional Integrals and Derivatives: Theory and applications*. Gordon and Breach, New York, (1998).

[7] Y. Luchko, H. M. Srivastava, *Computers and Mathematics with Applications*. **29**, 73 (1995).

[8] A. Babakhani, V. D. Gejji, *Journal of Mathematical Analysis & Applications*, **278**, 434 (2003).

[9] S. Saha Ray, R. K. Bera, *Applied Mathematics & Computation*. **167**, 561 (2005).

[10] D. Zhi-Qiang, L. M. P. de Lima João, M. P. de Lima Isabel, V. P. Singh, *Water resources research*. **42**, (2006).

[11] M. T. van Genuchten, P. J. Wierenga, *Soil Science Society Of America Journal*. **40**, 473, (1976).

[12] R. Gorenflo, A. A. Kilbas, F. Mainardi, S. V. Rogosin, *Mittag-Leffler Functions, Related Topics and Applications*. Springer, Berlin, (2014).

[13] A. Giusti, *Nonlinear Dynamics*. **93(3)**, 1757 (2018).

[14] D. Baleanu, *Physica Scripta.* **T136**, 014006 (2009).

[15] D. Baleanu, J. I. Trujillo, *Communication of Nonlinear Science & Numerical Simulation.* **15(5)**, 1111 (2010).

[16] G. S. F. Frederico, D. F. M. Torres, *Nonlinear Dynamics.* **53(3)**, 215 (2008).

[17] J. A. Tenreiro Machado, *Nonlinear Dynamics.* **57(1-2)**, 253 (2009).

[18] M. K. Fung, *Chinese Journal of Physics.* **35(6)**, 789 (1997).

[19] R. Schumer, D. A. Benson, M. M. Meerschaert, S. W. Wheatcraft, *Journal of Contaminant Hydrology.* **48**, 69 (2001).

[20] O. P. Agrawal, *Nonlinear Dynamics.* **38(4)**, 323 (2004).

[21] B. J. Hong, D. C. Lu, *Journal of Basic and Applied Physics.* **1(3)**, 73 (2012).

[22] E. A. B. Abdel-Salam, Z. I. A. Al-Muhiameed, *Mathematical Problems in Engineering.* **2015**, 1 (2015).

[23] M. Duarte Ortigueira, J. A. Tenreiro Machado, *Journal of Computational Physics.* **293**, 4 (2015)..

[24] B. J. West, *Reviews of Modern Physics.* **86**, 1169 (2014).

[25] A. A. Kilbas, H. M. Srivastava, J. J. Trujillo, *Theory and Applications of Fractional Differential Equations.* Elsevier, Amsterdam, (2006).

[26] D. A. Benson, M. M. Meerschaert, J. Revielle, *Advanced Water Resources.* **51**, 479 (2013).

[27] J. P. Roop, *Journal of Computational and Applied Mathematics.* **193**, 243 (2006).

[28] P. P. Egeghy, D. A. Vallero, E. A. C. Hubal, *Environmental science & policy .* **14(8)**, 950 (2011).

[29] K. Kanchan, A. K. Gorai, P. Goyal, *Asian Journal of Atmospheric Environment.* **9(2)**, 101 (2015).

[30] P. G. Georgopoulos, A. F. Sasso, S. S. Isukapalli, P. J. Lioy, D. A. Vallero, M. Okino, *Journal of exposure science & environmental epidemiology.* **19(2)**, 149 (2009).

[31] D. A. Vallero, *Environmental contaminants: assessment and control.* Elsevier, (2010).

[32] J. Mitchell, J. A. Arnot, O. Jolliet, P. G. Georgopoulos, S. Isukapalli, S. Dasgupta, *Science of the total environment.* **458**, 555 (2013).

[33] N. Kwan-Hoong, *Non-ionizing radiations-sources, biological effects, emissions and exposures Kuala Lumpur.* (2003).

[34] S. Mathew, M. Rajagopalan, J. P. Abraham, D. Balakrishnan, A. G. madevi, *Natural radioactivity content in soil and indoor air of chellanam.* Radiation Protection and Dosimetry, (2012).

[35] G. Gadd, *Endeavour.* **20(4)**, 150 (1996).

[36] M. Eisenbud, T. F. Gesell, *Environmental radioactivity: from natural, industrial, and military sources.* Academic Pr, (1997).

[37] L. Verschaeve, *Journal Critical Reviews in Environmental Science and Technology.* **44(12)**, 1313 (2014).

[38] D. J. Jacob, *Introduction to Atmospheric Chemistry.* Princeton University Press, New Jersey, (1999).

[39] J. J. Jetter, Z. S. Guo, J. A. Mcbrian, M. R. Flynn, *The science of the total environment.* **295**, 51 (2002).

[40] J. M. Stockie, *SIAM Review.* **53**, 349 (2011).

[41] R. M. Harrison, H. A. McCartney, *Atmospheric environment.* **14**, 233 (1980).

[42] H. Balde, *Modélisation de la pollution atmosphérique de scalaires passifs par faibles vents.* Thèse de doctorat, Université D'Every Val D'Essonne, (2011).

[43] A. Doury, R. Gerard, M. Picol, *Abaques d'évaluation Directe des tranferts atmosphériques d'effluents gazeux.* Rapport DSN 84, (1980).

[44] O. Grandamas, Ph. Hubert, P. Pags, *Analyse critique des logiciels de dispersion atmosphérique.* CEPN, Rapport 157, (1989).

[45] J. R. Garratt, *The Atmospheric Boundary Layer.* Cambridge University Press, (1994).

[46] T. R. Oke, *Boundary Layer Climates.* Routledge, London, (1988).

[47] B. Crabol, F. Eberbach, D. Manesse, R. Martens, K. Massmeyer, M. Monfort, K. Nester, H. Schnadt, *Modèle franco-allemand pour le calcul de la dispersion atmosphérique en cas d'accident nucléaire.* Rapport technique DPEA/SECRI/121, IPSN, (1999).

[48] R. B. Stull, *An Introduction to Boundary Layer Meteorology.* Kluwer Academic Publishers, Springer Netherlands, XIV, 670, (1988).

[49] A. Einstein, *Annalen der Physik.* **17**, 549 (1905).

[50] B. Duplantier, *Séminaire Poincaré.* **1**, 155 (2005).

[51] R. Lewis Fry, *Containing Papers of a Mathematical and Physical Character.* **110**, 709 (1926).

[52] H. Scher, E. W. Montroll, *Physical Review B.* **12(6)**, 2455 (1975).

[53] E. W. Montroll, K. E. Shuler, *Advances in Chemical Physics.* **1**, 361 (2007).

[54] B. Mandelbrot, *The fractal geometry of nature.* WH freeman & Co, (1983).

[55] R. Metzler, J. Klafter, *Physics Reports.* **339**, 1 (2000).

[56] M. Bromly, C. Hinz, *Water Resources Research.* **40**, 1 (2004).

[57] K. J. Falconer, *Fractal geometry : mathematical foundations and applications.* John Wiley & Sons Inc, New york, (2003).

[58] B. O'Shaughnessy, P. Itamar, *Physical Review Letters.* **54**, 455 (1985).

[59] J. Klafter, M. F. Shlesinger, G. Zumofen, *Physics today.* **49(2)**, 33 (1996).

[60] R. Muralidhar, D. Ramkrishna, H. Nakanishi, D. Jacobs, *Physica A: Statistical Mechanics and its Applications.* **167(2)**, 539 (1990).

[61] V. M. Kenkre, E. W. Montroll, M. F. Shlesinger, *Journal of Statistical Physics.* **9(1)**, 45 (1973).

[62] D. Delbosco, L. Rodino, *Journal of Mathematical Analysis and Applications.* **204**, 609 (1996).

[63] J. Sabatier, O. P. Agrawal, J. A. Tenreiro Machado, *Advances in fractional calculus.* Springer, New York, (2007).

[64] L. W. Blank, T. M. Roberts, R. A. Skeffington, *Nature.* **336**, 27, (1988).

[65] G. Landmann, M. Bonneau, *Forest decline and atmospheric deposition effects in the French mountains.* Springer-Verlag, Heidelberg, Berlin, (1995).

[66] C. Langebartels, W. Heller, G. Führer, M. Lippert, S. Sirnons, H. J. Sandermann, *ecotoxicology and environmental safety.* **41**, 62 (1998).

[67] N. T. Keen, O. C. Taylor, *Plant Physiol.* **55**, 731 (1975).

[68] M. Schraudner, U. Graf, C. Langebartels, H. Sandermann, *Proceedings of the Royal Society of Edinburgh.* **102B**, 55 (1994).

[69] H. Eckey-Kaltenbach, D. Ernst, W. Heller, H. Sandermann, *Plant Physiology.* **104**, 67 (1994).

[70] D. T. Tingey, L. T. Gail, L. M. Gumpertz, W. E. Hogsett, *Agriculture and Environment.* **7(3)**, 243 (1982).

[71] C. Langebartels, W. Heller, D. Ernst, M. Lippert, C. Lütz, H.-D. Payer, H. Sandermann, *Ozone responses of trees: Results from controlled chamber exposure in the GSF phytotron. In Forest Decline and Ozone: A Comparison of Controlled Chamber and Field Experiments.* Ecological Studies, Springer, Berlin, (1997).

[72] D. P. Byres, T. J. Dean, J. D. Johnson, *The New Phytologist.* **120(1)**, 61 (1992).

[73] P. B. Reich, *Tree Physiology.* **3(1)**, 63 (1987).

[74] S. Chandrasekhar, *Reviews of Modern Physics.* **15**, 1 (1943).

[75] G. Metcalfe, M. F. M. Speetjens, D. R. Lester, H. J. H. Clercx, *Advances in Applied Mechanics.* **45**, 109 (2012).

[76] H. R. Seyf, B. Nikaaein, *International Journal of Thermal Sciences.* **58**, 36 (2012).

[77] Agence Internationale de l'Energie Atomique (AIEA), *Collection Documents techniques de l'AIEA*, (1981).

[78] A. Merle-Széréméta, J. Brenot, A. Thomassin, *Le Groupe Radioécologie Nord-Cotentin (GRNC) Etude Nord-Cotentin : méthodologie de l'analyse de sensibilité et d'incertitude.* Congrès SFRP, Tours, 19-21 juin (2001).

[79] S. Pal Arya, *Introduction to micrometeorology, Second edition.* Academic Press, San Diego, (2001).

[80] D. Maro, *Transfert des radionucléides sous forme de gaz et d'aérosols dans les environnements complexes : études expérimentales de dispersion atmosphérique et d'échange aux interfaces.* Mémoire d'habilitation à diriger la recherche, Institut de Radioprotection et de Sécurité Nucléaire (IRSN), Université des Sciences de Nantes, École doctorale SPIGA (Sciences pour l'Ingénieur, Géosciences, Architecture), Spécialité: Physique de l'atmosphère (2011).

[81] J. M. Dumas, G. Lhiaubet, G. Lemarois, G. Ducros, *Fission Product Transport Processes in Reactor Accidents, Fuel Behavior and Fission Product Release under Realistic Hydrogen Conditions with Comparisons between Heva 06 Test Results and Vulcain Computations, First edition.* CRC Press, Boca Raton (1990).

[82] N. J. Pattenden, R. S. Cambray, K. Playford, *Geochimica Cosmochimica Acta.* **45**, 93 (1981a).

[83] N. J. Pattenden, R. S. Cambray, K. Playford, J. D. Eakins, E. M. R. Fisher, *I.A.E.A.-S.M.-.* **248/138**, 201 (1981b).

[84] N. J. Pattenden, R. S. Cambray, K. Playford, J. D. Eakins, E. M. R. Fisher, *(198 I). Atmospheric measurements on radionuclides previously discharged to sea. In The Impacts of Radionuclides into the Marine Environment.* IAEA STI/PUB/565, Vienna (1980).

[85] A. V. Borges, B. Delille, L. S. Schiettecatte, F. Gazeau, G. Abril, M. Frankignoulle, *Limnology and Oceanography.* **49(5)**, 1630 (2004).

[86] G. Abril, H. Etcheber, P. Le Hir, P. Bassoullet, B. Boutier, M. Frankignoulle, *Limnology and Oceanography.* **44(5)**, 1304 (1999).

[87] J. H. Seinfeld, S. N. Pandis, *Atmospheric Chemistry and Physics: From Air Pollution to Climate Change, 3rd Edition.* John Wiley & Sons, New Jersey (2016).

[88] I. N. Ogorodnikov, V. A. Pustovarov, A. V. Kruzhalov, L. I. Isaenko, M. Kirm, G. Zimmerer, *Physics of the Solid State.* **42**, 464 (2000).

[89] A. Doury, *Une méthode de calcul pratique et générale pour la prévision numérique des pollutions véhiculées par 1'atmosphère.* Rapport CEA-R-4280 (Rév. 1), CENService de documentation, Gif-sur-Yvette (1976).

[90] G. Delibrias, *Le Journal de Physique et le Radium. Physique Appliquée.* **15(S5)**, 78 (1954).

[91] J. H. Seinfeld, *Atmospheric Chemistry and Physics of Air Pollution.* Wiley, New York (1986).

[92] J. H. Seinfeld, S. N. Pandis, *Atmospheric Chemistry and Physics.* John Wiley & Sons, New Jersey (1998).

[93] L. Jingfu, *Environmental Pollutants and Bioavailability.* **32(1)**, 68 (2020).

[94] Wout Slob, M. N. Pieters, *Risk Analysis.* **18(6)**, 787 (1998).

[95] W. F. Heidenreich, R. Hoogenveen, *Risk Analysis.* **21(1)**, 103 (2001).

[96] L. Järup, *British Medical Bulletin.* **68**, 167 (2003).

[97] D. Fullerton, G. E. Metcalf, *Journal of Public Economics.* **80(2)**, 249 (2001).

[98] G. E. Metcalf. *Journal of Public Economics.* **87(2)**, 313 (2003).

[99] O. G. Sutton, *Micrometeorology.* McGIraw-Hill, New York, (1953).

[100] A. S. Monin, A. M. Obukhov, *Geophysical Institute Academy of Sciences USSR.* **24**, 151 (1954). By *Bulletin of the American Meteorological Society, T-R-174, AF.* **19**, 604 (1936).

[101] J.-P. Détrie, P. Jarrault, *Revue de géographie alpine.* **4**, 865 (1969).

[102] B. Sportisse, *Pollution atmosphérique des processus à la modélisation.* Springer, New York, (2008).

[103] G. De Moor, *Couche limite atmosphérique et turbulence, les bases de la micrométéorologie dynamique. Cours et manuels nº 16 de Météo-France.* ENM, France, (2006).

[104] L. Menut, *Étude expérimentale et théorique de la couche limite atmosphérique en agglomération parisienne.* Thèse de doctorat, Université Pierre et Marie Curie, France, (1997).

[105] F. Pearson Lees, *Loss prevention in the process industries, Chap. 15 : Emission et dispersion.* Butterworth Heinemann, Oxford, (1996).

[106] O. Reynolds, *On the dynamical theory of incompressible viscous fluids and the determination of the criterion.* Philosophical Transactions of the Royal Society, London, (1895).

[107] F. Archambeau, N. Méchitoua, M. Sakiz, *International Journal on Finite Volumes.* **1**, 1, (2004).

[108] S. P. Arya, *Air Pollution Meteorology and Dispersion.* Oxford University Press, New York, (1999).

[109] L. Bai, J. Wang, X. Ma, H. Lu, *International Journal of Environmental Research and Public Health.* **15(4)**, 780 (2018).

[110] N. Oreskes, K. Shrader-Frechette, K. Belitz, *Sciences.* **263**, 641 (1994).

[111] S. R. Hanna, G. A. Briggs, J. Deardorf, B. A. Eagan, F. A. Gifford, F. Pasquill,*Bulletin of the American Meteorological Society.* **58(12)**, 1305 (1977).

[112] A. Doury, *Quelques réflexions sur le comportement thermodynamique de l'ozonosphère.* Pollution atmosphérique, 140, (1993).

[113] F. Pasquill, *Atmospheric Diffusion.* Van Nostrand, London, (1962).

[114] S. R. Hanna, P. J. Drivas, *Guidelines for the use of vapor cloud dispersion models.* Published by CCPS/AIChE, 345 East 47th St., New York, NY 10017, (1987).

[115] R. H. Schulze, D. Turner, *Practical guide to atmospheric dispersion modeling.* Trinity Consultants Inc., Texas, (1996).

[116] R. M. Lyon, F. Scott, *Water Resources Research.* **31(1)**, 213 (1995).

[117] T. K. Mikkelsen, S. E. Larsen, *Nuclear technology.* **67**, 56 (1984).

[118] M. Sharan, P. Kumar, *Atmospheric Environment.* **43**, 2268 (2009).

[119] J. S. Irwin, *Atmospheric Environment.* **13**, 191 (1979).

[120] C. J. Mooney, J. D. Wilson, *Boundary-Layer Meteorology.* **64**, 291 (1993).

[121] M. Abramowitz, I. A. Stegun, *Handbook of Mathematical Functions with Formulas, Graphs and Mathematical Tables, Chapter 15.* Dover Publ., Inc., New York, (1972).

[122] M. Sharan, S. Gupta, *Atmospheric Environment.* **36(1)**, 97 (2002).

[123] S. R. Hanna, *Journal of Applied Meteorology and Climatology.* **20**, 242 (1981).

[124] J. H. Seinfeld, *Atmospheric Chemistry and Physics of Air Pollution.* Wiley, New York, (1986).

[125] J. M. Ema'a Ema'a, G. H. Ben-Bolie, P. O. Ateba, *Atmospheric research.* **120**, 162 (2013).

[126] A. Gettelman, R. B. Rood, *Climate Models: A Users Guide to Earth System Models.* Springer, New York, (2016).

[127] C. M. E. Pompei, E. D. L. Alves, E. M. Vieira, L. C. Campos, *International Journal of Environmental Science and Technology.* **17**, 1387 (2020).

[128] L. J. Briley, W. S. Ashley, R. B. Rood, A. Krmenec, *Theoretical and Applied Climatology.* **127(3)**, 643 (2017).

[129] A. M. Vieira-de-melo, J. M. Santos, I. Mavroidis, J. Reis, *Building and Environment.* **56(8)**, 8 (2012).

[130] Y. Fraigneau, *Études numériques de l'évolution diurne de l'ozone dans la région d'une agglomération.* Thése de Doctorat, Rouen, (1996).

[131] J.-F. Louis, *Boundary-Layer Meteorology.* **17(2)**, 187 (1979).

[132] J.-F. Louis, M. Tiedtke, J.-F. Geleyn, *A short history of the PBL parametrization at ECMWF.* Proceding ECMWF Workshop on Planetary Layer parametrization Reading, (1982).

[133] S. Heinz, H. Van Dop, *Atmospheric Environment.* **33**, 2031 (1999).

[134] S. Wortmann, M. T. Vilhena, D. M. Moreira, D. Buske, *Atmospheric Environment.* **39(12)**, 2187 (2009).

[135] D. M. Moreira, M. T. Vilhena, T. Tirabassi, D. Buske, R. Cotta, *Atmospheric Environment.* **39**, 6289 (2005).

[136] D. M. Moreira, M. T. Vilhena, D. Buske, T. Tirabassi, *Atmospheric Research.* **92(1)**, 1 (2009).

[137] D. Buske, M. T. Vilhena, T. Tirabassi, B. Bodmann, *Journal of Environmental Protection.* **3**, 1124 (2012).

[138] D. M. Moreira, M. T. Vilhena, T. Tirabassi, C. Costa, B. Bodmann, *Water, Air and Soil Pollution.* **177(1)**, 411 (2006).

[139] C. F. Segatto, M. T. Vilhena, *Proceedings of Mathematics and Computational Reactor Physics and Enviromental Analysis in Nuclear Applications.* **1**, 1618 (1999).

[140] H. Scher, M. F. Shlesinger, J. T. Bendler, *Physics Today.* **44**, 26 (1991).

[141] E. W. Montroll, G. H. Weiss, *Journal of Mathematical Physics.* **10**, 753 (1969).

[142] E. W. Montroll, H. Scher, *Journal of Statistical Physics.* **9**, 101 (1973).

[143] J. Klafter, A. Blumen, M. F. Shlesinger, *Physical Review A.* **35**, 3081 (1987).

[144] W. I. Smirnow, *Lehrgang der hoK heren Mathematik, Vols. III/2 and IV/1.* VEB Deutscher Verlag der Wissenschaften, Berlin, (1988).

[145] K. B. Oldham, J. Spanier, *The Fractional Calculus.* Academic Press, New York, (1974).

[146] R. Hilfer, *Applications of Fractional Calculus in Physics.* World Scientific, Singapore, (1999).

[147] K. S. Miller, B. Ross, *An Introduction to the Fractional Calculus and Fractional Differential Equations.* Wiley, New York, (1993).

[148] E. Barkai, R. Metzler, J. Klafter, *Physical Review E.* **61**, 132 (2000).

[149] A. D. Michal, *Proceedings of the National Academy of Sciences.* **24**, (1938).

[150] V. I. Averbukh, O. G. Smolyanov, *Russian Mathematical Surveys.* **22**, (1967).

[151] K. M. Kolwankar, A. D. Gangal, *Chaos.* **6**, 505 (1996).

[152] Y. S. Mishura, *Stochastic calculus for fractional Brownian motion and related processes.* Springer-Verlag, Berlin, (2008).

[153] I. M. Sokolov, *First Steps in Random Walks-From Tools to Applications.* Oxford University Press, (2015).

[154] F. Ben Adda, *Nonlinear Analysis.* **47**, 5423 (2001).

[155] F. Ben Adda, *Comptes rendus hebdomadaires des sciences de l'Académie des sciences.* **326**, 787 (1998).

[156] G. Calcagni, *Physical Review D.* **84**, 061501(R) (2011).

[157] I. Podlubny, *Fractional differential equations.* Academic Press, San Diego, (1999).

[158] B. Ross, *A Brief History and Exposition of the Fundamental Theory of Fractional Calculus.* Fractional Calculus and its Applications, Berlin, (1975).

[159] X. J. Yang, *Prespacetime Journal.* **3(9)**, 913 (2012).

[160] X. J. Yang, *Journal of Applied Library and Information Science.* **1(1)**, 1 (2012).

[161] X. J. Yang, *Advanced Local Fractional Calculus and Its Applications.* World Science Publisher, New York, (2012).

[162] M. S. Hu, D. Baleanu, X. J. Yang, *Mathematical Problems in Engineering.* **2013**, 1 (2013).

[163] L. Machta, *Global scale atmospheric mixing.* Advances in Geophysics 18 B, Academic Press, 33-56 (1974).

[164] I. L. Karol, V. I. Ivanhoc, V. M. Kolobaskin, O. I. Leypunsky, V. I. Nekrasov, A. N. Gudkov, N. P. Ushakova, *International Association of Meteorology and Atmospheric Physics.* **5**, (1972).

[165] P. H. Gudiksen, A. W. Fairhall, R. J. Reed, *Journal of Geophysical Research.* **73**, 4461 (1968).

[166] J. B. Bassingthwaighte, L. S. Liebovitch, B. J. West, *Fractal Physiology.* Oxford University Press, Oxford, (1994).

[167] J. M. Ema'a Ema'a, G. H. Ben-Bolie, P. A. Owono, *Atmospheric Research.* **120**, 162 (2013).

[168] P. Kumar, M. Sharan, *Proceedings of the Royal Society.* **466**, 383 (2010).

[169] J. Ma, S. M. Daggupaty, *Environmental Modeling & Assessment.* **3**, 239 (1998).

[170] J. M. Ema'a Ema'a, *Modélisation de la dispersion et du dépôt sec des polluants rejétés dans l'atmosphère.* Thèse de Doctorat, Université de Yaoundé 1, (2013).

[171] J. M. Ema'a Ema'a, G. H. Ben-Bolie, P. Ele Abiama, A. Zarma, P. A. Owono, *Boundary-Layer Meteorology.* **155(2)**, (2015).

[172] I. S. Gradshteyn, I. M. Ryshik, *Table of Integrals, Series, and Products*, Academic Press, New York, (1980).

[173] M. D. Ortigueira, F. J. Coito, *Computers & Mathematics with Applications.* **59**, 1782 (2010).

[174] Y. Luchko, *Mathematical Modelling of Natural Phenomena.* **11(3)**, **1** (2016).

[175] A. Pelliccioni, T. Tirabassi, *Il nuovo cimento C.* **31(3)**, 253 (2008).

[176] P. Kumar, M. Sharan, *Proceedings of the Royal Society A.* **466**, 383 (2010).

[177] K. S. M. Essa, M. E. Soad, M. Embaby, *Atmospheric Research.* **84**, 337 (2007).

[178] J. S. P. Guerrero, L. C. G. Pimentel, J. F. de Oliveira-Júnior, P. F. Lavalle Heilbron Filho, A. G. Ulke, *Atmospheric Environment.* **55**, 201 (2012).

[179] T. Tirabassi, *Air Pollution and turbulence Modeling and Application.* **978**, 1 (2010).

[180] S. Havlin, D. Ben-Avraham, *Advances in Physics.* **36**, 695 (1987).

[181] M. T. Barlow, A. Grigor'yan, T. Kumagai, *Journal fï£¡r die reine und angewandte Mathematik.* **626**, 135 (2009).

[182] C. Gianluca, *Advances in Theoretical and Mathematical Physics.* **16**, 549 (2012).

[183] G. M. Zaslavsky, *Physics Reports.* **371**, 461 (2002).

[184] A. K. Blackadar. *Turbulence and Diffusion in the Atmosphere: Lectures in Environmental Sciences.* Springer-Verlag, Berlin, (1997).

[185] G. A. Gonï£¡alves, D. Buske, R. S. Quadros, G. J. Weymar, *International Journal of Development Research.* **8**, 20535 (2018).

[186] A. G. Cherstvy, R. Metzler, *Physical Review E.* **90(1)**, 012134 (2014).

[187] D. Buske, B. Bodmann, M. T. Vilhena, R. S. De Quadros, *American Journal of Environmental Engineering.* **5(1A)**, 1 (2015).

[188] R. B. Smith, *Boundary Layer Meteorology.* **139**, 501 (2011).

[189] G. H. Weiss, *Journal of Statistical Physics.* **80**, 2880 (1984).

[190] V. E. Tarasov, *Communications in Nonlinear Science and Numerical Simulation.* **30(1)**, 1 (2016).

[191] J. Vanterler, E. C. de Oliveira, *Progress in Fractional Differentiation and Applications.* **4(4)**, 479 (2018).

[192] J. Sabatier, C. Farges, *Journal of Computational and Applied Mathematics.* **339**, 30 (2018).

[193] M. D. Ortigueira, J. T. Machado, *Communications in Nonlinear Science and Numerical Simulation.* **82** 105022 (2020).

[194] A. G. O. Goulart, J. M. Lazo, J. M. S. Suarez, D. M. Moreira, *Journal of Fluid Mechanics.* **477**, 9 (2017).

[195] P. Kumar, S. K. Singh, P. Ngae, A. A. Feiz, G. Turbelin, *Atmospheric Research.* **197**, 84 (2017).

[196] Ŏzisik M. Necati, *Heat Conduction.* John Wiley & Sons, New York, (1980).

[197] R. Gorenflo, Y. Luchko, M. Yamamoto, *Fractional Calculus and Applied Analysis.* **18(3)**, 799 (2015).

[198] V. Kolokoltsov, *Fractional Calculus and Applied Analysis.* **18(4)**, 1039 (2015).

[199] S. R. Hanna, J. C. Chang, D. G. Strimaitis, *Atmospheric Environment. Part A. General Topics.* **27(15)**, 2265 (1993).

[200] K. S. M. Essa, A. S. Shalaby, M. A. E. Ibrahim, A. M. Mosallem, *Pure and Applied Geophysics.* **177**, 4545 (2020).

[201] K. S. Nisar, *Frontiers in Physics.* **8**, 33 (2020).

[202] A. Cayley, *Philosophical Transactions of the Royal Society.* **148**, 17 (1858).

[203] B. Bonilla, M. Rivero, J. J. Trujillo, *Applied Mathematics and Computation.* **187**, 68 (2007).

[204] A. Kadem, D. Baleanu, *On one method for solving fractional transport equation.* International Workshop on New Trends in Science and Technology, Ankara, (2008).

[205] D. M. Moreira, A. M. Moret, *Meteorological Society.* **57**, 185 (2018).

[206] D. Moreira, M. Vilhena, *Air Pollution and Turbulence: Modeling and Applications.* Taylor & Francis Ltd, New York, (2019).

[207] J. H. Seinfeld, *Atmospheric Chemistry and Physics of Air Pollution.* Wiley, New York, (1986).

[208] S. M. Khaled Essa, F. Mubarak, A. Abo Bakr, *World Applied Sciences Journal.* **34(10)**, 1399 (2016).

[209] A. Godec, R. Metzler, *Journal of Physics A: Mathematical and Theoretical.* **50(8)**, 084001 (2017).

[210] V. Sposini,R. Metzler, G. Oshanin, *New Journal of Physics.* **21(7)**, 073043 (2019).

[211] S. G. Samko, A. A. Kilbas, O. I. Marichev. *Fractional Integrals and Derivatives-Theory and Applications.* Gordon and Breach, Linghorne, (1993).

[212] R. Metzler, J. Klafter, *Physics Reports.* **339**, 1 (2000).

[213] R. Metzler, J. Klafter, *Journal of Physics A: Mathematical and Theoretical.* **37**, R161 (2004).

[214] B. J. West, *Reviews of Modern Physics.* **86**, 1169 (2014).

[215] Y. Li, R. Mei, Y. Xu, J. Kurths, J. Duan, R. Metzler, *New Journal of Physics.* **22(5)**, 053016 (2020).

[216] A. A. Kilbas, H. M. Srivastava, J. J. Trujillo, *Theory and Applications of Fractional Differential Equations.* Elsevier, Amsterdam, (2006).

[217] E. Awad, R. Metzler, *Fractional Calculus and Applied Analysis.* **23(1)**, 55 (2020).

[218] K. Diethelm, *The Analysis of Fractional Differential Equations: An Application-Oriented Exposition Using Differential Operators of Caputo Type.* Springer-Verlag, Berlin Heidelberg, (2010).

[219] I. Eliazar, R. Metzler, S. Reuveni, *Physical Review E.* **100(2)**, 020104 (2019).

[220] R. Metzler, *AIP Conference Proceedings.* **1579(1)**, 89 (2014).

[221] A. G. O. Goulart, J. M. Lazo, J. M. S. Suarez, D. M. Moreira, *Journal of Fluid Mechanics.* **477**, 9 (2017).

[222] E. M. E. Zayed, M. A. M. Abdelaziz, *Mathematical Problems in Engineering.* **2012**, 725061 (2012).

[223] O. Güner, A. Bekir, A. C. Cevikel, *The European Physical Journal Plus.* **130(146)**, 1 (2015).

[224] A. Bekir, O. Güner, O. Unsal, M. Mirzazadeh, *Journal of Applied Analysis and Computation.* **6(1)**, 131 (2016).

[225] Q. Zhao, S. K. Liu, Z. T. Fu, *Communications in Theoretical Physics.* **43**, 615 (2005).

[226] Y. Zhang, *Advances in Difference Equations.* **65**, 1 (2014).

[227] J.-H. He, *International Journal of Turbo & Jet Engines.* **14**, 23 (1997).

[228] J.-H. He, *Chaos,Solitons and Fractals.* **19**, 847 (2004).

[229] A. A. Kilbas, H. M. Srivastava, J. J. Trujillo, *Theory and applications of fractional differential equations.* Elsevier, Amsterdam, (2006).

[230] O. P. Agrawal, *J. Mathematical Analysis and Applications.* **272(1)**, 368 (2002).

[231] E. A. B. Abdel-Salam, Z. I. A. Al-Muhiameed, *Mathematical Problems in Engineering.* **2015**, 1 (2015).

[232] O. Unsal, O. Güner, A. Bekir, A. C. Cevikel, *AIP Conference Proceedings.* **1798(1)**, 020167 (2017).

[233] X. J. Yang, D. Baleanu, H. M. Srivastava, *Local Fractional Integral Transforms and Their Applications.* Academic Press (Elsevier), London, (2016).

[234] J.-H. He, S. K. Elagan, Z. B. Li, *Physics Letter A.* **376(4)**, 257 (2012).

[235] J. M. Burger, *Advances in Applied Mechanics.* **1**, 171 (1948).

[236] J. D. Cole, *Quarterly of Applied Mathematics.* **9**, 225 (1951).

[237] S. Sahoo, S. Ray, *Mathematical Methods in the Applied Sciences.* **40**, 106 (2016).

[238] G. Jumarie, *Computers and Mathematics with Applications.* **51**, 1367 (2006).

[239] N. Taghizadeh, M. Najad, *Journal of Computational and Applied Mathematics.* **4**, 390 (2012).

[240] Z. Feng, *Journal of Physics A.* **35**, 343 (2002).

[241] N. Bourbaki, *Elements of mathematics.* Commutative algebra, Hermann, Addison-Wesley, Paris, (1972).

[242] H. Yéepez-Martínez, J. F. Gómez-Aguilar, I. O. Sosa, J. M. Reyes, J. Torres-Jiménez, *Revista Mexicana de Física.* **62**, 310 (2016).

[243] G. A. Briggs, *Diffusion Estimation for Small Emissions.* Tennessee: NOAA Oak Ridge, 1973.

[244] W. M. Cox, J. A. Tikvart, *Atmospheric Environment.* **24A**, 2387 (1990).

[245] M. Sharan, M. Modani, *Atmospheric Environment.* **40**, 3479 (2006).

[246] P. Kumar, M. Sharan, *Environmental Modeling & Assessment.* **19(6)**, 487 (2014).

[247] P. Cagnetti, M. C. Cirillo, *DIMULA, un codice multisorgente per il calcolo della concentrazione in aria, al livello del suolo, di inquinanti atmosferici.* ENEA RTI/STUDI-VALSAMB, (1982).

[248] R. Gorenflo, F. Mainardi, S. V. Rogosin, *Handbook of Fractional Calculus with Applications.* **1**, 269 (2019).

[249] M. Sharan, M. Modani, *Atmospheric Environment.* **40**, 3469 (2006).

[250] S. E. Gryning, E. Lyck, *The Copenhagen tracer experiments: Reporting of measurements.* Risï£¡-R-1054(rev.1)(EN), (2002).

[251] M. L. Barad, *Project Prairie Grass, a Field Program in Diffusion (Vol. II).* Geophysical Research Papers No. 59, Air Force Cambridge Research Centre-TR-58-235(II), (1958).

[252] U. N. Katugampola, *Applied Mathematics and Computation.* **215**, 860 (2000).

[253] J. Klafter, M. F. Shlesinger, *Proceedings of the National Academy of Sciences.* **83(4)**, 848 (1986).

[254] S. Wortmann, M. T. Vilhena, D. M. Moreira, D. Buske, *Atmospheric Environment.* **39**, 2171 (2005).

[255] H. R. Olesen, *International Journal of Environment and Pollution.* **5**, 693 (2014).

[256] A. A. M. Holtslag, F. T. M. Nieuwstadt, *Boundary-Layer Meteorology.* **36**, 201 (1986).

[257] P. Kumar, M. Sharan, *Proceedings of the Royal Society A: Mathematical, Physical and Engineering Sciences.* **466(2114)**, 383 (2009).

[258] M. L. Barad, *Geophysical Research Paper.* **59**, (1958).

[259] H. R. Olesen, *International Journal of Environmental Pollution.* **5**, 693 (1995).

[260] S.-E. Gryning, A. A. M. Holtslag, J. S. Irwin, B. Sivertsen, *Atmospheric Environment.* **21**, 79 (1987).

[261] M. Sharan, S. K. Singh, J. P. Issartel, *Pure and applied geophysics.* **169(3)**, 483 (2012).

[262] G. Pandey, M. Sharan, *Atmospheric Environment.* **202**, 105 (2019).

[263] S. Sahoo, S. Ray, *Mathematical Methods in the Applied Sciences.* **40**, 106 (2016).

[264] J. Zhao, B. Tang, S. Kumar, Y. Hou, *Mathematical Problems in Engineering.* **2012**, 11 (2012).

[265] M. Younis, A. A. Zafar, K. Ul-Haq, M. Rahman, *American Journal of Computational and Applied Mathematics.* **3(2)**, 81 (2013).

[266] H. Yéepez-Martínez, J. F. Gómez-Aguilar, I. O. Sosa, J. M. Reyes, J. Torres-Jiménez, *Revista Mexicana de Física.* **62**, 310 (2016).

[267] S. Y. Lou, B. Tong, H. C. Hu, X. Y. Tang, *Journal of Physics A: Mathematical and General.* **39**, 513 (2006).

[268] S.-E. Gryning, E. J. Lyck, *Journal of Applied Meteorology and Climatology.* **23**, 651 (1984).

[269] S.-E. Gryning, A. A. M. Holtslag, *Atmospheric Environment.* **21**, 79 (1987).

[270] A. Taloni, A. Chechkin, J. Klafter, *EPL (Europhysics Letters).* **97(3)**, 30001 (2012).

[271] J. Paneva-Konovska, *From Bessel to Multi-Index Mittag Leffler Functions: Enumerable Families, Series in them and Convergence.* World Scientific Publishing, London (2016).

[272] J. Beran, *Statistics for Long-Memory Processes.* Chapman and Hall, (1994).

[273] C. W. J. Granger, *Journal of Econometrics.* **14(2)**, 227 (1980).

[274] P. S. Laplace, *Annales de chimie et de physique.* **XVIII**, 305 (1821).

[275] S. Baek, D. Lee, J. Kim, S. H. Hong, O. Kim, M. Ree, *Advanced Functional Materials.* **17**, 2637 (2007).

[276] P. J. Torvik, R. L. Bagley, *Journal of Applied Mechanics.* **51**, 294 (1984).

[277] A. Atangana, D. Baleanu, *Thermal Science. 20*, 763 (2016).

[278] A. A. Alderremy, K. M. Saad, P. Agarwal, S. Aly, S. Jain, *Physica A: Statistical Mechanics and its Applications.* **545**, 123806 (2020).

[279] M. D. Ortigueira, J. A. T. Machado, *Journal of Computational Physics.* **293**, 4 (2015).

[280] D. Stauffer, H. E. Stanley, *From Newton to Mandelbrot: A Primer in Theoretical Physics.* Springer-Verlag, New York, (1990).

[281] P. M. Gleiss, P. F. Stadler, A. Wagner et al., *Advances in Complex Systems.* **4**, 207 (2001).

[282] Mi Lv, J. Ma, *Neurocomputing.* **205**, 375 (2016).

[283] D. W. Dockery, C. A. Pope, X. Xu, J. D. Spengler, J. H. Ware, M. E. Fay, F. E. Speizer, *New England Journal of Medicine*, **329(24)**, 1753 (1993).

[284] G. Polichetti, S. Cocco, A. Spinali, V. Trimarco, A. Nunziata, *Toxicology.* **261(1-2)**, 1 (2009).

[285] J. S. Irwin, *Atmospheric Environment.* **13**, 191 (1979).

[286] A. L. Hodgkin, A. F. Huxley, *The Journal of Physiology.* **117**, 500 (1952).

[287] Mi Lv, C. N. Wang, G. D. Ren, J. Ma, X. Song, *Nonlinear Dynamics.* **85**, 1479 (2016).

[288] F. Wu, C. Wang, Y. Xu, J. Ma, *Scientific Reports.* **6**, (2016).

[289] T. C. Kofané, M. Fokou, A. Mohamadou, E. Yomba, *International Journal of Non-Linear Mechanics.* **112**, (2018).

[290] W. R. Chappel, W. R., J. Mordenti, *Advances in Drug Research.* **1** (1991).

[291] Mi Lv, J. Ma, *Neurocomputing.* **205**, 375 (2016).

[292] S. Brunak, B. Lautrup, *Neural Networks: Computer with intuition.* World Scientific Publishing, Singapor, (1990).

[293] E. A. Ermakova, E. E. Schnol, M. A. Panteelev, A. A. Butylin, V. Volpert, F. I. Ataullakhanov, *Plos One.* **4(2)**, (2017).

[294] Z. P. Kilpatrick, P. C. Bressloff, *Journal of Physics D: Applied Physics.* **239**, 547 (2010b).

[295] K. Frank, L. Tauc, *Cellular Function of Membrane Transport.* Prentice-Hall, New Jersey, (1964).

[296] R. Fitzhugh, *Biophysical Journal.* **1**, 445 (1961).

[297] T. Dauxois, M. Peyrard, *Physics of solitons, Chapter 3.* Cambridge University Press, Cambridge, (2006).

[298] N. M. Markovic, P. N. Ross, *Surface Science Reports.* **454)**, 117 (2002).

[299] P. J. Gilman, *Physical Chemistry.* **68**, 70 (1964).

[300] W. O. Davis, *Journal of Chemical Physics.* **43(8)**, 2809 (1965).

[301] Y. Wada, T. Yoshida, M. Tsuji, Y. Tamaura, *Energy Conversion and Management.* **36**, 641 (1995).

[302] W. Jin, C. Zhang, P. Zhang, Y. Fan, N. Xu, *AIChE journal.* **52**, 2545 (2006).

[303] S. Y. Savinov, H. Lee, H. K. Song, B.-Ki Na, *Industrial & Engineering Chemistry Research.* **38**, 2540 (1999).

[304] S. B. Tooski, *Physics of Plasmas*, **16**. 103302 (2009).

[305] A. C. Dillon, K. M. Jones, T. A. Bekkedahl, C.-H. Kiang, D. S. Bethune, M. J. Heben, *Nature.* **386**, 377 (1997).

[306] A. Zuttel, C. Nützenadel, P. Sudan, Ph. Mauron, C. Emmenegger, S. Rentsch, L. Schlapbach, A. Weidenkaff, T. Kiyobayashi, *Journal of Alloys and Compounds.* **676**, 330 (2002).

[307] A. Sen, D. P. Ahalpara, A. Thyagaraja, G. S. Krishnaswami, *Communications in Nonlinear Science and Numerical Simulation.* **17**, 4115 (2012).

[308] X. Fan, J. Yin, *Mathematica Aeterna.* **2(3)**, 273 (2012).

[309] D. J. Benney, *Journal of Mathematics and Physics.* **45**, 52 (1966).

[310] S. Yomosa, *Journal of the Physical society of Japan.* **56**, 506 (1987).

[311] E. C. Whipple, T. G. Northrop, D. A. Mendis, *Journal of Geophysical Research.* **90**, 7450 (1985).

[312] C. K. Goertz, *Reviews of Geophysics.* **27**, 271 (1989).

Publications resulting from the thesis

1- A S **Tagne Tankou**, J M Ema'a Ema'a, G H Ben-Bolie, D Buske *A new truncated M-fractional derivative for air pollutant dispersion.* Indian Journal of Physics, **94(11)**, 1777-1784 (2020) (Springer Nature)

https://doi.org/10.1007/s12648-019-01619-z

2- **TANKOU TAGNE** ALAIN SYLVAIN, ELE ABIAMA PATRICE, EMA'A EMA'A JEAN MARIE, OWONO ATEBA PIERRE and BEN-BOLIE GERMAIN HUBERT *Analytical solution of the steady-state atmospheric fractional diffusion equation in a finite domain.* Pramana Journal of Physics, **95(1)**, 2-9 (2021) Indian Academy of Science (Springer Nature)

https://doi.org/10.1007/s12043-020-02034-4

3- Alain Sylvain **Tankou Tagne**, Patrice Ele Abiama, Jean Marie Ema'a Ema'a, Pierre Owono Ateba, Germain Hubert Ben-Bolie, *A three-dimensional fractional solution for air contaminants dispersal in the planetary boundary layer.* Heliyon, **7(5)**, e07005 (2021)

https://doi.org/10.1016/j.heliyon.2021.e07005.